

# **On the Transmission of Light through Random Media**

PROEFSCHRIFT

TER VERKRIJGING VAN DE GRAAD VAN DOCTOR  
AAN DE RIJSUNIVERSITEIT TE LEIDEN, OP GEZAG  
VAN DE RECTOR MAGNIFICUS DR. W. A. WAGENAAR,  
HOGLERAAR IN DE FACULTEIT DER SOCIALE WETENSCHAPPEN,  
VOLGENS BESLUIT VAN HET COLLEGE VAN DEKANEN  
TE VERDEDIGEN OP DONDERDAG 16 OKTOBER 1997  
TE KLOKKE 16.15 UUR

DOOR

**Jeroen Clemens Jozef Paasschens**

GEBOREN TE VALKENSWAARD IN 1970

Promotiecommissie:

Promotor: Prof. dr. C. W. J. Beenakker  
Referent: Prof. dr. G. W. 't Hooft  
Overige leden: Prof. dr. L. J. de Jongh  
Prof. dr. J. M. J. van Leeuwen  
Prof. dr. G. Nienhuis  
Prof. dr. ir. W. van Saarloos

Het onderzoek beschreven in dit proefschrift heeft plaatsgevonden op het Philips Natuurkundig Laboratorium te Eindhoven, als onderdeel van het Philips onderzoeksprogramma, en is tevens onderdeel van het wetenschappelijk programma van de Nederlandse Organisatie voor Wetenschappelijk Onderzoek (NWO).

The work described in this thesis has been carried out at the Philips Research Laboratories Eindhoven, the Netherlands, as part of the Philips research programme, and is also part of the scientific programme of the Netherlands Organization for Scientific Research (NWO).

About the cover:

The cover shows the image of a cat, distorted by a piece of frosted glass (an example of a random medium). The original image is regained upon reflection in a special "phase-conjugating" mirror (studied in the last chapter of this thesis). From Jack Feinberg, *Optics Letters* 7, 486 (1982), used with permission of the author.

aan alle mensen met kanker

... la vraye Philosophie, dans laquelle on conçoit la cause de tous les effets naturels par des raisons de mechanicque. Ce qu'il faut faire à mon avis, ou bien renoncer à tous esperance de jamais rien comprendre dans la Physique.

... de ware Filosofie, waarin men mechanische redenen veronderstelt als oorzaak van alle natuurlijke effecten. Dit moet men volgens mij wel doen, of anders alle hoop opgeven ooit iets van Natuurkunde te begrijpen.

Christiaan Huygens,  
Traité de la Lumiere.



# Contents

<b>1</b>	<b>Introduction</b>	<b>1</b>
1.1	Medical imaging . . . . .	1
1.2	Random lasers . . . . .	3
1.3	Phase-conjugating mirror . . . . .	5
1.4	Analogies between photons and electrons . . . . .	6
1.5	Radiative transfer theory . . . . .	9
1.6	Diffusion approximation . . . . .	11
1.7	Scattering theory . . . . .	12
1.8	Numerical simulations . . . . .	14
1.9	This thesis . . . . .	16
	References . . . . .	19
<b>2</b>	<b>Accuracy of the diffusion equation with extrapolated-boundary condition</b>	<b>23</b>
2.1	Exact calculation of the transmittance . . . . .	24
2.2	Comparison with the diffusion approximation . . . . .	27
	References . . . . .	31
<b>3</b>	<b>Exact solution of the time-dependent Boltzmann equation</b>	<b>33</b>
3.1	Calculation of the Fourier-transformed intensity . . . . .	34
3.2	Inversion of the Fourier transform . . . . .	37
3.2.1	Two dimensions . . . . .	38
3.2.2	Four dimensions . . . . .	39
3.2.3	Three dimensions . . . . .	40
3.2.4	Ballistic peak . . . . .	43
3.3	Decay length and dispersion relation . . . . .	44
3.4	Conclusion . . . . .	46
3.A	Numerical inversion of the Fourier transform in 3 dimensions	47
3.B	Anisotropic scattering . . . . .	48
3.B.1	Formal exact solution . . . . .	49
3.B.2	Kratky-Porod theory . . . . .	50
3.B.3	Decay length . . . . .	52
	References . . . . .	55

---

<b>4</b>	<b>Influence of boundaries on the imaging of objects in turbid media</b>	<b>57</b>
4.1	Perturbation theory for general objects . . . . .	58
4.1.1	Born series . . . . .	60
4.1.2	Small objects . . . . .	61
4.1.3	Strength of specific objects . . . . .	64
4.1.4	Example . . . . .	67
4.1.5	Amplitude modulated sources . . . . .	68
4.2	Optimal boundaries . . . . .	68
4.2.1	Sources and boundaries . . . . .	68
4.2.2	Green functions . . . . .	72
4.2.3	Reflecting boundaries . . . . .	75
4.2.4	Experimental results . . . . .	77
4.2.5	Absorbing boundaries . . . . .	85
4.3	Conclusions . . . . .	90
	References . . . . .	93
<b>5</b>	<b>Probability of reflection by a random laser</b>	<b>95</b>
5.1	Calculation of the albedo . . . . .	96
5.2	Probability distribution of the albedo . . . . .	99
5.3	Numerical simulations and conclusions . . . . .	101
	References . . . . .	103
<b>6</b>	<b>Duality between absorption and amplification</b>	<b>105</b>
6.1	Proof of duality . . . . .	106
6.2	Single mode example . . . . .	108
6.3	Numerical simulations and conclusions . . . . .	111
	References . . . . .	113
<b>7</b>	<b>Localization in a non-conservative disordered multi-mode waveguide</b>	<b>115</b>
7.1	Formulation of the scattering problem . . . . .	117
7.2	Fokker-Planck equation . . . . .	118
7.3	Localization length . . . . .	123
7.3.1	Single-mode waveguide . . . . .	123
7.3.2	Multi-mode waveguide . . . . .	125
7.4	Numerical results and conclusions . . . . .	127
	References . . . . .	129

<b>8 Brightness of a phase-conjugating mirror behind a random medium</b>	<b>131</b>
8.1 Formulation of the problem . . . . .	132
8.2 Phase-incoherent solution . . . . .	135
8.2.1 Radiative transfer theory . . . . .	135
8.2.2 Neglect of angular correlations . . . . .	136
8.2.3 Exact solution of the Boltzmann equation . . . . .	137
8.3 Phase-coherent solution . . . . .	140
8.3.1 Scattering matrices . . . . .	140
8.3.2 Random-matrix theory . . . . .	143
8.3.3 Numerical simulations . . . . .	149
8.4 Comparison with Andreev reflection . . . . .	150
8.A Calculations in the coherent regime . . . . .	152
References . . . . .	159
<b>Samenvatting</b>	<b>161</b>
<b>List of Publications</b>	<b>165</b>
<b>Curriculum Vitæ</b>	<b>167</b>



# 1 Introduction

In optics, a random medium is a system where the dielectric constant  $\varepsilon(\mathbf{r})$  varies randomly as function of the position  $\mathbf{r}$ . Light propagating through such a medium is scattered by the fluctuations in  $\varepsilon$ . Furthermore, a non-zero imaginary part of  $\varepsilon$  leads to absorption or amplification of the radiation. In this thesis we study the transmission of light through various types of random media. The initial motivation of this research was a problem in medical imaging.

## 1.1 Medical imaging

The human body is a random medium, at least on a certain length scale. Due to the structure of cells and their components the dielectric constant of human tissue fluctuates randomly from point to point. The goal of medical imaging is to study the inside of a body, by transmitting radiation through it. X-rays have been used for that purpose for over a century, but they damage the tissue. Therefore it is advantageous to use longer wavelengths in the near infrared or in the visible parts of the spectrum. In this frequency region the scattering is greatly enhanced with respect to that of x-rays. It is a difficult problem to reconstruct an image from light which has been multiply scattered.

An additional complication is absorption, which should be as low as possible. The absorption by tissue is dominated by the absorption in water. In the range between small (ionizing) wavelengths and wavelengths too large for imaging purposes, the absorption minimum of water is around 500 nm. Near that wavelength, however, blood (haemoglobin) and pigments (melanin) have their absorption peak. The effective absorption by tissue is smallest at approximately 800 nm. Experiments are therefore done in the near-infrared regime.

There are two major applications of medical imaging. First of all, one can study the skin. The small thickness of the skin means that the amount of scattering can be rather low. The second application is the detection of tumors. This is possible either inside the head or in the female breast (mammography). Both regions of the body are void of bones and hence relatively homogeneous. Our research was motivated by the problem of

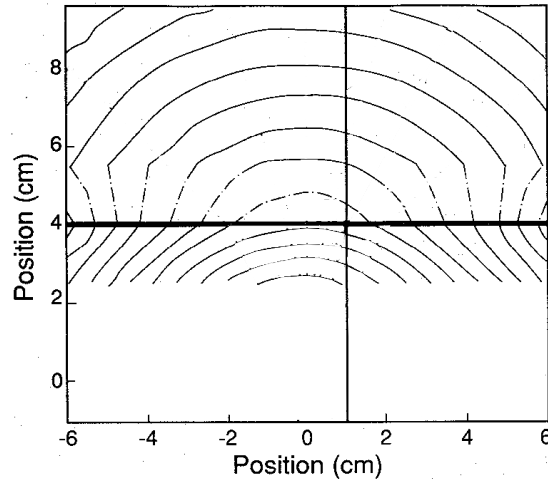


**Figure 1.1:** Refraction of a photon-density wave. Shown are constant phase contours (in  $20^\circ$  intervals) for the propagation of a diffusive photon-density wave through a planar boundary that separates two regions with different mean free path. From Ref. [1].

optical mammography.

The goal of mammography is the detection of an object, the tumor, inside a tissue, which is rather homogenous. This is done by detecting at various points around the breast the amount of light transmitted, coming from a single source. By repeating the measurement for different sources one gathers a large amount of data, from which in principle the interior of the breast can be reconstructed.

To be able to do a reconstruction, one needs to understand first the optical properties of the tissue when no tumor or other inhomogeneity is present. These are determined by two length scales, the mean free path for scattering and the absorption length. The angle-dependence of scattering is also of importance. (In general, tissue scatters predominantly in the forward direction.) The next step is to calculate the influence of such an inhomogeneity on the detected signals. The sensitivity of the measurement depends on the geometry and boundary conditions, and on the positions of the sources and detectors.

The source of light need not be a continuous wave, but could be a short pulse. The time-dependence of the detected signal can be used to gain extra information from the medium. Alternatively, one can use an

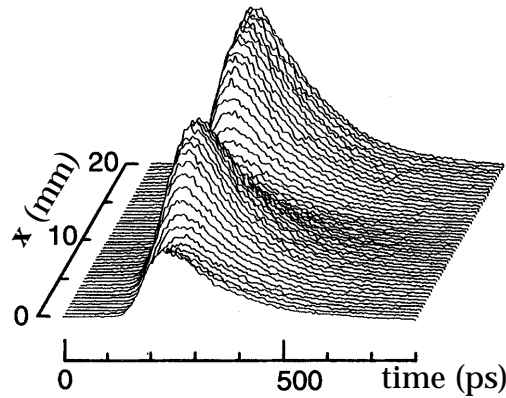


**Figure 1.2:** Time-dependent intensity profiles after transmission through a thin slab. Different scans belong to different positions along the slab, which contains large objects at  $x = 0$  mm and  $x = 10$  mm. From Ref. [3].

amplitude or frequency modulated source. The phase of the detected signal then contains additional information from the medium. When using amplitude modulation one speaks of a photon-density wave. In Fig. 1.1 we show refraction of a photon-density wave (interference has also been observed [2]). The difference with normal waves is that photon-density waves have a decay length which is of the same order of magnitude and smaller than the wavelength.

Although time-resolved or frequency-modulated experiments are more complicated than continuous-wave experiments, the reconstruction of the image can be simpler. An example of this is shown in Fig. 1.2. In a time-resolved measurement, the smallest times correspond to the shortest light paths. When an object is in between the source and detector, short light paths can not go around the object. Hence the small-time data can be used for direct projection imaging. To have sufficient accuracy the medium must not be too wide, since the amount of light with short path lengths decays exponentially with the thickness of the medium.

## 1.2 Random lasers

The term “random laser” was coined by Wiersma *et al.* [4], in response to an experiment by Lawandy *et al.* [5] on amplification of light in a strongly scattering medium. To make a laser one needs an amplifying medium

with a feedback mechanism. Usually feedback is provided by two mirrors. The light moves back and forth between the mirrors. Stimulated emission by atoms which have been pumped into an excited state leads to gain. Transmission through the (partially reflecting) mirrors leads to loss. The laser threshold is crossed when gain exceeds loss.

A random laser is a laser where feedback is provided by scattering by disorder, rather than by mirrors. It has an analogy with a nuclear reactor. Inside a reactor neutrons are generated by fission. These neutrons then move through the medium, and undergo scattering. Some of the neutrons are lost, either at the outer boundary, or at the cadmium control rods. They may also cause a new fission process. The threshold for the nuclear reaction is reached when, on average, each neutron generates another neutron before being lost.

Already in 1967 Letokhov [6] invoked this analogy to describe lasing in stellar atmospheres. He also argued that a mirrorless laser could be useful as a frequency standard, because the central frequency of the emitted radiation is set by the atomic transition frequency, and not by the geometry of the system. The recent practical interest in mirrorless lasers is motivated by futuristic applications such as “laser paint” [7]. The scientific interest is to study the interplay of amplification and localization.

A precursor of localization is the effect known as “weak localization”, manifested in the coherent backscattering peak [8, 9]. Consider a random medium that is illuminated by a plane wave. The light can pass through the medium via many different paths. These paths will interfere constructively or destructively, depending on the difference in path length. For any path there is also the time-reversed path, of the same length. These two paths will always interfere constructively, which results in an enhancement by a factor of two of the probability for closed paths, or equivalently of the intensity of light reflected at the angle of incidence. This coherent backscattering peak has a width of order  $\lambda/l$ , where  $\lambda$  is the wave vector of the light and  $l$  is the transport mean free path.

The effect of amplification on the coherent backscattering peak was investigated experimentally [10] and theoretically [11, 12]. The medium studied in the experiment consists of Ti:sapphire powders which amplify the light, doped with  $\text{Ti}_2\text{O}_3$  particles which have a large dielectric constant and cause scattering. As is shown in Fig. 1.3 the amplification leads to a narrowing of the backscattering peak. The reason is that the tails of the peak are due to short paths, and these are amplified less than long paths.

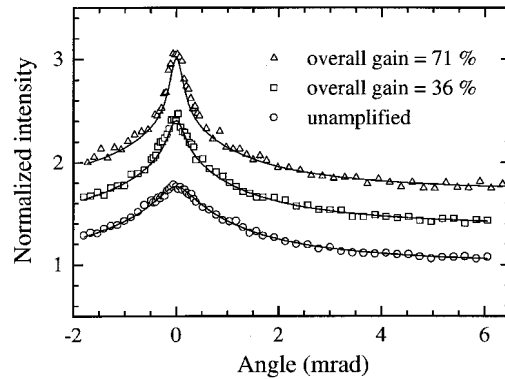


**Figure 1.3:** Backscattering peak in an amplifying medium. From Ref. [10].

### 1.3 Phase-conjugating mirror

Phase conjugation is the effect that an incoming wave  $\propto \cos(kx - \omega t)$  is reflected as a wave  $\propto \cos(-kx - \omega t)$ , with opposite sign of the phase  $kx$ . This is equivalent to reversing the sign of the time  $t$ , so that phase conjugation is sometimes called a time-reversal operation. The reflected wave has a wavevector precisely opposite to that of the incoming wave, and therefore propagates back along the incoming path. This is called retro-reflection. The differences between an ordinary mirror and a phase-conjugating mirror are depicted in Fig. (1.4) for two simple cases: an incoming plane wave and an incoming spherical wave.

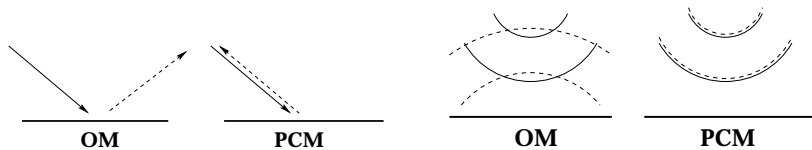


**Figure 1.4:** Reflection by an ordinary mirror (OM) and a phase-conjugating mirror (PCM) of a plane wave (left) and a spherical wave (right).

There exist various methods to create a phase-conjugating mirror [13–16]. A widely used method is the technique of four-wave mixing [13]. It makes use of a substance with a large third-order non-linear suscepti-

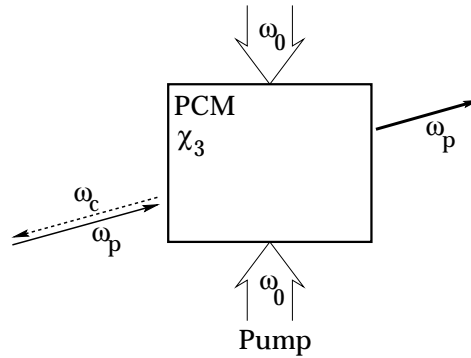


**Figure 1.5:** Four-wave mixing cell which constitutes a phase-conjugating mirror (PCM). The medium has a non-linear susceptibility  $\chi_3$ . Two pump beams at frequency  $\omega_0$  are counter-propagating. A probe beam at frequency  $\omega_p$  enters and is amplified. In addition a fourth beam at frequency  $\omega_c = 2\omega_0 - \omega_p$  is reflected in the opposite direction as the probe beam.

bility  $\chi_3$ . Examples are  $\text{BaTiO}_3$  and  $\text{CS}_2$ . The material is pumped by two counter-propagating beams, both at the same frequency  $\omega_0$  (see Fig. 1.5). A third beam, the probe beam, impinges on the material with a much smaller amplitude and a slightly different frequency  $\omega_p$ . The non-linear susceptibility leads to an amplification of the probe beam, and to the generation of a fourth beam. Basically two photons of the pump beams are converted into one photon for the third and fourth beam each. Energy conservation dictates that the frequency  $\omega_c$  of the fourth beam equals  $2\omega_0 - \omega_p$ . Momentum conservation dictates that its wavevector is opposite to that of the probe beam.

A phase-conjugating mirror can be used for wave-front reconstruction [14]. Imagine an incoming plane wave, that is distorted by some inhomogeneity. When this distorted wave falls on the mirror, it is phase conjugated and retro-reflected. Due to the time-reversal effect, the inhomogeneity that originally distorted the wave now changes it back to the original plane wave. An experimental example is shown in Fig. 1.6. We refer to Refs. [15–18] for a further introduction of phase conjugation.

## 1.4 Analogies between photons and electrons

In the previous sections we gave an overview of the subjects considered in this thesis. Much of our intuition comes from the analogous problems

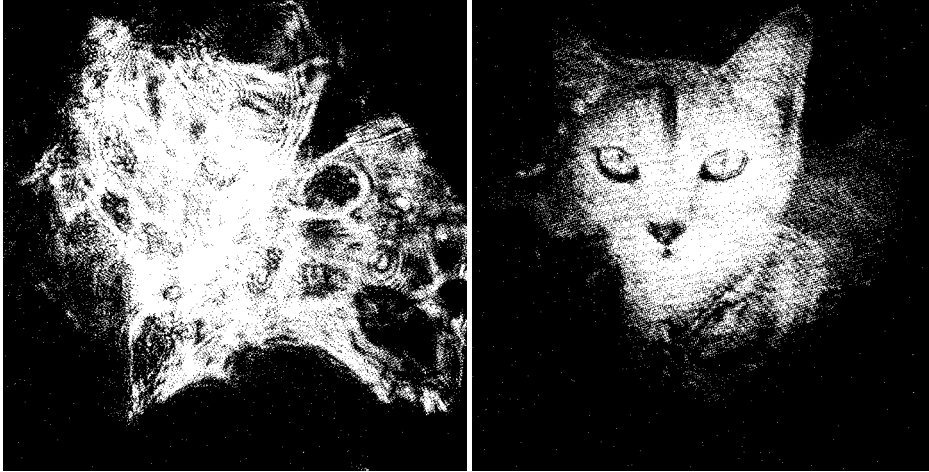


**Figure 1.6:** Experimental example of phase conjugation. In both photographs the image of a cat was distorted by transmitting it through a piece of frosted glass, and reflecting it back through the same piece of glass. This yields a unrecognizable image (left panel) when reflected by an ordinary mirror and the original image when reflected by a phase-conjugating mirror (right panel). From Ref. [19].

in solid-state physics, involving scattering of electrons instead of light. We introduce the analogies in this section.

The electric and magnetic fields  $E(\mathbf{r}, \omega)$  and  $B(\mathbf{r}, \omega)$  (at point  $\mathbf{r}$  and frequency  $\omega$ ) satisfy Maxwell's equations,

$$\nabla \cdot \varepsilon(\mathbf{r}, \omega) \mathbf{E} = 0, \quad (1.1a)$$

$$\nabla \cdot \mathbf{B} = 0, \quad (1.1b)$$

$$\nabla \times \mathbf{E} - i\omega \mathbf{B} = 0, \quad (1.1c)$$

$$\nabla \times \mathbf{B} + \varepsilon(\mathbf{r}, \omega) \frac{i\omega}{c^2} \mathbf{E} = 0. \quad (1.1d)$$

We assume that the relative magnetic permeability is unity and that the relative dielectric constant  $\varepsilon(\mathbf{r}, \omega)$  is isotropic. Eliminating the magnetic field from Eq. (1.1) one finds for the electric field the equation

$$\nabla^2 \mathbf{E} + \varepsilon(\mathbf{r}, \omega) \frac{\omega^2}{c^2} \mathbf{E} = \nabla(\nabla \cdot \mathbf{E}). \quad (1.2)$$

The vector character (polarization) of the light is a complication which in disordered media is usually insignificant (since the multiple scattering

randomizes the polarization). It is convenient to analyze a scalar wave equation, obtained from Eq. (1.2) by replacing the vector field  $\mathbf{E}$  by a scalar field  $E$  and setting the right-hand-side equal to zero. The result is the Helmholtz equation,

$$\nabla^2 E + \varepsilon(\mathbf{r}, \omega) \frac{\omega^2}{c^2} E = 0. \quad (1.3)$$

The scalar description is exact for effectively two-dimensional systems, where the dielectric constant varies only in the  $xy$ -plane, the polarization of the electric field being in the  $z$ -direction.

The Helmholtz equation (1.3) for classical waves has the same form as the Schrödinger equation

$$-\frac{\hbar^2}{2m} \nabla^2 \Psi(\mathbf{r}) + V(\mathbf{r}) \Psi(\mathbf{r}) = U \Psi(\mathbf{r}) \quad (1.4)$$

for quantum mechanical waves ( $\Psi(\mathbf{r})$  is the wave function,  $U$  is the energy and  $V(\mathbf{r})$  is the potential). This is the basis for the analogy between electronic and optical systems [20]. To make the correspondence we write the Helmholtz equation (1.3) as

$$-\nabla^2 E + c^{-2} [1 - \varepsilon(\mathbf{r}, \omega)] \omega^2 E = c^{-2} \omega^2 E. \quad (1.5)$$

We see that the correspondence with the Schrödinger equation (1.4) requires

$$\Psi(\mathbf{r}) \leftrightarrow E(\mathbf{r}), \quad (1.6a)$$

$$2mU/\hbar^2 \leftrightarrow \omega^2/c^2, \quad (1.6b)$$

$$2mV(\mathbf{r})/\hbar^2 \leftrightarrow [1 - \varepsilon(\mathbf{r}, \omega)] \omega^2/c^2. \quad (1.6c)$$

Using these mappings one can try to find similarities and differences between optical and electronic systems. We mention some of these.

The Schrödinger and Helmholtz equations are mathematically equivalent at any fixed value of energy  $U$  and frequency  $\omega$ . However because of the different way in which  $U$  and  $\omega$  appear in the two equations, the solutions to the two equations are different when considering a range of  $U$  or  $\omega$ . In particular, the time-dependent equations (obtained by Fourier-transformation with respect to  $U$  or  $\omega$ ) are entirely different in the electronic and optical cases. The Schrödinger equation has a first-order time-derivative while the Helmholtz equation has a second-order time-derivative. This leads to the different dispersion relations for light and electrons.

Furthermore, the frequency dependence of  $[1 - \varepsilon(\mathbf{r}, \omega)]\omega^2$  would be analogous to a time-dependent potential  $V(\mathbf{r}, t)$ , whereas the electronic problem has a time-independent potential  $V(\mathbf{r})$ . This difference leads for instance to a discrepancy between the group velocity of a wave and the energy velocity [21]. In this thesis we will restrict ourselves mainly to a single frequency, so that these effects are not important.

A difference which will be important here is that photons can be created or absorbed, in contrast to electrons. The difference manifests itself in the fact that the potential for electrons is real, while the dielectric constant  $\varepsilon = \varepsilon' + i\varepsilon''$  may be complex. Absorption corresponds to  $\varepsilon'' > 0$ . Amplification by stimulated emission corresponds to  $\varepsilon'' < 0$ .

Another difference between electronic and optical systems lies in the fact that the real part of  $\varepsilon$  is positive ( $\varepsilon' > 0$ , except for metals, but then substantial absorption takes place within a single wavelength). This implies for the corresponding electronic system that the energy is always larger than the potential,  $U > V(\mathbf{r})$ . Hence the simple tunnel barrier, familiar from quantum mechanics, does not exist in optics. The scattering due to a fluctuating dielectric constant cannot be as strong as that of a fluctuating potential with peaks higher than the energy of the electrons. Localization of light in three-dimensional systems requires strong disorder and is therefore much more difficult to achieve than for electrons [22–24]. In one-dimensional geometries (length much greater than width) localization sets in for arbitrary weak disorder, if the system is long enough. The localization length  $\xi$  in a disordered waveguide, (number of propagating modes  $N$ , mean free path  $l$ ) is given by  $\xi \simeq Nl$ . The transmittance decays exponentially  $\propto e^{-L/\xi}$  for lengths  $L \gg \xi$ . In this thesis we will only consider one-dimensional localization.

In the next sections we describe the three techniques we will use in this thesis. If interference effects can be neglected, then the theory of radiative transfer is the most convenient starting point. Otherwise, we will use a scattering theory, which fully accounts for interference effects. The third method is a numerical method, a solution of the Helmholtz equation discretized on a lattice.

## 1.5 Radiative transfer theory

The theory of radiative transfer was developed to study the propagation of electromagnetic radiation through stellar atmospheres [25–28]. In such a medium the free propagation of energy is randomly interrupted by a

scattering process, which changes the propagation direction or causes a loss of energy (absorption). When viewing the scattering process in time, the light can visit some parts of space multiple times. In the theory of radiative transfer the resulting correlations are not taken into account, but every scattering process is treated independently. The other basic approximation is that interference effects are disregarded.

The central quantity is the intensity  $I(\mathbf{r}, t, \hat{\mathbf{s}})$ , being the energy flux per unit solid angle at position  $\mathbf{r}$  and time  $t$ , in the direction  $\hat{\mathbf{s}}$ . Its evolution is governed by the Boltzmann equation, also called the equation of radiative transfer,

$$\frac{1}{v} \frac{\partial I(\mathbf{r}, t, \hat{\mathbf{s}})}{\partial t} + \hat{\mathbf{s}} \cdot \nabla I(\mathbf{r}, t, \hat{\mathbf{s}}) = l^{-1} Q(\mathbf{r}, t, \hat{\mathbf{s}}) - (l^{-1} + l_a^{-1}) I(\mathbf{r}, t, \hat{\mathbf{s}}). \quad (1.7)$$

Here  $v = c/n$  is the velocity of propagation (with  $c$  the speed of light in vacuum and  $n$  the index of refraction),  $l$  is the mean free path for scattering and  $l_a$  the absorption length. The quantity  $Q$  consists of all the light scattered from directions  $\hat{\mathbf{s}}'$  to  $\hat{\mathbf{s}}$ ,

$$Q(\mathbf{r}, t, \hat{\mathbf{s}}) = \int \frac{d\hat{\mathbf{s}}'}{\Omega_d} F(\hat{\mathbf{s}} \cdot \hat{\mathbf{s}}') I(\mathbf{r}, t, \hat{\mathbf{s}}'), \quad (1.8)$$

with a weight function  $F(\hat{\mathbf{s}} \cdot \hat{\mathbf{s}}')$  known as the phase function. The angular integral is normalized by the area  $\Omega_d = 2\pi^{d/2}/\Gamma(\frac{1}{2}d)$  of the unit sphere in  $d$  dimensions. The anisotropy parameter

$$g = \int \frac{d\hat{\mathbf{s}}'}{\Omega_d} F(\hat{\mathbf{s}} \cdot \hat{\mathbf{s}}') \hat{\mathbf{s}} \cdot \hat{\mathbf{s}}' \quad (1.9)$$

is a measure of the amount of anisotropy of the scattering.

The angular average of the intensity

$$\bar{I}(\mathbf{r}, t) = \int \frac{d\hat{\mathbf{s}}}{\Omega_d} I(\mathbf{r}, t, \hat{\mathbf{s}}) \quad (1.10)$$

determines the energy density

$$u(\mathbf{r}, t) = v^{-1} \Omega_d \bar{I}(\mathbf{r}, t). \quad (1.11)$$

Together with the net flux

$$\mathbf{F}(\mathbf{r}, t) = \int d\hat{\mathbf{s}} I(\mathbf{r}, t, \hat{\mathbf{s}}) \hat{\mathbf{s}}, \quad (1.12)$$

it satisfies the continuity equation

$$\frac{\partial}{\partial t} u(\mathbf{r}, t) + \nabla \cdot \mathbf{F} = -v l_a^{-1} u(\mathbf{r}, t), \quad (1.13)$$

as one can verify by integrating Eq. (1.7).

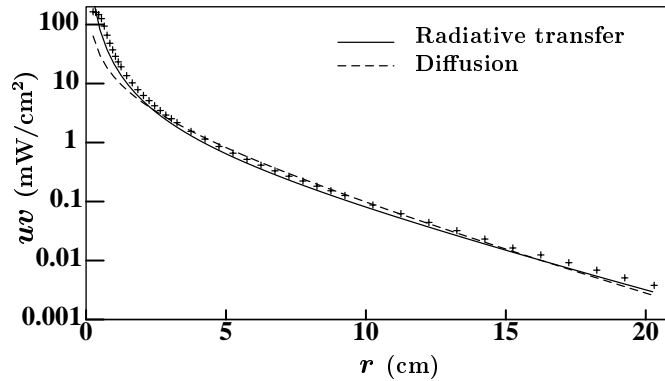


**Figure 1.7:** Energy density (times velocity)  $uv$  as a function of distance  $r$  to the source. The system has a mean free path  $l = 2.34$  cm, is anisotropic with  $g = 0.734$ , and is highly absorbing,  $l_a = 8.47$  cm. Nonetheless, the diffusion approximation (dashed) is nowhere far of from the calculation using radiative transfer theory (solid), and both are close to the experimental data (crosses). From Ref. [32].

## 1.6 Diffusion approximation

After the light has undergone multiple scattering, the angular dependence of the intensity will be weak. In this diffusive regime the equation of radiative transfer can be simplified to a diffusion equation, in which the angular variable has been eliminated. To derive the diffusion equation [26,27] one retains only the linear dependence of  $I$  on  $\hat{s}$ ,

$$I(\mathbf{r}, t, \hat{s}) \simeq \frac{1}{\Omega_d} [vu(\mathbf{r}, t) + d\hat{s} \cdot \mathbf{F}(\mathbf{r}, t)]. \quad (1.14)$$

We multiply the Boltzmann equation by  $\hat{s}$  and integrate over  $\hat{s}$ . Using the ansatz (1.14) we find

$$\frac{1}{v} \frac{\partial}{\partial t} \mathbf{F}(\mathbf{r}, t) + \frac{v}{d} \nabla u(\mathbf{r}, t) = -[l^{-1}(1-g) + l_a^{-1}] \mathbf{F}. \quad (1.15)$$

The two terms involving the time derivative on the left-hand-side and the absorption length on the right-hand-side should be neglected for a consistent approximation [29–31] (see also section 3.3). To find the correct expressions to the next order in  $l/l_a$  one needs to take higher order terms in the ansatz (1.14) into account as well. From Eq. (1.15) we find Fick's law

$$\mathbf{F}(\mathbf{r}, t) = -D \nabla u(\mathbf{r}, t), \quad (1.16)$$

with the diffusion constant  $D = vl_{\text{tr}}/d$  and the transport mean free path  $l_{\text{tr}} = l/(1 - g)$ . Combining Eqs. (1.13) and (1.15) we find the diffusion equation

$$\frac{\partial}{\partial t}u(\mathbf{r}, t) = D\nabla^2u(\mathbf{r}, t) - vl_a^{-1}u(\mathbf{r}, t). \quad (1.17)$$

The diffusion approximation breaks down within a transport mean free path from a source or a boundary, or if  $l_a \lesssim l_{\text{tr}}$ . That it works well can be seen in Fig. 1.7. In this experiment [32] the energy profile was measured resulting from a time-independent point-like source in an infinite medium. Although the result from the radiative transfer equation describes the experimental data better, the diffusion approximation is not far off, even though  $l_{\text{tr}} \simeq l_a$ .

## 1.7 Scattering theory

To include interference effects, neglected in the radiative transfer theory, we use a scattering approach. To this end the region where scattering takes place is embedded into a waveguide (see Fig. 1.8). The modes in the waveguide are normalized such that each of them carries the same flux. We assume that there are  $N$  propagating modes in the waveguide to the left of the scattering region, and  $N$  to the right. Any incoming or outgoing wave can be expanded as a sum of these  $2N$  modes,

$$E^{\text{in}} = \sum_{n=1}^{2N} u_n E_n^{\text{in}}, \quad E^{\text{out}} = \sum_{n=1}^{2N} v_n E_n^{\text{out}}. \quad (1.18)$$

The complex coefficients are combined into two vectors

$$\mathbf{u} = (u_1, u_2, \dots, u_{2N}), \quad \mathbf{v} = (v_1, v_2, \dots, v_{2N}). \quad (1.19)$$

The outgoing amplitudes  $v_n$  are linearly related to the incoming amplitudes  $u_n$ ,

$$\mathbf{v} = \mathbf{S}\mathbf{u}. \quad (1.20)$$

The  $2N \times 2N$  scattering matrix  $\mathbf{S}$  is symmetric,  $\mathbf{S} = \mathbf{S}^T$ , due to time reversal symmetry, and it is also unitary,  $\mathbf{S}^{-1} = \mathbf{S}^\dagger$ , due to flux conservation (when no absorption is present).

For simplicity we will usually assume a scalar wave, disregarding polarization effects. We consider a waveguide with constant cross-section

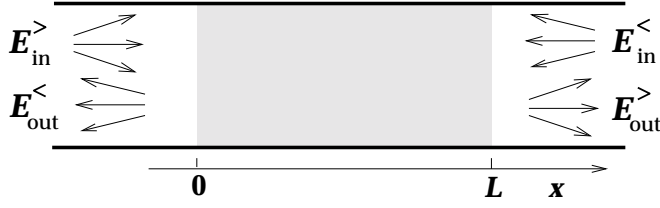


**Figure 1.8:** Schematic view of the scattering geometry in a waveguide.

(transverse coordinate vector  $\rho$ ) and dielectric constant  $\varepsilon = 1$ . The modes are given by

$$E_n^>(\rho, z, t) = k_n^{-1/2} \Psi_n(\rho) \exp(+ik_n z - i\omega t), \quad (1.21a)$$

$$E_n^<(\rho, z, t) = k_n^{-1/2} \Psi_n(\rho) \exp(-ik_n z - i\omega t). \quad (1.21b)$$

The superscript  $>$  ( $<$ ) indicates a wave moving to the right (left) along the  $z$ -axis, with frequency  $\omega$  and wavenumber

$$k_n = (\omega^2/c^2 - k_{\perp,n}^2)^{1/2}. \quad (1.22)$$

The functions  $\Psi_n(\rho)$  are eigenfunctions of the Helmholtz equation

$$\nabla^2 \Psi_n(\rho) = -k_{\perp,n}^2 \Psi_n(\rho), \quad (1.23)$$

in the cross-sectional plane of the waveguide. We will take the simplified condition that they vanish at the boundary. For the case of 2-dimensional scattering, we have

$$\Psi_n(\rho) = \sin\left(\frac{n\pi y}{W}\right) \quad (1.24)$$

where  $\rho = y$ ,  $W$  is the width of the waveguide and  $k_{\perp,n} = n/\pi W$ .

The scattering matrix

$$\mathbf{S} = \begin{pmatrix} \mathbf{r}_{11} & \mathbf{t}_{12} \\ \mathbf{t}_{21} & \mathbf{r}_{22} \end{pmatrix} \quad (1.25)$$

is described by two  $N \times N$  transmission matrices  $\mathbf{t}_{21}(\omega)$  and  $\mathbf{t}_{12}(\omega)$  (transmission from left to right and from right to left) plus two  $N \times N$  reflection matrices  $\mathbf{r}_{11}(\omega)$  and  $\mathbf{r}_{22}(\omega)$  (reflection from left to left and from right to right). In the absence of absorption (when  $\mathbf{S}$  is unitary), the reflection and transmission matrices can be decomposed as [33, 34]

$$\begin{aligned} \mathbf{r}_{11} &= i\mathbf{V}\sqrt{\mathbf{1}-\mathbf{T}}\mathbf{V}^T, & \mathbf{r}_{22} &= i\mathbf{U}\sqrt{\mathbf{1}-\mathbf{T}}\mathbf{U}^T, \\ \mathbf{t}_{12} &= \mathbf{V}\sqrt{\mathbf{T}}\mathbf{U}^T, & \mathbf{t}_{21} &= \mathbf{U}\sqrt{\mathbf{T}}\mathbf{V}^T. \end{aligned} \quad (1.26)$$

Here  $\mathbf{U}$  and  $\mathbf{V}$  are  $N \times N$  unitary matrices and  $\mathbf{T}$  is a diagonal matrix with the transmission eigenvalues  $T_n \in [0, 1]$  on the diagonal.

For a random medium, the scattering matrix is a random matrix, with some probability distribution. To compute averages we can use the techniques of random-matrix theory (two reviews of the random-matrix theory of phase-coherent scattering are Refs. [33, 34]). In a good approximation (called the isotropy approximation) the matrices  $\mathbf{U}$  and  $\mathbf{V}$  are uniformly distributed over the unitary group. For large systems,  $l \ll L \ll Nl$ , the density of transmission eigenvalues is bimodal,

$$\rho(T) = \frac{N}{2(L/l^* + 1)} \frac{1}{T\sqrt{1-T}}, \quad (1.27)$$

with a peak near zero and one and a cut-off for exponentially small  $T$ . The scaled mean free path  $l^*$  differs from the transport mean free path  $l_{\text{tr}}$  by a numerical factor

$$l^*/l_{\text{tr}} = \sqrt{\pi} \Gamma(\frac{1}{2}d + \frac{1}{2}) / \Gamma(\frac{1}{2}d + 1). \quad (1.28)$$

## 1.8 Numerical simulations

To test the analytical results we compare with numerical simulations of phase-coherent multiple scattering, using the recursive Green function technique [35–38]. The technique was developed for the Schrödinger equation, and therefore assumes a real potential. This is equivalent to the Helmholtz equation with a real dielectric constant. We will use the technique also for systems having absorption or amplification, which implies a complex dielectric constant. Therefore we will repeat in short the theory behind the simulations to show that they are still valid in this case.

The Helmholtz equation (1.3) is discretized on a square lattice (lattice constant  $b$ ):

$$E_{i,a-1} + E_{i,a+1} + E_{i+1,a} + E_{i-1,a} - 4E_{i,a} + \left(\varepsilon_{ia}\omega^2 b^2/c^2\right) E_{ia} = 0. \quad (1.29)$$

The width  $M$  is finite ( $a = 0, 1, \dots, M+1$ ), while the length is infinite ( $i = 0, \pm 1, \pm 2, \pm 3, \dots$ ). The boundary conditions are

$$E_{i,0} = E_{i,M} = 0, \quad \text{for all } i. \quad (1.30)$$

The geometry is therefore the same as that of Fig. 1.8. We introduce disorder in a segment of length  $L$  ( $i = 1, 2, \dots, L$ ), by letting the relative dielectric constant  $\varepsilon_{ia}$  fluctuate from site to site between  $1 \pm \delta\varepsilon$ . Outside this region, we take  $\varepsilon_{ia} = 1$ . In the leads ( $i \leq 0$  and  $i > L$ ) there are  $N$  propagating modes. The number  $N$  depends on the frequency  $\omega b/c$ . We seek the  $2N \times 2N$  scattering matrix  $\mathbf{S}$ , for an ensemble of different realizations of the disorder.

The scattering matrix is related [35] to the (retarded) Green function  $G_{nm}(z_p, z_q)$ , projected onto modes  $n$  and  $m$  at two points  $z_p, z_q$  in the leads  $p, q = 1, 2$ . To compute  $G$  we use the recursive Green function technique, which we explain following MacKinnon [37]. The Green function on the lattice can be found from the equation

$$(Z\delta_{ij}\delta_{ab} - H_{ia,jb})G_{jb,kc} = \delta_{ik}\delta_{ac}, \quad (1.31)$$

with implicit summation over repeated indices. The matrix  $H$  is the discretized Helmholtz operator,

$$H_{ia,jb} = \delta_{ij}(\delta_{a,b-1} + \delta_{a,b+1}) + \delta_{ab}(\delta_{i,j-1} + \delta_{i,j+1}) + \delta_{ij}\delta_{ab}(\varepsilon_{ia}\omega^2 b^2/c^2 - 4), \quad (1.32)$$

the parameter  $Z$  is a positive imaginary infinitesimal. The calculation of  $G$  requires a matrix inversion. This can be done efficiently in a recursive way, by adding slices of the disordered region, one at a time.

We take the elements belonging to one slice, at constant  $i$ , together, writing

$$(\mathbf{H}_{ij})_{a,b} = H_{ia,jb}, \quad (\mathbf{G}_{ij})_{a,b} = G_{ia,jb}. \quad (1.33)$$

Equation (1.31) then becomes

$$(Z\delta_{ij}\mathbf{1} - \mathbf{H}_{ij})\mathbf{G}_{jk} = \delta_{ik}\mathbf{1}. \quad (1.34)$$

We start with the Green function  $\mathbf{G}_{ij}^{(I)}$  for a semi-infinite system, where  $i, j \leq I$ . This Green function can be found analytically for  $I \leq 0$ , where no disorder is present. We add one slice at a time until  $I = L$ , doing the calculation numerically. The full Green function can then be found from the Green function for  $i \leq L$  and that for  $i > L$ , which can again be calculated analytically since no disorder is present in that region. The calculation of  $\mathbf{G}^{(I+1)}$  from  $\mathbf{G}^{(I)}$  can be done using the equations [37]

$$\mathbf{G}_{I+1,I+1}^{(I+1)} = (Z\mathbf{1} - \mathbf{H}_{I+1,I+1} - \mathbf{H}_{I+1,I}\mathbf{G}_{I,I}^{(I)}\mathbf{H}_{I,I+1})^{-1}, \quad (1.35a)$$

$$\mathbf{G}_{I+1,i}^{(I+1)} = \mathbf{G}_{I+1,I+1}^{(I+1)}\mathbf{H}_{I+1,I}\mathbf{G}_{I,i}^{(I)}, \quad (1.35b)$$

$$\mathbf{G}_{i,I+1}^{(I+1)} = \mathbf{G}_{i,I}^{(I)} \mathbf{H}_{I,I+1} \mathbf{G}_{I+1,I+1}^{(I+1)} \quad (1.35c)$$

$$\mathbf{G}_{i,j}^{(I+1)} = \mathbf{G}_{i,j}^{(I)} + \mathbf{G}_{i,I}^{(I)} \mathbf{H}_{I,I+1} \mathbf{G}_{I+1,I+1}^{(I+1)} \mathbf{H}_{I+1,I} \mathbf{G}_{I,j}^{(I)} \quad (1.35d)$$

where  $i, j \leq I$ . Once we know  $G$ , the scattering matrix, projected onto modes  $n$  and  $m$ , follows from

$$(\mathbf{S}_{pq})_{mn} = i\delta_{pq}\delta_{mn} + \sqrt{v_n v_m} G_{nm}(z_p, z_q). \quad (1.36)$$

Here  $\mathbf{S}_{pq}$  is a reflection matrix for  $p = q$  and a transmission matrix for  $p \neq q$ , and  $v_n = (4 - \{\omega^2 b^2 / c^2 - 4 + 2 \cos[n\pi / (M + 1)]\}^2)^{-1/2}$  is the velocity along the waveguide of mode  $n$ .

The recursive method has the following advantages. For every slice added, the matrix one has to invert remains of size  $M \times M$ . The computation time required, therefore, scales linearly with  $L$ . Furthermore the method is stable, in contrast to transfer matrix calculations, which we do not discuss here. The derivation does not require  $H$  to be Hermitian, and therefore holds also for complex dielectric constant, i.e. for systems with absorption or amplification.

To compare the numerical results with the theory we need to extract the mean free path  $l^*$  from the numerical data. This can be done by computing the average transmission  $\langle T \rangle \equiv \langle N^{-1} \text{Tr} \mathbf{t}_{12} \mathbf{t}_{12}^\dagger \rangle$  averaged over disorder realizations, for a large number of modes  $N$ . The mean free path is then obtained from

$$\langle T \rangle = \frac{1}{1 + L/l^*}. \quad (1.37)$$

which is a good approximation for  $N \gg 1$  [39].

## 1.9 This thesis

In the first three chapters following this introduction, we ignore interference effects. The theme of the first two chapters is the accuracy of the diffusion approximation to the theory of radiative transfer in the stationary (chapter 2) and the time-dependent case (chapter 3). The following chapter describes the use of the diffusion approximation for imaging purposes (chapter 4). In the next four chapters we include interference effects. The theme of those chapters is the interplay of phase-coherent multiple scattering with amplification (chapters 5–7) and phase conjugation (chapter 8).

### **Extrapolated-boundary condition for the diffusion equation**

As mentioned in section 1.6, the diffusion approximation is easier to use than the full theory of radiative transfer, described in section 1.5. This approximation is accurate far from boundaries and sources. In a finite system, one needs to supplement the diffusion equation with boundary conditions, derived from the equation of radiative transfer. In chapter 2, we investigate this problem for a slab geometry, with a step in the index of refraction at the boundary. We calculate the transmittance in the diffusion approximation, and compare with the exact solution of the equation of radiative transfer.

### **Propagation of a pulse through a random medium**

In chapter 3, we extend the comparison between the theory of radiative transfer and the diffusion approximation, to the time-dependent case. We study the spreading of a light-pulse in an unbounded disordered medium. Within the diffusion approximation the intensity distribution is Gaussian in space, centered at  $r = 0$  and with a width  $\sim \sqrt{Dt}$ . From the equation of radiative transfer we find that the intensity has two peaks: a ballistic peak at time  $t = r/c$ , in addition to the diffusion peak at  $t \simeq r^2/D$ . Forward scattering adds a tail to the ballistic peak in 2 and 3 dimensions,  $\propto (ct - r)^{-1/2}$  and  $\propto -\ln(ct - r)$ , respectively. This tail has not been noticed previously.

### **Influence of boundaries on the imaging of objects in turbid media**

To image objects that are present in a random medium, one needs to know how sensitive measurements are to different kinds of objects, and to the position of those objects. In chapter 4 we calculate this sensitivity for objects which have a different absorption with respect to the background, and for objects which differ in the scattering parameters. The medium that contains the objects will be bounded, and in practice the sources and detectors are at the boundaries. Using the previous results we compare three systems, an unbounded medium, a medium having a black boundary, and a medium having a mirror as boundary. We calculate the influence of the boundaries on the sensitivity. Our results are confirmed by experiments.

### **Probability of reflection by a random laser**

We start the study of the interplay of disorder and amplification with the “random laser” introduced in section 1.2. In chapter 5 we consider the

reflection of light from an amplifying random medium. We calculate the sample-to-sample fluctuations of the albedo  $a$  (the ratio of reflected and incident flux). The average albedo equals that calculated from theories which do not take interference into account. We find, as expected, a laser threshold, where the disorder and amplification are such that the average albedo diverges, and we compute the enhancement of fluctuations close to the laser threshold. Beyond the laser threshold, the distribution of  $a$  remains well-defined, with a finite modal value and divergent moments. This distribution is however unstable due to spontaneous emission events.

### Localization with absorption or amplification

In chapters 6 and 7 we study the effect of amplification on the localization length  $\xi$  of a disordered waveguide. As discussed in section 1.4 the transmittance of these quasi-one-dimensional systems decays exponentially  $\propto e^{-L/\xi}$  in the large- $L$  limit. In the presence of absorption, the decay length  $\xi$  becomes shorter. We show that dual systems, which differ only in the sign of the imaginary part of  $\varepsilon$ , have the same decay length. Hence, contrary to intuition, amplification suppresses the transmittance of a long waveguide in the same way as absorption does. We use random-matrix theory to calculate the localization lengths for systems with one and with many modes, and compare with numerical simulations.

### Random medium in front of a phase conjugating mirror

Optical phase-conjugation was introduced in section 1.3. In chapter 8 we study the combination of a disordered medium and a phase-conjugating mirror. As in previous chapters, we calculate the total flux reflected, for given incoming flux. We compare the incoherent theory of radiative transfer, with a phase-coherent scattering theory. The two approaches agree if the frequency shift  $\Delta\omega$  acquired at the phase-conjugating mirror is large compared to the inverse of the mean dwell time  $\tau_{\text{dwell}}$  of a photon in the disordered region. However, radiative transfer theory fails completely in the opposite regime,  $\Delta\omega \ll 1/\tau_{\text{dwell}}$ . We also consider the angular dependence of the reflected intensity for an incident wave, to study wave-front reconstruction. Perfect phase conjugation means that all of the light is retro-reflected in the incident direction. This is possible only for a narrow range of angles of incidence. The diffusive scattering by disorder prevents perfect phase conjugation, but not completely: a clear peak in the reflected intensity persists at the angle of incidence.

## Bibliography

- [1] M. A. O'Leary, D. A. Boas, B. Chance, and A. G. Yodh, *Phys. Rev. Lett.* **69**, 2658 (1992).
- [2] J. M. Schmitt, A. Knüttel, and J. R. Knutson, *J. Opt. Soc. Am. A* **9**, 1832 (1992).
- [3] D. G. Papaioannou, G. W. 't Hooft, J. J. M. Baselmans, and M. J. C. van Gemert, *Appl. Opt.* **34**, 6144 (1995).
- [4] D. S. Wiersma, M. P. van Albada, and A. Lagendijk, *Nature* **373**, 203 (1995).
- [5] N. M. Lawandy, R. M. Balachandran, A. S. L. Gomes, and E. Sauvain, *Nature* **368**, 436 (1994).
- [6] V. S. Letokhov, *Pis'ma Zh. Eksp. Teor. Fiz.* **4**, 477 (1966) [*JETP Lett.* **4**, 321 (1966)]; V. S. Letokhov, *Pis'ma Zh. Eksp. Teor. Fiz.* **5**, 262 (1967) [*JETP Lett.* **5**, 212 (1967)].
- [7] D. S. Wiersma and A. Lagendijk, *Physics World* **10**, 33 (Jan. 1997).
- [8] M. P. van Albada and A. Lagendijk, *Phys. Rev. Lett.* **55**, 2692 (1985).
- [9] E. Akkermans, P. E. Wolf, and R. Maynard, *Phys. Rev. Lett.* **56**, 1471 (1986).
- [10] D. S. Wiersma, M. P. van Albada, and A. Lagendijk, *Phys. Rev. Lett.* **75**, 1739 (1995).
- [11] A. Yu. Zyuzin, *Europhys. Lett.* **26**, 517 (1994).
- [12] S. C. Feng and Z.-Q. Zhang, *Phys. Rev. B* **54**, 3240 (1996).
- [13] R. W. Hellwarth, *J. Opt. Soc. Am.* **67**, 1 (1977).
- [14] B. Ya. Zel'dovich, V. I. Popovichev, V. V. Ragul'skii, and F. S. Faizullov, *ZhETF Pis. Red.* **15**, 160 (1972) [*JETP Lett.* **15**, 109 (1972)].
- [15] R. A. Fisher, editor, *Optical Phase Conjugation* (Academic, New York, 1983).
- [16] B. Ya. Zel'dovich, N. F. Pilipetskiĭ, and V. V. Shkunov, *Principles of Phase Conjugation* (Springer, Berlin, 1985).

- [17] V. Shkunov and B. Ya. Zel'dovich, *Sci. Am.* **253** (12), 40 (1985).
- [18] D. M. Pepper, *Sci. Am.* **254** (1), 56 (1986).
- [19] J. Feinberg, *Opt. Lett.* **7**, 486 (1982).
- [20] W. van Heteren and D. Lenstra, editors, *Analogies in Optics and Micro Electronics* (Kluwer, Dordrecht, 1990).
- [21] A. Lagendijk and B. A. van Tiggelen, *Phys. Rep.* **270**, 143 (1996).
- [22] S. John, *Phys. Rev. Lett.* **53**, 2169 (1984).
- [23] P. Sheng, editor, *Scattering and Localization of Classical Waves in Random Media* (World Scientific, Singapore, 1990).
- [24] S. John, *Phys. Today* **44** (5), 32 (1991).
- [25] S. Chandrasekhar, *Radiative Transfer* (Dover, New York, 1960).
- [26] A. Ishimaru, *Wave Propagation and Scattering in Random Media* (Academic, New York, 1978).
- [27] A. J. Welch and M. J. C. van Gemert, editors, *Optical-Thermal Response of Laser-Irradiated Tissue* (Plenum, New York, 1995).
- [28] J. Lenoble, editor, *Radiative Transfer in Scattering and Absorbing Atmospheres: Standard Computational Procedures* (A. Deepak, Hampton, Virginia, 1985).
- [29] A. Ya. Polishchuk, S. Gutman, M. Lax, and R. R. Alfano, *J. Opt. Soc. Am. A* **14**, 230 (1997).
- [30] H. C. van de Hulst, *Multiple Light Scattering* (Academic, New York, 1980).
- [31] M. Bassani, F. Martelli, G. Zaccanti, and D. Contini, *Opt. Lett.* **22**, 853 (1997).
- [32] K. Rinzema, L. H. P. Murrer, W. M. Star, and J. J. ten Bosch, unpublished (1996).
- [33] A. D. Stone, P. A. Mello, K. A. Muttalib, and J.-L. Pichard, in: *Mesoscopic Phenomena in Solids*, edited by B. L. Altshuler, P. A. Lee, and R. A. Webb (North-Holland, Amsterdam, 1991).

- 
- [34] C. W. J. Beenakker, *Rev. Mod. Phys.* **69**, 731 (1997).
- [35] P. A. Lee and D. S. Fisher, *Phys. Rev. Lett.* **47**, 882 (1981).
- [36] D. J. Thouless and S. Kirkpatrick, *J. Phys. C* **14**, 235 (1981).
- [37] A. MacKinnon, *Z. Phys. B* **59**, 385 (1985).
- [38] H. U. Baranger, D. P. DiVincenzo, R. A. Jalabert, and A. D. Stone, *Phys. Rev. B* **44**, 10637 (1991).
- [39] M. J. M. de Jong, *Phys. Rev. B* **49**, 7778 (1994).



## 2 Accuracy of the diffusion equation with extrapolated-boundary condition

Multiple scattering of light in a turbid medium is well described by the theory of radiative transfer [1–3]. This theory is based on a Boltzmann equation for the stationary intensity  $I(\mathbf{r}, \hat{\mathbf{s}})$  of monochromatic light at position  $\mathbf{r}$  and with wave vector in the direction  $\hat{\mathbf{s}}$ . In the simple case of isotropic and non-absorbing scatterers (with mean free path  $l$ ), the Boltzmann equation takes the form

$$l \hat{\mathbf{s}} \cdot \nabla I(\mathbf{r}, \hat{\mathbf{s}}) = -I(\mathbf{r}, \hat{\mathbf{s}}) + \bar{I}(\mathbf{r}). \quad (2.1)$$

Far from boundaries the angle-averaged intensity, given here for 3 dimensions,

$$\bar{I}(\mathbf{r}) \equiv \int \frac{d\hat{\mathbf{s}}}{4\pi} I(\mathbf{r}, \hat{\mathbf{s}}) \quad (2.2)$$

satisfies the diffusion equation

$$\nabla^2 \bar{I}(\mathbf{r}) = 0, \quad (2.3)$$

which is easier to solve than the Boltzmann equation. The diffusion equation breaks down within a few mean free paths from the boundary, and one needs to return to the Boltzmann equation in order to determine  $\bar{I}(\mathbf{r})$  near the boundaries.

A great deal of work has been done on the choice of boundary conditions for the diffusion equation which effectively incorporate the non-diffusive boundary layer [1, 2, 4–8]. These studies have led to the so called “extrapolated-boundary condition”

$$\bar{I}(\mathbf{r}) = -\xi \hat{\mathbf{n}} \cdot \nabla \bar{I}(\mathbf{r}), \quad (2.4)$$

where  $\mathbf{r}$  is a point on the boundary and  $\hat{\mathbf{n}}$  is a unit vector perpendicular to the boundary and pointing outwards. Equation (2.4) implies that a linear density profile extrapolates to zero at a distance  $\xi$  beyond the boundary. The extrapolation length  $\xi$  is of the order of the mean free path.

In this chapter we consider transmission through a slab of finite thickness  $L$ . We compute the transmittance  $T$ , the ratio between the incident

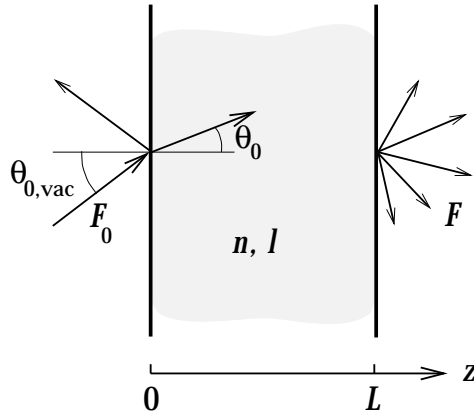


**Figure 2.1:** A sketch of the slab geometry. The disordered medium (thickness  $L$ ) has a refractive index  $n$  (relative to the outside) and a mean free path  $l$ . The slab is illuminated by a plane wave incident at an angle  $\theta_{0,\text{vac}}$ , which is refracted to an angle  $\theta_0$  inside the medium. The transmittance  $T$  is the ratio of the transmitted flux  $F$  and the incident flux  $F_0$ .

flux and the transmitted flux, by solving the Boltzmann equation numerically. Previous work on this problem used the diffusion equation with the extrapolated-boundary condition [9–12] (or an alternative large- $L/l$  approximation [7]) to derive convenient analytical formulas for the dependence of  $T$  on  $L$  and  $l$ , on the refractive index of the slab, and on the angle of incidence. It is the purpose of the present study to determine the accuracy of these formulas, by comparison with the results from the Boltzmann equation. We generalize and extend a previous study by De Jong [13] in the context of electrical conduction through a disordered metal, where the issue of refractive-index mismatch and angular resolution has not been considered.

## 2.1 Exact calculation of the transmittance

We consider a slab containing a disordered medium between the planes  $z = 0$  and  $z = L$  (see Fig. 2.1). The intensity  $I(\mathbf{r}, \hat{\mathbf{s}})$  depends only on the  $z$ -coordinate and on the angle  $\theta$  between  $\hat{\mathbf{s}}$  and the  $z$ -axis. We define  $\mu \equiv \cos \theta$ . The Boltzmann equation (2.1) takes the form

$$l\mu \frac{\partial}{\partial z} I(z, \mu) = -I(z, \mu) + \bar{I}(z), \quad 0 < z < L, \quad (2.5a)$$

$$\bar{I}(z) = \frac{1}{2} \int_{-1}^1 d\mu I(z, \mu). \quad (2.5b)$$

We supplement Eq. (2.5) with boundary conditions at  $z = 0$  and  $z = L$  that describe reflection due to a refractive index mismatch, with reflection probability  $R(\mu)$ :

$$I(0, \mu) = R(\mu)I(0, -\mu) + I_0(\mu), \quad \mu > 0, \quad (2.6a)$$

$$I(L, -\mu) = R(\mu)I(L, \mu). \quad \mu > 0, \quad (2.6b)$$

The boundary condition at  $z = 0$  also contains the intensity due to a planar source with angular distribution  $I_0(\mu)$  inside the medium. Note that the angular distribution is different from that outside the medium, due to refraction at the boundary and due to the fact that part of the light is reflected before even entering the medium.

The Boltzmann equation (2.5) with boundary conditions (2.6) implies for  $\bar{I}(z)$  an integral equation of the Schwarzschild-Milne type [1, 6, 7, 13]

$$\begin{aligned} \bar{I}(z) = M_0(z) + \int_0^L dz' \bar{I}(z') \Big[ & M_1(z - z') + \\ & M_2(z + z') + M_2[(L - z) + (L - z')] + \\ & M_3(z - z') + M_3[(L - z) - (L - z')] \Big]. \end{aligned} \quad (2.7)$$

We have defined the kernels

$$M_1(z) = \int_0^1 \frac{d\mu}{2l\mu} e^{-|z|/l\mu}, \quad (2.8a)$$

$$M_2(z) = \int_0^1 \frac{d\mu}{2l\mu} N(\mu)R(\mu)e^{-z/l\mu}, \quad (2.8b)$$

$$M_3(z) = \int_0^1 \frac{d\mu}{2l\mu} N(\mu)R^2(\mu)e^{-(2L+z)/l\mu}. \quad (2.8c)$$

The factor  $N$  is given by

$$N(\mu) = \left(1 - R^2(\mu)e^{-2L/l\mu}\right)^{-1}. \quad (2.9)$$

The kernels  $M_1$ ,  $M_2$ , and  $M_3$  describe propagation from  $z'$  to  $z$  with zero, an odd number, and an even number of reflections, respectively. The source term  $M_0$  is given by

$$M_0(z) = \frac{1}{2} \int_0^1 d\mu N(\mu)I_0(\mu) \left[ e^{-z/l\mu} + R(\mu)e^{-(2L-z)/l\mu} \right]. \quad (2.10)$$

Once  $\bar{I}(z)$  is known, the intensities  $I(z, \mu)$  and  $I(z, -\mu)$  with  $\mu > 0$  follow from

$$I(z, \mu) = I_0(\mu)N(\mu)e^{-z/l\mu} + \int_0^z \frac{dz'}{l\mu} e^{(z'-z)/l\mu} \bar{I}(z') + N(\mu)R(\mu)e^{-z/l\mu} \\ \times \int_0^L \frac{dz'}{l\mu} \left( e^{-z'/l\mu} + R(\mu)e^{-(2L-z')/l\mu} \right) \bar{I}(z'), \quad (2.11a)$$

$$I(z, -\mu) = I_0(\mu)N(\mu)R(\mu)e^{-(2L-z)/l\mu} + \int_z^L \frac{dz'}{l\mu} e^{(z-z')/l\mu} \bar{I}(z') \\ + N(\mu)R(\mu)e^{-(2L-z)/l\mu} \\ \times \int_0^L \frac{dz'}{l\mu} \left( e^{z'/l\mu} + R(\mu)e^{-z'/l\mu} \right) \bar{I}(z'). \quad (2.11b)$$

This is a solution of the Boltzmann equation (2.5) with boundary conditions (2.6), as can be checked by substitution. Integration over all  $\mu$  then yields the Schwarzschild-Milne equation (2.7). We solve the integral equation (2.7) numerically, by discretizing the interval  $(0, L)$ , so that it reduces to a matrix equation [13].

The quantity of interest is the transmittance  $T$ , defined as the ratio of the flux  $F$  that is transmitted through the slab and the flux  $F_0$  incident from the source,

$$T = F/F_0. \quad (2.12)$$

The transmitted flux is given by

$$F = 2\pi \int_{-1}^1 d\mu \mu I(z, \mu), \quad (2.13)$$

where  $c$  is the speed of light in the medium. The flux is independent of  $z$ , because there is no absorption. The total incident flux (including the flux which is reflected at the slab boundary before entering the medium) is given by

$$F_0 = 2\pi \int_{\mu_c}^1 d\mu \frac{\mu I_0(\mu)}{1 - R(\mu)}. \quad (2.14)$$

We assume that the medium in the slab has a refractive index  $n > 1$  (relative to the refractive index outside the slab). The lower bound  $\mu_c$  in the integral, defined by  $\mu_c \equiv (1 - 1/n^2)^{1/2}$ , is the cosine of the angle at which total internal reflection occurs [ $R(\mu) \equiv 1$  for  $\mu < \mu_c$ ]. For  $0 < \mu < \mu_c$  the reflection probability is given by the Fresnel formula for unpolarized light,

$$R(\mu) = \frac{1}{2} \left| \frac{\mu_{\text{vac}} - n\mu}{\mu_{\text{vac}} + n\mu} \right|^2 + \frac{1}{2} \left| \frac{n\mu_{\text{vac}} - \mu}{n\mu_{\text{vac}} + \mu} \right|^2, \quad (2.15a)$$

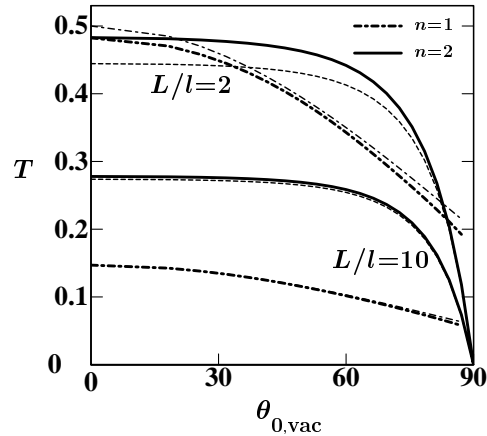


**Figure 2.2:** Transmittance as a function of the incident angle  $\theta_{0,\text{vac}}$  for two different values of  $L$  and  $n$ . The thick curves are computed from the Boltzmann equation, the thin curves are the diffusion approximation (2.20).

$$\mu_{\text{vac}} \equiv [1 - n^2(1 - \mu^2)]^{1/2}. \quad (2.15b)$$

The relation between  $\mu_{\text{vac}} = \cos \theta_{\text{vac}}$  and  $\mu = \cos \theta$  is Snell's law, such that the angle of incidence  $\theta_{\text{vac}}$  outside the medium (in "vacuum") is refracted to an angle  $\theta$  in the medium (see Fig. 2.1).

We have calculated the transmittance for the case of plane-wave illumination,  $I_0(\mu) = I_0 \delta(\mu - \mu_0)$ . The results are shown in Fig. 2.2, where  $T$  is plotted as a function of the angle of incidence  $\theta_{0,\text{vac}}$  outside the medium [ $\mu_{0,\text{vac}} = \cos \theta_{0,\text{vac}}$  is related to  $\mu_0$  by Eq. (2.15b)]. We show results for two different ratios  $L/l$  and two values of  $n$  (thick curves). For  $n = 1$  the transmittance is non-zero for all incident angles, but numerical difficulties prevent us from going beyond  $\theta_{0,\text{vac}} \simeq 87^\circ$ . The thin curves in Fig. 2.2 are the results of the diffusion approximation, which we discuss in the following section.

## 2.2 Comparison with the diffusion approximation

The diffusion approximation for the transmittance has been studied by several authors [9–12]. Here we briefly describe this approach, and then compare the result with the numerical solution of the Boltzmann equation.

In a slab geometry the diffusion equation with extrapolated-boundary

condition takes the form [cf. Eqs. (2.3) and (2.4)]

$$\frac{d^2}{dz^2} \bar{I}(z) = 0, \quad 0 < z < L, \quad (2.16)$$

with boundary conditions

$$\bar{I}(0) = \xi \bar{I}'(0), \quad \bar{I}(L) = -\xi \bar{I}'(L). \quad (2.17)$$

We assume plane-wave illumination of the boundary  $z = 0$ , at an angle  $\theta_{0,\text{vac}}$  with the positive  $z$ -axis. A fraction  $1 - R(\mu_0)$  of the incident flux  $F_0$  enters the medium, and is first scattered on average at  $z = \mu_0 l$ . [We recall that  $\mu_0 = \cos \theta_0$ , where  $\theta_0$  corresponds to  $\theta_{0,\text{vac}}$  after refraction, cf. Eq. (2.15b).] This plane-wave illumination is incorporated into the diffusion equation (2.16) as a source term,

$$\frac{d^2}{dz^2} \bar{I}(z) + \frac{3}{4\pi l} [1 - R(\mu_0)] F_0 \delta(z - \mu_0 l) = 0. \quad (2.18)$$

The solution of Eq. (2.18) with boundary condition (2.17) is

$$\bar{I}(z) = \begin{cases} \frac{3}{4\pi l} \frac{(\xi + z)(L + \xi - \mu_0 l)}{L + 2\xi} [1 - R(\mu_0)] F_0, & \text{if } 0 < z < \mu_0 l, \\ \frac{3}{4\pi l} \frac{(\xi + \mu_0 l)(L + \xi - z)}{L + 2\xi} [1 - R(\mu_0)] F_0, & \text{if } \mu_0 l < z < L. \end{cases} \quad (2.19)$$

The transmitted flux  $F = -\frac{4}{3}\pi \bar{I}'(L)$  divided by the incident flux  $F_0$  leads to the transmittance in the diffusion approximation,

$$T_{\text{diff}} = [1 - R(\mu_0)] \frac{\xi + \mu_0 l}{L + 2\xi}. \quad (2.20)$$

This simple analytical formula combines results in the literature by Kaplan et al. [9] (who considered normal incidence) and by Nieuwenhuizen and Luck [7] (who considered the Schwarzschild-Milne equation in the diffusive limit  $L \gg l$ ).

We still need to specify the value of the extrapolation length  $\xi$ . We will use an expression due to Zhu, Pine, and Weitz [14],

$$\xi = \frac{2}{3} l \frac{1 + C_2}{1 - C_1}, \quad (2.21)$$

where the coefficients  $C_1$  and  $C_2$  are the first two moments of  $R(\mu)$ ,

$$C_1 = 2 \int_0^1 d\mu \mu R(\mu), \quad (2.22a)$$

$$C_2 = 3 \int_0^1 d\mu \mu^2 R(\mu), \quad (2.22b)$$

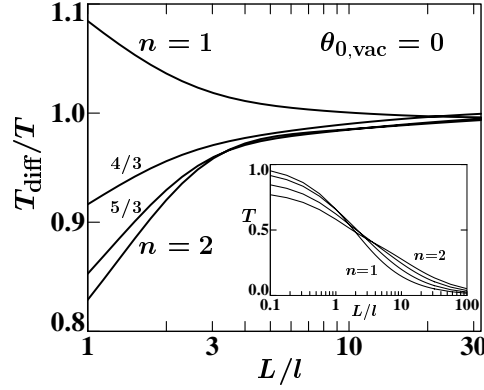


**Figure 2.3:** Ratio of the transmittance  $T_{\text{diff}}$  according to the diffusion approximation and the exact result  $T$  according to the Boltzmann equation, for normal incidence  $\theta_{0,\text{vac}} = \theta_0 = 0$ . The inset shows  $T$  as a function of  $L/l$ , for the same values of  $n$  as the main plot.

normalized such that  $C_1 = C_2 = R$  for an angle-independent reflection probability  $R(\mu) = R$ . Comparison of Eq. (2.21) with a numerical solution of the Boltzmann equation in a semi-infinite medium by Aronson [8] shows that it accurately describes the length over which the linear density profile extrapolates to zero. The difference is largest for  $n = 1$ , when Eq. (2.21) gives  $\xi = \frac{2}{3}l$  while the Boltzmann equation gives an extrapolation length of  $0.7104l$  which is somewhat larger [1, 7]. The transmittance  $T_{\text{diff}}$  is compared in Figs. 2.2 and 2.3 with the exact  $T$  from the Boltzmann equation.

Once the transmittance  $T$  for plane-wave illumination as a function of  $\mu_{0,\text{vac}} = \cos \theta_{0,\text{vac}}$  is known, one can compute the transmittance  $T_{\text{tot}}$  for diffusive illumination by integrating over the angles of incidence,

$$T_{\text{tot}} = 2 \int_0^1 d\mu_{0,\text{vac}} \mu_{0,\text{vac}} T(\mu_{0,\text{vac}}). \quad (2.23)$$

The diffusion approximation (2.20) and (2.21) yields the analytical formula

$$T_{\text{diff,tot}} = n^2 \left( \frac{3L}{4l} + \frac{1+C_2}{1-C_1} \right)^{-1}. \quad (2.24)$$

In the absence of a refractive-index mismatch ( $n = 1$ ,  $C_1 = C_2 = 0$ ) this formula has been found [13] to agree with the Boltzmann equation within 3% for all  $L/l$ . For  $n > 1$  the relative error in Eq. (2.24) is comparable to that shown in Fig. 2.3 for the transmittance at normal incidence.

In conclusion, we have computed the transmittance of a turbid medium of mean free path  $l$  and length  $L$  from the Boltzmann equation as a function of the angle of incidence. We compared the results from the diffusion equation to this exact solution. The difference between the two transmittances stays below 6% for  $L > 3l$  and  $1 < n < 2$ . The diffusion approximation overestimates the transmittance for  $n = 1$  and underestimates it in the presence of a significant refractive index mismatch. The relative error is largest for large refractive index mismatch.

## Bibliography

- [1] S. Chandrasekhar, *Radiative Transfer* (Dover, New York, 1960).
- [2] A. Ishimaru, *Wave Propagation and Scattering in Random Media*, Vols. 1 & 2 (Academic, New York, 1978).
- [3] H. C. van de Hulst, *Multiple Light Scattering* (Academic, New York, 1980).
- [4] R. G. Giovanelli, *Optica Acta* **2**, 153 (1955).
- [5] A. Lagendijk, R. Vreeker, and P. de Vries, *Phys. Lett. A* **136**, 81 (1989).
- [6] I. Freund, *Phys. Rev. A* **45**, 8854 (1992).
- [7] Th. M. Nieuwenhuizen and J. M. Luck, *Phys. Rev. E* **48**, 569 (1993).
- [8] R. Aronson, in *Progress in Biomedical Optics; Proceedings of Photon Migration and Imaging in Random Media and Tissues*, edited by B. Chance, R. R. Alfano, and A. Katzir, Vol. 1888 (SPIE, Los Angeles, 1993).
- [9] P. D. Kaplan, M. H. Kao, A. G. Yodh, and D. J. Pine, *Appl. Opt.* **32**, 3828 (1993).
- [10] J. H. Li, A. A. Lisianski, T. D. Cheung, D. Livdan, and A. Z. Genack, *Europhys. Lett.* **22**, 675 (1993).
- [11] R. C. Haskell, L. O. Svaasand, T. Tsay, T. Feng, M. S. McAdams, and B. J. Tromberg, *J. Opt. Soc. Am. A* **11**, 2727 (1994).
- [12] S. Fantini, M. A. Franceschini, and E. Gratton, *J. Opt. Soc. Am. B* **11**, 2128 (1994).
- [13] M. J. M. de Jong, *Phys. Rev. B* **49**, 7778 (1994).
- [14] J. X. Zhu, D. J. Pine, and D. A. Weitz, *Phys. Rev. A* **44**, 3948 (1991).



### 3 Exact solution of the time-dependent Boltzmann equation

The spreading of a pulse of particles or radiation through a random medium has attracted considerable attention in several fields of physics, such as astrophysics, optics, and solid-state physics [1–3]. In each of these systems it is possible to generate a pulse of energy, consisting of electromagnetic or acoustic waves, or electrons. The pulse then propagates through the medium, with a certain intensity  $\bar{I}(\mathbf{r}, t)$  at point  $\mathbf{r}$  and time  $t$ . In the long time limit it is accurately given by the diffusion expression

$$\bar{I}_{\text{diff}}(\mathbf{r}, t) = \frac{1}{(4\pi Dt)^{d/2}} \exp\left(-\frac{r^2}{4Dt}\right). \quad (3.1)$$

Here  $r = |\mathbf{r}|$  is the distance to the source, assumed to be isotropic,  $t$  is the time,  $d$  is the dimension of the system,  $D = cl/d$  is the diffusion coefficient, and  $l$  is the mean free path for elastic and isotropic scattering. We disregard here any interference effects, effects of inelastic scattering, or absorption.

The diffusion result is very useful, but has certain shortcomings. First of all, it has a non-zero value at every position even though the energy needs some time to propagate from source to detector. Hence for  $r > ct$  the correct  $\bar{I}$  should be identically zero. Furthermore, large deviations from the diffusion approximation can be expected at any  $r$ , for short times  $t < l/c$ . More accurate expressions for the probability density as function of position and time have been proposed [4–8], based on the Boltzmann equation (also known as the equation of radiative transfer [9,10]), of which the diffusion equation is the long-time limit.

In this chapter we will present exact solutions of the equation of radiative transfer, and compare with approximate expression in the literature [4, 6, 8]. The solution in 1 dimension has been given a long time ago by Hemmer [11];

$$\begin{aligned} \bar{I}(r, t) = & \frac{1}{2}e^{-ct/2l} \left[ \delta(r - ct) + \frac{1}{2l}\Theta(ct - r) \right. \\ & \left. \times \left( I_0(\sqrt{c^2t^2 - r^2}/2l) + ct \frac{I_1(\sqrt{c^2t^2 - r^2}/2l)}{\sqrt{c^2t^2 - r^2}} \right) \right], \quad d = 1, \quad (3.2) \end{aligned}$$

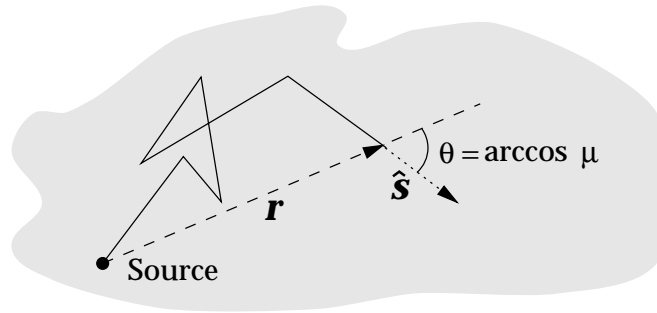


**Figure 3.1:** Schematic drawing of scattering in a random medium. Shown is a single path involving  $N = 5$  scattering events.

where  $I_0$  and  $I_1$  are Bessel functions, and the step function  $\Theta(x)$  is zero for  $x < 0$  and 1 for  $x > 0$ . We will generalize this solution to higher dimensions, using a path integral method [12, 13]. In 2 and 4 dimensions we are able to give explicit expressions. In 3 dimensions the solution is given in terms of its Fourier transform. Using the results for  $d = 2$  and 4 we construct an interpolation for  $d = 3$ , which is correct within a few percent. A qualitative difference with existing results is that in 2 and 3 dimensions the ballistic peak at  $r = ct$  is accompanied by a tail resulting from single-scattering events. The analytical shape of this tail is  $\propto (ct - r)^{-1/2}$  and  $\propto -\ln(ct - r)$  for  $d = 2$  and 3, respectively.

Our presentation is organized as follows. In section 3.1 we derive the Fourier transform  $\bar{I}(k, \omega)$  of the intensity  $\bar{I}(r, t)$  for any dimension. In section 3.2 we invert the Fourier transform to get the time and position dependent intensity. We give analytical results for  $d = 2$  and 4, and numerical results plus an interpolation formula for  $d = 3$ . We compare our results with the literature, and discuss the ballistic peak in some detail. In section 3.3 we calculate the decay length and use the result to give a diffusion-like equation for the intensity which does not include the angular degree of freedom. This equation might be useful in other geometries as well. We conclude in section 3.4.

### 3.1 Calculation of the Fourier-transformed intensity

The theory of radiative transfer describes the place  $r$  and time  $t$  dependence of the intensity  $I(r, t, \hat{s})$  of radiation, propagating in the direction  $\hat{s}$

(see Fig. 3.1). It is based on the Boltzmann equation [9, 10]

$$\frac{\partial}{c \partial t} I(\mathbf{r}, t, \hat{\mathbf{s}}) + \hat{\mathbf{s}} \cdot \nabla I(\mathbf{r}, t, \hat{\mathbf{s}}) = -(l^{-1} + l_a^{-1}) I(\mathbf{r}, t, \hat{\mathbf{s}}) + l^{-1} \bar{I}(\mathbf{r}, t) + c^{-1} S(\mathbf{r}, t, \hat{\mathbf{s}}), \quad (3.3a)$$

$$\bar{I}(\mathbf{r}, t) = \int \frac{d\hat{\mathbf{s}}'}{\Omega_d} I(\mathbf{r}, t, \hat{\mathbf{s}}'). \quad (3.3b)$$

Here  $S$  is the source term,  $l$  is the mean free path, and  $l_a$  is the absorption length. The integration is performed over all directions  $\hat{\mathbf{s}}'$  in  $d$  dimensions, normalized by the surface area  $\Omega_d = 2\pi^{d/2}/\Gamma(d/2)$  of the unit sphere. We have assumed isotropic scattering.

The dependence of the intensity on the absorption is through a  $\mathbf{r}$  and  $\hat{\mathbf{s}}$  independent factor  $\exp(-ct/l_a)$ . Without loss of generality we can therefore leave the absorption out of our considerations in the following, taking effectively  $l_a \rightarrow \infty$ . We take the isotropic point source

$$S(\mathbf{r}, t, \hat{\mathbf{s}}) = \delta(\mathbf{r})\delta(t), \quad (3.4)$$

and seek for a solution to Eq. (3.3) for  $t > 0$ . (We may set  $I \equiv 0$  for  $t < 0$ .) Due to the spherical symmetry,  $I(\mathbf{r}, t, \hat{\mathbf{s}})$  and  $\bar{I}(\mathbf{r}, t)$  only depend on  $r = |\mathbf{r}|$ ,  $t$ , and  $\mu = \hat{\mathbf{s}} \cdot \mathbf{r}/r$ . The Boltzmann equation (3.3) simplifies to

$$l \left( \frac{\partial}{c \partial t} + \mu \frac{\partial}{\partial r} + \frac{1 - \mu^2}{r} \frac{\partial}{\partial \mu} \right) I(r, t, \mu) = -I(r, t, \mu) + \bar{I}(r, t) + \frac{l\delta(r)\delta(t)}{\Omega_d r^{d-1} c}, \quad (3.5a)$$

$$\bar{I}(r, t) = \int_{-1}^1 d\mu \rho_d(\mu) I(r, t, \mu). \quad (3.5b)$$

The weight function  $\rho_d(\mu)$  is defined by

$$\rho_d(\mu) = \frac{\Gamma(d/2)}{\sqrt{\pi} \Gamma[(d-1)/2]} (1 - \mu^2)^{d/2-3/2}, \quad d > 1. \quad (3.6)$$

In 1 dimension we find  $\rho_1(\mu) = \frac{1}{2}\delta(\mu - 1) + \frac{1}{2}\delta(\mu + 1)$ .

To solve the Boltzmann equation it is useful not to make use of the spherical symmetry initially. We consider separately the contributions to the intensity from  $N = 0, 1, 2, \dots$  scattering events,

$$I(\mathbf{r}, t, \hat{\mathbf{s}}) = \sum_{N=0}^{\infty} I_N(\mathbf{r}, t, \hat{\mathbf{s}}), \quad \bar{I}(\mathbf{r}, t) = \sum_{N=0}^{\infty} \bar{I}_N(\mathbf{r}, t). \quad (3.7)$$

Such a decomposition is customary in the theory of random walks [13, 14] It is also at the basis of the path-integral method for the theory of the Boltzmann equation [12]. The partial intensities  $I_N$  satisfy

$$\left(\frac{\partial}{c\partial t} + \hat{\mathbf{s}} \cdot \nabla + l^{-1}\right) I_N(\mathbf{r}, t, \hat{\mathbf{s}}) = l^{-1} \bar{I}_{N-1}(\mathbf{r}, t), \quad N > 0, \quad (3.8a)$$

$$\left(\frac{\partial}{c\partial t} + \hat{\mathbf{s}} \cdot \nabla + l^{-1}\right) I_0(\mathbf{r}, t, \hat{\mathbf{s}}) = c^{-1} S(\mathbf{r}, t). \quad (3.8b)$$

The differential operators on the left-hand-side can be integrated, to yield

$$I_N(\mathbf{r}, t, \hat{\mathbf{s}}) = l^{-1} \int_0^\infty d\mathbf{r}_0 e^{-r_0/l} \bar{I}_{N-1}(\mathbf{r} - \mathbf{r}_0 \hat{\mathbf{s}}, t - r_0/c), \quad (3.9a)$$

$$I_0(\mathbf{r}, t, \hat{\mathbf{s}}) = c^{-1} \int_0^\infty d\mathbf{r}_0 e^{-r_0/l} S(\mathbf{r} - \mathbf{r}_0 \hat{\mathbf{s}}, t - r_0/c). \quad (3.9b)$$

Similarly, we find for the angular average of the intensity

$$\bar{I}_N(\mathbf{r}, t) = \int d\mathbf{r}_0 p_0(\mathbf{r}_0) \bar{I}_{N-1}(\mathbf{r} - \mathbf{r}_0, t - r_0/c), \quad (3.10a)$$

$$\bar{I}_0(\mathbf{r}, t) = l c^{-1} \int d\mathbf{r}_0 p_0(\mathbf{r}_0) S(\mathbf{r} - \mathbf{r}_0, t - r_0/c), \quad (3.10b)$$

where we defined

$$p_0(\mathbf{r}) = \frac{e^{-r/l}}{\Omega_d l r^{d-1}}. \quad (3.11)$$

Using the source (3.4) we can give the explicit expression for the ballistic intensities ( $N = 0$ )

$$I_0(\mathbf{r}, t, \hat{\mathbf{s}}) = e^{-ct/l} \delta(\mathbf{r} - ct\hat{\mathbf{s}}) \Theta(t) = e^{-ct/l} \frac{\delta(r - ct) \delta(\mu - 1^-)}{\Omega_d r^{d-1} \rho_d(\mu)}, \quad (3.12a)$$

$$\bar{I}_0(\mathbf{r}, t) = \frac{e^{-ct/l}}{\Omega_d r^{d-1}} \delta(r - ct). \quad (3.12b)$$

The  $1^-$  in the delta function denotes that it is a single-sided delta function having all its weight in the region  $\mu \leq 1$ . The solution of the recursion relations (3.10) and consequently of Eq. (3.9) then is

$$\bar{I}_N(\mathbf{r}, t) = l \left[ \prod_{i=0}^N \int d\mathbf{r}_i p_0(\mathbf{r}_i) \right] \delta(ct - \sum_{i=0}^N r_i) \delta(\mathbf{r} - \sum_{i=0}^N \mathbf{r}_i), \quad (3.13a)$$

$$I_N(\mathbf{r}, t, \hat{\mathbf{s}}) = \Omega_d l \left[ \prod_{i=0}^N \int d\mathbf{r}_i p_0(\mathbf{r}_i) \right] \times \delta(ct - \sum_{i=0}^N r_i) \delta(\mathbf{r} - \sum_{i=0}^N \mathbf{r}_i) \delta(\hat{\mathbf{r}}_0 - \hat{\mathbf{s}}), \quad (3.13b)$$

where  $\hat{\mathbf{r}}_0 = \mathbf{r}_0/|\mathbf{r}_0|$ .

Summation over all  $N$  of Eq. (3.9) results in

$$I(\mathbf{r}, t, \hat{\mathbf{s}}) = I_0(\mathbf{r}, t, \hat{\mathbf{s}}) + l^{-1} \int_0^\infty d r_0 e^{-r_0/l} \bar{I}(\mathbf{r} - r_0 \hat{\mathbf{s}}, t - r_0/c), \quad (3.14)$$

and leads to the spherical analogue of the Schwarzschild-Milne equation [9]:

$$\bar{I}(\mathbf{r}, t) = \bar{I}_0(\mathbf{r}, t) + \int d\mathbf{r}_0 p(\mathbf{r}_0) \bar{I}(\mathbf{r} - \mathbf{r}_0, t - r_0/c). \quad (3.15)$$

At this point, we introduce the Fourier transform

$$\bar{I}(\mathbf{k}, \omega) = \int d\mathbf{r} \int_0^\infty dt e^{i(\omega t - \mathbf{k} \cdot \mathbf{r})} \bar{I}(\mathbf{r}, t), \quad (3.16)$$

which depends only on  $\omega$  and  $k = |\mathbf{k}|$ . We first compute the partial intensities  $\bar{I}_N(k, \omega)$ , by taking the Fourier transform of  $\bar{I}_N(\mathbf{r}, t)$ . The expression factorizes into  $N + 1$  equivalent integrals over  $\mathbf{r}_i$ , which can be performed. The result is

$$\bar{I}_N(\mathbf{k}, \omega) = c^{-1} l \left( \int_{-1}^1 \frac{d\mu \rho_d(\mu)}{1 - i\omega l/c + ikl\mu} \right)^{N+1} \quad (3.17a)$$

$$= c^{-1} l \left[ \frac{{}_2F_1\left(\frac{1}{2}, 1; \frac{1}{2}d; -k^2 l^2 (1 - i\omega l/c)^{-2}\right)}{1 - i\omega l/c} \right]^{N+1}, \quad (3.17b)$$

$$I_N(\mathbf{k}, \omega, \hat{\mathbf{s}}) = \bar{I}_{N-1}(k, \omega) \frac{1}{1 - i\omega l/c + ikl \cdot \hat{\mathbf{s}}}, \quad (3.17c)$$

where  ${}_2F_1$  is a hypergeometric function. This expression is the frequency and direction dependent analogue of the result for a random walk [13].

## 3.2 Inversion of the Fourier transform

In the previous section we have computed the Fourier transformed intensity for arbitrary dimension  $d$ . In this section we invert the Fourier transform, which can be done analytically for  $d = 2$  and  $d = 4$ , and numerically for  $d = 3$ .

### 3.2.1 Two dimensions

In two dimensions Eq. (3.17) simplifies to

$$\bar{I}_N(k, \omega) = c^{-1} l \left[ (1 - i\omega l/c)^2 + k^2 l^2 \right]^{-(N+1)/2}. \quad (3.18)$$

The ballistic  $N = 0$  term consists of a delta function in real space and is given in Eq. (3.12), (where  $\Omega_2 = 2\pi$ ). After inverse Fourier transformation with respect to  $k$  we find for  $N \geq 1$ :

$$\bar{I}_N(r, \omega) = \frac{1}{cl^2} \left( \frac{r}{2l(1 - i\omega l/c)} \right)^{(N-1)/2} \frac{K_{(N-1)/2}[(1 - i\omega l/c)r/l]}{\Gamma[(N+1)/2]}. \quad (3.19)$$

Using the representation

$$K_\nu(z) = \frac{\sqrt{\pi}(z/2)^\nu}{\Gamma(\nu + \frac{1}{2})} \int_0^\infty d\xi (\sinh \xi)^{2\nu} e^{-z \cosh \xi}, \quad (3.20)$$

and the substitution  $\cosh \xi = ct/r$ , one can see that Eq. (3.19) is the Fourier transform of

$$\bar{I}_N(r, t) = \frac{e^{-ct/l}}{2\pi l^2} \frac{1}{(N-1)!} \left( \frac{ct}{l} \right)^{N-2} \left( 1 - \frac{r^2}{c^2 t^2} \right)^{(N-2)/2} \Theta(ct - r), \quad N \geq 1. \quad (3.21)$$

Summing over  $N$ , and adding the ballistic  $N = 0$  term from Eq. (3.12), we find the total intensity

$$\begin{aligned} \bar{I}(r, t) &= \frac{e^{-ct/l}}{2\pi r} \delta(ct - r) \\ &+ \frac{\Theta(ct - r)}{2\pi lct} \left( 1 - \frac{r^2}{c^2 t^2} \right)^{-1/2} \exp \left[ l^{-1} (\sqrt{c^2 t^2 - r^2} - ct) \right]. \end{aligned} \quad (3.22)$$

The diffusion result (3.1), with  $D = cl/2$ , is recovered for  $t \gg r/c$ . It is remarkable that the diffusion approximation does not require that  $ct \gg l$ , but only that  $ct \gg r$ . We will see that this is special for two dimensions.

To obtain the angular resolved intensity  $I_N(\mathbf{r}, t, \hat{\mathbf{s}})$  we perform the integral over  $r_0$  in Eq. (3.14). The integrand vanishes for  $r_0 > r_{\max}$ , defined by

$$|\mathbf{r} - r_{\max} \hat{\mathbf{s}}| = ct - r_{\max} \iff r_{\max} = \frac{(ct)^2 - r^2}{2(ct - r\mu)}. \quad (3.23)$$

We thus find for the intensity the result ( $N \geq 1$ )

$$\begin{aligned} I_N(\mathbf{r}, t, \mu) &= \frac{1}{2\pi l^N (N-2)!} \int_0^{r_{\max}} dr_0 e^{-ct/l} \left[ (ct - r_0)^2 - (\mathbf{r} - r_0 \hat{\mathbf{s}})^2 \right]^{(N-3)/2} \\ &= \frac{e^{-ct/l}}{2\pi l^N (N-1)!} \frac{1}{ct - r\mu} \left( c^2 t^2 - r^2 \right)^{(N-1)/2} \Theta(ct - r). \end{aligned} \quad (3.24)$$

Summing over  $N$  and including the ballistic contribution (3.12) for  $N = 0$ , we find

$$\begin{aligned} I(\mathbf{r}, t, \hat{\mathbf{s}}) &= e^{-ct/l} \delta(\mathbf{r} - ct\hat{\mathbf{s}}) \\ &\quad + \frac{e^{-ct/l}}{2\pi l(ct - \mathbf{r} \cdot \hat{\mathbf{s}})} \exp\left( l^{-1} \sqrt{c^2 t^2 - r^2} \right) \Theta(ct - r). \end{aligned} \quad (3.25)$$

It is easy to check that this expression obeys the Boltzmann equation (3.5).

### 3.2.2 Four dimensions

In four dimensions the Fourier transformed intensity is given by

$$\bar{I}_N(k, \omega) = 2^{N+1} c^{-1} l \left( \sqrt{(1 - i\omega l/c)^2 + k^2 l^2} + 1 - i\omega l/c \right)^{-(N+1)}. \quad (3.26)$$

To invert the Fourier transform we use

$$\int \frac{d\mathbf{k}}{(2\pi)^4} e^{i\mathbf{k} \cdot \mathbf{r}} f(|\mathbf{k}|) = \frac{1}{4\pi^2 r} \int_0^\infty dk k^2 J_1(kr) f(k), \quad (3.27)$$

so that

$$\begin{aligned} \bar{I}_N(r, t) &= \frac{2^N e^{-ct/l}}{4\pi^3 i l^N r^{N+3}} \int_0^\infty dk J_1(kr) k^{-2N} \\ &\quad \times \int_{r/l-i\infty}^{r/l+i\infty} dz e^{zct/r} [\sqrt{x^2 + z^2} - z]^{N+1}. \end{aligned} \quad (3.28)$$

The integral over  $z$  yields  $i(N+1)(kr)^{N+1} J_{N+1}(kct) \Theta(t)$ . After integration over  $k$  we find, for  $N \geq 1$ ,

$$\bar{I}_N(r, t) = \frac{1}{\pi^2} e^{-ct/l} \frac{1}{ct l^3} \left( \frac{ct}{l} \right)^{N-3} \frac{N+1}{(N-1)!} \left[ 1 - \frac{r^2}{c^2 t^2} \right]^{N-1} \Theta(ct - r). \quad (3.29)$$

Again we sum over all  $N$ , and include the ballistic term  $N = 0$ , to find the total intensity

$$\bar{I}(r, t) = \frac{e^{-ct/l}}{2\pi^2 r^3} \delta(r - ct) + \frac{1}{(\pi l ct)^2} \left( 1 - \frac{r^2}{c^2 t^2} + \frac{2l}{ct} \right) \exp(-r^2/lct) \Theta(ct - r). \quad (3.30)$$

If both  $r$  and  $l$  are  $\ll ct$  we find the diffusion result (3.1), with diffusion constant  $D = \frac{1}{4}cl$ .

In the same way as we did for  $d = 2$  we can calculate the angular resolved intensity  $I(r, t, \mu)$  from Eqs. (3.14) and (3.29). We find ( $N \geq 1$ )

$$I(r, t, \mu) = \frac{\pi e^{-ct/l}}{2r^3} \delta(r - ct) \delta(\mu - 1^-) (1 - \mu^2)^{-1/2} + \frac{\Theta(ct - r)}{(\pi l ct)^2} \times e^{-r^2/lct} \frac{(1 - y^2)(1 + y^2 - 2\mu y) + 2(1 - \mu y)l/ct}{(1 + y^2 - 2\mu y)^2}, \quad (3.31)$$

where we have abbreviated  $y = r/ct$ . Again it can be checked that this expression obeys the Boltzmann equation (3.5).

### 3.2.3 Three dimensions

In three dimensions the Fourier transformed intensity reads

$$\bar{I}_N(k, \omega) = c^{-1} l \left[ \frac{1}{kl} \arctan \left( \frac{kl}{1 - i\omega l/c} \right) \right]^{N+1}. \quad (3.32)$$

The inverse can be evaluated analytically for  $N = 0$  and  $N = 1$ , but not for arbitrary  $N$ . An interpolation between the results (3.21) and (3.29) for  $d = 2$  and 4 suggests the approximation  $\bar{I}_N \propto [1 - r^2/(ct)^2]^{3N/4-1}$ . The coefficient 3/4 in the exponent ensures that the diffusion limit is obtained when  $r$  and  $l$  are both much smaller than  $ct$ . The solution (3.13) implies the normalization

$$\int dr \bar{I}_N(r, t) = \frac{1}{N!} \left( \frac{ct}{l} \right)^N e^{-ct/l}. \quad (3.33)$$

Taking this normalization into account, we find for  $N \geq 1$  the approximation

$$\bar{I}_N(r, t) \simeq \frac{e^{-ct/l}}{\pi l^3} \frac{\Gamma(\frac{3}{4}N + \frac{3}{2})}{\sqrt{\pi} N! \Gamma(\frac{3}{4}N)} \left( \frac{ct}{l} \right)^{N-3} \left( 1 - \frac{r^2}{c^2 t^2} \right)^{\frac{3}{4}N-1} \Theta(ct - r). \quad (3.34)$$

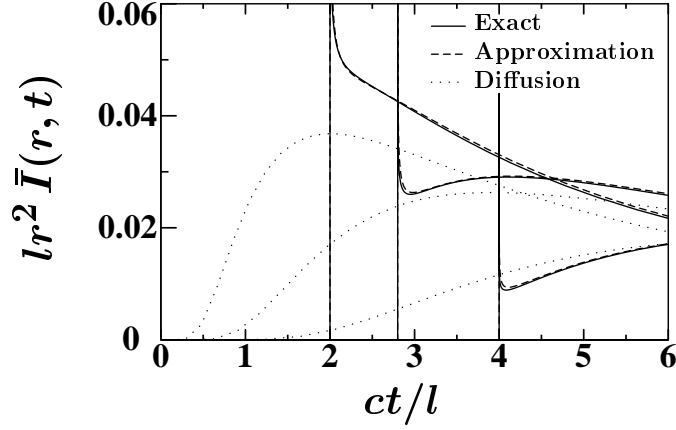


**Figure 3.2:** Angular average of the intensity as a function of time for  $r = 2.0l, 2.8l$  and  $4.0l$ , from left to right. The solid lines are the exact result (3.55), which is very close to the interpolation formula (3.35) (dashed lines). The dotted lines are the diffusion result (3.1). The intensity has a minimum for  $r$  greater than some  $r_c$ .

Because of its construction as an interpolation between two exact results, we expect Eq. (3.34) to be rather accurate.

The total intensity including the ballistic peak, becomes

$$\begin{aligned} \bar{I}(r, t) &\simeq \frac{e^{-ct/l}}{4\pi r^2} \delta(r - ct) + \Theta(ct - r) \\ &\quad \times \frac{(1 - r^2/c^2 t^2)^{1/8}}{(4\pi lct/3)^{3/2}} e^{-ct/l} G\left(\frac{ct}{l} \left[1 - \frac{r^2}{c^2 t^2}\right]^{3/4}\right), \end{aligned} \quad (3.35a)$$

$$G(x) = 8(3x)^{-3/2} \sum_{N=1}^{\infty} \frac{\Gamma(\frac{3}{4}N + \frac{3}{2})}{\Gamma(\frac{3}{4}N)} \frac{x^N}{N!}. \quad (3.35b)$$

In numerical calculations the function  $G(a)$  can be approximated within 1.6% by  $G(x) \simeq e^x \sqrt{1 + 2.026/x}$ . For  $l, r \ll ct$  the diffusion result (3.1) is regained, with  $D = cl/3$ .

To check the accuracy of this interpolation we have compared Eq. (3.35) with a numerical inversion of the Fourier transform (see appendix 3.A). In Fig. 3.2 we have plotted the intensity as a function of  $ct/l$  for three values of  $r/l$ . The dashed curves are the approximation (3.35). The difference is barely visible on this scale.

In Fig. 3.3 we compare our result with the literature. Perelman *et al.* [6] have improved upon the diffusion result by taking into account the finite

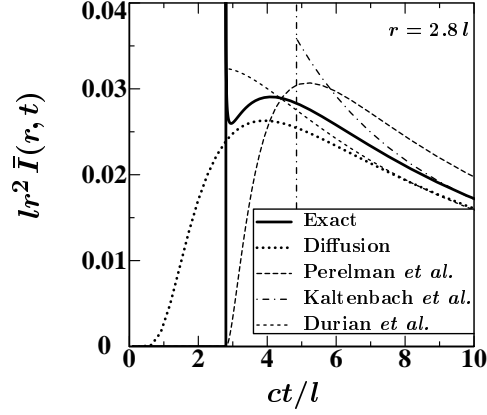


**Figure 3.3:** Average intensity as a function of time for  $r = 2.8l$ . The solid line is the exact result (3.55). The dotted line is the diffusion result (3.1), the short-dashed line is the result (3.36) from Perelman *et al.*, the dash-dotted line is the result (3.37) from Kaltenbach and Kaschke, and the long-dashed line is the result (3.38) from Durian and Rudnick.

velocity of light, such that the intensity vanishes for  $ct < r$ . Their result

$$\bar{I}(r, t) = \frac{\Gamma(3ct/4l + 5/2)}{\pi\sqrt{\pi}t^3 \Gamma(3ct/4l + 1)} \left(1 - \frac{r^2}{c^2t^2}\right)^{3ct/4l} \Theta(ct - r) \quad (3.36)$$

is shown short-dashed in Fig. (3.3). It does not contain the ballistic peak and overestimates the diffusion maximum. Another extension of the diffusion result is due to Kaltenbach and Kaschke [4],

$$\bar{I}(r, t) = \frac{3\sqrt{3}}{8\pi l^2} \exp(-ct/2l) \left[ 2\sqrt{3}\delta(ct - r\sqrt{3})l/r + \frac{\Theta(ct - r\sqrt{3})}{\sqrt{c^2t^2 - 3r^2}} I_1(\sqrt{c^2t^2 - 3r^2}/2l) \right], \quad (3.37)$$

and is also plotted in Fig. 3.3 (dash-dotted). The difference with the exact solution is clear. Recently also Durian and Rudnick [8] gave an extension to the diffusion result

$$\bar{I}(r, t) = \frac{e^{-3ct/2l}}{4\pi l^2} \left\{ \frac{l^2}{r} \delta'(ct - r) + \left( \frac{3l}{2ct} + \frac{9}{8} \right) \delta(ct - r) + \frac{9}{4l} \times \left[ I_1(3\sqrt{c^2t^2 - r^2}/2) + \frac{ct I_2(3\sqrt{c^2t^2 - r^2}/2)}{\sqrt{c^2t^2 - r^2}} \right] \Theta(ct - r) \right\}, \quad (3.38)$$

which is also plotted in Fig. 3.3 (long-dashed). Again, the difference with the exact solution is clear. Furthermore this expression introduces the derivative of the delta function, which is not positive everywhere.

### 3.2.4 Ballistic peak

The main qualitative new feature of our result is the tail of the ballistic peak at  $t = r/c$  (see Fig. 3.2). The ballistic peak itself consists of a delta function  $\bar{I}_0 \sim \delta(t - r/c)$  due to unscattered radiation. The tail towards larger  $t$  is due to radiation which has undergone a single forward scattering event. The shape of the tail is given by  $\bar{I}_1$ , which can be computed analytically for any dimension. The single-scattering intensity is given by Eq. (3.13) with  $N = 1$ . Since the integration is over a single delta function, we readily find

$$I_1(r, t, \mu) = \frac{e^{-ct/l}}{l\Omega_d} \frac{1}{ct - r\mu} \frac{1}{(ct - r_{\max})^{d-2}}, \quad (3.39)$$

where  $r_{\max}$  is given in Eq. (3.23). Integration over  $\mu$  with the weight function  $\rho_d(\mu)$  given in Eq. (3.6), yields

$$\bar{I}_1(r, t) = \frac{2^{d-2} e^{-ct/l}}{\Omega_d l (ct)^{2d-4}} (c^2 t^2 - r^2)^{(d-3)/2} {}_2F_1\left(\frac{1}{2}, d-2; \frac{1}{2}; \frac{r^2}{c^2 t^2}\right). \quad (3.40)$$

For dimensions greater than 3 the hypergeometric function  ${}_2F_1$  has a singularity for  $r \rightarrow ct$  which is canceled by the factor  $(c^2 t^2 - r^2)^{(d-3)/2}$ . The term  $\bar{I}_1$  therefore is finite at  $r = ct$  and contributes no tail to the ballistic peak for  $d > 3$ . In contrast, for  $d \leq 3$ , the term  $\bar{I}_1$  has an integrable singularity at  $r = ct$ , which adds a tail to the ballistic peak. The singularity is logarithmic in three dimensions,

$$\bar{I}_1(r, t) = \frac{e^{-ct/l}}{4\pi l c t r} \ln \frac{ct + r}{ct - r}, \quad d = 3, \quad (3.41)$$

and algebraic in two dimensions

$$\bar{I}_1(r, t) = \frac{e^{-ct/l}}{2\pi l} (c^2 t^2 - r^2)^{-1/2}, \quad d = 2. \quad (3.42)$$

In one dimension the ballistic peak has no tail, but is enhanced itself by a factor  $e^{ct/2l}$  [cf. Eq. (3.2)].

The tail of the ballistic peak in 2 and in 3 dimensions leads to a minimum in the intensity as function of time, provided  $r$  is large enough. For

this minimum to occur we need  $r > [(11 + 5\sqrt{5})/2]^{1/2} l \simeq 3.330l$  for  $d = 2$  and  $r \gtrsim 2.4l$  for  $d = 3$ . Note that also for anisotropic scattering the tail exists, but it will have different properties, depending on the phase functions.

### 3.3 Decay length and dispersion relation

We have calculated the time-dependence of the intensity for an infinite geometry. These have the remarkable property that they obey diffusion-like equations, which are equations for the angle-averaged intensity only, and therefore have a degree of freedom less than the Boltzmann equation (3.3). This result is interesting in itself. But it might also give an improvement of the diffusion equation which can be used in more general geometries than the unbounded geometry considered here, without need to take the angular degree of freedom into account. This can be useful in numerical calculations.

We need first to consider the decay length. Far from sources and boundaries the light intensity decays exponentially with decay length  $\kappa$ . In a spherical geometry we can write  $\bar{I} \propto e^{-\kappa r}/r$  (3 dimensions), while in a slab geometry  $\bar{I} \propto e^{-\kappa z}$ . This decay length depends on the mean free path, on the absorption length and for a time-dependent source,  $S \sim e^{-i\omega t}$ , also on the frequency  $\omega$ . Based on the diffusion equation different expressions have been presented for  $\kappa$  [8, 10, 15, 16]. Here we will calculate it exactly.

We consider again only isotropic scattering. We Fourier transform the Boltzmann equation (3.3) with respect to time:

$$(1 + \gamma)I(\mathbf{r}, \gamma, \hat{\mathbf{s}}) + l\hat{\mathbf{s}} \cdot \nabla I(\mathbf{r}, \gamma, \hat{\mathbf{s}}) = \bar{I}(\mathbf{r}, \gamma) + c^{-1}lS(\mathbf{r}, \omega), \quad (3.43)$$

where we defined

$$\gamma = l/l_a - i\omega l/c. \quad (3.44)$$

Note that we need to take the absorption length explicitly into account here, in contrast to section 3.1. When the source is distant, we can start with neglecting its contribution and search for a self-consistent solution. This can be most easily done in a slab geometry where the intensity only depends on  $z$ ,  $\mu \equiv \hat{\mathbf{s}} \cdot \hat{\mathbf{z}}$  and on  $\gamma$ . We look for a solution of the form:  $I \propto e^{-\kappa z}$  and find

$$I(z, \gamma, \mu) = \frac{\bar{I}(z, \gamma)}{1 + \gamma - \mu\kappa l}. \quad (3.45)$$

Integrating over all angles  $\mu$ , taking the density  $\rho_d(\mu)$  from Eq. (3.6) into account, we find

$$1 = \frac{1}{1+\gamma} f_d[\kappa l/(1+\gamma)], \quad (3.46a)$$

$$f_d(x) = \int_0^1 d\mu \rho_d(\mu) \frac{2}{1-x^2\mu^2} = {}_2F_1\left(\frac{1}{2}, 1; \frac{1}{2}d; x^2\right). \quad (3.46b)$$

The hypergeometric function can be expressed in terms of elementary functions for any integer dimension. When  $f_d$  can be inverted one can find  $\kappa l$  as function of  $\gamma$ . Otherwise one has only an implicit equation. The result is

$$\kappa^2 l^2 = \gamma(1+\gamma), \quad d=1, \quad (3.47a)$$

$$\kappa^2 l^2 = \gamma(2+\gamma), \quad d=2, \quad (3.47b)$$

$$\frac{\kappa l}{\tanh \kappa l} = 1 + \gamma, \quad d=3, \quad (3.47c)$$

$$\kappa^2 l^2 = \begin{cases} 4\gamma, & d=4, \gamma < 1, \\ (1+\gamma)^2, & d=4, \gamma > 1. \end{cases} \quad (3.47d)$$

The relation for  $d=3$  has already been found for pure absorption ( $\omega = 0$ ) [16].

We can interpret the relation between decay length and frequency as a dispersion relation. From this dispersion relation one can pose a corresponding equation for the angular average of the intensity itself, of which the diffusion equation is the small frequency and small absorption limit. Hence from the Boltzmann equation, which is an equation for the angle-resolved intensity, we can now find an equation for the angular average itself.

To find an equation in the space-time domain, we rewrite the dispersion relations (3.47) using the substitutions

$$\kappa^2 \rightarrow \nabla^2; \quad \gamma \rightarrow l/l_a + c^{-1}l\partial/\partial t. \quad (3.48)$$

This leads to the following equations for  $d=1, 2$  and  $4$

$$l^2 \nabla^2 \bar{I} = \left( \frac{l^2}{l_a^2} + \frac{l}{l_a} + \frac{l^2}{c^2} \frac{\partial^2}{\partial t^2} + \frac{l}{c} \frac{\partial}{\partial t} \right) \bar{I} + \text{Source}, \quad d=1, \quad (3.49a)$$

$$l^2 \nabla^2 \bar{I} = \left( \frac{l^2}{l_a^2} + \frac{2l}{l_a} + \frac{l^2}{c^2} \frac{\partial^2}{\partial t^2} + \frac{2l}{c} \frac{\partial}{\partial t} \right) \bar{I} + \text{Source}, \quad d=2, \quad (3.49b)$$

$$l^2 \nabla^2 \bar{I} = \left( \frac{4l}{l_a} + \frac{4l}{c} \frac{\partial}{\partial t} \right) \bar{I} + \text{Source}, \quad d=4. \quad (3.49c)$$

Now we can check whether the time-resolved solutions we found indeed obey these equations. For 1 dimension, we know that the diffusion ansatz (1.14) is exact. When taking all derivatives with respect to time into account while deriving the diffusion equation, we find again Eq. (3.49a). Hence this equation is exact for one dimension. Indeed the solution given by Hemmer [11] [Eq. (3.2)] obeys the equation above. For 2 dimensions, the time-resolved intensity is given by  $\bar{I}(r, t) = \bar{I}_0(r, t) + \bar{I}_s(r, t)$ . The scattered part  $\bar{I}_s(r, t)$  obeys equation (3.49b) with the ballistic part  $\bar{I}_0$  as source. Hence for arbitrary sources in an infinite medium, Eq. (3.49b) can be used, taking as source term the distribution of the unscattered light. For  $d = 4$  we find that the time-resolved solution obeys the equation above (which is the normal diffusion equation), as long as  $t > r/c$ .

The case of 3 dimensions is more difficult, due to the more complex dispersion relation. To find an approximate diffusion-like equation, that can be used for instance in numerical simulations, one can do two things: One can expand  $\gamma$  as function of  $\kappa^2 l^2$  or one can expand  $\kappa^2 l^2$  as a function of  $\gamma$ . Using the substitutions (3.48) one then finds either

$$\left(\frac{l}{l_a} + \frac{l}{c} \frac{\partial}{\partial t}\right) \bar{I} = \frac{1}{3} l^2 \nabla^2 \bar{I} - \frac{1}{45} (l^2 \nabla^2)^2 \bar{I} + \dots, \quad (3.50a)$$

or

$$l^2 \nabla^2 \bar{I} = 3 \left(\frac{l}{l_a} + \frac{l}{c} \frac{\partial}{\partial t}\right) \bar{I} + \frac{3}{5} \left(\frac{l}{l_a} + \frac{l}{c} \frac{\partial}{\partial t}\right)^2 \bar{I} + \dots. \quad (3.50b)$$

The latter equation, without the higher order terms, has already been given in Ref. [15]. A disadvantage of taking only a finite number of terms into account, is that the position of the ballistic peak is predicted incorrectly.

### 3.4 Conclusion

We have presented exact solutions to the time-dependent Boltzmann equation (or equation of radiative transfer). The method used is based on a summation over the paths, that brings a particle from source to some position  $r$ , after  $N$  scattering events. This method has been used before, both in connection with the Boltzmann equation [12] and in the theory of random walks [13, 14, 17]. However as far as we know the exact solution presented here was not known. We have shown that, at least in the unbounded geometry considered here, the exact solution obeys a diffusion-like equation which does not have an angular degree of freedom, and which might therefore be easier to use in other geometries.

An important feature of the exact solution is the tail to the ballistic peak, which has not been noticed in the literature, either in analytical studies [4, 6, 8], in experimental results [18], or in numerical simulations based on the Monte Carlo method [14, 16, 19] (the tail is barely noticeable in the numerical simulations of Ref. [8]). The tail requires a continuum description; it is not present in lattice models [14] for a random walk. Experimentally the observation of the tail is challenging, since the time resolution needed is below the scattering mean free time.

### 3.A Numerical inversion of the Fourier transform in 3 dimensions

In Eq. (3.32) we gave an analytical expression for  $\bar{I}_N(k, \omega)$  in 3 dimensions. To find the real space intensity  $\bar{I}(r, t)$  we have to sum over all the number  $N$  of scattering events and invert the Fourier Transform. In this Appendix we show how this can be done numerically. This is not straightforward, because of the singularity at  $r = ct$ . For notational simplicity we take  $l = c = 1$  in what follows.

The sum of the contributions for  $N \geq 4$  is has no singularity and is smooth at  $t = r$ . It is given by

$$\sum_{N=4}^{\infty} \bar{I}_N(r, t) = \frac{1}{4\pi^3 r} \int_0^{\infty} dk k^{-3} \sin(kr) \int_{-\infty}^{\infty} d\omega e^{-i\omega t} \times \arctan^5\left(\frac{k}{1-i\omega}\right) \left[ k - \arctan\left(\frac{k}{1-i\omega}\right) \right]^{-1}. \quad (3.51)$$

The integral over  $\omega$  can be done by contour integration, closing the contour in the lower half of the complex plane. The contribution from the pole  $k = \arctan[k/(1-i\omega)]$  is given by

$$\bar{I}_{\text{pole}}(k, t) = 2\pi \exp(tk/\tan k - t) \frac{k^2}{\sin^2 k} \Theta(\pi/2 - k). \quad (3.52)$$

To calculate the contribution from the branch cut between  $\omega = -i - k$  and  $\omega = -i + k$  we parametrize  $\omega = -i + \xi k$ . We find

$$\bar{I}_{\text{cut}}(k, t) = \frac{\pi e^{-t}}{4k^2} \int_{-1}^1 d\xi \left[ \cos(kt\xi) \frac{4k^2(5\Lambda^4 - 10\Lambda^2\pi^2 + \pi^4) + (\Lambda^2 + \pi^2)^2(3\Lambda^2 - \pi^2)}{(4k^2 - \Lambda^2 - \pi^2)^2 + 16k^2\Lambda^2} \right] \quad (3.53)$$

$$2 \sin(kt\xi) \Lambda \frac{2k^2(3\Lambda^2 - \pi^2)(\Lambda^2 - 3\pi^2) + (\Lambda^2 - \pi^2)(\Lambda^2 + \pi^2)^2}{(4k^2 - \Lambda^2 - \pi^2)^2 + 16k^2\Lambda^2} \Big],$$

where we have abbreviated  $\Lambda(\xi) = 2 \operatorname{artanh} \xi$ . Next we calculate the contributions for  $N \leq 3$ . The ballistic term  $\bar{I}_0$  is already given in Eq. (3.12) and the single scattering term  $\bar{I}_1$  in Eq. (3.41). For  $N = 2, 3$  we use the same parametrization as above, but interchange the integrals over  $k$  and  $\xi$ . We find

$$\bar{I}_2(r, t) = \frac{e^{-t}}{16\pi r} \int_{r/t}^1 d\xi \left( 3\Lambda^2 - \pi^2 \right), \quad (3.54a)$$

$$\bar{I}_3(r, t) = \frac{e^{-t}}{8\pi r} \int_{r/t}^1 d\xi \Lambda \left( \Lambda^2 - \pi^2 \right) (t\xi - r). \quad (3.54b)$$

The total intensity is then given by

$$\bar{I}(r, t) = \sum_{N=0}^3 \bar{I}_N(r, t) + \frac{1}{4\pi^3 r} \int_0^\infty dk k \sin(kr) [\bar{I}_{\text{pole}}(k, t) + \bar{I}_{\text{cut}}(k, t)]. \quad (3.55)$$

These integrals can be calculated numerically without problems.

### 3.B Anisotropic scattering

Up till now, we have only considered the case of isotropic scattering, where the phase function is constant. In this appendix we will summarize some results from literature about the time-dependence of the intensity when the scattering is *not* isotropic, which can serve as a background for the reader. We will extend the results to the calculation of the decay length. For anisotropic scattering the phase-function introduces many extra degrees of freedom, which makes it much more difficult to find exact expressions.

Parts of the theory presented here are a result from the study of flexible polymer chains. A polymer consists in general of a large molecule consisting of a chain of repeating units. These units have a more or less fixed length. At the bonds between two units the angle between them can vary. The structure of such a polymer can be seen as a random walk with a fixed step length. In this sense it is similar to a photon path in a disordered medium. Hence the calculation of the intensity  $\bar{I}(r, t)$  is similar to the calculation of the distance between begin and end point of the polymer, given the number of units, or the total chain length. We refer to Refs. [20, 21] for a review about this problem in polymer theory, and to Refs. [22, 23] for recent developments.

### 3.B.1 Formal exact solution

The Boltzmann equation for anisotropic scattering is given by

$$\frac{1}{c} \frac{\partial I(\mathbf{r}, t, \hat{\mathbf{s}})}{\partial t} + \hat{\mathbf{s}} \cdot \nabla I(\mathbf{r}, t, \hat{\mathbf{s}}) = l^{-1} Q(\mathbf{r}, t, \hat{\mathbf{s}}) - (l^{-1} + l_a^{-1}) I(\mathbf{r}, t, \hat{\mathbf{s}}), \quad (3.56a)$$

$$Q(\mathbf{r}, t, \hat{\mathbf{s}}) = \int \frac{d\hat{\mathbf{s}}'}{\Omega_d} F(\hat{\mathbf{s}} \cdot \hat{\mathbf{s}}') I(\mathbf{r}, t, \hat{\mathbf{s}}'). \quad (3.56b)$$

The quantity  $Q$  consists of all the light scattered from directions  $\hat{\mathbf{s}}'$  to  $\hat{\mathbf{s}}$ . This scattering is no longer isotropic but given by the phase function  $F(\hat{\mathbf{s}} \cdot \hat{\mathbf{s}}')$ . The first moment of the normalized phase function is a measure of the anisotropy

$$g = \int \frac{d\hat{\mathbf{s}}'}{\Omega_d} F(\hat{\mathbf{s}} \cdot \hat{\mathbf{s}}') \hat{\mathbf{s}} \cdot \hat{\mathbf{s}}'. \quad (3.57)$$

The transport mean free path is given by  $l_{\text{tr}} = l/(1 - g)$ . It is this length that determines the diffusion constant  $D = cl_{\text{tr}}/d$  [10].

Jernigan [24] has described a method to find systematic approximations for the intensity, which we will repeat here in short (see also Ref. [20]). We consider only  $d = 3$ . Again we assume spherical geometry such that the intensity depends only on  $r$ ,  $t$ , and  $\mu$ . We can then write the phase function as

$$F(\mu, \mu') = \sum_m g_m P_m(\mu) P_m(\mu'), \quad (3.58)$$

where  $P_m(\mu)$  are the Legendre Polynomials. From the normalization we have  $g_0 = 1$ . The anisotropy factor is given by  $g = g_1/3$ .

Consider now the moments of the intensity [25]

$$u_{m,q} = \langle P_m(\mu)(r/l_{\text{tr}})^{2q-m} \rangle \equiv \frac{1}{2} \int_{-1}^1 d\mu \int_0^{ct} dr r^2 I(r, t, \mu) P_m(\mu) (r/l_{\text{tr}})^{2q-m}. \quad (3.59)$$

Instead of Fourier-transforming we now Laplace transform with respect to time:

$$I(r, p, \mu) = \int_0^\infty dt e^{-pt} I(r, t, \mu). \quad (3.60)$$

After this Laplace transform we arrive at the following equation for the moments

$$[pl_{\text{tr}}/c + \frac{1 - a_m}{1 - g}] u_{m,q} = \frac{m(2q+1)}{2m+1} u_{m-1,q-1} + \frac{2(q-m)(m+1)}{2m+1} u_{m+1,q}. \quad (3.61)$$

Due to normalization one has  $u_{0,0} = 1/p$ . This equation generates the Laplace transforms of various moments. Furthermore the inverse Laplace transform is easily performed since all expression will give rational functions in  $p$  with the roots of the denominator given. Hence, for any phase-function one can find exact expressions for the moments  $u_{m,q}(t)$ . For instance, we have independent of dimension and of phase function:

$$\langle r^2 \rangle = 2ct l_{\text{tr}} - 2l_{\text{tr}}^2(1 - e^{-ct/l_{\text{tr}}}); \quad \langle \mu r \rangle = l_{\text{tr}}(1 - e^{-ct/l_{\text{tr}}}). \quad (3.62)$$

Next we define the auxiliary variable

$$\rho^2 = 3r^2/2u_{0,1}(t), \quad (3.63)$$

which depends both on  $r$  and on  $t$ , and the parameters

$$h_{2n}(t) = \langle \rho^{-1} H_{2n+1}(\rho) \rangle / 2^{2n+2} (2n+1)!. \quad (3.64)$$

The  $H$  are the Hermite polynomials. The averages defined in Eq. (3.64) can be easily calculated using the known moments. The first two are given by  $h_0 = \frac{1}{2}$  and  $h_2 = 0$ . The intensity is now given by [20]

$$\bar{I}(r, t) = \left( \frac{3}{2\pi u_{0,1}(t)} \right)^{3/2} \rho^{-1} e^{-\rho^2} \sum_{n=0}^{\infty} h_{2n}(t) H_{2n+1}(\rho). \quad (3.65)$$

Note that, since for  $n > 1$  and  $t \rightarrow \infty$  the parameters  $h_{2n}(t)$  vanish, one regains the diffusion result (3.1).

Equation (3.65) is an exact expression for all possible phase functions. Although each step in the calculation is straightforward, the final expression becomes more complicated with increasing  $n$ . Hence this approximation is limited in its use. Since it is an approximation which gives systematic deviations from the diffusion result, one can expect it to be accurate for large  $r$  and  $t$ . The intensity around  $r = ct$  can not be calculated accurately with Eq. (3.65).

### 3.B.2 Kratky-Porod theory

As mentioned before, the intensity for anisotropic scattering depends on the phase function, and hence on all the parameters  $g_m$ . To reduce the number of free parameters, one can consider the limit of completely anisotropic scattering, where  $g \rightarrow 1$ . The important length scale is then  $l_{\text{tr}} = l/(1-g)$ , while  $l$  itself vanishes. In this limit, a single scattering changes

the propagation direction  $\hat{\mathbf{s}}$  only slightly. Hence many scattering events are necessary to change  $\hat{\mathbf{s}}$  appreciable. This means that  $\hat{\mathbf{s}}$  performs a random walk over the surface of the sphere. This random walk can be described by a diffusion equation on the unit sphere. The Boltzmann equation then assumes the form [7, 21, 26]

$$(d-1)l_{\text{tr}} \left[ \frac{\partial}{c\partial t} + \mu \frac{\partial}{\partial r} + \frac{1-\mu^2}{r} \frac{\partial}{\partial \mu} \right] I(r, t, \mu) = \nabla_{\mu}^2 I(r, t, \mu). \quad (3.66)$$

Here  $\nabla_{\mu}^2$  is the Laplacian on a unit-sphere (for  $d = 3$  this is the Legendre operator), and describes the diffusion of  $\mu$ . The general form of  $\nabla_{\mu}^2$  is

$$\nabla_{\mu}^2 = (1-\mu^2) \frac{\partial^2}{\partial \mu^2} - (d-1) \frac{\partial}{\partial \mu}. \quad (3.67)$$

In the study of polymers this limit is described by the Kratky-Porod theory [20]. One can find this limit also by using a phase-function with  $g_m = (2m+1)g^{m(m+1)/2}$  in 3 dimensions. This corresponds to a phase function  $F(1, \mu) \simeq \frac{1}{2} \exp[(\mu-1)/(1-g)]/(1-g)$  for  $g \sim 1$ , which is almost Gaussian in the scattering angle  $\theta$ . Several exact results have been found, mainly giving moments.

Equation (3.66) for finding the intensity is equivalent to a path integral [7, 21] formalism. In this formalism one makes a summation over all possible paths  $\mathbf{r}'(t')$ , as in section 3.1, with a constant velocity:  $|\mathbf{dr}'/dt'| = c$ . The weight factor of each path depends on its curvature, given by the inverse of the radius of curvature,  $\kappa(t) = |\mathbf{d}^2\mathbf{r}'/dt'^2|/c^2$ :

$$\bar{I}(\mathbf{r}, t) \propto \int \mathcal{D}\mathbf{r}'(t') \delta[\mathbf{r}'(t) - \mathbf{r}] \exp[-\frac{1}{2}cl_{\text{tr}} \int_0^t \kappa^2(t'') dt'']. \quad (3.68)$$

Let us discretize the path. Its total length is  $ct$ , and contains  $N$  straight parts, of length  $l = ct/N$ . The positions of scattering are given by  $\mathbf{r}_i$ . Define  $\mathbf{R}_i = \mathbf{r}_i - \mathbf{r}_{i-1}$ . For the velocity we then have  $\mathbf{v}_i = c\mathbf{R}_i/l \equiv c\hat{\mathbf{s}}_i$ , where  $\hat{\mathbf{s}}_i$  are unit vectors. This leads to the expression in Fourier space

$$\bar{I}(\mathbf{k}, t) \propto \left[ \prod_{i=1}^N \int \frac{d\mathbf{s}_i}{\Omega_d} \right] \exp\left[ \frac{Nl_{\text{tr}}}{ct} \sum_{i=2}^N \hat{\mathbf{s}}_i \cdot \hat{\mathbf{s}}_{i-1} + ict\mathbf{k} \cdot \frac{1}{N} \sum_{i=1}^N \mathbf{s}_i \right]. \quad (3.69)$$

The normalization is given by  $\bar{I}(\mathbf{k} = 0, t) = 1$ . This path integral is similar to the partition function of a 1-dimensional classical Heisenberg model in an (imaginary) magnetic field. The spins are then given by the  $\hat{\mathbf{s}}_i$ . A possible simplification might be found by demanding  $\hat{\mathbf{s}}_i \cdot \hat{\mathbf{s}}_{i-1} = g$ .

For the path integral (3.68) or the differential equation (3.66) Daniels [27] gave an exact solution in the form of a continued fraction in terms of  $k$  and the Laplace variable  $p$  (here given for  $d = 3$ ):

$$\bar{I}(k, p) = \frac{1}{p + \frac{1^2(1 \cdot 3)^{-1}k^2c^2}{p + (1 \cdot 2)c/2l_{tr} + \frac{2^2(3 \cdot 5)^{-1}k^2c^2}{p + (2 \cdot 3)c/2l_{tr} + \frac{3^2(5 \cdot 7)^{-1}k^2c^2}{p + (3 \cdot 4)c/2l_{tr} + \dots}}}, \quad (3.70)$$

Amic *et al.* [26] have found some exact results for the time-independent semi-infinite medium. Many other authors have given approximations for the intensity (or the equivalent quantity in polymer physics) [7, 20, 21, 23].

### 3.B.3 Decay length

Also for anisotropic scattering we can calculate the decay lengths. We use again the slab geometry, where the intensity is a function of  $z$ ,  $\mu$  and the parameter  $\gamma$ . Here we need a more general approach than that which we took for isotropic scattering. This more general approach leads to the same results as before in the case of isotropic scattering, but is more tedious. We expand the phase function and the intensity in ultraspherical polynomials, defined as polynomials of degree  $m$ , and orthogonal with respect to  $\rho_d(\mu)$ :

$$\int_{-1}^1 d\mu \rho_d(\mu) P_m(\mu) P_n(\mu) = S_m \delta_{mn}. \quad (3.71)$$

For three dimensions, the  $P_m$  are the Legendre polynomials with  $S_m = (2m + 1)^{-1}$ , while for two dimensions the  $P_m$  are the Chebyshev polynomials, with  $S_0 = 1$  and  $S_n = \frac{1}{2}$  for  $n > 1$ . Let us write

$$I(z, \mu) = \sum_m a_m(z) P_m(\mu), \quad (3.72)$$

$$A_{mn} = \int d\mu P_m(\mu) P_n(\mu) \mu \rho_d(\mu). \quad (3.73)$$

The matrix  $\mathbf{A}$  has only non-zero components when  $m = n \pm 1$ . Using these expression in the Boltzmann equation we find

$$\frac{A_{mn}}{S_m(1 + \gamma) - S_m^2 g_m} l \partial_z a_n(z) = a_m. \quad (3.74)$$

The smallest decay length in the system corresponds to the largest eigenvalue of the matrix on the left-hand-side. We note that the spectrum of this matrix is symmetric around 0.

For any dimension and phase function we can analytically find the small  $\gamma$  expansion of  $\kappa l$ . The first term is given by the diffusion result

$$\kappa^2 l^2 = d(1 - g)\gamma. \quad (3.75)$$

Every next term needs an extra term in the expansion of the phase function. It is therefore possible to find the term  $\propto \gamma^2$ , which will depend, apart from  $\kappa l$  and  $d$ , only on  $g_1$  and  $g_2$ . We present a single example for  $d = 2$  and the non-trivial phase function  $F(\mu) = 1 + 2g\mu$ . The decay length  $\kappa$  is again given in terms of  $l$ ,  $\gamma$  and  $g = g_1/2$  as

$$\kappa l = (1 + \gamma)\sqrt{1 - z^2}, \quad (3.76a)$$

$$z = \frac{-\gamma(1 + \gamma - 2g) + \sqrt{(1 + \gamma)^2(2 + \gamma)^2 + 4g\gamma^2(g - \gamma - 1)}}{2(1 + \gamma)^2}, \quad (3.76b)$$

which gives Eq. (3.47b) for  $g = 0$ .

The numerical calculation of the decay length is straightforward (the largest eigenvalue of a band matrix can be found numerically in a time proportional to the linear dimension of the matrix). Hence for almost any phase function, even for  $g$  close to 1, one can compute  $\kappa$  efficiently.



## Bibliography

- [1] L. C. Lee and J. R. Jokipii, *Astrophys. J.* **201**, 532 (1975).
- [2] A. Ishimaru, *J. Opt. Soc. Am.* **68**, 1045 (1978).
- [3] H. S. Carslaw and J. C. Jaeger, *Conduction of Heat in Solids* (Clarendon, Oxford, 1959).
- [4] J. Kaltenbach and M. Kaschke, in *Medical Optical Tomography: Functional Imaging and Monitoring*, edited by G. Müller (SPIE, Washington DC, 1993).
- [5] L. T. Perelman, J. Wu, I. Itzkan, and M. S. Feld, *Phys. Rev. Lett.* **71**, 1341 (1994).
- [6] L. T. Perelman, J. Wu, Y. Wang, I. Itzkan, R. R. Dasari, and M. S. Feld, *Phys. Rev. B* **51**, 6134 (1995).
- [7] A. Ya. Polishchuk, M. Zevallos, F. Liu, and R. R. Alfano, *Phys. Rev. E* **53**, 5523 (1996).
- [8] D. J. Durian and J. Rudnick, *J. Opt. Soc. Am. A* **14**, 235 (1997); **14**, 940 (1997).
- [9] S. Chandrasekhar, *Radiative Transfer* (Dover, New York, 1960).
- [10] A. Ishimaru, *Wave Propagation and Scattering in Random Media* (Academic, New York, 1978).
- [11] P. Chr. Hemmer, *Physica* **27**, 79 (1961).
- [12] J. M. Ziman, *Electrons and Phonons* (Clarendon, Oxford, 1960).
- [13] G. H. Weiss and R. J. Rubin, in *Advances in Chemical Physics*, edited by I. Prigogine and S. A. Rice, Vol. LII (Wiley, New York, 1983).
- [14] A. H. Gandjbakhche, G. H. Weiss, R. F. Bonner, and R. Nossal, *Phys. Rev. E* **48** 810 (1993).
- [15] A. Ya. Polishchuk, S. Gutman, M. Lax, and R. R. Alfano, *J. Opt. Soc. Am. A* **14**, 230 (1997).
- [16] S. L. Jacques, L. Wang, and A. M. Hielscher, in *Optical-Thermal Response of Laser-Irradiated Tissue*, edited by A. J. Welch and M. J. C. van Gemert (Plenum, New York, 1995).

- [17] G. H. Weiss, A. H. Gandjbakhche, and J. Masoliver. *J. Mod. Opt.* **42**, 1567 (1995).
- [18] K. M. Yoo, F. Liu, and R. R. Alfano, *Phys. Rev. Lett.* **64**, 2647 (1990); **65**, 2210 (1990).
- [19] Y. Yamada, Y. Hasegawa, and Y. Yamashita, *Appl. Opt.* **32**, 4808 (1993).
- [20] P. J. Flory, *Statistical Mechanics of Chain Molecules* (Wiley, New York, 1969).
- [21] K. F. Freed, in *Advances in Chemical Physics*, edited by I. Prigogine, and S. A. Rice, Vol. XXII (Wiley, New York, 1972).
- [22] J. Wilhelm and E. Frey, *Phys. Rev. Lett.* **77**, 2581 (1996).
- [23] D. Thirumalai and B.-Y. Ha, preprint (cond-mat/9705200).
- [24] R. L. Jernigan, Ph. D. Thesis (Stanford University, 1967); see also appendix E of Ref. [20].
- [25] J.J. Hermans and R. Ullman, *Physica* **18**, 951 (1952).
- [26] E. Amic, J. M. Luck, and Th. M. Nieuwenhuizen, *J. Phys. A* **29**, 4915 (1996).
- [27] H. E. Daniels, *Proc. Roy. Soc. Edinburgh* **63A**, 290 (1952).

## 4 Influence of boundaries on the imaging of objects in turbid media

For imaging the interior of a turbid medium several methods have been developed in the recent past. The imaging consists of two parts. First one has to define a geometry and a measurement. Next one has to reconstruct the interior of the medium with the data. For detection one has at ones disposal apart from continuous wave measurements also the time-resolved measurements and the photon density wave approach. For reconstruction one uses, amongst others, back-projection and algebraic reconstruction techniques. Both detection and reconstruction depend on the geometry of the medium, the positions of sources and detectors, and the character of the objects one wants to image.

Two factors are of experimental importance in detecting the object. The first is the accuracy of the measurements. In practice this depends on the strength of the signal: the larger the signal, the less the relative noise and therefore the larger the accuracy. The second is the sensitivity to inhomogeneities. This depends on the measurement method as well as on the position of the object with respect to the source and detector. For a given accuracy one can ask the question what kind of objects can still be detected and possibly reconstructed. Which measurement method is the best? Furthermore, since the boundaries are of influence on the measured signal, one can ask which kind of boundary is best for imaging.

To address these questions we will start with the calculation of the influence of an object on the measured signal. We are mainly interested in the order of magnitude of the effect, such that we can give a reasonable estimate of the accuracy needed to detect an object. We will generalize the methods given by Den Outer *et al.* [1] and Zhu *et al.* [2] to be able to split the effect of an object on a measurement into a geometry dependent part — including the boundaries, sources and detectors — and a pure object dependent part. Both parts depend furthermore on the optical parameters of the medium and possibly on the frequency of the amplitude modulation of the source. Time-dependent sources are related to the latter by a Fourier transform.

The treatment will lead to general formulas to estimate the effect of objects on measurements, for general geometries. We can then include the

influence of the boundaries of the medium, and compare these to measurements in an infinite medium. We will consider basically two kinds of boundaries. The first are those which reflect the major part of the light. This reflection can be due, for instance, to a mirror. The second boundary to be considered is that consisting of a transparent medium surrounding the turbid medium, with possible refractive index mismatch. When this mismatch vanishes, none of the light leaving the turbid medium will be reflected back and the boundary is equivalent to a completely black boundary.

To discuss the effects of boundaries we will consider the two basic classes of measurements, those in reflection and those in transmission. In the first case we will consider a semi-infinite medium, in the second a slab geometry. In both cases the source and detector are located at the surface. We argue that our results are qualitatively the same for other possibly more complex geometries.

The outline of this study is as follows. In section 4.1 we will calculate the influence of an object on a measurement. We will find a general formula which can be used in any geometry. The object dependent parameters are calculated for objects which have slightly different optical parameters compared to those of the background, as well as for a completely black object. We will calculate the sensitivity to both absorption and scattering. In section 4.2 we will address the question of optimal boundaries. To do this we need to describe the effects of boundaries and sources on the propagation of light. Subsequently we can estimate the difference in sensitivities between the different kinds of boundaries. The theoretical results are compared with experiments. Finally, in section 4.3 we present our conclusions.

## 4.1 Perturbation theory for general objects

Before we consider the influence of different boundaries, we first need to consider the sensitivity of a measurement for given perturbation of the absorption and scattering parameters. Hence we need to determine what the difference in a measurement is between a homogeneous medium and a medium with some perturbation. The precise quantity one measures depends on a lot of factors concerning the detector, amongst them being its shape, surface area and acceptance angle. In general however the measurement itself is proportional to the photon density at the detector position [3]. The photon density  $\Phi(\mathbf{r}, t)$  at position  $\mathbf{r}$  and at time  $t$  is described

by the diffusion equation [4]

$$\frac{\partial}{\partial t}\Phi(\mathbf{r}, t) - \nabla \cdot D(\mathbf{r})\nabla\Phi(\mathbf{r}, t) + v\mu_a(\mathbf{r})\Phi(\mathbf{r}, t) = S(\mathbf{r}, t). \quad (4.1)$$

The absorption coefficient  $\mu_a = l_a^{-1}$  and the transport scattering coefficient  $\mu_s = l_{tr}^{-1}$  can depend on the position in the medium. The diffusion constant  $D = v/3\mu_s$  ( $v$  is the velocity of the light) then also depends on position. We do not take any absorption dependence of the diffusion constant into account, as many other authors do [2–6], since corrections to  $D$  are of the same order as corrections to the diffusion equation itself [7–9]. For the diffusion equation to be valid one needs [4, 5]

$$\mu_a \ll \mu_s. \quad (4.2)$$

The source term  $S(\mathbf{r}, t)$  describes the density of photons generated per second. The diffusion equation (4.1) has to be supplemented with boundary conditions, which we will consider later on.

Since the diffusion theory can only handle photon densities, without being able to distinguish different directions of propagation, the source  $S$  has to be isotropic. For simplicity we will only consider point sources. A short discussion on non-isotropic light sources will be given in section 4.2, following Haskell *et al.* [3]. When the source is amplitude modulated, the photon density will be time dependent, although always non-negative. Taking only one Fourier component with frequency  $\omega$  into account, a source at position  $\mathbf{r}_s$  is then given by

$$S(\mathbf{r}, t) = S_\omega e^{-i\omega t} \delta(\mathbf{r} - \mathbf{r}_s). \quad (4.3)$$

Unless  $\omega = 0$  the corresponding photon density will be complex and have the same harmonic time-dependence.

We will formulate the theory in terms of Green functions. A Green function describes the propagation of light in a homogenous medium (no objects present), having only one source at an arbitrary position  $\mathbf{r}'$  (not necessarily the position  $\mathbf{r}_s$  of the physical source). From now on we will use  $\mu_a$  and  $\mu_s$  to characterize the homogenous background medium, and use extra subscripts to denote inhomogeneities. The Green function obeys the diffusion equation

$$-\nabla^2 G(\mathbf{r}, \mathbf{r}') + \kappa^2 G(\mathbf{r}, \mathbf{r}') = \delta(\mathbf{r} - \mathbf{r}') \quad (4.4)$$

with the same the boundary conditions as  $\Phi$ . Here  $\kappa = [(\mu_a v - i\omega)/D]^{1/2}$  is the inverse decay length of the background medium. For later use we

also define  $\kappa_0 = \kappa(\omega = 0) = \sqrt{3\mu_a\mu_s}$ , which is real. We suppose that the solution to equation (4.4) is known. The photon density for the homogenous medium is then given by

$$\Phi_0(\mathbf{r}) = \frac{S_\omega}{D}G(\mathbf{r}, \mathbf{r}_s). \quad (4.5)$$

The Green function obeys the symmetry of reciprocity [10],

$$G(\mathbf{r}, \mathbf{r}') = G(\mathbf{r}', \mathbf{r}), \quad (4.6)$$

which can be useful in calculations.

An important Green function in our calculations is that of the infinite medium given by

$$G_\infty(\mathbf{r} - \mathbf{r}_s) = \frac{1}{4\pi r}e^{-\kappa r}, \quad (4.7)$$

where  $r = |\mathbf{r} - \mathbf{r}_s|$  is the distance to the source. When  $\mathbf{r}$  and  $\mathbf{r}'$  are close together and far from boundaries all Green functions tend to  $G_\infty$ . We will use this when we consider the influence of small objects.

#### 4.1.1 Born series

For any source term  $S(\mathbf{r})$  the solution to the homogenous diffusion equation can be found as

$$\Phi(\mathbf{r}) = D^{-1} \int d\mathbf{r}' G(\mathbf{r}, \mathbf{r}') S(\mathbf{r}'). \quad (4.8)$$

Consider now the diffusion equation (4.1), at frequency  $\omega$ . Rewrite it such that the left-hand-side corresponds to the homogenous medium, and all terms due to perturbations of the optical parameters, as well as the physical source, are on the right-hand-side:

$$\begin{aligned} -\nabla^2\Phi(\mathbf{r}) + \kappa^2\Phi(\mathbf{r}) &= \frac{S_\omega}{D}\delta(\mathbf{r} - \mathbf{r}_s) + \frac{\Delta D(\mathbf{r})}{D}\nabla^2\Phi(\mathbf{r}) \\ &+ D^{-1}[\nabla D_{\text{obj}}(\mathbf{r})] \cdot [\nabla\Phi(\mathbf{r})] - 3\mu_s\Delta\mu_a(\mathbf{r})\Phi(\mathbf{r}). \end{aligned} \quad (4.9)$$

Here we introduced the perturbation in the absorption and in the diffusion constant

$$\Delta\mu_a(\mathbf{r}) = \mu_{a,\text{obj}}(\mathbf{r}) - \mu_a, \quad (4.10a)$$

$$\Delta D(\mathbf{r}) = D_{\text{obj}}(\mathbf{r}) - D. \quad (4.10b)$$

For the scattering parameter  $\Delta\mu_s(\mathbf{r})$  a similar relations holds. The complete right-hand-side of Eq. (4.9) then acts as a source in Eq. (4.8). In general one can therefore write the solution of the diffusion equation (after partial integration) as [11, 12]

$$\begin{aligned}\Delta\Phi(\mathbf{r}) &\equiv \Phi(\mathbf{r}) - \Phi_0(\mathbf{r}) \\ &= -3\mu_s \int d\mathbf{r}' G(\mathbf{r}, \mathbf{r}') \Delta\mu_a(\mathbf{r}') \Phi(\mathbf{r}') \\ &\quad - \int d\mathbf{r}' [\nabla_{\mathbf{r}'} G(\mathbf{r}, \mathbf{r}')] \frac{\Delta D(\mathbf{r}')}{D} \nabla_{\mathbf{r}'} \Phi(\mathbf{r}').\end{aligned}\quad (4.11)$$

By substituting the expression for  $\Phi$  itself in the right-hand-side, and repeating this for every new expression, one generates a series. Each term in this Born series contains only  $\Phi_0$  and  $G$  (which are proportional) or derivatives thereof, but no longer the complete photon density  $\Phi$ . This (infinite) Born series is a solution of the diffusion equation for any spatial variation of the optical parameters.

For systems where the perturbation of  $\mu_s$  and  $\mu_a$  is small, one can use the first order Born approximation, which implies that one replaces  $\Phi$  on the right-hand-side of Eq. (4.11) by the most important contribution  $\Phi_0$ . This is the basis of the forward calculation in many reconstruction techniques [11, 13–17], since it assumes that the measurements depend linearly on the perturbations.

#### 4.1.2 Small objects

Let us now consider a single small object. For an object at position  $\mathbf{r}_o$  to be small, its characteristic size  $a$  must obey

$$a \ll |\mathbf{r}_o - \mathbf{r}_s|, |\mathbf{r}_o - \mathbf{r}|, |\kappa|^{-1}. \quad (4.12)$$

Outside the object the perturbations of the optical parameters vanish ( $\Delta\mu_a = \Delta D = 0$ ). Let us first consider only a perturbation in  $\mu_a$ , i.e.  $\Delta D = 0$ . Since the object is small the Green function  $G(\mathbf{r}, \mathbf{r}')$  in the integral of Eq. (4.11) is nearly constant and we find

$$\Phi(\mathbf{r}) = \Phi_0(\mathbf{r}) - 3\mu_s G(\mathbf{r}, \mathbf{r}_o) \int_{\Omega} d\mathbf{r}' \Delta\mu_a(\mathbf{r}') \Phi(\mathbf{r}'), \quad (4.13)$$

where  $\Omega$  denotes the volume of the object. This still leads to a Born series. Every term of this series contains in the integral the photon density

$\Phi_0(\mathbf{r}') = S_\omega D^{-1} G(\mathbf{r}', \mathbf{r}_s)$ . Again, this Green function varies only little over the volume of the object. Therefore the photon density can be written as

$$\Phi(\mathbf{r}) = \Phi_0(\mathbf{r})[1 + qQ(\mathbf{r}_o; \mathbf{r}, \mathbf{r}_s)], \quad (4.14)$$

where  $Q$  is the sensitivity for absorption [2, 18, 19] defined by

$$Q(\mathbf{r}_o; \mathbf{r}, \mathbf{r}_s) = \frac{4\pi}{\kappa_0} \frac{G(\mathbf{r}, \mathbf{r}_o)G(\mathbf{r}_o, \mathbf{r}_s)}{G(\mathbf{r}, \mathbf{r}_s)}. \quad (4.15)$$

The dependence of  $Q$  on  $\mathbf{r}$  has a ‘‘banana’’ shape [20]. The (real) factor  $4\pi/\kappa_0$  is conventional and has been chosen to make  $Q$  unit-less and void of factors  $4\pi$  for the infinite medium. The rest of the Born series gives the strength  $q$  of the object

$$q = -\kappa_0 \frac{3\mu_s}{4\pi} \int_{\Omega} d\mathbf{r}' \Delta\mu_a(\mathbf{r}') \left( 1 - \frac{3\mu_s}{4\pi} \int_{\Omega} d\mathbf{r}'' \frac{\Delta\mu_a(\mathbf{r}'')}{|\mathbf{r}' - \mathbf{r}''|} (1 - \dots) \right). \quad (4.16)$$

The usefulness of Eq. (4.14) (and similarly of Eqs. (4.17) and (4.21) below) lies in the fact that the sensitivity for absorption  $Q$  does not depend on the object, only on its position, and that the strength of the object  $q$  does not depend on geometrical factors of the surrounding medium. The strength does depend on the spatial distribution of the perturbation of the absorption coefficient, i.e. on the shape of the object and its absorption contrast with respect to the background. Since any measurement depends only on the position of the object and its strength, the shape of the object and the precise distribution of the absorption inside the object is however not important for the measurement. This means for instance that a very small and completely black object can give the same result as a larger object with only moderate absorption, as long as both fulfill condition (4.12). This has consequences for reconstruction, in the sense that not all characteristics of objects can be reconstructed. We will give the strength  $q$  of several objects later on.

We can give the same analysis for an object which has no extra absorption ( $\Delta\mu_a = 0$ ) but which has a different diffusion constant than the background. The description of scattering objects introduces the gradient of the Green functions [cf. Eq. (4.11)]. Since we have two of them, one for light going from source to object and one for light going from object to detector, we need a matrix  $p_{ij}$  with two indices to describe the object. In the same way as above, we find

$$\Phi(\mathbf{r}) = \Phi_0(\mathbf{r})[1 + \sum_{i,j} p_{ij} P_{ij}(\mathbf{r}_o; \mathbf{r}, \mathbf{r}_s)]. \quad (4.17)$$

Here  $P_{ij}$  is the sensitivity for scattering,

$$P_{ij}(\mathbf{r}_o; \mathbf{r}, \mathbf{r}_s) = -\frac{4\pi}{\kappa_0^3} \frac{\nabla_{r_o,i} G(\mathbf{r}', \mathbf{r}_o) \nabla_{r_o,j} G(\mathbf{r}_o, \mathbf{r}_s)}{G(\mathbf{r}, \mathbf{r}_s)}. \quad (4.18)$$

Again the factor  $-4\pi/\kappa_0^3$  is conventional. The object is characterized by the symmetric matrix

$$p_{ij} = \frac{\kappa_0^3}{4\pi D} \int_{\Omega} d\mathbf{r}' \Delta D(\mathbf{r}') \left( \delta_{ij} - \frac{1}{4\pi D} \sum_k \int_{\Omega} d\mathbf{r}'' \Delta D(\mathbf{r}'') \right. \\ \left. \times \nabla_{r',i} \nabla_{r'',k} \frac{1}{|\mathbf{r}' - \mathbf{r}''|} (\delta_{kj} - \dots) \right). \quad (4.19)$$

For spherical symmetric objects the dipole term is a scalar  $p_{ij} = p\delta_{ij}$ . Then one does not need all elements of  $P_{ij}$ , but only the trace

$$P(\mathbf{r}_o; \mathbf{r}, \mathbf{r}_s) = \sum_i P_{ii}(\mathbf{r}_o; \mathbf{r}, \mathbf{r}_s) = -\frac{4\pi}{\kappa_0^3} \frac{\nabla_{r_o} G(\mathbf{r}', \mathbf{r}_o) \cdot \nabla_{r_o} G(\mathbf{r}_o, \mathbf{r}_s)}{G(\mathbf{r}, \mathbf{r}_s)}, \quad (4.20)$$

which is the vector product of the gradients of two Green functions [2]. For objects with less symmetry all components of  $p_{ij}$  can in principle be non-zero. But the deviation from the contribution  $p\delta_{ij}$  is generally small. Hence in all the examples we will use the simplified form (4.20).

A difference between absorbing objects described by Eq. (4.14) and scattering objects described by Eq. (4.17) is that the former actually take light away, while the latter mainly redistribute the light, such that the total amount of light detected does not necessarily change. The description of objects that include both scattering and absorption is somewhat more complex than above. We will not address this problem here. We only note that strengths describing the combination of absorption and scattering are negligible when the object is also small with respect to the absorption and scattering lengths of the object itself, since such a combination is always a higher order effect.

The next question to be asked is, what is the result for multiple objects. In first order all the different objects contribute linearly to the measurement. That is, for multiple objects, we can write

$$\Phi(\mathbf{r}) \simeq \Phi_0(\mathbf{r}) [1 + \sum_o q_o Q(\mathbf{r}_o; \mathbf{r}_s, \mathbf{r}_d) + \sum_o p_o P(\mathbf{r}_o; \mathbf{r}_s, \mathbf{r}_d)], \quad (4.21)$$

where the index  $o$  identifies the objects. Equations (4.14), (4.17) and (4.21) generalize the expressions given in Refs. [1,2,21]. We will see that the first

order approximation (4.21) is good, even when the difference between  $\Phi$  and  $\Phi_0$  is of the order of tens of percents. Note that Eq. (4.21) is basically the first order Born approximation discussed in section 4.1.1, but now with a more realistic description of single objects.

### 4.1.3 Strength of specific objects

Now we will give the explicit form of the strengths  $q$  and  $p$  for different objects. Not many of them can be calculated analytically however. For small objects and perturbations which are not too large we again only need to take into account the first term of the series in Eqs. (4.16) and (4.19). We find for an object with volume  $\Omega$  and only a small constant perturbation in absorption  $\Delta\mu_a$ :

$$q = -\frac{\kappa_0^3 \Omega \Delta\mu_a}{4\pi\mu_a}, \quad p = 0, \quad (4.22)$$

and for an object with only a small constant perturbation in scattering  $\Delta D$ :

$$p = \frac{\kappa_0^3 \Omega \Delta D}{4\pi D}, \quad q = 0. \quad (4.23)$$

For spherical objects of radius  $a$  one can find the results in Refs. [1, 2] for general values of the optical parameters of the background and the object. For the specific case of  $\Delta\mu_a = 0$ ,  $\Delta D = D_{\text{obj}} - D$  is constant inside the spherical object and for  $\kappa a \ll 1$ , these reduce to

$$p_{\text{sphere}} = (\kappa_0 a)^3 \frac{D_{\text{obj}} - D}{D_{\text{obj}} + 2D}. \quad (4.24)$$

One can show that the series of Eq. (4.19) gives the same result. Consequently, even for small radius  $a$  one needs to take the full series into account, when  $\Delta D$  itself is not small. When the scattering in the object increases,  $D_{\text{obj}}$  decreases, until  $p$  reaches a maximum value of  $-\frac{1}{2}(\kappa_0 a)^3$ . That  $p$  has a maximum is due to the fact that large scattering of the object implies that all the light will be reflected, almost at the point of entering. If this is so, the absolute amount of scattering given by the value of  $D_{\text{obj}}$  is no longer important. Also the opposite case of a very transparent object, with large  $D_{\text{obj}}$ , leads to a saturation value,  $p = (\kappa_0 a)^3$ . We see that as long as  $D_{\text{obj}}$  and  $D$  differ enough, their precise values are not important for the determination of  $p$ .

We observe that for weak objects the strengths  $p$  and  $q$  scale with the volume of the object. One can use this to rewrite Eq. (4.21) into its integral equivalent [12]

$$\Phi(\mathbf{r}) = \Phi_0(\mathbf{r}) \left[ 1 - \frac{3\mu_s}{4\pi} \int d\mathbf{r}_o \Delta\mu_a(\mathbf{r}_o) Q(\mathbf{r}_o; \mathbf{r}_s, \mathbf{r}) + \frac{3\kappa_0^3}{4\pi} \int d\mathbf{r}_o \frac{D_{\text{obj}}(\mathbf{r}_o) - D}{D_{\text{obj}}(\mathbf{r}_o) + 2D} P(\mathbf{r}_o; \mathbf{r}_s, \mathbf{r}) \right]. \quad (4.25)$$

For the case of  $\Delta D = 0$  and a large but constant  $\Delta\mu_a$  in the object,  $\kappa_{\text{obj}}a \gtrsim 1$ , one finds [1, 2]

$$q_{\text{sphere}} = -\kappa_0 a [1 - \tanh(\kappa_{\text{obj}}a) / \kappa_{\text{obj}}a], \quad p = 0. \quad (4.26)$$

In the limit of large absorption  $\kappa_{\text{obj}}a \gg 1$  this leads to the strength of a black sphere

$$q_{\text{black}} = -\kappa_0 a. \quad (4.27)$$

Note that again in the limit of large perturbations the precise value of the optical parameters of the object is no longer important. The strength (4.27) can also be found by solving the diffusion equation directly for a spherical object [20] assuming that the photon density vanishes on the boundary of the object:

$$\Phi(|\mathbf{r} - \mathbf{r}_o| = a) = 0. \quad (4.28)$$

That this boundary condition is not exact is well known [3, 4]. This is due to the approximate nature of the diffusion equation, which requires  $\mu_a \ll \mu_s$  [cf. Eq. (4.2)]. This is not the case inside a strongly absorbing object. Equation (4.28) works rather well, however, when corrections to length scales of the order of the scattering length  $\mu_s^{-1}$  are negligible. For a small absorbing sphere, this is no longer the case, since  $a$  can be of the same order as  $\mu_s^{-1}$ . Therefore Eq. (4.27) no longer holds. In the neighborhood of an absorbing boundary the photon density does not vanish. Instead it has an offset. A boundary condition which incorporates this effect [4] and hence generally gives more accurate results [3] is (see also section 4.2)

$$\Phi + \xi_{\text{ext}} \hat{\mathbf{n}} \cdot \nabla \Phi \Big|_{\text{at the surface}} = 0. \quad (4.29)$$

Here  $\hat{\mathbf{n}}$  is a unit vector perpendicular to the surface of the scattering medium and pointing outward. The extrapolation length  $\xi_{\text{ext}}$  is of the order of  $\mu_s^{-1}$ . Its precise value depends on the the ratio of refractive in-

dices [4, 22–24], cf. Eq. (4.40), and on the geometry. Solving the diffusion equation (4.1) with a spherical object but using the boundary condition (4.29) instead of Eq. (4.28) one finds

$$q_{\text{black}} = -\frac{\kappa_0 a^2}{a + \xi_{\text{ext}}}. \quad (4.30)$$

The length  $\xi_{\text{ext}}$  itself depends only weakly on  $a$ . For large  $a$  it takes the value of the semi-infinite medium [4]  $\xi_{\text{ext}} = 2/3\mu_s$ . In the limit of vanishing  $a$  its value is  $\xi_a$  and will be calculated in the following.

Consider a virtual sphere of radius  $a \ll \mu_s^{-1}$ . We know that for a given source strength  $S_\omega$  (in photons per second) the photon density at the position  $\mathbf{r}_o$  of this sphere is given by  $\Phi_0(\mathbf{r}_o)$ . The number of photons in the sphere is then given by  $4\pi\Phi_0 a^3/3$ . We can assume that none of the photons will be scattered in the volume. The distribution of their directions is uniform, as is their distribution over space. The frequency at which photons enter the object depends on the inverse time spent in the object, which itself depends on the position at the surface of the sphere at which the photon enters, and its direction. The average over all possible entry points and directions of the inverse dwell time is  $v/a$ . Would the sphere be completely black, a number of  $S_o = (4\pi\Phi_0 a^3/3) \times (v/a) = 4\pi\Phi_0 a^2 v/3$  photons would be absorbed per unit of time. Hence, the sphere acts as a negative source with strength  $S_o$ . The photon density can now be written as

$$\Phi(\mathbf{r}) = \Phi_0(\mathbf{r}) - \frac{S_o}{D} G(\mathbf{r}; \mathbf{r}_o). \quad (4.31)$$

Combining this with Eq. (4.14) we get  $q_{\text{black}} = -\mu_s \kappa_0 a^2$  and consequently  $\xi_a = \mu_s^{-1}$ , which is 3/2 times as large as  $\xi_{\text{ext}}$  for large  $a$ .

We see from Eq. (4.30) that a cross-over exists in the dependence of  $q_{\text{black}}$  on the radius  $a$ , between small black spheres,  $a\mu_s < 1$  and larger spheres  $a\mu_s > 1$ . It is fair to ask if such a cross-over exists for spheres that have only a small extra absorption, compared to the background ( $\Delta\mu_a a \ll 1$ ). We know that for spheres which obey the diffusion equation (and therefore have relatively small  $\mu_a$ ) Eq. (4.22) holds and hence  $q \sim a^3$ . For a very small sphere we can use the same arguments as above. The number of photons present is again  $4\pi\Phi_0(\mathbf{r}_o)a^3/3$ . The frequency at which these photons get absorbed more than in the background is  $\Delta\mu_a v$ . Using again Eq. (4.31) we find  $q = -a^3 \Delta\mu_a \mu_s \kappa_0$  conform Eq. (4.22). We see that no cross-over exists.

We can explain the cubic dependence on the radius  $a$  qualitatively as follows. For any  $a$  the number of photons entering the object is propor-

tional to the number of photons absorbed when the object would be perfectly black, *i.e.*  $\propto q_{\text{black}}$  from Eq. (4.30). When  $a$  is small this number scales with  $a^2$ . The average path length is linear in  $a$ . Consequently the extra absorption which determines  $q$  is cubic in  $a$ . When  $a$  gets larger, the number of photons entering the sphere scales with  $a$ . The average length a photon travels inside the sphere is then no longer linear in  $a$ : the photon will have a diffusive motion inside the sphere. Its average time in the sphere will be  $\sim a^2/D$ , and hence the average path length in the sphere will be  $\sim a^2\mu_s$ . Again we find that  $q$  is cubic in  $a$ .

#### 4.1.4 Example

Let us consider a simple situation to obtain some insight in the formulas, deriving the main dependencies on the parameters, as well as getting some feeling for the sensitivity to scattering and absorption. We take both the source and the detector at a distance  $r$  of the object, all three of them on a line. The sensitivities are then given by

$$Q = \frac{2}{\kappa_0 r}, \quad (4.32a)$$

$$P = \frac{2}{(\kappa_0 r)^3} (1 + \kappa r)^2. \quad (4.32b)$$

(Note the difference between the real  $\kappa_0$ , acting as a length scale, and the complex and frequency dependent  $\kappa$ .) In many cases of practical interest for medical imaging, the distance  $r$  between source and object is of the same order as  $|\kappa|^{-1}$ . This means that both sensitivities are of equal order. For large  $r$  and zero frequency they are even identical in this geometry. When taking a realistic spherical object, where  $q$  and  $p$  are given by Eqs. (4.22) and (4.24) we find for the perturbation in photon densities

$$\frac{\Delta\Phi_q}{\Phi_0} = -\frac{\Delta\mu_a}{3\mu_a} (\kappa_0 a)^3 \frac{2}{\kappa_0 r}, \quad (4.33a)$$

$$\frac{\Delta\Phi_p}{\Phi_0} = \frac{\Delta D}{3D + \Delta D} (\kappa_0 a)^3 \frac{2}{\kappa_0^3 r^3} (1 + \kappa r)^2, \quad (4.33b)$$

where the index  $q$  ( $p$ ) denotes a perturbation in absorption (scattering). We see that in general the perturbation due to scattering can be as large as that due to absorption. For medical imaging purposes we expect however that absorption is more important than scattering since in practice  $\Delta\mu_a/\mu_a \gg \Delta D/D$ .

### 4.1.5 Amplitude modulated sources

All formula's given above can be applied as well to the case of an amplitude modulated source. We will, as in the experiments, use the amplitude  $A$  and the phase  $\varphi$ ,

$$\Phi = A e^{i\varphi}, \quad (4.34)$$

and write  $\Phi_0 = A_0 e^{i\varphi_0}$  for the homogenous background medium. (For zero frequency  $\Phi$  itself is real and hence  $\varphi = 0$ .) Consider a perturbation in the photon density, which we can write as

$$\Delta\Phi = |\Delta\Phi| e^{i\vartheta}. \quad (4.35)$$

From this perturbation one needs to calculate the perturbation in  $A$  and  $\varphi$ . For small perturbations we can write

$$\frac{\Delta A}{A_0} = |\Delta\Phi| \cos(\vartheta - \varphi_0) / A_0 = \operatorname{Re} \left( \frac{\Delta\Phi}{\Phi_0} \right), \quad (4.36a)$$

$$\Delta\varphi = |\Delta\Phi| \sin(\vartheta - \varphi_0) / A_0 = \operatorname{Im} \left( \frac{\Delta\Phi}{\Phi_0} \right). \quad (4.36b)$$

We give explicit formulas for the same example as above, where the object is exactly in the middle between source and detector, both distances being equal to  $r$ . We get

$$\frac{\Delta A}{A_0} = \frac{2}{3} \left( \frac{a}{r} \right)^3 \left[ -\frac{\Delta\mu_a}{\mu_a} (\kappa_0 r)^2 + \frac{\Delta D}{3D + \Delta D} \operatorname{Re}(1 + \kappa r)^2 \right], \quad (4.37a)$$

$$\Delta\varphi = \frac{2}{3} \left( \frac{a}{r} \right)^3 \frac{\Delta D}{3D + \Delta D} \operatorname{Im}(1 + \kappa r)^2. \quad (4.37b)$$

In general we see that the amplitude difference  $\Delta A/A_0$  is mainly sensitive to absorption inside the object, while the phase  $\Delta\varphi$  is mainly sensitive to the extra scattering of the object. When the object is not on the line between source and detector the sensitivity has an extra exponential factor. Due to this factor both amplitude and phase can vary for a single object, even if it is purely extra absorbing or purely extra scattering.

## 4.2 Optimal boundaries

### 4.2.1 Sources and boundaries

The purpose of our research is to image an object inside some medium. This medium will in general be a finite one. It is well known that the

boundary of this medium affects the measurements. One boundary of interest is the open boundary, where only air or a transparent fluid is surrounding the medium. For the description of the scattering of light inside the medium this is almost equivalent to a complete black boundary, since no light that leaves the turbid medium will re-enter it. An open boundary can also be accompanied by a mismatch in the refractive index between the turbid medium and the medium outside. An opposite kind of boundary is also possible, i.e. a boundary with as much reflection as possible, such that only a little amount of light gets lost. This can be done by surrounding the medium with mirrors. Surrounding the medium by another diffusive medium gives a similar result, since also a diffusive medium reflects much of the light entering it. The question arises which of these two possibilities is best for imaging objects. In answering this question we have to take into account both the sensitivity to the object, as discussed in the previous section, and the possible accuracy of the measurement, which benefits from large photon densities having less noise. Both change with boundary conditions. Also the algorithm of reconstruction can favor a choice of boundaries. To study this problem we will start with describing the boundaries and the way we will treat them. Then we will look both at sensitivity and accuracy.

Typically the source consists of a fiber placed in the medium, or — in the case of an outer boundary — at the edge of the medium. Therefore the incoming light will be a directed beam of light, with some aperture. The diffusion theory assumes point sources. It is possible to model a directed beam by a point source [3]. One has to determine where the model point-source is located, given the physical source. Due to symmetry reasons this point source will be at some distance from the end of the fiber, but on its axis  $\hat{n}$ . This distance, which we will call  $\xi_{\text{in}}$  will depend on the aperture. It has been shown [25] that for a collimated beam, having a small aperture,  $\xi_{\text{in}} = \mu_s^{-1}$  is a reasonable choice. We will take this value in the following. Larger apertures will have smaller  $\xi_{\text{in}}$ . For the use of the diffusion theory one needs a (model) source as deep into the medium a possible. This means that when the system is to be described by a diffusion equation, a small aperture of a source at the boundary would be best.

When modeling a physical detector, the same arguments as above hold. The physical detector also consists of a fiber. We assume that it has also a small aperture. Due to the symmetry with respect to the source fiber, the intensity detected in this way will be proportional to the photon density a length  $\xi_{\text{in}}$  away from this detector. This symmetry between source and

detector is a result of reciprocity [10], cf. Eq. (4.6). There is another way of looking at this. The approximation one makes in deriving the diffusion equation from the theory of radiative transfer is to write the photon flux  $I(\mathbf{r}, \hat{\mathbf{s}})$  at position  $\mathbf{r}$  in the direction  $\hat{\mathbf{s}}$  as [4] [cf. Eq. (1.14)]

$$I(\mathbf{r}, \hat{\mathbf{s}}) = \frac{v}{4\pi} [\Phi(\mathbf{r}) - \mu_s^{-1} \hat{\mathbf{s}} \cdot \nabla \Phi] \simeq \frac{v}{4\pi} \Phi(\mathbf{r} - \mu_s^{-1} \hat{\mathbf{s}}). \quad (4.38)$$

The flux at the detector position, and pointing into the fiber is then

$$I(\mathbf{r}_d, -\hat{\mathbf{n}}) \simeq \frac{v}{4\pi} \Phi(\mathbf{r}_d + \xi_{\text{in}} \hat{\mathbf{n}}), \quad (4.39)$$

which is proportional to the photon density a length  $\xi_{\text{in}} = \mu_s^{-1}$  in front of the physical detector.

Apart from the sources, we need to model boundaries as well. This can be done by the boundary condition (4.29) [3, 4, 22, 26] (see also chapter 2). This boundary condition can be derived using conservation of light flux at the boundary in combination with the requirement that no light is entering the medium. (Note that sources at physical boundaries are modeled as point sources in the medium and do therefore not interfere with these boundary conditions.) The value of  $\xi_{\text{ext}}$  is given by [5, 22]

$$\xi_{\text{ext}} = \frac{2}{3\mu_s} \frac{1 + 3 \int_0^{\pi/2} d\theta R(\theta) \sin \theta \cos(\theta)^2}{1 + 2 \int_0^{\pi/2} d\theta R(\theta) \sin \theta \cos(\theta)}, \quad (4.40)$$

where  $R(\theta)$  is the reflectivity of the boundary for light incident under an angle  $\theta$ . The boundary condition (4.29) is however not always easy to handle. For small  $\xi_{\text{ext}}$  one can expand  $\Phi$  around its value at the boundary  $\mathbf{r}_b$ . Using the boundary condition (4.29) this results in  $\Phi(\mathbf{r}) \simeq (\mathbf{r} - \mathbf{r}_b - \xi_{\text{ext}} \hat{\mathbf{n}}) \cdot \nabla \Phi(\mathbf{r}_b)$ . Hence the photon density vanishes for  $\mathbf{r} = \mathbf{r}_b + \xi_{\text{ext}} \hat{\mathbf{n}}$ , i.e. at a distant  $\xi_{\text{ext}}$  outside the medium. This is basically the requirement of the so-called extrapolated boundary [4, 23, 24]: The density is extrapolated by a distance  $\xi_{\text{ext}}$  beyond the boundaries, at which point the photon density vanishes,

$$\Phi[(\mathbf{r} - \mathbf{r}_b) \cdot \hat{\mathbf{n}} = \xi_{\text{ext}}] = 0. \quad (4.41)$$

This simplification of the boundary condition can only be done when the photon density is approximately linear over a distant  $\xi_{\text{ext}}$ , consequently the extrapolated-boundary condition can only be used for  $\kappa \xi_{\text{ext}} \ll 1$ . This puts a restriction on the use of Eq. (4.41). It is however much more simple to handle than Eq. (4.29) in calculating the photon density and it has

therefore been used extensively in literature. Haskell *et al.* [3] showed that the difference between both boundary conditions is indeed small for reasonable optical parameters. We prefer to use the latter boundary condition (4.41) whenever possible.

The extrapolation length  $\xi_{\text{ext}}$  used in Eqs. (4.29) and (4.41) depends on the refractive index mismatch between the scattering medium and its surroundings [22]. It is of the order of a mean free path. It has a minimum of  $2/3\mu_s$  for the semi-infinite geometry [4] (its value when considering the theory of radiative transfer [27] is  $0.71\mu_s^{-1}$ ). It increases with refractive index mismatch, and can become several mean free paths long [23, 24]. Hence we can model the amount of Fresnel reflection at the boundary, which is due to this mismatch, by the value of  $\xi_{\text{ext}}$ .

The introduction of  $\xi_{\text{ext}}$  enlarges the system effectively with a distance of the order of the mean free path. One would therefore expect only a small correction to the results, of the order of  $\xi_{\text{ext}}/L$ , where  $L$  is a measure of the system size. This is however not true in the case where either source or detector is close to a boundary. The less deep the source is located, the larger the losses at the boundary will be, and consequently the smaller for example the transmission. As we will see, for small  $\xi_{\text{ext}}$ , the photon density scales with the distance between the (model) source and the boundary of the effective medium  $\xi \equiv \xi_{\text{ext}} + \xi_{\text{in}}$ . When calculating the absolute value of the photon density, the value of  $\xi_{\text{ext}}$  is important. The source strength  $S_\omega$  is of equal importance. Fresnel reflection at the boundary has its influence both on the source term and on the value of  $\xi_{\text{ext}}$ . Since it is in practice difficult to determine the source term, we will seek quantities that only depend on relative measurements. For these cases, the exact value of  $\xi_{\text{ext}}$  is not very important, as long as  $\kappa\xi_{\text{ext}}$  is small. For reflecting boundaries however  $\kappa\xi_{\text{ext}}$  can be large, in which case the value of  $\xi_{\text{ext}}$  is important.

We want to study the influence of the boundary extrapolation. Two limits are evident. First of all the limit  $\xi_{\text{ext}} \rightarrow \infty$ . In this limit the two boundary conditions (4.29) and (4.41) give different results. The former corresponds to having perfect mirrors at the boundaries, reflecting all the light. The latter corresponds to an infinite medium. Both are similar but not equivalent. The second limit is that of small  $\xi_{\text{ext}}$ . This is almost equivalent to completely absorbing boundaries, or a surrounding medium which does not scatter the light and which has (almost) matching refractive index. Both will be considered. When considering good reflecting mirrors, we assume that measurements are made using small fibers, that penetrate the mirrors, instead of measuring the small amount of light that is transmitted through the mirrors.

### 4.2.2 Green functions

To determine the sensitivities  $Q$  and  $P$  and their dependence on the boundary, we first need to calculate the Green functions [28]. We will start with a semi-infinite medium since this is the most simple case, and it already gives some insight. The medium occupies the half space  $z > 0$ . The source is as before located at  $r_s$ . The difference in the  $xy$ -plane between  $r$  and  $r_s$  is the lateral distance  $\rho$ . The system is cylindrically symmetric, so that the Green function and other resulting quantities only depend on  $\rho = |\rho|$ , and not on the direction of  $\rho$ . It is useful to perform a Fourier transform in the  $xy$ -plane, writing

$$\begin{aligned} G_s(\rho, z, z_s) &= \int \frac{d^2\mathbf{q}}{(2\pi)^2} e^{i\mathbf{q}\cdot\rho} G_s(\mathbf{q}, z, z_s) \\ &= \int_{\kappa}^{\infty} \frac{d\alpha}{2\pi} J_0(\rho\sqrt{\alpha^2 - \kappa^2}) \alpha G_s(\alpha; z, z_s). \end{aligned} \quad (4.42)$$

The subscript  $s$  refers to “semi-infinite”, and  $J_0$  is a Bessel function. The change to the variable  $\alpha^2 = \kappa^2 + \mathbf{q}^2$  is introduced for later convenience. For amplitude modulated sources  $\kappa$ , and therefore  $\alpha$ , will be complex. However, for notational simplicity we will write the integral over  $\alpha$  as being from  $\kappa$  to  $\infty$ . To find the Green function we need to solve Eq. (4.4). After Fourier transformation we get

$$\left(-\frac{\partial^2}{\partial z^2} + \alpha^2\right)G_s(\alpha; z, z_s) = \delta(z - z_s). \quad (4.43)$$

Since we do not want to restrict the value of  $\xi_{\text{ext}}$  yet, we will use the boundary condition (4.29). The solution for the Green function at fixed  $\alpha$  is then given by

$$G_s(\alpha; z, z_s) = \frac{1}{2\alpha} \left( e^{\alpha z_{\min}} - \frac{1 - \alpha\xi_{\text{ext}}}{1 + \alpha\xi_{\text{ext}}} e^{-\alpha z_{\min}} \right) e^{-\alpha z_{\max}}, \quad (4.44)$$

as can be checked by substitution. We defined  $z_{\min} = \min(z, z_s)$  and  $z_{\max} = \max(z, z_s)$ . The Green function in real space is then given by

$$G_s(\rho, z, z_s) = \int_{\kappa}^{\infty} \frac{d\alpha}{4\pi} J_0(\rho\sqrt{\alpha^2 - \kappa^2}) \left( e^{\alpha z_{\min}} - \frac{1 - \alpha\xi_{\text{ext}}}{1 + \alpha\xi_{\text{ext}}} e^{-\alpha z_{\min}} \right) e^{-\alpha z_{\max}}. \quad (4.45)$$

Equation (4.7) for the Green function  $G_{\infty}$  in the infinite medium can be found from Eq. (4.45), by considering a source and a final position far into

the medium,  $\kappa z_{\min} \gg 1$ . Then the boundary will not have any influence and we find

$$G_{\infty}(\rho, z, z_s) = \int_{\kappa}^{\infty} \frac{d\alpha}{4\pi} J_0(\rho\sqrt{\alpha^2 - \kappa^2}) e^{-\alpha(z_{\max} - z_{\min})} = \frac{1}{4\pi r} e^{-\kappa r}, \quad (4.46)$$

where  $r^2 = \rho^2 + (z - z_s)^2$ . Using this equality one can rewrite the Green function (4.45) for the semi-infinite medium as [3]

$$G_s(\rho, z, z_s) = \frac{1}{4\pi r} e^{-\kappa r} + \frac{1}{4\pi r_+} e^{-\kappa r_+} - \frac{2}{\xi_{\text{ext}}} \int_{-\infty}^{-z_s} dz' \frac{1}{4\pi r'} e^{-\kappa r'} e^{(z'+z_s)/\xi_{\text{ext}}}, \quad (4.47)$$

where  $r_+^2 = \rho^2 + (z + z_s)^2$  and  $r'^2 = \rho^2 + (z - z')^2$ . This expression can be interpreted as follows. The first term is the result from the original source, when no boundaries are present. The second term describes the propagation of light from a source just on the other side of the physical boundary at  $z = 0$ , which we call the mirror source. The last term describes the propagation of light from a distribution of sources on the  $z$ -axis between  $z' = -\infty$  and  $z' = -z_s$ . The density of this distribution is a Poisson distribution  $\xi_{\text{ext}}^{-1} e^{(z'+z_s)/\xi_{\text{ext}}}$  and has a total strength of  $-2$ .

We can now model the different boundaries by taking the limiting values of  $\xi_{\text{ext}}$ . For perfectly reflecting boundaries,  $\xi_{\text{ext}} \rightarrow \infty$ , the distribution of sources at  $z'$  has a vanishing contribution for any position. Hence the Green function has only two terms, that of the original and that of the mirror source.

Taking the other limit,  $\xi_{\text{ext}} \rightarrow 0$ , the distribution term is limited to the one point  $z' = -z_s$ . The Green function then exists of a term describing the propagation from the original source and a term describing the propagation from the mirror source, but with total strength  $-1$ . For  $\xi_{\text{ext}} = 0$  the Green function itself vanishes at the boundary whereas for  $\xi_{\text{ext}} \rightarrow \infty$  its derivative with respect to  $z$  vanishes. This can also be seen directly from the boundary condition (4.29). For a realistic absorbing boundary the value of  $\xi_{\text{ext}}$  does not vanish completely. For small values we can write Eq. (4.44) as

$$G_s(\alpha; z, z_s) = \frac{1}{2\alpha} \left( e^{\alpha z_{\min}} - e^{-\alpha(z_{\min} + 2\xi_{\text{ext}})} \right) e^{-\alpha z_{\max}}, \quad \kappa \xi_{\text{ext}} \ll 1. \quad (4.48)$$

This expression and the resulting Green function  $G(\rho, z, z_s)$  describe again two sources, one at the original source position, and one (with strength  $-1$ ) at  $-z_s - 2\xi_{\text{ext}}$ . The Green function then indeed vanishes at the extrapolated boundary  $z = -\xi_{\text{ext}}$ , according to the boundary condition (4.41). In

real space the resulting Green function is given by [29]

$$G_s(\rho, z, z_s) = G_\infty(\sqrt{(z - z_s)^2 + \rho^2}) - G_\infty(\sqrt{(z - z_s - 2\xi_{\text{ext}})^2 + \rho^2}), \quad z > z_s. \quad (4.49)$$

For large but finite  $\xi_{\text{ext}}$  it is not possible to find an expression such that the Green function or its derivative vanishes at the same position for every  $\alpha$ . Therefore no extrapolated boundary in any sense can be used for good but not perfect mirrors. Qualitatively a mirror which is not perfectly reflecting can be described by using a mirror source of a somewhat smaller strength. For quantitative calculations however one needs to use the full expression (4.47).

The next geometry we consider is that of the slab. The slab geometry consists of a medium of infinite extent in both the  $x$  and  $y$ -direction, but limited between two boundaries in the  $z$ -direction:  $0 < z < L$ . In a slab geometry two qualitatively different measurements are possible. The first is a reflection measurement, which is similar to a reflection measurement at a semi-infinite medium. The second is a transmission measurement where source and detector are on two opposite boundaries. For every finite convex medium, any measurement is either like a reflection measurement or like a transmission measurement. For our discussion it suffices to consider these two possibilities as general prototypes.

As we did for the semi-infinite medium, we take the physical source at  $z = 0$ , pointing into the medium. We then need to solve Eq. (4.44) to find the Green function. The boundary condition (4.29) takes the explicit form

$$G_L(0, z_s) = \xi_{\text{ext}} \partial_z G(z, z_s)|_{z=0}, \quad (4.50a)$$

$$G_L(L, z_s) = -\xi_{\text{ext}} \partial_z G(z, z_s)|_{z=L}, \quad (4.50b)$$

for the slab geometry considered here. We find

$$G_L(\alpha; z, z_s) = \frac{\left( e^{\alpha z_{\text{min}}} - F e^{-\alpha z_{\text{min}}} \right) \left( e^{\alpha(L - z_{\text{max}})} - F e^{-\alpha(L - z_{\text{max}})} \right)}{2\alpha \left( e^{\alpha L} - F^2 e^{-\alpha L} \right)}, \quad (4.51a)$$

$$F = \frac{1 - \alpha \xi_{\text{ext}}}{1 + \alpha \xi_{\text{ext}}}. \quad (4.51b)$$

The Green function in real space is then given by

$$G_L(\rho, z, z_s) = \int_{\kappa}^{\infty} \frac{d\alpha}{4\pi} J_0(\sqrt{\alpha^2 - \kappa^2} \rho) 2\alpha G_L(\alpha; z, z_s). \quad (4.52)$$

Expression (4.52) can be simplified when we can make use of the boundary condition (4.41) instead of (4.29). This results again in the use of mirror sources [30]. In the slab geometry the system consists of two extrapolated boundaries, where the photon density has to vanish. To find the Green function one needs a mirror source for each of this two boundaries. Each mirror source also needs its own image in both boundary planes, which in turn need their own images. This leads to an infinite number of mirror sources, all regularly spaced. The formula for the Green function  $G_L$  of the slab then reads [30]

$$G_L(\mathbf{r}, \mathbf{r}_s) = \sum_{m=-\infty}^{\infty} \left( G_{\infty}(\mathbf{r}, \mathbf{r}_s + 2m(L + 2\xi_{\text{ext}})\hat{\mathbf{z}}) - G_{\infty}(\mathbf{r}, \sigma_z \mathbf{r}_s + 2m(L + 2\xi_{\text{ext}})\hat{\mathbf{z}}) \right). \quad (4.53)$$

Here  $\sigma_z$  is a mirror operation in the  $xy$ -plane:  $\sigma_z \mathbf{r} = \sigma_z(x, y, z) \equiv (x, y, -z)$ .

### 4.2.3 Reflecting boundaries

We now consider the differences between an infinite medium and a medium bounded by mirrors. Suppose that the source is at a boundary, which we model with  $z_s = \xi_{\text{in}} = \mu_s^{-1}$ . Then the source and its mirror image are separated by a distance of  $2\mu_s^{-1}$ . For positions not too close to the source the mirror source will appear as strong as the original source (the difference being a factor of the order of  $\kappa/\mu_s$  or  $1/\mu_s r$  smaller). Hence

$$G_s(\rho, z, \xi_{\text{in}}) \simeq 2G_{\infty}(\rho, z, \xi_{\text{in}}), \quad \xi \rightarrow \infty. \quad (4.54)$$

This enhancement appears for every position  $\mathbf{r}$ , and therefore the Green function from source to a detector at the same boundary, is enhanced by a factor of 2. The Green function from source to object, well away from a boundary is also enhanced. For symmetry reasons the Green function from object to detector is enhanced by the same factor. Bearing the definition (4.15) of the sensitivity for absorption in mind, we see that this sensitivity itself gets also enhanced by a factor of 2, for the measurement in reflection described here:

$$Q_{\text{mirror}} \simeq 2Q_{\infty}, \quad \text{reflection experiment.} \quad (4.55)$$

Next we consider a transmission experiment. The Green functions from source to object and from object to detector get enhanced by a factor of 2 with respect to the Green function of the infinite medium, as before.

The Green function from source to detector gets an enhancement factor of 2 due to the mirror close to the source. The mirror at the detector however is not the same mirror. Hence for symmetry reasons alone also at the detector we get an enhancement of two. The total enhancement for the Green function from source to detector is then 4. For the sensitivity to absorption  $Q$  we then find

$$Q_{\text{mirror}} \simeq Q_{\infty}, \quad \text{transmission experiment.} \quad (4.56)$$

Another way of looking at this is using a mirror object instead of mirror sources and detectors. One can then easily see that in reflection one actually measures two objects, one on each side of the boundary, one of them a mirror-object. In transmission, the mirror objects will be either too far away from source or from the detector to be measured. Corrections to this simple picture have to be made when the system size  $L$  is such that  $\exp(-\kappa L) \simeq 1$ , or when the object is close to boundary. In the former case one needs the full expression for the Green function in a slab geometry (4.52). When the object is close to a boundary, but far from both source and detector, the ratio between  $Q_{\text{mirror}}$  and  $Q_{\infty}$  is again 2.

A mirror that is almost perfectly reflecting can be described qualitatively by a mirror source of a somewhat smaller strength than 1. The enhancement factors discussed above get smaller than 2, but are still present. For mirrors reflecting only a part of the light the value of  $\xi_{\text{ext}}$  decreases even more. In those cases there is even less difference between an infinite medium and a bounded medium. The Green function in the infinite medium is such that  $\Phi \simeq \kappa^{-1}\Phi'$ . Therefore the boundary condition (4.29) is almost fulfilled by  $G_{\infty}$  when  $\kappa\xi_{\text{ext}} \simeq 1$ . For boundaries that are even less reflecting — we will show experimental examples of this — the sensitivity is somewhere between that of an infinite medium and that of a medium with absorbing boundaries. These different boundaries will be compared in specific geometries later on. We can conclude that the influence of mirrors on the Green function is only a factor of the order 1, with respect to the infinite system.

The arguments presented above hold also for the sensitivity to scattering  $P$ . Since the difference between an infinite system and a system with good mirrors is only a factor between 1 and 2, we can conclude that a boundary with good mirrors is qualitatively equivalent to an infinite system:

$$Q_{\text{mirror}} \simeq Q_{\infty}, \quad P_{\text{mirror}} \simeq P_{\infty}, \quad (4.57)$$

the difference being only a factor of order 1.

For black boundaries the situation is entirely different. For small  $\xi_{\text{ext}}$  the source and its mirror have different sign. Hence the difference of these two sources determines the Green function. Instead of  $G_{\infty}$  itself, its derivative becomes important. In this case there will be also differences between sensitivity for absorption and for scattering. It is difficult to compare the sensitivities for absorbing boundaries with those of an infinite medium using only general principles, as above. For the case of absorbing boundaries we will do some explicit calculations below. Before we do this however, we first describe the experimental results.

#### 4.2.4 Experimental results

The experimental setup to measure the influence of various kinds of boundaries on the detectability of objects is as follows: As a turbid medium a fish tank filled with 1% intralipid<sup>®</sup> is used. Intralipid is an emulsion of soybean oil in water, commercially available in concentrations of 10% and 20%. We diluted the 10% solution ten times to obtain a transport scattering coefficient of  $\mu_s = 0.85 \text{ mm}^{-1}$  and an absorption coefficient of  $\mu_a = 7 \cdot 10^{-4} \text{ mm}^{-1}$ , resulting in  $\kappa_0 = 0.042 \text{ mm}^{-1}$ . The light from a temperature stabilized semiconductor laser operating at 670 nm is administered via a multi-mode fiber with a diameter of 1 mm. The light intensity at the fiber end in the fish tank is approximately 1.2 mW. The detector position is determined by one end of a second multi-mode fiber which is connected at the other end to a Hamamatsu H5783-01 photomultiplier, having a maximum sensitivity of  $3 \cdot 10^3 \text{ A/W}$  at 670 nm. An electrometer measures directly the current output of the photomultiplier, and after A/D conversion the data is archived in a computer. The source and detector fibers are positioned in the fish tank, either with small white delrin holders to resemble an infinite medium, in the 1 mm holes of black perspex plates, or in the holes of polished aluminum plates acting as reflecting boundaries.

Both absorbing as well as scattering objects are studied. The absorbing object is a 5 mm diameter cylinder made of black delrin with a height of 5 mm. A computer controlled stepper motor holding a 2 mm diameter white delrin rod attached to the cylinder makes it possible to move the object freely through the fish tank. The rod has a negligible influence in comparison to the black cylinder. The scattering object is a hollow white cylinder with an internal diameter of 8.4 mm and an effective height of 55 mm filled with 20% intralipid. In order to correct for any absorbing effects of the delrin container each measurement is followed by a second one in which the container is filled with the same concentration as the

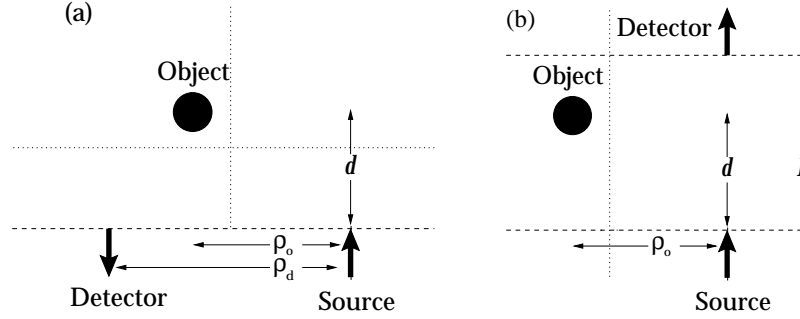


**Figure 4.1:** Schematic view of the geometry used for experiments and theory. (a) For measurements in reflection the source-detector distance in the  $xy$ -plane is denoted by  $\rho_d$ . The position of the object is given by its lateral coordinate  $\rho_o$  and its depth  $d$ . The dashed line shows the position of the physical boundary, when present. The object is moved along the horizontal dotted line for the measurements of Figs. 4.2 and 4.4, and along the vertical dotted line for the measurements of Figs. 4.3 and 4.5. The scale of the object corresponds to the black cylinder. (b) For measurements in transmission  $L$  is the thickness of the slab in the  $z$ -direction. The position of the object is again given by  $\rho_o$  and  $d$ . The dashed lines show the position of the physical boundaries, when present. The object is moved along the vertical dotted line for the measurements of Figs. 4.6 and 4.7.

surrounding medium i.e. 1% intralipid. Only the differences of two of such scans are displayed in the figures.

In Fig. 4.1(a) we show the geometry for the measurements in reflection (we discuss the experiments in transmission later on). We performed two measurements. For both we have taken a fixed source-detector distance  $\rho_d = 30$  mm. The object is then either scanned parallel to the line source-detector, with constant  $d$ , or over the symmetry line,  $\rho_o = \rho_d/2$ , with varying  $d$ . For all situations we have measured the signal with and without an object. The difference is then normalized by the measured signal without the object, which equals the ratio of photon densities  $\Delta\Phi/\Phi_0$ .

To compare the experimental results with theory we used Eqs. (4.15) and (4.20) to calculate the sensitivities  $Q$  and  $P$ . The Green functions we used are Eq. (4.7) for the infinite medium, Eq. (4.49) for the semi-infinite medium with absorbing boundaries, Eq. (4.47) for the semi-infinite medium with reflecting boundaries, and Eq. (4.52) for the slab. For the absorbing cylinder we took the value of  $Q$  at the center-point of the object and multiplied it with  $q$  to find  $\Delta\Phi_q/\Phi_0$ . Since the scattering object is

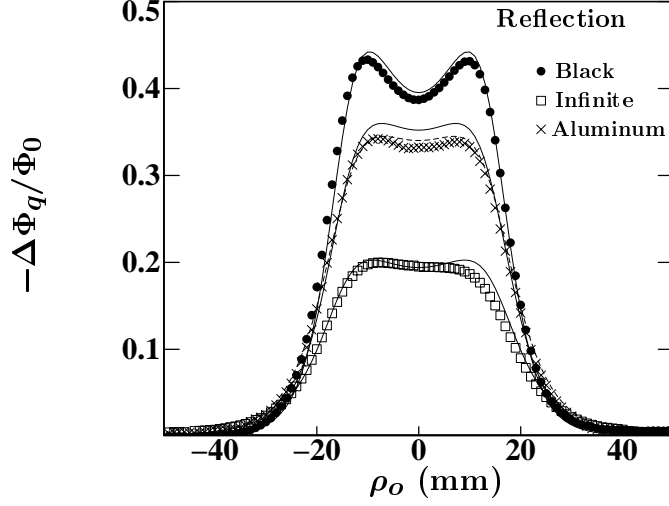


**Figure 4.2:** Sensitivity to absorption  $\Delta\Phi_q/\Phi_0 = qQ$  in a reflection measurement as a function of the lateral position  $\rho_o$ . The source detector distance  $\rho_d$  is 30 mm. The depth  $d$  of the object is 10 mm. The data points are for an infinite medium (squares), a semi-infinite medium with reflecting aluminum boundaries (crosses), and a semi-infinite medium with absorbing boundaries (dots). The solid curves are the corresponding theoretical lines. The dashed curve is for a reflecting gold mirror.

large, we cannot use the value of  $P$  at only one point. Instead we use Eq. (4.25) to find  $\Delta\Phi_p$ , with  $D/D_{\text{obj}} = 20$ . For later comparison we calculate the strength as if it were a small object and find  $p = -0.025$ .

To determine  $q$  we use Eq. (4.30) for  $q_{\text{black}}$ , with an effective radius  $a$ . We determine  $a$  by assuming that it is such that the surface of the effective sphere  $4\pi a^2$  equals the surface of the cylinder  $\pi d(h + d/2)$ . The reason for taking the surface is that  $q$  scales approximately with  $a^2$ . We find  $a = 3.06$  mm. Since this is already larger than a mean free path, we choose for  $\xi_{\text{ext}}$  its value for large  $a$ , which is  $0.67\mu_s^{-1} = 0.79$  mm. We find  $q = -0.10$ .

The different boundaries are characterized by the value of the extrapolation length  $\xi_{\text{ext}}$ , as defined in Eq. (4.40). For the black boundaries we find  $\mu_s\xi_{\text{ext}} = 0.67$ . For the aluminum plates, having a refractive index of  $1.4 - 6.28i$ , we use  $\mu_s\xi_{\text{ext,AI}} = 7.34$ . For a theoretical comparison we also calculated the results for a gold-coated mirror, with a refractive index of  $0.134 - 3.65i$  and hence  $\mu_s\xi_{\text{ext,Au}} = 28.0$ .

In Fig. 4.2 we show the results for the sensitivity to the absorbing object. The scan is parallel to the line joining the source and the detector.

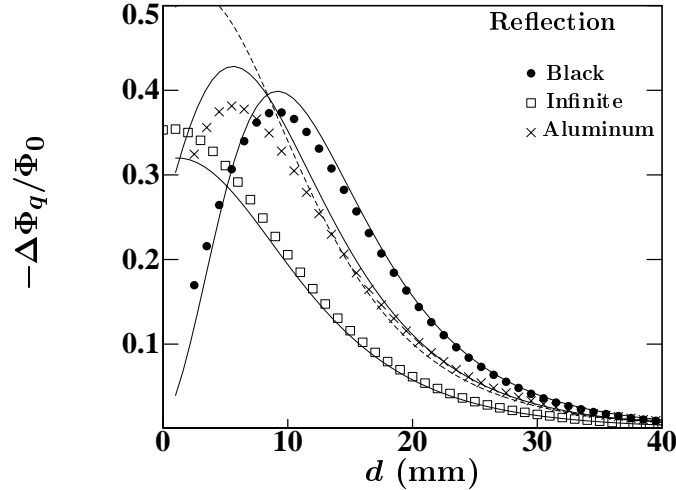


**Figure 4.3:** Sensitivity to absorption  $\Delta\Phi_q/\Phi_0 = qQ$  in a reflection measurement. The parameters are the same as in Fig. 4.2, but now the lateral distance  $\rho_o$  is fixed at  $\rho_d/2 = 15$  mm and the depth  $d$  is varied.

The three sets of data show the measurements for an infinite medium and for a semi-infinite medium with either absorbing or reflecting (aluminum) boundary. The corresponding theoretical results are shown with solid lines. The two maxima are at positions  $\rho_o$  such that the object is in front of either source or detector. The correspondence between experiment and theory is good, even though up to 45% of the light is already absorbed by the object. Remember that the theory is based on the assumption of small objects. This does however not mean that only small  $\Delta\Phi/\Phi_0$  can be described, as long as the strength  $q$  is calculated from the full expression in Eq. (4.16). No adjustable parameters have been used. The dashed theoretical line is for a semi-infinite reflecting (gold) boundary, which has a higher reflectivity than the aluminum boundary. For the same source-detector distance we also scanned the object over the symmetry line,  $\rho_o = \rho_d/2$ . The results are plotted in Fig. 4.3. Again the correspondence is quite good.

We note that the sensitivity  $Q$  is proportional to the data in the figures. One can see in Figs. 4.2 and 4.3 that in general the sensitivity for the semi-infinite medium with absorbing boundaries will be larger than that with reflecting boundaries or than that of the infinite medium. This is not true for objects close to absorbing boundaries, where the amount of light is small. The sensitivity  $Q$  of the semi-infinite medium with reflect-

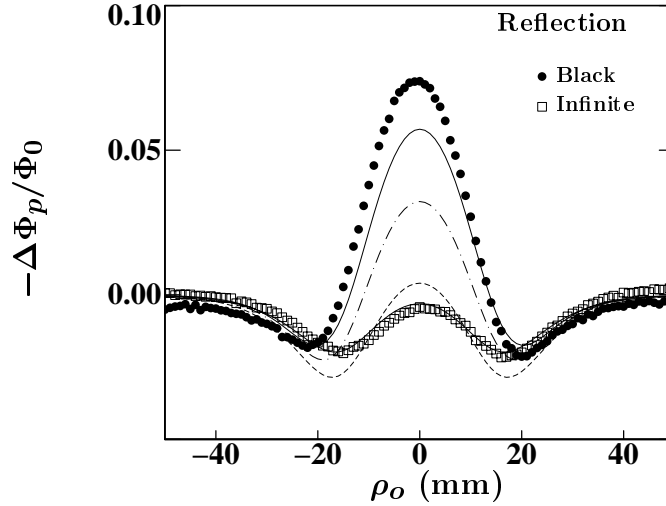


**Figure 4.4:** Sensitivity to scattering  $\Delta\Phi_p/\Phi_0$  in a reflection measurement as a function of the lateral position  $\rho_o$ , with  $\rho_d = 30$  mm, as in Fig. 4.2. The data points are for an infinite medium (squares,  $d = 15$  mm) and a semi-infinite medium with absorbing boundaries (dots,  $d = 17$  mm). The solid curves are the corresponding theoretical lines. The dashed-dotted line is the theoretical curve for the aluminum mirror, the dashed curve for a gold mirror ( $d = 15$  mm for both).

ing boundaries seems to be in the middle between the two other cases. As mentioned before this results from the fact that the aluminum mirrors reflect an amount of light which is in between that of the absorbing boundary and of that part of the infinite medium which is on the other side of the dashed line in Fig. 4.1. The dashed curve shows a sensitivity which is proportional to the sensitivity in the infinite medium, as described by Eq. (4.55). For  $d \gtrsim 10$  mm the difference between a good mirror (dashed curve) and a not so good mirror (crosses, solid curve) is minimal. (The exact curves depend on the values of  $\xi_{\text{ext}}$ .) Although the Green function in general increases when the reflection of the boundary increases, the sensitivity, involving 3 Green functions, has a behaviour which is different. When the object is close to the boundary the sensitivity for an aluminum mirror drops, since the amount of light near the boundary is low. For the gold mirror the sensitivity keeps rising and will be maximal at the boundary itself. Therefore the difference between a good mirror and a not so good mirror is mainly visible close to boundaries, at least for reflection experiments.

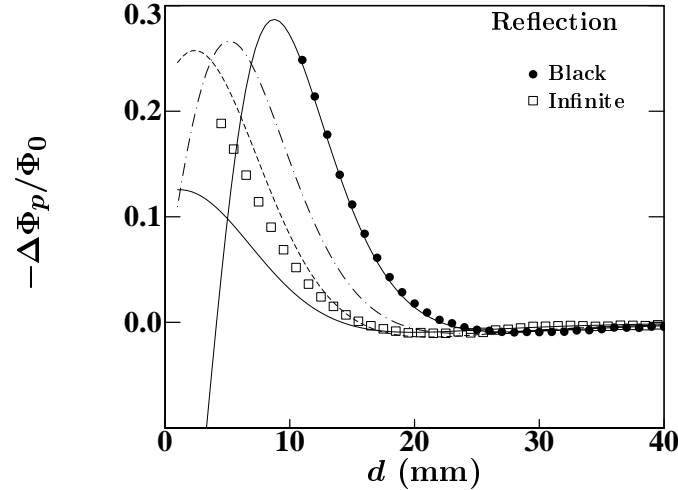


**Figure 4.5:** Sensitivity to scattering  $\Delta\Phi_p/\Phi_0$  in a reflection measurement as a function of the depth  $d$ , with  $\rho_o = \rho_d/2 = 15$  mm, as in Fig. 4.3. The solid theoretical curves correspond to the data points. The dashed-dotted curve is the curve for an aluminum mirror, the dashed curve for a gold mirror.

We also measured the sensitivity for scattering  $P$ . The results are shown in Figs. 4.4 and 4.5 for the same geometries as in Figs. 4.2 and 4.3, respectively. The data points are for an infinite medium and a medium with absorbing boundaries. The theoretical curves again correspond to the data points. Systematic errors include the determination of the position of the scattering object and the drift of the detector during the measurement. Due to the subtraction of two measurements these small errors lead to larger errors in the determination of  $\Delta\Phi_p$ . The final error is equivalent to an error of the order of 1 mm, which is already large enough to explain the discrepancies between theory and experiment. Note that the form of the curves agrees quite well with the theory.

We also calculated the theoretical curves for an aluminum boundary, which is shown in Figs. 4.4 and 4.5, dash-dotted to signify that no experimental results were available, and for a gold mirror (shown dotted). We observe again that the semi-infinite medium with reflecting boundaries is similar to the infinite medium.

The expression (4.20) for  $P$  may take on negative values. This happens when the scattering of a photon density wave from the object is effectively backwards. Such a negative sensitivity means that the detected signal will

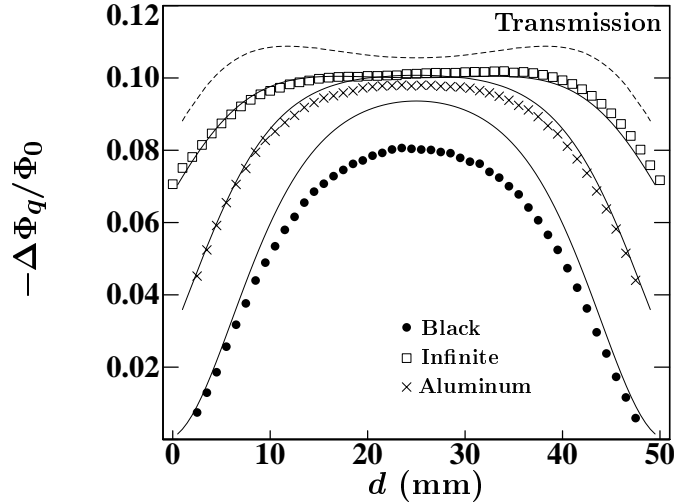


**Figure 4.6:** Sensitivity to absorption  $\Delta\Phi_q/\Phi_0 = qQ$  in a transmission measurement as a function of the depth  $d$ , with  $\rho_o = 15$  mm. The solid curves are the theoretical values, the dashed line shows again the curve for a gold mirror. The thickness of the slab is  $L = 50$  mm.

increase when the object scatters more strongly. For absorbing objects a change of sign is not possible. For Fig. 4.4 we observe this effect when  $\rho_o$  is large enough. This implies a faster decrease in  $P$  than we observed for  $Q$ . In the geometry of Fig. 4.5 the sensitivity to scattering  $P$  becomes negative when either  $d$  is large, or when  $d$  is small and the boundary is absorbing. In the latter case the photon density wave will travel from the source into the medium, turn back to the object, which is close to the boundary. There it will reflect effectively backwards and propagate to the detector, again avoiding the absorbing boundary. This effectively backward reflection implies a negative sensitivity  $P$ .

To give a full comparison between infinite systems and finite systems with different kind of boundaries, it is not enough to consider only reflection measurements. As we discussed before, for a finite medium all measurements are either like reflection or like transmission measurements. The geometry we chose for transmission experiments is one where the source and detector are opposite to each other (head on) as in Fig. 4.1(b). The thickness of the slab is  $L = 50$  mm. The object is scanned along a line parallel to the source-detector line, at a distance  $\rho_o$ . The depth of the object  $d$  is again varied. Results are shown in Figs. 4.6 and 4.7 for the absorbing

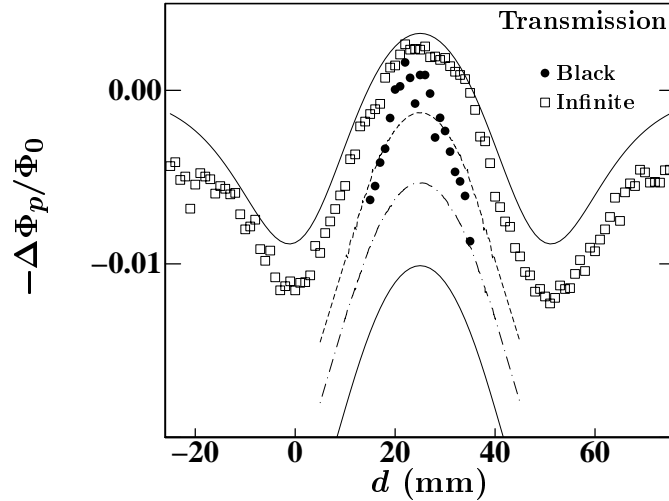


**Figure 4.7:** Sensitivity to scattering  $\Delta\Phi_p/\Phi_0$  in a transmission measurement as a function of the depth  $d$ . The thickness of the slab is  $L = 50$  mm, as in Fig. 4.6. For the infinite medium (squares)  $\rho_o = 19$  mm, for the semi-infinite medium (dots)  $\rho_o = 15$  mm. Note that the domain of  $d$  for the infinite medium is larger than in the previous figure. The solid theoretical curve correspond to the data points. The dashed-dotted curve is the curve for an aluminum mirror, the dashed curve for a gold mirror ( $\rho_o = 15$  mm for both).

and the scattering object, respectively. We have theoretically investigated also a geometry which is finite in two directions instead of one, and found no qualitative difference with the slab.

As is shown in Eq. (4.56) the sensitivity in a transmission experiment when the object is not close to a boundary is the same for an infinite medium and for a medium with mirrors. The amount of reflection is not very important in this case, as can be observed in Fig. 4.6. When the object is closer to the boundary, one can again observe differences between good and not so good mirrors.

The results shown in Fig. 4.7 are noisy, due to the smallness of  $\Delta\Phi_p/\Phi_0$ . A systematic shift can be observed between the data points of the absorbing medium and the theory. Again this is either due to a drift in the detector, or a small error in determining the position of the object, which result in larger errors after the subtraction of two measurements. Qualitatively there is only a slight difference between the different boundaries in this case.

### 4.2.5 Absorbing boundaries

Using the experimental results we could already qualitatively compare the absorbing boundary with the infinite medium. Here we will give some quantitative results to compare the infinite medium with media having absorbing boundaries. To find simple expressions in the case of absorbing boundaries we will take  $\xi = \xi_{\text{in}} + \xi_{\text{ext}}$  small. This results in approximate expressions that can be used for qualitative discussions. Since the model point source is very close to the boundary, we can take the terms in Eq. (4.53) pairwise together

$$G_{\infty}(\mathbf{r}, \mathbf{r}_s) - G_{\infty}(\mathbf{r}, \mathbf{r}_s - 2\xi\hat{\mathbf{z}}) \simeq 2\xi\hat{\mathbf{z}} \cdot \nabla_{\mathbf{r}_s} G_{\infty}(\mathbf{r}_d, \mathbf{r}_s - \xi\hat{\mathbf{z}}). \quad (4.58)$$

We note that the argument  $\mathbf{r}_s - \xi\hat{\mathbf{z}} \equiv \tilde{\mathbf{r}}_s$  is a point at the (extrapolated) boundary. Using Eq. (4.58) we can write for the total Green function for the slab

$$G_L(\mathbf{r}, \mathbf{r}_s) = 2\xi\hat{\mathbf{z}} \cdot \nabla_{\tilde{\mathbf{r}}_s} \sum_m G_{\infty}(\mathbf{r}, \tilde{\mathbf{r}}_s + 2mL\hat{\mathbf{z}}). \quad (4.59)$$

Since the Green function for the infinite medium depends only on the difference between the two points  $\mathbf{r}$  and  $\mathbf{r}'$ , i.e.  $G_{\infty}(\mathbf{r}, \mathbf{r}') = G_{\infty}(\mathbf{r} - \mathbf{r}')$ , we can write the Green function for light going to the detector at position  $\mathbf{r}_d$  as

$$G_L(\mathbf{r}_d, \mathbf{r}) = \pm 2\xi\hat{\mathbf{z}} \cdot \nabla_{\tilde{\mathbf{r}}_d} \sum_m G_{\infty}(\tilde{\mathbf{r}}_d + 2mL\hat{\mathbf{z}}, \mathbf{r}). \quad (4.60)$$

Here  $\tilde{\mathbf{r}}_d = \mathbf{r}_d \mp \xi\hat{\mathbf{z}}$  is also a point at the (extrapolated) boundary. The upper signs belong to a reflection measurement, where the detected light propagates in the negative  $z$ -direction. The lower signs corresponds to a transmission measurement. There can however be no doubt which sign to take, since the Green function is always positive.

For calculating  $G_L(\mathbf{r}_d, \mathbf{r}_s)$  we can use Eq. (4.59) and evaluate it at  $\mathbf{r}_d = \tilde{\mathbf{r}}_d \pm \xi\hat{\mathbf{z}}$ . We again use the derivative with respect to  $\tilde{\mathbf{r}}_d$  to find  $G_L(\mathbf{r}_d, \mathbf{r}_s) = \pm \xi\hat{\mathbf{z}} \cdot \nabla_{\tilde{\mathbf{r}}_d} G_L(\tilde{\mathbf{r}}_d, \mathbf{r}_s)$ . The photon density can now easily be found. When only one absorbing object is present with strength  $q$  we find

$$\begin{aligned} \Phi_L(\mathbf{r}_d) &= \frac{S_{\omega}}{D} \left( G_L(\mathbf{r}_d, \mathbf{r}_s) + \frac{4\pi q}{\kappa_0} G_L(\mathbf{r}_d, \mathbf{r}_o) G_L(\mathbf{r}_o, \mathbf{r}_s) \right) \\ &= \pm 2\xi^2 \frac{S_{\omega}}{D} (\hat{\mathbf{z}} \cdot \nabla_{\tilde{\mathbf{r}}_s}) (\hat{\mathbf{z}} \cdot \nabla_{\tilde{\mathbf{r}}_d}) \sum_m \left[ G_{\infty}(\tilde{\mathbf{r}}_d, \tilde{\mathbf{r}}_s + 2mL\hat{\mathbf{z}}) \right. \\ &\quad \left. + 2 \frac{4\pi q}{\kappa_0} \sum_{m'} G_{\infty}(\tilde{\mathbf{r}}_d + 2m'L\hat{\mathbf{z}}, \mathbf{r}_o) G_{\infty}(\mathbf{r}_o, \tilde{\mathbf{r}}_s + 2mL\hat{\mathbf{z}}) \right]. \quad (4.61) \end{aligned}$$

In general the sums over  $m$  and  $m'$  will only have a few terms that are important, due to the exponential decay of  $G_\infty$ .

Let us first consider the semi-infinite medium. Since  $L \rightarrow \infty$  we only have to take  $m = m' = 0$  in the sums. Furthermore, only measurements in reflection are possible. We find from Eq. (4.61) that

$$\Phi_s(r_d) = \frac{2\xi^2 S_\omega}{D} (\hat{\mathbf{z}} \cdot \nabla_{\tilde{\mathbf{r}}_s})(\hat{\mathbf{z}} \cdot \nabla_{\tilde{\mathbf{r}}_d}) \left[ G_\infty(\tilde{\mathbf{r}}_d, \tilde{\mathbf{r}}_s) + \frac{8\pi q}{\kappa_0} G_\infty(\tilde{\mathbf{r}}_d, \mathbf{r}_o) G_\infty(\mathbf{r}_o, \tilde{\mathbf{r}}_s) \right]. \quad (4.62)$$

We can compare this to the equation we would have found in the infinite medium,

$$\Phi_\infty(r_d) = \frac{S_\omega}{D} \left[ G_\infty(\mathbf{r}_d, \mathbf{r}_s) + \frac{4\pi q}{\kappa_0} G_\infty(\mathbf{r}_d; \mathbf{r}_o) G_\infty(\mathbf{r}_o; \mathbf{r}_s) \right]. \quad (4.63)$$

So basically the photon density at the detector for the semi-infinite medium is given by that for the infinite medium, differentiated to both source and detector position. Furthermore we see that an extra factor 2 appeared in front of  $q$ . This enhancement is similar to that of Eq. (4.55). The sensitivity to absorption  $Q = (\Phi - \Phi_0)/q\Phi_0$  can be found rather easily from the expressions above.

As an example let us consider the case where source, object and detector are all in the same plane (see Fig.4.1). Only the depth  $d$  of the object into the medium, and the lateral distances  $\rho_d$  and  $\rho_o$  are of importance. Define  $d_s = z_o - z_s$  and  $d_d = z_o - z_d$ . Of course,  $d_d$  and  $d_s$  have the same value  $d$ , but the functional dependence of  $\Phi$  on both differs. Hence we have to consider them separately when taking derivatives. The two differential operators become

$$(\hat{\mathbf{z}} \cdot \nabla_{\tilde{\mathbf{r}}_{s,d}}) \rightarrow -\frac{\partial}{\partial d_{s,d}}. \quad (4.64)$$

Three distances are needed:  $r_1$  from source to object,  $r_2$  from object to detector, and  $r_{12}$  from source to detector. They are given by

$$r_1 = \sqrt{\rho_o^2 + d_s^2}; \quad r_2 = \sqrt{(\rho_o - \rho_d)^2 + d_d^2}; \quad r_{12} = \sqrt{\rho_d^2 + (d_d - d_s)^2}. \quad (4.65)$$

We calculate the photon density  $\Phi_\infty$  for the infinite geometry and  $\Phi_s$  for the semi-infinite geometry, both at the detector position  $r_d$ . The results are

$$\Phi_{\infty,0} = \frac{S_\omega}{4\pi D} \frac{1}{r_{12}} e^{-\kappa r_{12}}, \quad (4.66a)$$

$$\Delta\Phi_\infty = \frac{S_\omega}{4\pi D} \left( \frac{q}{\kappa_0 r_1 r_2} e^{-\kappa(r_1+r_2)} \right), \quad (4.66b)$$

$$\Phi_{s,0} = \frac{S_\omega}{4\pi D} 2\xi^2 \frac{1 + \kappa r_{12}}{r_{12}^3} e^{-\kappa r_{12}}, \quad (4.66c)$$

$$\Delta\Phi_s = \frac{S_\omega}{4\pi D} \left( 4q\xi^2 d^2 \frac{(1 + \kappa r_1)(1 + \kappa r_2)}{\kappa_0 r_1^3 r_2^3} e^{-\kappa(r_1+r_2)} \right). \quad (4.66d)$$

From these results we calculate the sensitivities

$$Q_\infty = \frac{r_{12}}{\kappa r_1 r_2} e^{-\kappa_0(r_1+r_2-r_{12})}, \quad (4.67a)$$

$$Q_s = 2 \frac{(1 + \kappa r_1)(1 + \kappa r_2)}{1 + \kappa r_{12}} \frac{d^2 r_{12}^2}{r_1^2 r_2^2} Q_\infty. \quad (4.67b)$$

We note that these do no longer depend on the value of  $\xi$ . The expressions for the sensitivity for scattering can be calculated readily, but are rather lengthy, and will not be presented here.

In many practical cases the ratio  $dr_{12}/r_1 r_2$  will be of the order of unity. Only when the source-detector distance remains fixed and the objects are far away from both, this ratio decreases. But then the influence of the object on the measurement is negligible, due to the exponential decay of  $Q$ . Hence, in practice,  $Q_s/Q_\infty$  is of the same order as  $(1 + \kappa r_{12})$  (which means order 1 if  $\kappa r_{12} \ll 1$  and order  $\kappa r_{12}$  when  $\kappa r_{12} \gg 1$ ). The black boundary can therefore increase sensitivity. A price has to be paid however. The total intensity detected in the semi-infinite system will be largely decreased with respect to the infinite medium. This can be seen from the ratio

$$\frac{\Phi_{\infty,0}}{\Phi_{s,0}} = 2 \left( \frac{\xi}{r_{12}} \right)^2 (1 + \kappa r_{12}), \quad (4.68)$$

which is always small ( $\xi \simeq \mu_s^{-1}$ ). (We always assume source-detector distances to be larger than a few scattering lengths.) The decrease in intensity due to the finiteness of the medium is mainly due to a loss of intensity at the boundary close to the source and close to the detector.

For the quantitative discussion in the slab geometry we consider only the situation where source, detector and object are on the same line,  $\rho_o = \rho_d = 0$ . Furthermore we assume that the object is not too close to the boundary. Then the result [taking only the most important terms in the sum of Eq. (4.61)] is

$$Q_\infty = \frac{L}{\kappa_0 r_1 r_2}, \quad (4.69a)$$

$$Q_{\text{slab}} = \frac{L^2}{r_1 r_2} \frac{(1 + \kappa r_1)(1 + \kappa r_2)}{2 + 2\kappa L + \kappa^2 L^2} Q_{\infty}, \quad (4.69b)$$

$$P_{\infty} = \frac{(1 + \kappa r_1)(1 + \kappa r_2)L}{\kappa_0^3 r_1^2 r_2^2}, \quad (4.69c)$$

$$P_{\text{slab}} = \frac{(2 + 2\kappa r_1 + \kappa^2 r_1^2)(2 + 2\kappa r_2 + \kappa^2 r_2^2)L^3}{(2 + 2\kappa L + \kappa^2 L^2)\kappa_0^3 r_1^3 r_2^3}. \quad (4.69d)$$

Note that  $r_1 + r_2 = L$ . From this we find that for large  $\kappa$  there is no difference in the sensitivities between the slab and the infinite system. This is basically due to the fact that for large absorption a boundary has only a local effect. At the position of the object the difference between a source at a boundary and a source in an infinite medium is no longer visible, apart from an overall prefactor. The same holds for the boundary at the position of the detector. Therefore the sensitivity is the same in both cases. In a reflection measurement this is not true since the propagation of light from source to detector is everywhere influenced by the boundary. For small  $\kappa$  the sensitivity  $Q_{\text{slab}}$  will be a factor  $L^2/2r_1 r_2 > 2$  larger than  $Q_{\infty}$  and  $P_{\text{slab}}$  will be even a factor  $2L^2/r_1 r_2 > 8$  larger than  $P_{\infty}$ . From the expressions we also see that the sensitivities can be large for small  $r_1$  or  $r_2$ , increasing the sensitivity when the object is close to the source or detector, even more so when the boundaries are absorbing. The expressions (4.69) are however are no longer correct close to the boundary.

Again we note that the enhancement is relatively small, compared to the loss in detected signal. The ratio between the detected signals in this geometry is given by

$$\frac{\Phi_{\text{slab}}}{\Phi_{\infty}} = \left(\frac{\xi}{L}\right)^2 (2 + 2\kappa L + \kappa^2 L^2). \quad (4.70)$$

As was the case in the semi-infinite geometry, this ratio is small, mainly due to the  $\xi^2$  term, which is a result from the boundary. Hence again a large price has to be paid to increase sensitivity.

In comparing the infinite medium with the semi-infinite medium with absorbing boundaries we comment on some other features. Consider anew Fig. 4.3. All curves show a maximum at some depth  $d$  and a decrease in the sensitivity for larger depths. The difference between the different boundaries seems to be only in the position of this maximum, giving the position of the maximal sensitivity. The sensitivities for an infinite medium are centered around the line between source and detector. One can say that the photon density wave propagates along this line, although of course

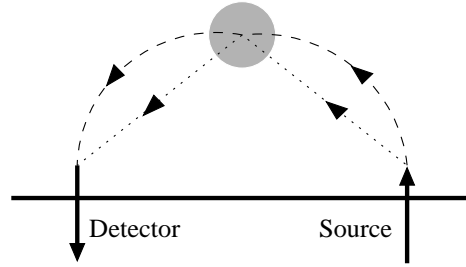


**Figure 4.8:** Schematic view of the propagation of photon density waves in a reflection measurement, as schematically shown in Fig. 4.1. The arrows show the average direction of the photon density flow. The two thick arrows show the propagation if light in and just outside the source and detector fiber. The dotted arrows are for an infinite medium, where propagation is direct. The dashed arrows are for a semi-infinite medium with absorbing boundaries, where the propagation avoids the boundary.

single light paths can be much more complex. For absorbing boundaries the Green functions and therefore the sensitivities (almost) vanish at the boundaries. This implies that when the line between source and detector lies close to a boundary, the centerline of the sensitivity — the line where for different  $\rho_0$  the maximum value of  $Q$  can be found — will curve away from this boundary. Consequently the propagation direction will be curved (see Fig. 4.8). The maximum shown in Fig. 4.3 lies away from the boundary, at larger depths than that of the infinite medium (or medium with reflecting boundaries). This means that the semi-infinite medium is not really more sensitive to absorbing objects, but rather the spatial location of this sensitivity is changed.

As a next point, we note that the strength  $p$  of the scattering object, [calculated using Eq. (4.23)] is about 4 times as small as that of the absorbing object we used. Furthermore, the scattering object is large and therefore it has some parts in regions with low sensitivity for scattering. Nonetheless the measured effects are almost as big as those of absorbing objects, at least in reflection measurements. Therefore the sensitivity for scattering  $P$  is in general larger than the sensitivity for absorption  $Q$ . The difference of about a factor 5 appears mainly close to the boundary, and for absorbing boundaries almost everywhere. The latter is due to two reasons. First of all scattering objects have an influence which scales with the gradient of the Green function, rather than with the Green function itself. Since the decrease of  $G$  is larger for an absorbing boundary, the sensitivity will

increase. Secondly, consider the position at  $\rho_o = 15$  mm and  $d = 10$  mm, which can be found in both Fig. 4.2 and 4.3. For the infinite medium, an extra term  $\cos \theta$  appears, where  $\theta$  is the angle between the source-object and the object-detector line. This term enters due to the inner product. In the semi-infinite medium however, the angle  $\theta$ , which is the angle between the two gradients of the Green function, will be smaller. This reflects a photon density wave that does not propagate straight from source to object. As discussed before and shown schematically in Fig. 4.8, the propagation will rather be curve-linear due to the absorbing boundary. Upon arriving at the object, it will propagate more parallel to the boundary than in the infinite medium. Also the propagation from object to detector will be such that its direction at the object is almost parallel to the boundary. The effective  $\cos \theta$  will therefore be larger than in the infinite medium.

The difference between the sensitivities for absorption and scattering implies that  $|\Delta\Phi/\Phi_0|$  for an object with a given  $\Delta D/D$  is larger than for an object with the same  $\Delta\mu_a/\mu_a$ . In practice however the variation in absorption can be an order of magnitude larger than the variation in scattering. Therefore measurements will in general be more sensitive to absorption than to scattering.

### 4.3 Conclusions

We have studied the influence of different boundaries on the detection of objects. To do this we started with a derivation of the expressions that give the values of the photon density — which are proportional to measurements — when the optical parameters are not constant, but rather vary in space. We have shown a clear distinction between geometrical factors, given by the sensitivities  $Q$  and  $P$ , and the strength of (small) objects  $q$  and  $p$ . These can be calculated independently. We have shown how to calculate the strengths even when the scattering or absorption in the object is not small and have improved the expressions from the literature for a completely black spherical object.

The experiments we performed are done with a cylindrical object, while the theoretical value of  $q$  was derived only for a spherical object. From this we note two things. First, experimentally it is nearly impossible to see the difference between different shapes of objects, in our case a sphere and a cylinder. As mentioned before, this means that for small objects only the value  $q$  (or  $p$ ) can be measured, and that nearly nothing about precise shape can be found. Secondly, even though we did not calculate the ex-

act value of  $q$  for a cylindrical object, we are able to give a rather good estimate using the theory for a sphere.

Next we have compared the different boundaries. For a boundary of a good mirror, such as gold, the sensitivity is merely a constant times the sensitivity of an infinite medium. This constant is nearly two for a measurement in reflection and approximately one for a measurement in transmission. For a medium with absorbing boundaries the sensitivity in reflection can become rather large, when the decay constant  $\kappa$  is large, compared to the inverse source-detector distance. For moderate  $\kappa$  however, the difference with an infinite medium lies mainly in the spatial position of the sensitivity, rather than in a difference between the values themselves. Close to absorbing boundaries the sensitivity vanishes. For a system bounded by a not so good mirror, like the aluminum mirror we used in the experiments, the sensitivity is in between that of an infinite medium and that with absorbing boundaries.

Considering the effects of sensitivity to the object and total intensity detected, we see that there is a trade-off between the two. Since the effect of loss of intensity when using black boundaries is much larger than the loss of sensitivity, we argue that for detecting objects an infinite system, or one with good mirrors, is better than a finite one, or one with not so good mirrors. Furthermore the infinite medium has another advantage: formulas, like those for the photon density and sensitivities, will be more simpler. This simplifies the reconstruction. Since in practice an infinite medium is difficult to achieve in the circumstances needed for medical imaging, a finite system with a rather good reflecting boundary resembles the infinite medium enough to be a useful for both forward calculations and for reconstruction techniques.



## Bibliography

- [1] P. N. den Outer, Th. M. Nieuwenhuizen, and A. Lagendijk, *J. Opt. Soc. Am. A* **10**, 1209 (1993).
- [2] X. D. Zhu, S. Wei, S. C. Feng, and B. Chance, *J. Opt. Soc. Am. A* **13**, 494 (1996).
- [3] R. C. Haskell, L. O. Svaasand, T. Tsay, T. Feng, M. S. McAdams, and B. J. Tromberg, *J. Opt. Soc. Am. A* **11**, 2727 (1994).
- [4] A. Ishimaru, *Wave Propagation and Scattering in Random Media* (Academic, New York, 1978).
- [5] W. M. Star, in *Optical-thermal Response of Laser-Irradiated Tissue*, edited by A. J. Welch and M. J. C. van Gemert (Plenum, New York, 1995).
- [6] D. A. Boas, M. A. O'Leary, B. Chance, and A. G. Yodh, *Proc. Nat. Acad. Sci. USA* **91**, 4887 (1994).
- [7] A. Ya. Polishchuk, S. Gutman, M. Lax, and R. R. Alfano, *J. Opt. Soc. Am. A* **14**, 230 (1997).
- [8] K. Furutsu and Y. Yamada, *Phys. Rev. E* **50**, 3634 (1994).
- [9] M. Bassani, F. Martelli, G. Zaccanti, and D. Contini, *Opt. Lett.* **22**, 853 (1997).
- [10] K. M. Case and P. F. Zweifel, *Linear Transport Theory* (Addison-Wesley, Reading, 1967).
- [11] R. Freyer, U. Hampel, M. Forejtek, and C. T. Luu, in *Progress in Biomedical Optics; Proceedings of Photon Propagation in Tissues*, edited by B. Chance, D. T. Delpy, G. J. Müller, and A. Katzir, Vol. 2626 (SPIE, Barcelona, 1995).
- [12] M. R. Ostermeyer and S. L. Jacques, *J. Opt. Soc. Am. A* **14**, 255 (1997).
- [13] S. R. Arridge, M. Schweiger, M. Hiraoka, and D. T. Delpy, *Med. Phys.* **20**, 299 (1993).
- [14] H. Jiang, K. D. Paulsen, and U. L. Österberg, *Phys. Med. Biol.* **41**, 1483 (1996).

- [15] S. B. Colak, D. G. Papaioannou, G. W. 't Hooft, M. B. van der Mark, H. Schomberg, J. C. J. Paasschens, J. B. M. Melissen, and N. A. A. J. van Asten, *Appl. Opt.* **36**, 180 (1997).
- [16] Y. Yao, Y. Wang, Y. Pei, W. Zhu, and R. L. Barbour, *J. Opt. Soc. Am. A* **14**, 325 (1997).
- [17] W. Zhu, Y. Wang, Y. Yao, J. Chang, H. L. Graber, and R. L. Barbour, *J. Opt. Soc. Am. A* **14**, 799 (1997).
- [18] S. Feng, F. Zeng, and B. Chance, in *Progress in Biomedical Optics; Proceedings of Photon Migration and Imaging in Random Media and Tissues*, edited by B. Chance, R. R. Alfano, and A. Katzir, Vol. 1888 (SPIE, Los Angeles, 1993).
- [19] J. C. Schotland, J. C. Haselgrove, and J. S. Leigh, *Appl. Opt.* **32**, 448 (1993).
- [20] S. Feng, F. Zeng, and B. Chance, *Appl. Opt.* **34**, 3826 (1995).
- [21] Th. M. Nieuwenhuizen and M. C. W. van Rossum, *Phys. Lett. A* **177**, 102 (1993).
- [22] J. X. Zhu, D. J. Pine, and D. A. Weitz, *Phys. Rev. A* **44**, 3948 (1991).
- [23] R. Aronson, in *Progress in Biomedical Optics; Proceedings of Photon Migration and Imaging in Random Media and Tissues*, edited by B. Chance, R. R. Alfano, and A. Katzir, Vol. 1888 (SPIE, Los Angeles, 1993).
- [24] Th. M. Nieuwenhuizen and J. M. Luck, *Phys. Rev. E* **48**, 569 (1993).
- [25] D. J. Durian, *Phys. Rev. E* **50**, 857 (1994).
- [26] C. P. Gonatas, M. Miwa, M. Ishii, J. Schotland, B. Chance, and J. S. Leigh, *Phys. Rev. E* **48**, 2212 (1993).
- [27] S. Chandrasekhar, *Radiative Transfer* (Dover, New York, 1960).
- [28] S. R. Arridge, M. Cope, and D. T. Delpy, *Phys. Med. Biol.* **37**, 1531 (1992).
- [29] S. Fantini, M. A. Franceschini, and E. Gratton, *J. Opt. Soc. Am. B* **11**, 2128 (1994).
- [30] M. S. Patterson, B. Chance, and B. C. Wilson, *Appl. Opt.* **28**, 2331 (1989).

## 5 Probability of reflection by a random laser

Recent experiments on turbid laser dyes [1–4] have drawn attention to the remarkable properties of amplifying disordered media. The basic issue is to understand the interplay of phase-coherent multiple scattering and amplification (or absorption) of radiation. A quantity which measures this interplay is the albedo  $a$ , which is the power reflected by the medium divided by the incident power. A thick disordered slab which is optically passive has  $a = 1$ . Absorption leads to  $a < 1$  and amplification to  $a > 1$ . As the amplification increases the laser threshold is reached, at which the average albedo becomes infinitely large [5]. Such a generator was referred to by its inventor V. S. Letokhov as a “laser with incoherent feedback” [6], because the feedback of radiation is provided by random scattering and not by mirrors — as in a conventional laser.

The current renewed interest in random lasers owes much to the appreciation that randomness is not the same as incoherence. Early theoretical work on this problem was based on the equation of radiative transfer [7], which ignores phase coherence. Zyuzin [8] and Feng and Zhang [9] considered interference effects on the average albedo  $\bar{a}$ , averaged over different configurations of the scattering centra. Their prediction of a sharpening of the backscattering peak in the angular distribution of the average reflected intensity has now been observed [3]. The other basic interference effect is the appearance of large, sample-specific fluctuations of the albedo around its average. These diverge faster than the average on approaching the laser threshold [10], so that  $\bar{a}$  is no longer characteristic for the albedo of a given sample. In this chapter we will show that, while all moments of the distribution function  $P(a)$  of the albedo diverge at the laser threshold, its modal value  $a_{\max}$  remains finite. The modal value is the value of  $a$  at which  $P(a)$  is maximal, and hence it is the most probable value measured in a single experiment. The diagrammatic perturbation theory of Refs. [8–10] can only give the first few moments of  $a$ , and hence can not determine  $a_{\max}$ . Here we develop a non-perturbative random-matrix theory for the entire distribution of the reflection matrix, from which  $P(a)$  can be computed directly.

We contrast the two cases of absorption and amplification. In the case of absorption,  $P(a)$  is a Gaussian with a width  $\delta a$  smaller than the average  $\bar{a}$  by an order  $1/N$ , where  $N \simeq S/\lambda^2 \gg 1$  is the number of modes associated

with an illuminated area  $S$  and wavelength  $\lambda$ . In the case of amplification, both  $\delta a$  and  $\bar{a}$  increase strongly on approaching the laser threshold — in a manner which we compute precisely. Below threshold, the mean and modal value of  $a$  coincide. Above threshold, the mean is infinite while the modal value is found to be

$$a_{\max} = 1 + 0.8\gamma N. \quad (5.1)$$

Here  $\gamma$  denotes the amplification per mean free path, assumed to be in the range  $N^{-2} \ll \gamma \ll 1$ . The existence of a finite  $a_{\max}$  is due to the finiteness of the number of modes  $N$  in a surface area  $S$  (ignored in radiative transfer theory). Since  $a_{\max}$  scales with  $N$  and hence with  $S$ , and the incident power scales with  $S$ , it follows that the reflected power scales *quadratically* rather than *linearly* with the illuminated area. We suggest the name “superreflection” for this phenomenon. To measure the albedo in the unstable regime above the laser threshold we propose a time-resolved experiment, consisting of illumination by a short intense pulse to pump the medium beyond threshold, rapidly followed by a weak pulse to measure the reflected intensity before spontaneous emission has caused substantial relaxation.

Our work on this problem was motivated by a recent paper by Pradhan and Kumar [11] on the case  $N = 1$  of a single-mode waveguide. We discovered the anomalous scaling with area in an attempt to incorporate the effects of mode-coupling into their approach.

## 5.1 Calculation of the albedo

We consider the reflection of a monochromatic plane wave (frequency  $\omega$ , wavelength  $\lambda$ ) by a slab (thickness  $L$ , area  $S$ ) consisting of a disordered medium (mean free path  $l$ ) which either amplifies or absorbs the radiation. We denote by  $\sigma$  the amplification per unit length, a negative value of  $\sigma$  indicating absorption. The parameter  $\gamma = \sigma l$  is the amplification (or absorption) per mean free path. We treat the case of a scalar wave amplitude, and leave polarization effects for future study. A discrete number  $N$  of scattering channels is defined by imbedding the slab in an optically passive waveguide without disorder (see Fig. 5.1, inset). The number  $N$  is the number of modes which can propagate in the wave guide at frequency  $\omega$ . The  $N \times N$  reflection matrix  $\mathbf{r}$  contains the amplitudes  $r_{mn}$  of waves reflected into mode  $m$  from an incident mode  $n$ . (The basis states of  $r$  are normalized such that each carries unit power.) The reflection eigenvalues  $R_n$  ( $n = 1, 2, \dots, N$ ) are the eigenvalues of the matrix product  $\mathbf{r}\mathbf{r}^\dagger$ . The

matrix  $\mathbf{r}$  is determined by the  $R_n$ 's and by a unitary matrix  $U$ ,

$$r_{mn} = \sum_k U_{mk} U_{nk} \sqrt{R_k}. \quad (5.2)$$

Note that  $r_{mn} = r_{nm}$  because of time-reversal symmetry. From  $\mathbf{r}$  one can compute the albedo  $a$  of the slab, which is the ratio of the reflected and incident power:

$$a = \sum_m |r_{mn}|^2 = \sum_k U_{nk} U_{nk}^* R_k. \quad (5.3)$$

For a statistical description we consider an ensemble of slabs with different configurations of scatterers. As in earlier work on optically passive media [12], we make the isotropy assumption that the matrix  $U$  is uniformly distributed in the unitary group. This assumption breaks down if the transverse dimension  $W$  of the slab is much greater than its thickness  $L$ , but is expected to be reasonable if  $W \lesssim L$ . As a consequence of isotropy,  $a$  becomes statistically independent of the index  $n$  of the incident mode. We further assume that the wavelength  $\lambda$  is much smaller than both the mean free path  $l$  and the amplification length  $1/\sigma$ . The evolution of the reflection eigenvalues with increasing thickness  $L$  of the slab can then be described by a Brownian motion process. To describe this evolution it is convenient to use the parametrization

$$R_n = 1 + \mu_n^{-1}, \quad \mu_n \in (-\infty, -1) \cup (0, \infty). \quad (5.4)$$

The  $L$ -dependence of the distribution  $P(\mu_1, \mu_2, \dots, \mu_N)$  of the  $\mu$ 's is governed by the Fokker-Planck equation

$$l \frac{\partial P}{\partial L} = \frac{2}{N+1} \sum_{i=1}^N \frac{\partial}{\partial \mu_i} \mu_i (1 + \mu_i) \left[ \frac{\partial P}{\partial \mu_i} + P \sum_{j \neq i} \frac{1}{\mu_j - \mu_i} \gamma(N+1) P \right], \quad (5.5)$$

with initial condition  $\lim_{L \rightarrow 0} P = N \prod_i \delta(\mu_i + 1)$ . In the single-channel case ( $N = 1$ ), the term  $\sum_{j \neq i}$  is absent and Eq. (5.5) reduces to the differential equation studied by Pradhan and Kumar [11, 13]. The multi-channel case is essentially different due to the coupling of the eigenvalues by the term  $\sum_{j \neq i} (\mu_j - \mu_i)^{-1}$ . This term induces a *repulsion* of closely separated eigenvalues. Equation (5.5) with  $\gamma = 0$  is known as the Dorokhov-Mello-Pereyra-Kumar (DMPK) equation [14, 15], and has been studied extensively in the context of electronic conduction [16]. We have generalized the derivation to  $\gamma \neq 0$ , by adapting the approach of Ref. [15] to a non-unitary scattering matrix. Details of this derivation are given in chapter 7.

The average  $\bar{a} \equiv \langle a \rangle$  and the variance  $\text{Var } a \equiv \langle (a - \bar{a})^2 \rangle$  of the albedo (5.3) can be computed by first averaging  $U$  over the unitary group and

then evaluating moments of the  $R_k$ 's by means of Eq. (5.5) [17]. In the limit  $N \rightarrow \infty$  we obtain the differential equations

$$l \frac{d}{dL} \bar{a} = (\bar{a} - 1)^2 + 2\gamma \bar{a}, \quad (5.6a)$$

$$l \frac{d}{dL} \text{Var } a = 4(\bar{a} - 1 + \gamma) \text{Var } a + 2N^{-1} \bar{a}(\bar{a} - 1)^2. \quad (5.6b)$$

Corrections are smaller by a factor  $|\gamma N^2|^{-1/2}$ , which we assume to be  $\ll 1$ . Equation (5.6a) for the average albedo is a known result of radiative transfer theory [18]. Equation (5.6b) for the variance is new. It describes the sample-specific fluctuations of the albedo due to interference of multiply scattered waves. Integration of Eq. (5.6) yields

$$\bar{a} = 1 - \gamma + (2\gamma - \gamma^2)^{1/2} \tan t, \quad (5.7a)$$

$$\begin{aligned} \text{Var } a = (8N \cos^4 t)^{-1} & \left( 4\gamma(1 - 2\gamma)L/l + 2\gamma(1 + \gamma) - 4\gamma^2 \cos 2t \right. \\ & + 2\gamma(1 - \gamma) \cos 4t + (2 - \gamma)^{-1}(2\gamma - \gamma^2)^{1/2} \\ & \left. \times [4\gamma(1 - \gamma) \sin 2t - (1 - 4\gamma + 2\gamma^2) \sin 4t] \right). \end{aligned} \quad (5.7b)$$

We have abbreviated  $t = (2\gamma - \gamma^2)^{1/2} L/l - \arcsin(1 - \gamma)$ .

Plots of Eq. (5.7) as a function of  $\gamma$  are shown in Fig. 5.1, for two values of  $L/l$ . (The data points are numerical simulations, discussed later.) In the case of absorption ( $\gamma < 0$ ), the large- $L$  limits

$$\bar{a}_\infty = 1 - \gamma - (\gamma^2 - 2\gamma)^{1/2}, \quad (5.8a)$$

$$\text{Var } a_\infty = \frac{1}{2N} \frac{\bar{a}_\infty(1 - \bar{a}_\infty)^2}{1 - \gamma - \bar{a}_\infty}, \quad (5.8b)$$

can be obtained directly from Eq. (5.6) by equating the right-hand-side to zero. The limit (5.8) is reached when  $L/l \gg (\gamma^2 - 2\gamma)^{-1/2}$ . In the case of amplification ( $\gamma > 0$ ), Eq. (5.7) holds for  $L$  smaller than the critical length

$$L_c = l(2\gamma - \gamma^2)^{-1/2} \arccos(\gamma - 1) \quad (5.9)$$

at which  $\bar{a}$  and  $\text{Var } a$  diverge. This is the laser threshold [5, 18]. For  $\gamma < 0$  the large- $L$  limit of the probability distribution  $P(a)$  of the albedo is well described by a Gaussian, with mean and variance given by Eq. (5.8a). (The tails are non-Gaussian, but carry negligible weight.) The modal value  $a_{\max}$  of the albedo equals  $\bar{a}$ . For  $\gamma > 0$  the large- $L$  limit of  $P(a)$  can not be reconstructed from its moments, but needs to be determined directly. We will see that while  $\bar{a}$  diverges,  $a_{\max}$  remains finite.

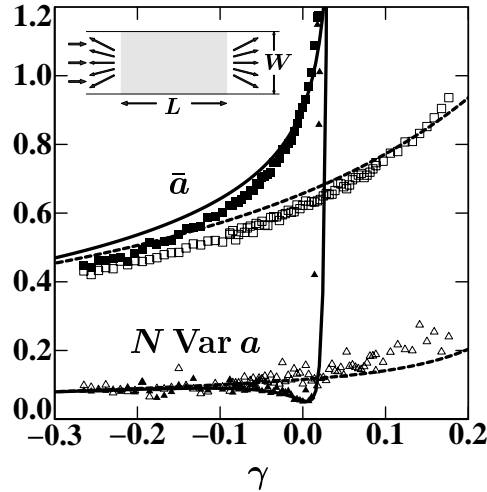


**Figure 5.1:** Comparison between theory and simulation of the average albedo  $\bar{a}$  (upper curves, squares) and the variance  $\text{Var } a$  (lower curves, triangles) for  $L/l = 1.92$  (dashed curves, open markers) and  $L/l = 9.58$  (solid curves, filled markers). Negative  $\gamma$  corresponds to absorption, positive  $\gamma$  to amplification. The curves are the theoretical result (5.7). The data points are a numerical simulation of a two-dimensional lattice ( $L = 50d$  and  $250d$ ;  $W = 51d$ ,  $N = 21$ ), averaged over 100 realizations of the disorder. The inset shows schematically the system under consideration.

## 5.2 Probability distribution of the albedo

The large- $L$  limit  $P_\infty(\mu_1, \mu_2, \dots, \mu_N)$  of the distribution of the  $\mu$ 's is obtained by equating to zero the expression between square brackets in Eq. (5.5). The result is

$$P_\infty = C \prod_i \exp\left(-\gamma(N+1)\mu_i\right) \prod_{i < j} |\mu_j - \mu_i|, \quad (5.10)$$

with  $C$  a normalization constant. Equation (5.10) holds for both positive and negative  $\gamma$ , but the support of  $P_\infty$  depends on the sign of  $\gamma$ : All  $\mu$ 's have to be  $> 0$  for  $\gamma > 0$  (amplification) and  $< -1$  for  $\gamma < 0$  (absorption). In what follows we take  $\gamma > 0$ . The function (5.10) is known in random-matrix theory as the distribution of the *Laguerre ensemble* [19]. The density  $\rho(\mu) = \langle \sum_i \delta(\mu - \mu_i) \rangle$  of the  $\mu$ 's is a series of Laguerre polynomials, hence

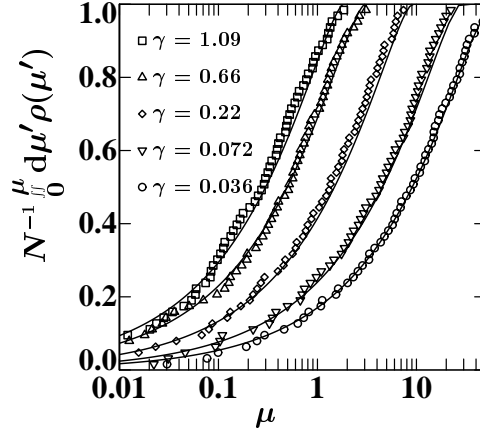


**Figure 5.2:** Comparison between theory and simulation of the cumulative density of the variables  $\mu_n$  (related to the reflection eigenvalues by  $R_n = 1 + \mu_n^{-1}$ ). Curves are computed from the density (5.11) of the Laguerre ensemble; data points are from the simulation ( $L = 500d = 19.2l$ ,  $W = 151d$ ,  $N = 63$ ), for a single realization of the disorder. (This is sufficient, since fluctuations in the  $\mu_n$ 's are small, of the order of their spacing.)

the name. For  $\gamma N^2 \gg 1$  one has asymptotically

$$\rho(\mu) = (N/\pi) \left( 2\gamma/\mu - \gamma^2 \right)^{1/2}, \quad 0 < \mu < 2/\gamma. \quad (5.11)$$

The square-root singularity at  $\mu = 0$  in Eq. (5.11) is cut off in the exact density [20], such that  $\rho = \gamma N^2$  if  $\mu \lesssim 1/\gamma N^2$ . The cumulative density is plotted in Fig. 5.2, together with the numerical simulations (discussed below).

We seek the distribution function of the albedo

$$P(a) = \left\langle \delta \left( a - 1 - \sum_k U_{nk} U_{nk}^* \mu_k^{-1} \right) \right\rangle. \quad (5.12)$$

The average  $\langle \dots \rangle$  consists of the average of  $U$  over the unitary group followed by the average of the  $\mu_k$ 's over the Laguerre ensemble. The averages can be done analytically for  $N^{-2} \ll \gamma \ll 1$  (in the continuum approximation [21], i.e. by ignoring the discreteness of the eigenvalues), and numerically for any  $N, \gamma$  (by Monte Carlo integration, i.e. by randomly sampling the Laguerre ensemble).

The analytical result is an inverse Laplace transform,

$$P(a) = \frac{1}{2\gamma N} \int_{-i\infty}^{i\infty} \frac{ds}{2\pi i} \exp \left[ \frac{1}{2} s(a-1)/\gamma N - 2f(s) \right] \left[ 1 + \frac{1}{4} f(s) \right]^2, \quad (5.13a)$$

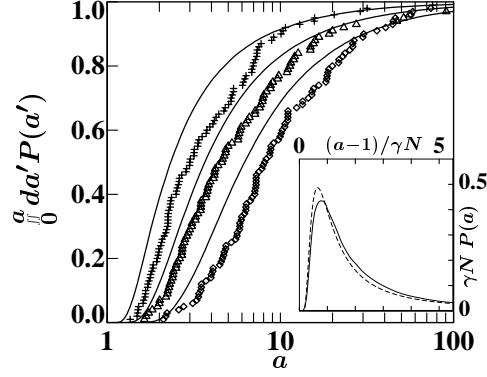


**Figure 5.3:** Comparison between theory and simulation of the cumulative probability distribution of the albedo beyond the laser threshold ( $L = 500d = 19.2l$ ,  $\gamma = 0.07$ ). Solid curves are obtained by numerically averaging over the Laguerre ensemble; data points are the results of the simulation, averaged over 100 realizations of the disorder. The three sets of data are for  $W = 25d$ ,  $N = 10$  (plusses),  $W = 51d$ ,  $N = 21$  (triangles), and  $W = 101d$ ,  $N = 42$  (diamonds). The inset compares the continuum approximation (5.13) for  $P(a)$  (dashed) with the exact large- $N$  limit of the Laguerre ensemble (solid).

where  $f$  is an implicit function of the Laplace variable  $s$ :

$$\left(s - \frac{1}{2}f + \frac{1}{2}\sqrt{4f + f^2}\right)^{-1/2} + 2\left(f - \sqrt{4f + f^2}\right)^{-1} + 1 = 0. \quad (5.13b)$$

The continuum approximation (5.13) is plotted in Fig. 5.3 (inset, dashed curve). It is close to the exact numerical large- $N$  result (solid curve). The modal value  $a_{\max}$  is given by Eq. (5.1). The distribution  $P(a)$  drops off  $\propto \exp[-2\gamma N/(a-1)]$  for smaller  $a$  and  $\propto a^{-5/3}$  for larger  $a$ , so that all moments diverge.

### 5.3 Numerical simulations and conclusions

To test these predictions of random-matrix theory on a model system, we have carried out numerical simulations of the analogous electronic Anderson model with a complex scattering potential, using the recursive Green function technique [22]. The disordered medium is modeled by a two-dimensional square lattice (lattice constant  $d$ , length  $L$ , width  $W$ ). The dielectric constant  $\varepsilon = \varepsilon' + i\varepsilon''$  has a real part  $\varepsilon'$  which fluctuates from

site to site between  $1 \pm \delta\varepsilon$ , and a non-fluctuating imaginary part  $\varepsilon''$ . The multiple scattering of a scalar wave  $\Psi$  (wave number  $k = 2\pi/\lambda$ ) is described by discretizing the Helmholtz equation  $(\nabla^2 + k^2\varepsilon)\Psi = 0$ . The mean free path  $l$  which enters in Eq. (5.5) is obtained from the average albedo  $\bar{a} = (1 + l/L)^{-1}$  without amplification ( $\varepsilon'' = 0$ ). We choose  $k^2 = 1.5d^{-2}$ ,  $\delta\varepsilon = 1$ , leading to  $l = 26.1d$ . The parameter  $\sigma$  (and hence  $\gamma = \sigma l$ ) is obtained from the analytical solution of the discretized Helmholtz equation in the absence of disorder ( $\delta\varepsilon = 0$ ). The complex longitudinal wavenumber  $k_n$  of transverse mode  $n$  then satisfies the dispersion relation

$$\cos k_n d + \cos n\pi d/W = 2 - \frac{1}{2}(kd)^2(1 + i\varepsilon''), \quad (5.14)$$

and leads to  $\sigma = -2N^{-1} \text{Im} \sum_n k_n$ . The albedo (5.3) was computed for normal incidence. Data points in Figs. 1–3 are the numerical results. The agreement with the analytical predictions is quite satisfactory, given that there are *no adjustable parameters*.

In conclusion, we have presented a random-matrix theory for the reflection matrix of a disordered medium with absorption or amplification. In the limit  $L \rightarrow \infty$  of a semi-infinite medium, the distribution of the reflection eigenvalues is that of the Laguerre ensemble. The corresponding distribution of the albedo is a Gaussian in the case of absorption, with mean and variance given by Eq. (5.8). In the case of amplification, the distribution is given by Eq. (5.13), with diverging moments and a finite modal value (5.1) proportional to the number of transverse modes. We have also considered finite  $L$ , and have computed precisely how the mean and variance of the albedo diverge on approaching the laser threshold [Eq. (5.7)]. We have considered a model with stimulated but without spontaneous emission of radiation. This allowed us to examine the light reflected in response to an incident wave, separately from spontaneously generated light. We have restricted ourselves here to sample-to-sample fluctuations in the albedo at a single frequency. Large fluctuations in the albedo as a function of frequency for a single sample are to be expected as well, and might be more accessible experimentally. Finally, we mention the extension to diffusive, rather than plane-wave illumination. The average albedo is the same, but the fluctuations are different [23].

## Bibliography

- [1] N. M. Lawandy, R. M. Balachandran, A. S. L. Gomes, and E. Sauvain, *Nature* **368**, 436 (1994).
- [2] W. L. Sha, C.-H. Liu, and R. R. Alfano, *Opt. Lett.* **19**, 1922 (1994).
- [3] D. S. Wiersma, M. P. van Albada, and A. Lagendijk, *Phys. Rev. Lett.* **75**, 1739 (1995).
- [4] For a critical discussion of random lasers, see the article by A. Z. Genack and J. M. Drake [*Nature* **368**, 400 (1994)], and the correspondence between the authors of Refs. [1] and [3] [*Nature* **373**, 203 (1995)].
- [5] V. S. Letokhov, *Pis'ma Zh. Eksp. Teor. Fiz.* **5**, 262 (1967) [*JETP Lett.* **5**, 212 (1967)].
- [6] V. S. Letokhov, *Zh. Eksp. Teor. Fiz.* **53**, 1442 (1967) [*Sov. Phys. JETP* **26**, 835 (1968)]; N. N. Lavrinovich and V. S. Letokhov, *ibid.* **67**, 1609 (1974) [**40**, 800 (1975)].
- [7] A. Ishimaru, *Wave Propagation and Scattering in Random Media* (Academic, New York, 1978).
- [8] A. Yu. Zyuzin, *Europhys. Lett.* **26**, 517 (1994).
- [9] S. Feng and Z.-Q. Zhang, unpublished.
- [10] A. Yu. Zyuzin, *Phys. Rev. B* **51**, 5274 (1995).
- [11] P. Pradhan and N. Kumar, *Phys. Rev. B* **50**, 9644 (1994).
- [12] P. A. Mello, E. Akkermans, and B. Shapiro, *Phys. Rev. Lett.* **61**, 459 (1988).
- [13] The  $N = 1$  limit of Eq. (5.5) was actually obtained as early as 1959 in the course of a radio-engineering problem: M. E. Gertsenshtein and V. B. Vasil'ev, *Teor. Veroyatn. Primen.* **4**, 424 (1959); **5**, 3(E) (1960) [*Theor. Probab. Appl.* **4**, 391 (1959); **5**, 340(E) (1960)].
- [14] O. N. Dorokhov, *Pis'ma Zh. Eksp. Teor. Fiz.* **36**, 259 (1982) [*JETP Lett.* **36**, 318 (1982)].
- [15] P. A. Mello, P. Pereyra, and N. Kumar, *Ann. Phys.* **181**, 290 (1988).

- [16] C. W. J. Beenakker, *Mod. Phys. Lett. B* **8**, 469 (1994).
- [17] This “method of moments” was developed for the DMPK equation by P. A. Mello and A. D. Stone, *Phys. Rev. B* **44**, 3559 (1991).
- [18] A. C. Selden, *Opt. Comm.* **10**, 1 (1974).
- [19] B. V. Bronk, *J. Math. Phys.* **6**, 228 (1965).
- [20] T. Nagao and K. Slevin, *J. Math. Phys.* **34**, 2317 (1993).
- [21] F. J. Dyson, *J. Math. Phys.* **3**, 157 (1962).
- [22] H. U. Baranger, D. P. DiVincenzo, R. A. Jalabert, and A. D. Stone, *Phys. Rev. B* **44**, 10637 (1991). The computer code for the recursive Green’s function calculation was kindly made available to us by Dr. Jalabert.
- [23] For example, the albedo  $a' = N^{-1} \sum_{n,m} |r_{mn}|^2$  in the case of diffusive illumination has  $\text{Var } a'_\infty = \frac{1}{2} N^{-2} (2 - \gamma)^{-2}$  instead of Eq. (5.8b).

## 6 Duality between absorption and amplification

Localization of electromagnetic waves in a random medium has attracted much interest [1], since the original proposals of John [2] and Anderson [3]. An essential difference with localization of electrons is the absence of a conservation law for photons. Light is absorbed or amplified — while retaining the phase coherence — if the dielectric constant has a non-zero imaginary part. The intensity of the radiation which has propagated without reflection over a distance  $L$  is then multiplied by a factor  $e^{\sigma L}$ , with  $\sigma$  negative (positive) for absorption (amplification). The interplay of absorption and localization has been studied extensively [2–8]. For the one-dimensional problem of a disordered single-mode waveguide (length  $L$ , mean free path  $l$ ), the result for the transmittance  $T$  (being the ratio of transmitted and incident flux) is [6, 7]:

$$\langle \ln T \rangle = (\sigma - l^{-1}) L, \quad (6.1)$$

where  $\langle \dots \rangle$  denotes an average over disorder. Equation (6.1) was derived for  $\sigma < 0$ , corresponding to absorption.

In this chapter we address the question: What happens for amplification? Since  $T = e^{\sigma L}$  in the absence of reflection for both positive and negative  $\sigma$ , one might surmise that Eq. (6.1) holds both for absorption and amplification. This is correct for short waveguides. However, as first noted by Zhang [9], the asymptotic result for  $L \rightarrow \infty$  is

$$\langle \ln T \rangle = (-|\sigma| - l^{-1}) L + O(1). \quad (6.2)$$

We will show that exponential decay of the transmittance in the case of amplification,  $\langle \ln T \rangle \simeq -L/\xi$ , is in fact implied by its exponential decay in the case of absorption, with a duality relation between decay lengths:

$$\xi(\sigma) = \xi(-\sigma). \quad (6.3)$$

This duality relation extends beyond the strictly one-dimensional case of Eq. (6.2), the only essential ingredient being an exponentially decaying transmittance in an absorbing system. Contrary to intuition, amplification suppresses the transmittance in the large- $L$  limit just as much as absorption does.

Experimentally, a random amplifying medium can be realized in a turbid laser dye or a powdered laser crystal [10–12]. Stimulated emission of radiation leads to a dielectric constant with a negative imaginary part, corresponding to  $\sigma > 0$ . We do not present a complete theory for such a “random laser”, because we ignore spontaneous emission [13]. Still, because of the different time scales for stimulated and spontaneous emissions, we believe that a time-resolved experiment in a waveguide geometry might give evidence for the localization of stimulated emission, before spontaneous emission sets in.

## 6.1 Proof of duality

To prove the duality relation (6.3) we consider the propagation of monochromatic radiation (scalar amplitude  $E$ , wavenumber  $k$ ), described by the Helmholtz equation

$$\mathcal{H}E(\mathbf{r}) = 0, \quad \mathcal{H} = \nabla^2 + k^2\varepsilon(\mathbf{r}). \quad (6.4)$$

(We suppose that all polarization-sensitive phenomena are absent.) Disorder leads to spatial fluctuations of the real part  $\varepsilon'$  of the dielectric constant. In the absence of disorder  $\varepsilon' = 1$ . A non-zero imaginary part  $\varepsilon''$  makes the system non-conservative. For the general duality relation it is irrelevant whether  $\varepsilon''$  depends on  $\mathbf{r}$  or not. The sign of  $\varepsilon''$  determines whether the system is locally absorbing ( $\varepsilon'' > 0$ ) or amplifying ( $\varepsilon'' < 0$ ). For a constant  $\varepsilon''$  the parameter  $\sigma$  introduced above is given by

$$\sigma = -2k \operatorname{Im} \sqrt{1 + i\varepsilon''}, \quad (6.5)$$

where the argument of the square root is chosen in the interval  $(-\frac{1}{2}\pi, \frac{1}{2}\pi)$ .

The dual symmetry underlying Eq. (6.3) is formulated in its general form in terms of scattering matrices. We assume that the system consists of a scattering region of length  $L$ , in which  $\varepsilon = \varepsilon' + i\varepsilon''$ , embedded in an  $N$ -mode waveguide with  $\varepsilon = 1$  (see Fig. 6.2, inset). The scattering matrix  $\mathbf{S}$  is a  $2N \times 2N$  matrix relating incoming and outgoing modes. It has the block structure

$$\mathbf{S} = \begin{pmatrix} \mathbf{r}' & \mathbf{t}' \\ \mathbf{t} & \mathbf{r} \end{pmatrix}, \quad (6.6)$$

where  $\mathbf{r}, \mathbf{r}'$  are the reflection matrices and  $\mathbf{t}, \mathbf{t}'$  the transmission matrices. The transmittances and reflectances are defined as

$$\begin{aligned} T &= N^{-1} \text{Tr} \mathbf{t} \mathbf{t}^\dagger, & R &= N^{-1} \text{Tr} \mathbf{r} \mathbf{r}^\dagger, \\ T' &= N^{-1} \text{Tr} \mathbf{t}' \mathbf{t}'^\dagger, & R' &= N^{-1} \text{Tr} \mathbf{r}' \mathbf{r}'^\dagger. \end{aligned} \quad (6.7)$$

Here  $T$  and  $R$  are the transmitted and reflected flux divided by the incident flux from the left. Similarly,  $T'$  and  $R'$  correspond to incident flux from the right. (Note that in the previous chapter we used  $a$  instead of  $R$ .) By taking the trace in Eq. (6.7) we are assuming diffuse illumination, i.e. that the incident flux is equally distributed over the  $N$  modes. In the absence of gain or loss ( $\varepsilon'' = 0$ ) the scattering matrix is unitary,  $\mathbf{S} \mathbf{S}^\dagger = 1$ . This relation expresses flux conservation and relies upon Hermiticity of the Helmholtz operator,  $\mathcal{H} = \mathcal{H}^\dagger$  at  $\varepsilon'' = 0$ . For non-zero  $\varepsilon''$  we have  $\mathcal{H}(-\varepsilon'') = \mathcal{H}^\dagger(\varepsilon'')$ , which implies the duality relation

$$\mathbf{S}(-\varepsilon'') \mathbf{S}^\dagger(\varepsilon'') = 1. \quad (6.8)$$

[If  $\varepsilon''$  depends on  $\mathbf{r}$  the duality relation refers to a change of sign for the complete function  $\varepsilon''(\mathbf{r}) \rightarrow -\varepsilon''(\mathbf{r})$ .]

Let us now examine the consequences of the duality relation (6.8) for the reflection and transmission matrices of two systems which differ only in the sign of  $\varepsilon''$ . (We call these systems “dual”.) We assume that one of the two dual systems (indicated by a subscript  $-$ ) is globally absorbing, so that all elements of  $\mathbf{t}_-$  and  $\mathbf{t}'_-$  tend to zero in the limit  $L \rightarrow \infty$ , while  $\mathbf{r}_-$  and  $\mathbf{r}'_-$  remain finite. Expanding the inverse of  $\mathbf{S}_-$  to first order in the transmission matrices and equating the result to  $\mathbf{S}_+^\dagger$ , we find

$$\mathbf{r}_+^\dagger = \mathbf{r}_-^{-1} + O(\mathbf{t}^2), \quad \mathbf{r}'_+^\dagger = \mathbf{r}'_-^{-1} + O(\mathbf{t}^2), \quad (6.9)$$

$$\mathbf{t}_+^\dagger = -\mathbf{r}'_-^{-1} \mathbf{t}'_- \mathbf{r}_-^{-1} + O(\mathbf{t}^2). \quad (6.10)$$

We introduce the transmission and reflection eigenvalues  $\mathcal{T}_n, \mathcal{T}'_n, \mathcal{R}_n, \mathcal{R}'_n$ , being the eigenvalues of, respectively,  $\mathbf{T} = \mathbf{t} \mathbf{t}^\dagger, \mathbf{T}' = \mathbf{t}' \mathbf{t}'^\dagger, \mathbf{R} = \mathbf{r} \mathbf{r}^\dagger, \mathbf{R}' = \mathbf{r}' \mathbf{r}'^\dagger$ . Because of time-reversal symmetry  $\mathbf{S}_- \mathbf{S}_+^* = 1$ . Together with Eq. (6.8) this implies that  $\mathbf{S}$  is a symmetric matrix. It follows that  $\mathbf{t}' = \mathbf{t}^T$ , hence  $\mathcal{T}_n = \mathcal{T}'_n$  and  $T = T'$ . The reflectances  $R$  and  $R'$  may differ. Equation (6.9) directly yields a duality relation for the reflection eigenvalues in the limit  $L \rightarrow \infty$ ,

$$\mathcal{R}_n(\varepsilon'') = \mathcal{R}_n^{-1}(-\varepsilon''). \quad (6.11)$$

Equations (6.9) and (6.10) together imply that the matrices  $\mathbf{T}' \mathbf{R}'^{-1}$  and  $\mathbf{T}_+ \mathbf{R}_+^{-1}$  have the same eigenvalues. The duality relation for the transmission eigenvalues follows from the following lemma:

Let  $\mathbf{A}(L)$  be a matrix function of  $L$  with exponentially decreasing eigenvalues  $a_n(L)$ . The eigenvalue localization lengths  $\xi_n$  are defined by  $\xi_n^{-1} = -\lim_{L \rightarrow \infty} L^{-1} \ln a_n(L)$ . Let  $\mathbf{B}(L)$  be another non-singular matrix function whose elements remain finite as  $L \rightarrow \infty$ . Then the matrix  $\mathbf{AB}$  has the same eigenvalue localization lengths as  $\mathbf{A}$ .

It follows that the matrices  $\mathbf{T}_+$ ,  $\mathbf{T}_+ \mathbf{R}_+^{-1}$ ,  $\mathbf{T}'_- \mathbf{R}'_-^{-1}$ ,  $\mathbf{T}'_-$ , and hence  $\mathbf{T}_-$  all have the same eigenvalue localization lengths. Explicitly,

$$-\lim_{L \rightarrow \infty} L^{-1} \ln \mathcal{T}_n(\varepsilon'') = -\lim_{L \rightarrow \infty} L^{-1} \ln \mathcal{T}_n(-\varepsilon''). \quad (6.12)$$

The transmittance  $T = N^{-1} \sum_n \mathcal{T}_n$  is dominated by the largest transmission eigenvalue, which is the  $\mathcal{T}_n$  with the largest localization length:  $\xi = \max(\xi_1, \xi_2, \dots, \xi_N)$ . This completes the proof of Eq. (6.3), since we have shown that all, and in particular the largest, transmission eigenvalues of dual systems have the same localization length.

## 6.2 Single mode example

The case  $N = 1$  of a single-mode waveguide can be analyzed in more detail. The joint probability distribution  $P(R, T, L)$  of reflectance and transmittance evolves with increasing  $L$  according to a Fokker-Planck equation (which we will derive in chapter 7),

$$\begin{aligned} l \frac{\partial P}{\partial L} = & -\frac{\partial}{\partial R} [(1-R)^2 + 2\sigma l R] P + \frac{\partial^2}{\partial R^2} R(1-R)^2 P \\ & -\frac{\partial}{\partial T} T(\sigma l - 1 + R) P + \frac{\partial^2}{\partial T^2} T^2 R P \\ & - 2 \frac{\partial^2}{\partial R \partial T} T R (1-R) P. \end{aligned} \quad (6.13)$$

The two parameters  $l$  and  $\sigma$  are spatial averages over length scales much smaller than the total length  $L$  of the waveguide. Equation (6.13) holds if the wavelength  $\lambda$  is much smaller than both  $l$  and  $1/|\sigma|$ . (This is not a restrictive assumption for an optical system.) For  $\sigma < 0$  (absorption), this equation is equivalent to the moment equation of Freilikher, Pustilnik, and Yurkevich [7]. For  $\sigma > 0$  (amplification) their method of moments cannot be used, because all moments of  $R$  diverge when  $L$  exceeds the laser threshold  $L_c$ , as has been shown in the previous chapter. The derivation of Eq. (6.13) proceeds along the lines of Ref. [14], where the case  $\sigma = 0$  was considered. On integration over  $T$  it reduces to a well known [15–17]

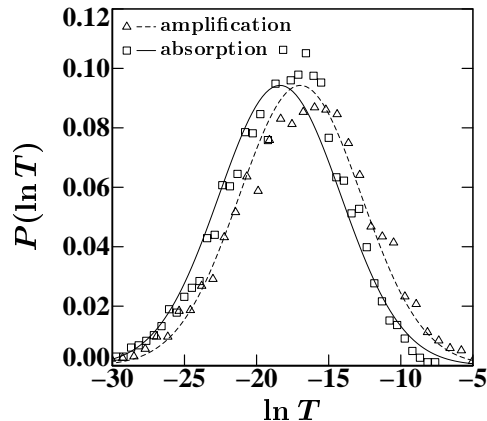


**Figure 6.1:** Probability distribution of the logarithm of the transmittance of a single-mode waveguide, for  $L/l = 15.4$  and  $\gamma = 0.2$  (triangles, dashed curve),  $\gamma = -0.2$  (squares, solid curve). The data points are provided by a numerical simulation (same parameters as in Fig. 6.2), the curves are a Gaussian distribution of  $\ln T$  with mean and variance given by Eqs. (6.15) and (6.16). There is a slight offset between the distributions for absorption and amplification because the system is not fully in the large- $L$  limit.

Fokker-Planck equation for  $P(R, L) = \int dT P(R, T, L)$ . The limit  $L \rightarrow \infty$  of  $P(R, L)$  was studied in chapter 5 and in Refs. [16, 17]. In terms of the variable  $\mu = 1/(R-1)$  it reads

$$P(\mu) = \begin{cases} 2\gamma e^{-2\gamma\mu} \theta(\mu) & \text{for } \gamma > 0, \\ -2\gamma e^{-2\gamma(1+\mu)} \theta(-1-\mu) & \text{for } \gamma < 0, \end{cases} \quad (6.14)$$

where we have defined  $\gamma = \sigma l$ . The function  $\theta(x) = 1$  for  $x > 0$  and 0 otherwise.

Using this asymptotic distribution we have computed from Eq. (6.13) the first two moments of  $\ln T$  in the large- $L$  limit. The result for the average is

$$\langle \ln T \rangle = -(1 + |\gamma|) L/l + 2c(\gamma), \quad (6.15a)$$

$$c(\gamma) = \begin{cases} 0 & \text{for } \gamma < 0, \\ \mathbf{C} + \ln 2\gamma - e^{2\gamma} \text{Ei}(-2\gamma) & \text{for } \gamma > 0, \end{cases} \quad (6.15b)$$

where  $\mathbf{C}$  is Euler's constant and  $\text{Ei}(x) = \int_{-\infty}^x dt e^t/t$  is the exponential integral [ $c(\gamma) \approx -2\gamma \ln \gamma$  if  $0 < \gamma \ll 1$ ]. Equation (6.15) agrees with Refs. [6, 7, 9], and demonstrates that the inverse localization length  $\xi^{-1}(\sigma) =$

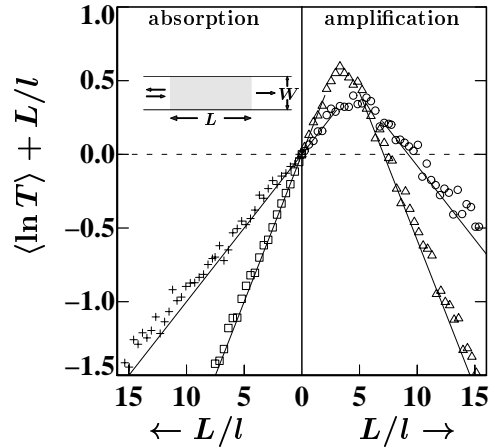


**Figure 6.2:** Numerical simulation of the transmittance of a single-mode waveguide ( $W = d$ ,  $k^2 = 0.5d^{-2}$ ,  $\delta\varepsilon = 0.2$ ,  $l = 521d$ ,  $N = 1$ ), averaged over  $10^4$  realizations of the disorder. The right half of the figure is for amplification (circles:  $\gamma = 0.1$ ; triangles:  $\gamma = 0.2$ ), the left half is for absorption (crosses:  $\gamma = -0.1$ ; squares:  $\gamma = -0.2$ ). The solid lines are the analytical asymptotes from Eq. (6.15). Their slope is independent of the sign of  $\gamma$ , in agreement with the duality relation (6.3). The inset shows the geometry considered.

$(1 + |\gamma|)l^{-1} = l^{-1} + |\sigma|$  is independent of the sign of  $\sigma$  — in accordance with the general duality relation (6.3). In Fig. 6.2 we compare the theoretical result (6.15) with numerical simulations (to be discussed later). For the variance we find

$$\text{Var} \ln T = 2 \left[ 1 + 2|\gamma|e^{2|\gamma|} \text{Ei}(-2|\gamma|) \right] L/l + O(1), \quad (6.16)$$

in agreement with Ref. [7] for  $\gamma < 0$ . Note that  $\sqrt{\text{Var} \ln T} \ll \langle \ln T \rangle$  for  $L/l \gg 1$ . Evaluation of higher moments shows that the distribution of  $\ln T$  tends to a Gaussian for  $L \rightarrow \infty$ . (The tails are non-Gaussian, but contain negligible weight.) We have plotted two examples in Fig. 6.1.

These results hold in the large- $L$  limit. For short waveguides instead of Eq. (6.15) one has  $\langle \ln T \rangle = -(1 - \gamma)L/l$ . The cross-over length is the lasing threshold  $L_c \simeq lc(\gamma)/|\gamma|$ , at which  $\langle T \rangle$  diverges for  $\gamma > 0$ . Below this length stimulated emission *enhances* transmission through the waveguide. On larger length scales stimulated emission *reduces* transmission. In contrast, the reflectance is enhanced on every length scale [16, 17], as discussed in chapter 5.

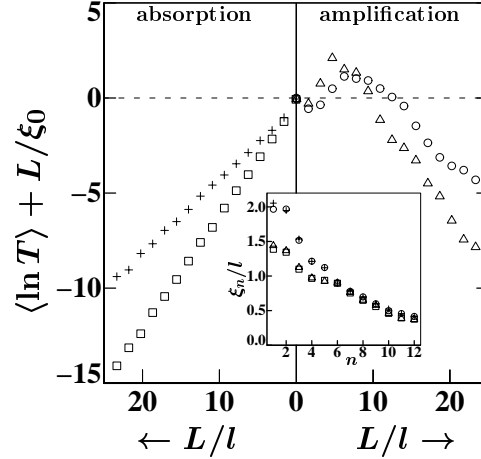


**Figure 6.3:** Numerical simulation of the transmittance of a multi-mode waveguide ( $W = 25d$ ,  $k^2 = 2.0d^{-2}$ ,  $\delta\varepsilon = 0.375$ ,  $l = 29.6d$ ,  $N = 12$ ), averaged over 50 realizations of the disorder. The parameter  $\xi_0 = (N + 1)l/2$  is the localization length of the system in the absence of absorption or amplification. The right half of the figure is for amplification (circles:  $\sigma = 0.0035d^{-1}$ ; triangles:  $\sigma = 0.0071d^{-1}$ ), the left half is for absorption (crosses:  $\sigma = -0.0035d^{-1}$ ; squares:  $\sigma = -0.0071d^{-1}$ ). The inset shows the eigenvalue localization lengths,  $\xi_n^{-1} \equiv -\lim_{L \rightarrow \infty} L^{-1} \ln T_n$ . These lengths  $\xi_n$  were computed from the  $L$ -dependence of  $T_n$  for  $L$  up to  $40l$  and a single realization of the disorder. The duality between absorption and amplification is verified with good accuracy.

### 6.3 Numerical simulations and conclusions

To test these analytical predictions for  $N = 1$ , and to investigate also the multi-mode case, we have numerically solved a discretized version of the Helmholtz equation (6.4), on a two-dimensional square lattice (lattice constant  $d$ , length  $L$ , width  $W$ ). The real part  $\varepsilon'$  of the dielectric constant was chosen randomly from site to site with a uniform distribution between  $1 \pm \delta\varepsilon$ . The imaginary part  $\varepsilon''$  of the dielectric constant had the same value at each site. The scattering matrix for the multi-mode case was computed using the recursive Green function technique, originally developed for the electronic Anderson model [18]. (For the case  $N = 1$  a transfer-matrix method [8,9] turned out to be more convenient.) Simulations with  $\varepsilon'' = 0$  were used to obtain  $l$ , from the relation [19]

$$-\lim_{L \rightarrow \infty} L^{-1} \langle \ln T \rangle = \left[ \frac{1}{2}(N + 1)l \right]^{-1}. \quad (6.17)$$

The parameter  $\sigma$  was determined from Eq. (6.5). Results for the single-mode case are shown in Figs. 6.2 and 6.1, and for the multi-mode case in Fig. 6.3. The duality relation between the localization lengths for absorption and amplification is verified with good accuracy, both for the single- and for the multi-mode case. Furthermore, for  $N = 1$  we find good agreement with the results (6.15) and (6.16) of the Fokker-Planck equation.

In conclusion, we have demonstrated that stimulated emission of radiation in a disordered waveguide *reduces* the decay length, in the same way as absorption does. This paradoxical result is an immediate consequence of the exact duality relation (6.8) between the scattering matrices of two systems with complex conjugated dielectric constants. The dual symmetry between absorption and amplification has been supported by an explicit computation of the decay lengths, both analytically (for the single-mode case) and numerically (for the single- and multi-mode cases).

## Bibliography

- [1] S. John, *Phys. Today* **44** (5), 32 (1991); P. Sheng, editor, *Scattering and Localization of Classical Waves in Random Media* (World Scientific, Singapore, 1990).
- [2] S. John, *Phys. Rev. Lett.* **53**, 2169 (1984).
- [3] P. W. Anderson, *Phil. Mag. B* **52**, 505 (1985).
- [4] R. L. Weaver, *Phys. Rev. B* **47**, 1077 (1993).
- [5] M. Yosefin, *Europhys. Lett.* **25**, 675 (1994).
- [6] R. Rammal and B. Doucot, *J. Phys. (France)* **48**, 509 (1987).
- [7] V. Freilikher, M. Pustilnik, and I. Yurkevich, *Phys. Rev. Lett.* **73**, 810 (1994).
- [8] A. K. Gupta and A. M. Jayannavar, *Phys. Rev. B* **52**, 4156 (1995).
- [9] Z. Q. Zhang, *Phys. Rev. B* **52**, 7960 (1995).
- [10] N. M. Lawandy, R. M. Balachandran, A. S. L. Gomes, and E. Sauvain, *Nature* **368**, 436 (1994).
- [11] W. L. Sha, C.-H. Liu, and R. R. Alfano, *Opt. Lett.* **19**, 1 922 (1994).
- [12] D. S. Wiersma, M. P. van Albada, and A. Lagendijk, *Phys. Rev. Lett.* **75**, 1739 (1995).
- [13] A. Yu. Zyuzin, *Phys. Rev. E* **51**, 5274 (1995).
- [14] P. A. Mello, P. Pereyra, and N. Kumar, *Ann. Phys. (N.Y.)* **181**, 290 (1988).
- [15] M. E. Gertsenshtein and V. B. Vasil'ev, *Teor. Veroyatn. Primen.* **4**, 424 (1959); **5**, 3(E) (1960) [*Theor. Probab. Appl.* **4**, 3 91 (1959); **5**, 340(E) (1960)].
- [16] W. Kohler and G. C. Papanicolaou, *SIAM J. Appl. Math.* **30**, 263 (1976).
- [17] P. Pradhan and N. Kumar, *Phys. Rev. B* **50**, 9644 (1994).

- [18] H. U. Baranger, D. P. DiVincenzo, R. A. Jalabert, and A. D. Stone, *Phys. Rev. B* **44**, 10637 (1991).
- [19] O. N. Dorokhov, *Sol. State Comm.* **51**, 381 (1984).

## 7 Localization in a non-conservative disordered multi-mode waveguide

Localization of waves in one-dimensional random media has been studied extensively, both for optical and for electronic systems [1, 2]. An analytical solution for the case of weak disorder (mean free path  $l$  much greater than the wavelength  $\lambda$ ) was obtained as early as 1959 by Gertsenshtein and Vasil'ev [3]. The transmittance  $T$  (being the ratio of transmitted and incident flux) has a log-normal distribution for large lengths  $L$  of the system, with a mean  $\langle \ln T \rangle = -L/\xi$  characterized by a localization length  $\xi$  equal to the mean free path.

This early work was concerned with the propagation of classical waves, and hence included also the effect of absorption. In the presence of absorption the transmittance decays faster, according to [4,5]  $\langle \ln T \rangle = (\sigma - l^{-1})L$ , where  $\sigma < 0$  and  $|\sigma|$  is the inverse absorption length. Absorption is the result of a positive imaginary part  $\varepsilon''$  of the (relative) dielectric constant  $\varepsilon = \varepsilon' + i\varepsilon''$ . For a homogeneous  $\varepsilon''$  one has

$$\sigma = -2k \operatorname{Im} \sqrt{1 + i\varepsilon''} \approx -k\varepsilon'' a, \quad \text{if } |\varepsilon''| \ll 1, \quad (7.1)$$

where  $k$  is the wavenumber. A negative  $\varepsilon''$  corresponds to amplification by stimulated emission of radiation, with inverse amplification length  $\sigma > 0$ . Propagation of waves through amplifying one-dimensional random media has been studied in Refs. [6–9], and already in chapter 6 of this thesis. In the limit  $L \rightarrow \infty$  amplification also leads to a faster decay of the transmittance, according to  $\langle \ln T \rangle = (-|\sigma| - l^{-1})L$  [cf. Eq. (6.2)] [8].

A natural extension of these studies is to waveguides which contain more than a single propagating mode. Localization in such “quasi-one-dimensional” systems has been studied on the basis of a scaling theory [10], a supersymmetric field theory [11], or a Fokker-Planck equation [12, 13]. It is found that the localization length for  $N$  modes is enhanced by a factor of  $N$  relative to the single-mode case. These investigations were concerned with quantum mechanical, rather than classical waves, and therefore did not include absorption. It is the purpose of the present study to extend the Fokker-Planck approach of Dorokhov, Mello, Pereyra, and Kumar [12, 13] (DMPK) to include the effects on the transmittance of a non-zero imaginary part of the dielectric constant.

According to the general duality relation discussed in chapter 6, the localization length is an even function of  $\sigma$  for any  $N$ ,

$$\xi(\sigma) = \xi(-\sigma). \quad (7.2)$$

It follows that both absorption and amplification lead to a faster decay of the transmittance for large  $L$ . For  $N \gg 1$  we find that, in good approximation,

$$\frac{1}{\xi} = \frac{2}{(N+1)l} + (\sigma^2 + 2|\sigma|/l)^{1/2}. \quad (7.3)$$

This result becomes exact in the two limits  $|\sigma| \gg 1/N^2l$  and  $|\sigma| \ll 1/N^2l$ . We compare with numerical simulations of the Helmholtz equation, and find reasonably good agreement over the whole range of  $\sigma$ .

The outline of this chapter is as follows. In section 7.1 we formulate the scattering problem and summarize the duality relation from chapter 6. In section 7.2 we derive a Fokker-Planck equation for the transmission and reflection eigenvalues  $\mathcal{T}_n, \mathcal{R}_n, n = 1, 2, \dots, N$ . These are eigenvalues of the matrix products  $\mathbf{t}\mathbf{t}^\dagger$  and  $\mathbf{r}\mathbf{r}^\dagger$ , respectively, where  $\mathbf{t}$  and  $\mathbf{r}$  are the transmission and reflection matrices of the waveguide. For  $\sigma = 0$  the Fokker-Planck equation is the DMPK equation [12, 13]. A reduced Fokker-Planck equation, containing only the  $\mathcal{R}_n$ 's, was previously obtained and studied in chapter 5. To obtain the localization length one needs to include also the  $\mathcal{T}_n$ 's, which are no longer related to the  $\mathcal{R}_n$ 's when  $\sigma \neq 0$ . We find that a closed Fokker-Planck equation containing  $\mathcal{R}_n$ 's and  $\mathcal{T}_n$ 's exists only for  $N = 1$ . If  $N > 1$  there appears an additional set of "slow variables," consisting of eigenvectors of  $\mathbf{r}\mathbf{r}^\dagger$  in a basis where  $\mathbf{t}\mathbf{t}^\dagger$  is diagonal. (These new variables do not appear when  $\sigma = 0$ , because then  $\mathbf{r}\mathbf{r}^\dagger$  and  $\mathbf{t}\mathbf{t}^\dagger$  commute.) Because of these additional relevant variables we have not been able to make as much progress in the solution of the Fokker-Planck equation for  $\sigma \neq 0$  as one can for  $\sigma = 0$  [14]. In section 7.3 we show that a closed evolution equation for  $\langle \ln T \rangle$  can be obtained if  $|\sigma| \gg 1/N^2l$ , which leads to the second term in Eq. (7.3). (This term could also have been obtained from the incoherent radiative transfer theory for  $\sigma < 0$ , but not for  $\sigma > 0$ .) To contrast the multi-mode and single-mode cases, we also briefly discuss in section 7.3 the derivation of the localization length for  $N = 1$ , which we have postponed in the previous chapter. Finally, in section 7.4 we compare the analytical results for the multi-mode case with numerical simulations.

## 7.1 Formulation of the scattering problem

We consider a random medium of length  $L$  with a spatially fluctuating dielectric constant  $\varepsilon = \varepsilon' + i\varepsilon''$ , embedded in an  $N$ -mode waveguide with  $\varepsilon = 1$ . The scattering matrix  $\mathbf{S}$  is a  $2N \times 2N$  matrix relating incoming and outgoing modes at frequency  $\omega$ . It has the block structure

$$\mathbf{S} = \begin{pmatrix} \mathbf{r}' & \mathbf{t}' \\ \mathbf{t} & \mathbf{r} \end{pmatrix}, \quad (7.4)$$

where  $\mathbf{r}$ ,  $\mathbf{r}'$  are the reflection matrices and  $\mathbf{t}$ ,  $\mathbf{t}'$  the transmission matrices. We introduce the sets of transmission and reflection eigenvalues  $\{\mathcal{T}_n\}$ ,  $\{\mathcal{T}'_n\}$ ,  $\{\mathcal{R}_n\}$ ,  $\{\mathcal{R}'_n\}$ , being the eigenvalues of, respectively,  $\mathbf{t}\mathbf{t}^\dagger$ ,  $\mathbf{t}'\mathbf{t}'^\dagger$ ,  $\mathbf{r}\mathbf{r}^\dagger$ ,  $\mathbf{r}'\mathbf{r}'^\dagger$ . Total transmittances and reflectances are defined as

$$\begin{aligned} T &= N^{-1} \text{Tr } \mathbf{t}\mathbf{t}^\dagger, & R &= N^{-1} \text{Tr } \mathbf{r}\mathbf{r}^\dagger, \\ T' &= N^{-1} \text{Tr } \mathbf{t}'\mathbf{t}'^\dagger, & R' &= N^{-1} \text{Tr } \mathbf{r}'\mathbf{r}'^\dagger. \end{aligned} \quad (7.5)$$

Here  $T$  and  $R'$  are the transmitted and reflected flux divided by the incident flux from the left. Similarly,  $T'$  and  $R$  correspond to incident flux from the right. By taking the trace in Eq. (7.5) we are assuming diffuse illumination, i.e. that the incident flux is equally distributed over the  $N$  modes. Two systems which differ only in the sign of  $\varepsilon''(\mathbf{r})$  are called dual. Scattering matrices of dual systems are related by

$$\mathbf{S}(\varepsilon'')\mathbf{S}^\dagger(-\varepsilon'') = 1, \quad (7.6)$$

[cf. Eq. (6.8)]. This duality relation takes the place of the unitarity constraint when  $\varepsilon'' \neq 0$ .

An optical system usually possesses time-reversal symmetry, as a result of which  $\mathbf{S}(\varepsilon'')\mathbf{S}^*(-\varepsilon'') = 1$ . Combining this relation with Eq. (7.6), we find that  $\mathbf{S} = \mathbf{S}^T$  is a symmetric matrix. Hence  $\mathcal{T}_n = \mathcal{T}'_n$  and  $T = T'$ . (The reflectances  $R$  and  $R'$  may differ.) The case of broken time-reversal symmetry, might also be physically relevant [15] and will be included here for completeness. In the absence of time-reversal symmetry  $S$  is an arbitrary complex matrix.

The duality relation (7.6) has consequences for the reflection and transmission eigenvalues of two dual systems. If  $N = 1$  the relation

$$T(\varepsilon'')/R(\varepsilon'') = T'(-\varepsilon'')/R'(-\varepsilon'') \quad (7.7)$$

holds for all  $L$ . If  $N \geq 1$  we have two relations for  $L \rightarrow \infty$ ,

$$\lim_{L \rightarrow \infty} \mathcal{R}_n(\varepsilon'') = \lim_{L \rightarrow \infty} \mathcal{R}_n^{-1}(-\varepsilon''), \quad (7.8)$$

$$\lim_{L \rightarrow \infty} L^{-1} \ln \mathcal{T}_n(\varepsilon'') = \lim_{L \rightarrow \infty} L^{-1} \ln \mathcal{T}_n(-\varepsilon''). \quad (7.9)$$

The transmittance  $T = N^{-1} \sum_n \mathcal{T}_n$  is dominated by the largest transmission eigenvalue, hence

$$\lim_{L \rightarrow \infty} L^{-1} \ln T(\varepsilon'') = \lim_{L \rightarrow \infty} L^{-1} \ln T(-\varepsilon''). \quad (7.10)$$

In other words, two dual systems have the same localization length, as stated in Eq. (7.2).

## 7.2 Fokker-Planck equation

We derive a Fokker-Planck equation for the evolution of the distribution of scattering matrices with increasing length  $L$  of the waveguide. In the absence of gain or loss ( $\sigma = 0$ ), the evolution equation is known as the Dorokhov-Mello-Pereyra-Kumar (DMPK) equation [12, 13]. Original derivations of this equation relied on the unitarity of the scattering matrix, making use of the invariant measure on the unitary group and the polar decomposition of a unitary matrix. These derivations cannot readily be generalized to the case  $\sigma \neq 0$ , in particular because the scattering matrix no longer admits a polar decomposition. (This means that the matrix products  $\mathbf{r}\mathbf{r}^\dagger$  and  $\mathbf{t}\mathbf{t}^\dagger$  do not commute.) The alternative derivation of the DMPK equation of Ref. [14] does not use the polar decomposition and is suitable for our purpose.

Without loss of generality we can write the transmission and reflection submatrices of the scattering matrix as follows,

$$\mathbf{S} = \begin{pmatrix} \mathbf{r}' & \mathbf{t}' \\ \mathbf{t} & \mathbf{r} \end{pmatrix} = \begin{pmatrix} \mathbf{U}\sqrt{\mathbf{R}'}\mathbf{W} & \mathbf{U}'\sqrt{\mathbf{T}'}\mathbf{Z} \\ \mathbf{V}\sqrt{\mathbf{T}}\mathbf{W}' & -\mathbf{V}'\sqrt{\mathbf{R}}\mathbf{Z}' \end{pmatrix}. \quad (7.11)$$

Here  $\mathbf{U}, \mathbf{U}', \mathbf{V}, \mathbf{V}', \mathbf{W}, \mathbf{W}', \mathbf{Z}, \mathbf{Z}'$  are  $N \times N$  unitary matrices, while  $\mathbf{R}, \mathbf{R}', \mathbf{T}, \mathbf{T}'$  are diagonal matrices whose elements are the reflection and transmission eigenvalues  $\{\mathcal{R}_n\}, \{\mathcal{R}'_n\}, \{\mathcal{T}_n\}, \{\mathcal{T}'_n\}$ . For  $\sigma = 0$ , the unitarity constraint  $\mathbf{S}\mathbf{S}^\dagger = \mathbf{1}$  implies  $\mathbf{U} = \mathbf{U}', \mathbf{V} = \mathbf{V}', \mathbf{W} = \mathbf{W}', \mathbf{Z} = \mathbf{Z}'$ , and  $\mathbf{R} = \mathbf{R}' = \mathbf{1} - \mathbf{T} = \mathbf{1} - \mathbf{T}'$ . Equation (7.11) then constitutes the polar decomposition of the scattering matrix. In this case one can derive a Fokker-Planck equation for the evolution of only transmission or only reflection eigenvalues.

If  $\sigma \neq 0$ , the Fokker-Planck equation contains both the transmission and reflection eigenvalues, as well as elements of the matrix  $\mathbf{Q} = \mathbf{V}^\dagger \mathbf{V}'$  relating eigenvectors of  $\mathbf{t}\mathbf{t}^\dagger$  and  $\mathbf{r}\mathbf{r}^\dagger$ . The only constraint on the scattering matrix if  $\sigma \neq 0$  is imposed by time-reversal symmetry, which requires  $\mathbf{S} = \mathbf{S}^T$ , hence  $\mathbf{W} = \mathbf{U}^T$ ,  $\mathbf{Z} = \mathbf{V}^T$ ,  $\mathbf{W}' = \mathbf{U}'^T$ ,  $\mathbf{Z}' = \mathbf{V}'^T$ ,  $\mathbf{T} = \mathbf{T}'$ .

The Fokker-Planck equation describes the evolution of slow variables after the elimination of fast variables. In our problem fast variables vary on the scale of the wavelength  $\lambda$ , while slow variables vary on the scale of the mean free path  $l$  or the amplification length  $\sigma^{-1}$ . We assume that both  $l$  and  $\sigma^{-1}$  are much greater than  $\lambda$ . The slow variables include  $\{\mathcal{R}_n\}$ ,  $\{\mathcal{T}_n\}$  and elements of  $\mathbf{Q} = \mathbf{V}^\dagger \mathbf{V}'$ . We denote this set of slow variables collectively by  $\{\Phi_n\}$ . Each  $\Phi_i$  is incremented by  $\delta\Phi_i$  if a thin slice of length  $\delta L$  ( $\lambda \ll \delta L \ll l$ ) is added to the waveguide of length  $L$ . The increments are of order  $(\delta L/l)^{1/2}$  and can be calculated perturbatively. We specify an appropriate statistical ensemble for the scattering matrix  $\delta\mathbf{S}$  of the thin slice and compute moments of  $\delta\Phi_i$ . The first two moments are of order  $\delta L/l$ ,

$$\langle \delta\Phi_i \rangle = a_i \delta L/l + O(\delta L/l)^{3/2}, \quad (7.12a)$$

$$\langle \delta\Phi_i \delta\Phi_j \rangle = a_{ij} \delta L/l + O(\delta L/l)^{3/2}. \quad (7.12b)$$

Higher moments have no term of order  $\delta L/l$ . According to the general theory of Brownian motion [16], the Fokker-Planck equation for the joint probability distribution  $P(\{\Phi_n\}, L)$  reads

$$l \frac{\partial P}{\partial L} = - \sum_i \frac{\partial}{\partial \Phi_i} a_i P + \frac{1}{2} \sum_{ij} \frac{\partial^2}{\partial \Phi_i \partial \Phi_j} a_{ij} P. \quad (7.13)$$

The average  $\langle \dots \rangle$  in Eq. (7.12) is defined by the statistics of  $\delta\mathbf{S}$ . We specify this statistics using simplifying features of the waveguide geometry (length  $\gg$  width), which justify the equivalent-channel or isotropy approximation [13, 17]. We assume that amplification or absorption in the thin slice is independent of the scattering channel. This entails the relation

$$\delta\mathbf{S}\delta\mathbf{S}^\dagger = 1 + \bar{\sigma} \delta L. \quad (7.14)$$

Here  $\bar{\sigma}$  is a modal and spatial average of the inverse amplification length  $\sigma$ . If  $\varepsilon''$  is spatially constant, one has

$$\bar{\sigma} = -\frac{2k}{N} \sum_{n=1}^N \text{Im}(1 - \omega_n^2/\omega^2 + i\varepsilon'')^{1/2}, \quad (7.15)$$

where  $\omega_n$  is the cutoff frequency of mode  $n$ . For  $N \rightarrow \infty$ , the sum over modes can be replaced by an integral. The result depends on the dimensionality of the waveguide,

$$\bar{\sigma} = -2k\varepsilon'', \text{ for a 3D waveguide,} \quad (7.16a)$$

$$\bar{\sigma} = -(\pi/2)k\varepsilon'', \text{ for a 2D waveguide,} \quad (7.16b)$$

where we have used that  $\varepsilon'' \ll 1$ .

Equation (7.14) ensures the existence of a polar decomposition for  $\delta\mathbf{S}$ ,

$$\delta\mathbf{S} = \begin{pmatrix} \mathbf{U}_0\sqrt{\delta\mathbf{R}}\mathbf{W}_0 & \mathbf{U}_0\sqrt{\delta\mathbf{T}}\mathbf{Z}_0 \\ \mathbf{V}_0\sqrt{\delta\mathbf{T}}\mathbf{W}_0 & -\mathbf{V}_0\sqrt{\delta\mathbf{R}}\mathbf{Z}_0 \end{pmatrix}, \quad (7.17)$$

with  $\delta\mathbf{T} + \delta\mathbf{R} = 1 + \bar{\sigma}\delta L$ . Note that a polar decomposition for  $\delta\mathbf{S}$  does not imply a polar decomposition for  $\mathbf{S}$ , because the special block structure of Eq. (7.17) is lost upon composition of scattering matrices. We make the isotropy assumption that the matrices  $\mathbf{U}_0$ ,  $\mathbf{V}_0$ ,  $\mathbf{W}_0$ ,  $\mathbf{Z}_0$  are uniformly distributed in the unitary group. In the presence of time reversal symmetry one has  $\mathbf{W}_0 = \mathbf{U}_0^\top$  and  $\mathbf{Z}_0 = \mathbf{V}_0^\top$ . In the absence of time reversal symmetry all four unitary matrices are independent. The diagonal matrices  $\delta\mathbf{R}$  and  $\delta\mathbf{T}$  may have arbitrary distributions. We specify the first moments,

$$\langle \text{Tr } \delta\mathbf{R} \rangle = N \delta L / l, \quad (7.18a)$$

$$\langle \text{Tr } \delta\mathbf{T} \rangle = N + N(\gamma - 1) \delta L / l, \quad (7.18b)$$

where we have defined  $\gamma = \bar{\sigma}l$ . The mean free path  $l$  in Eq. (7.18) is related to the mean free path  $l_{\text{tr}}$  of radiative transfer theory by [14]

$$l = (4/3)l_{\text{tr}}, \text{ for a 3D waveguide,} \quad (7.19a)$$

$$l = (\pi/2)l_{\text{tr}}, \text{ for a 2D waveguide.} \quad (7.19b)$$

This completes the specification of the statistical ensemble for  $\delta\mathbf{S}$ .

We need the increments  $\Delta\mathcal{R}_n$ ,  $\Delta\mathcal{T}_n$  of reflection and transmission eigenvalues to first order in  $\delta L/l$ ,

$$\Delta\mathcal{R}_n = \Delta R_{nn}^{(1)} + \Delta R_{nn}^{(2)} + \sum_{m \neq n} \frac{\Delta R_{nm}^{(1)} \Delta R_{mn}^{(1)}}{\mathcal{R}_n - \mathcal{R}_m}, \quad (7.20a)$$

$$\Delta\mathcal{T}_n = \Delta T_{nn}^{(1)} + \Delta T_{nn}^{(2)} + \sum_{m \neq n} \frac{\Delta T_{nm}^{(1)} \Delta T_{mn}^{(1)}}{\mathcal{T}_n - \mathcal{T}_m}. \quad (7.20b)$$

The matrices of perturbation  $\Delta R^{(1)}$ ,  $\Delta R^{(2)}$ ,  $\Delta T^{(1)}$ , and  $\Delta T^{(2)}$  are expressed through unitary matrices  $\mathbf{Q} = \mathbf{V}^\dagger \mathbf{V}'$ ,  $\tilde{\mathbf{U}} = \mathbf{Z}' \mathbf{U}_0$ ,  $\tilde{\mathbf{W}} = \mathbf{W}_0 \mathbf{V}'$  and diagonal matrices  $\mathbf{T}$ ,  $\mathbf{R}$ ,  $\delta \mathbf{T}$ ,  $\delta \mathbf{R}$ :

$$\Delta R^{(1)} = \left[ \sqrt{\mathbf{R}} \tilde{\mathbf{U}} \sqrt{\delta \mathbf{R}} \tilde{\mathbf{W}} (1 - \mathbf{R}) + \text{H.c.} \right], \quad (7.21a)$$

$$\begin{aligned} \Delta R^{(2)} = & -\sqrt{\mathbf{R}} \tilde{\mathbf{U}} (1 - \delta \mathbf{T}) \tilde{\mathbf{U}}^\dagger \sqrt{\mathbf{R}} + \tilde{\mathbf{W}}^\dagger \delta \mathbf{R} \tilde{\mathbf{W}} \\ & + \sqrt{\mathbf{R}} \tilde{\mathbf{U}} \sqrt{\delta \mathbf{R}} \tilde{\mathbf{W}} \tilde{\mathbf{W}}^\dagger \sqrt{\delta \mathbf{R}} \tilde{\mathbf{U}}^\dagger \sqrt{\mathbf{R}} - \left[ \frac{1}{2} \tilde{\mathbf{W}}^\dagger (1 - \delta \mathbf{T}) \tilde{\mathbf{W}} \mathbf{R} \right. \\ & \left. + \sqrt{\mathbf{R}} \tilde{\mathbf{U}} \sqrt{\delta \mathbf{R}} \tilde{\mathbf{W}} \sqrt{\mathbf{R}} \tilde{\mathbf{U}} \sqrt{\delta \mathbf{R}} \tilde{\mathbf{W}} (1 - \mathbf{R}) + \text{H.c.} \right], \end{aligned} \quad (7.21b)$$

$$\Delta T^{(1)} = - \left[ \mathbf{Q} \sqrt{\mathbf{R}} \tilde{\mathbf{U}} \sqrt{\delta \mathbf{R}} \tilde{\mathbf{W}} \mathbf{Q}^\dagger \mathbf{T} + \text{H.c.} \right], \quad (7.21c)$$

$$\begin{aligned} \Delta T^{(2)} = & \mathbf{Q} \sqrt{\mathbf{R}} \tilde{\mathbf{U}} \sqrt{\delta \mathbf{R}} \tilde{\mathbf{W}} \mathbf{Q}^\dagger \mathbf{T} \mathbf{Q} \tilde{\mathbf{W}}^\dagger \sqrt{\delta \mathbf{R}} \tilde{\mathbf{U}}^\dagger \sqrt{\mathbf{R}} \mathbf{Q}^\dagger \\ & - \left[ \frac{1}{2} \mathbf{Q} \tilde{\mathbf{W}}^\dagger (1 - \delta \mathbf{T}) \tilde{\mathbf{W}} \mathbf{Q}^\dagger \mathbf{T} \right. \\ & \left. - \mathbf{Q} \sqrt{\mathbf{R}} \tilde{\mathbf{U}} \sqrt{\delta \mathbf{R}} \tilde{\mathbf{W}} \sqrt{\mathbf{R}} \tilde{\mathbf{U}} \sqrt{\delta \mathbf{R}} \tilde{\mathbf{W}} \mathbf{Q}^\dagger \mathbf{T} + \text{H.c.} \right]. \end{aligned} \quad (7.21d)$$

(The abbreviation H.c. stands for Hermitian conjugate.) The moments (7.12) are computed by first averaging over the unitary matrices  $\mathbf{U}_0$ ,  $\mathbf{W}_0$  and then averaging over  $\delta \mathbf{R}$  and  $\delta \mathbf{T}$  using Eq. (7.18). Averages over unitary matrices follow from

$$\langle U_{nk} U_{ml}^* \rangle = \frac{1}{N} \delta_{nm} \delta_{kl}, \quad (7.22a)$$

$$\langle U_{nk} U_{mk} U_{pl}^* U_{ql}^* \rangle = \frac{1}{N(N+1)} \delta_{kl} (\delta_{np} \delta_{mq} + \delta_{nq} \delta_{mp}). \quad (7.22b)$$

Without time-reversal symmetry averages over  $\mathbf{U}_0$  and  $\mathbf{W}_0$  are independent. With time-reversal symmetry we have  $\mathbf{W}_0 = \mathbf{U}_0^\dagger$  so that only a single average remains. The results are

*With time-reversal symmetry*

$$\begin{aligned} (l/\delta L) \langle \delta \mathcal{R}_n \rangle = & 1 + 2(\gamma - 1) \mathcal{R}_n + \frac{\mathcal{R}_n}{N+1} \left( \mathcal{R}_n + \sum_m \mathcal{R}_m \right) \\ & + \frac{1}{N+1} \sum_{m \neq n} \frac{\mathcal{R}_n (1 - \mathcal{R}_m)^2 + \mathcal{R}_m (1 - \mathcal{R}_n)^2}{\mathcal{R}_n - \mathcal{R}_m}, \end{aligned} \quad (7.23a)$$

$$(l/\delta L) \langle \delta \mathcal{R}_n \delta \mathcal{R}_m \rangle = \frac{4\delta_{nm}}{N+1} \mathcal{R}_n (1 - \mathcal{R}_n)^2, \quad (7.23b)$$

$$(l/\delta L) \langle \delta \mathcal{T}_n \rangle = \mathcal{T}_n (\gamma - 1) + \frac{\mathcal{T}_n}{N+1} \left( A_{nn} + \sum_{m \neq n} \frac{\mathcal{T}_m A_{nm} + \mathcal{T}_n A_{mm}}{\mathcal{T}_n - \mathcal{T}_m} \right)$$

$$+ F_{nn} + \sum_{m \neq n} F_{nm} \frac{\mathcal{T}_n + \mathcal{T}_m}{\mathcal{T}_n - \mathcal{T}_m}, \quad (7.23c)$$

$$(l/\delta L) \langle \delta \mathcal{T}_n \delta \mathcal{T}_m \rangle = \frac{2}{N+1} \left( \delta_{nm} \mathcal{T}_n^2 A_{nn} + \mathcal{T}_n \mathcal{T}_m F_{nm} \right), \quad (7.23d)$$

$$(l/\delta L) \langle \delta \mathcal{T}_n \delta \mathcal{R}_m \rangle = -\frac{4}{N+1} \mathcal{T}_n \mathcal{R}_m (1 - \mathcal{R}_m) |Q_{nm}|^2. \quad (7.23e)$$

Without time-reversal symmetry

$$(l/\delta L) \langle \delta \mathcal{R}_n \rangle = 1 + 2(\gamma - 1) \mathcal{R}_n + \frac{\mathcal{R}_n}{N} \sum_m \mathcal{R}_m + \frac{1}{N} \sum_{m \neq n} \frac{\mathcal{R}_n (1 - \mathcal{R}_m)^2 + \mathcal{R}_m (1 - \mathcal{R}_n)^2}{\mathcal{R}_n - \mathcal{R}_m}, \quad (7.24a)$$

$$(l/\delta L) \langle \delta \mathcal{R}_n \delta \mathcal{R}_m \rangle = \frac{2\delta_{nm}}{N} \mathcal{R}_n (1 - \mathcal{R}_n)^2, \quad (7.24b)$$

$$(l/\delta L) \langle \delta \mathcal{T}_n \rangle = \mathcal{T}_n (\gamma - 1) + \frac{\mathcal{T}_n}{N} \left( A_{nn} + \sum_{m \neq n} \frac{\mathcal{T}_m A_{nm} + \mathcal{T}_n A_{mm}}{\mathcal{T}_n - \mathcal{T}_m} \right), \quad (7.24c)$$

$$(l/\delta L) \langle \delta \mathcal{T}_n \delta \mathcal{T}_m \rangle = \frac{2\delta_{nm}}{N} \mathcal{T}_n^2 A_{nn}, \quad (7.24d)$$

$$(l/\delta L) \langle \delta \mathcal{T}_n \delta \mathcal{R}_m \rangle = -\frac{2}{N} \mathcal{T}_n \mathcal{R}_m (1 - \mathcal{R}_m) |Q_{nm}|^2. \quad (7.24e)$$

We have abbreviated  $A_{nm} = (\mathbf{QRQ}^\dagger)_{nm}$  and  $F_{nm} = |(\mathbf{Q}\sqrt{\mathbf{R}}\mathbf{Q}^\dagger)_{mn}|^2$ .

The moments of  $\delta \mathcal{R}_n$  contain only the set of reflection eigenvalues  $\{\mathcal{R}_n\}$ , so that from Eq. (7.13) we can immediately write down a Fokker-Planck equation for the distribution of the  $\mathcal{R}_n$ 's. In terms of variables  $\mu_n = 1/(\mathcal{R}_n - 1) \in (-\infty, -1) \cup (0, \infty)$  it reads

$$l \frac{\partial}{\partial L} P(\{\mu_n\}, L) = \frac{2}{\beta N + 2 - \beta} \sum_{n=1}^N \frac{\partial}{\partial \mu_n} \mu_n (1 + \mu_n) \times \left[ \frac{\partial P}{\partial \mu_n} + \beta P \sum_{m \neq n} \frac{1}{\mu_m - \mu_n} + \gamma (\beta N + 2 - \beta) P \right], \quad (7.25)$$

as presented in chapter 5 without derivation. The symmetry index  $\beta = 1(2)$  corresponds to the case of unbroken (broken) time-reversal symmetry. The evolution of the reflection eigenvalues is independent of the transmission eigenvalues — but not vice versa. The evolution of the  $\mathcal{T}_n$ 's depends

on the  $\mathcal{R}_n$ 's, and in addition on the slow variables contained in the unitary matrix  $\mathbf{Q}$ . To obtain a closed Fokker-Planck equation we also need to compute increments and moments of  $\mathbf{Q}$ . The resulting expressions are lengthy and will not be written down here.

In the single-mode case ( $N = 1$ ) this complication does not arise, because  $Q = e^{i\varphi}$  drops out of the scalars  $A$  and  $F$ . The single transmission and reflection eigenvalues  $\mathcal{T}$ ,  $\mathcal{R}$  coincide with the transmittance and reflectance  $T$ ,  $R$  defined by Eq. (7.5). The resulting Fokker-Planck equation is

$$l \frac{\partial P}{\partial L} = -\frac{\partial}{\partial R} \left[ (1-R)^2 + 2\gamma R \right] P + \frac{\partial^2}{\partial R^2} R(1-R)^2 P - \frac{\partial}{\partial T} T(\gamma - 1 + R)P + \frac{\partial^2}{\partial T^2} T^2 R P - 2 \frac{\partial^2}{\partial T \partial R} T R (1-R) P. \quad (7.26)$$

In the case of absorption ( $\gamma < 0$ ), Eq. (7.26) is equivalent to the moments equations of Ref. [5].

## 7.3 Localization length

The limit  $L \rightarrow \infty$  of the distribution of the reflection eigenvalues follows directly from Eq. (7.25) by equating the left-hand-side to zero. The resulting distribution  $P_\infty$  is that of the Laguerre ensemble of random matrix theory [cf. Eq. 5.10],

$$P(\{\mu_n\}) \propto \prod_{i < j} |\mu_j - \mu_i|^\beta \prod_k \exp[-\gamma(\beta N + 2 - \beta)\mu_k]. \quad (7.27)$$

The distribution looks the same for both signs of  $\gamma$ , but the support (and the normalization constant) is different:  $\mu_n > 0$  for  $\gamma > 0$ , and  $\mu_n < -1$  for  $\gamma < 0$ . To determine the localization length we need the distribution of the transmission eigenvalues in the large- $L$  limit. We consider the cases  $N = 1$  and  $N \gg 1$ .

### 7.3.1 Single-mode waveguide

We compute the distribution  $P(T, L)$  of the transmittance through a single-mode waveguide in the limit  $L \rightarrow \infty$ , and extend the results of chapter 6. In the case of absorption ( $\gamma < 0$ ) this calculation was done by Rammal and Doucot [4], and by Freilikher, Pustilnik, and Yurkevich [5]. We generalize

their results to the case of amplification ( $\gamma > 0$ ). The two cases are essentially different because, while the mean value of  $R$  is finite in the case of absorption,

$$\langle R \rangle_\infty = 1 - 2\gamma e^{-2\gamma} \text{Ei}(2\gamma), \quad \text{for } \gamma < 0, \quad (7.28)$$

it diverges in the case of amplification. The mean value of  $\ln R$  is finite in both cases,

$$\langle \ln R \rangle_\infty = \begin{cases} \mathbf{C} + \ln 2\gamma - e^{2\gamma} \text{Ei}(-2\gamma), & \text{for } \gamma > 0, \\ -\mathbf{C} - \ln(-2\gamma) + e^{-2\gamma} \text{Ei}(2\gamma), & \text{for } \gamma < 0. \end{cases} \quad (7.29)$$

Here  $\mathbf{C}$  is Euler's constant and  $\text{Ei}(x) = \int_{-\infty}^x dt e^t/t$  is the exponential integral. The relation

$$\langle \ln R(\gamma) \rangle_\infty = -\langle \ln R(-\gamma) \rangle_\infty \quad (7.30)$$

holds, in accordance with the duality relation (7.8).

We now show that the asymptotic  $L \rightarrow \infty$  distribution of  $T$  is log-normal, with mean and variance of  $\ln T$  given by [cf. Eq. (6.15)]

$$\langle \ln T \rangle = -(1 + |\gamma|)L/l + 2c(\gamma) + O(L/l), \quad (7.31a)$$

$$c(\gamma) = \begin{cases} 0, & \text{for } \gamma < 0, \\ \mathbf{C} + \ln 2\gamma - e^{2\gamma} \text{Ei}(-2\gamma), & \text{for } \gamma > 0, \end{cases} \quad (7.31b)$$

$$\text{Var} \ln T = \left[ 2 + 4|\gamma|e^{2|\gamma|} \text{Ei}(-2|\gamma|) \right] L/l + O(1). \quad (7.31c)$$

The constant  $c(\gamma) \approx -2\gamma \ln \gamma$  if  $0 < \gamma \ll 1$ . Note that  $\text{Var} \ln T \ll \langle \ln T \rangle^2$  for  $L/l \gg 1$ . The localization length  $\xi = l(1 + |\gamma|)^{-1}$  is independent of the sign of  $\gamma$ , in accordance with the duality relation (7.2).

These results are easy to establish for the case of absorption, when Eq. (7.26) implies the evolution equations [4,5]

$$l \frac{\partial}{\partial L} \langle \ln T \rangle = -1 + \gamma, \quad l \frac{\partial}{\partial L} \text{Var} \ln T = 2\langle R \rangle, \quad \text{for } \gamma < 0. \quad (7.32)$$

Making use of the initial condition  $T \rightarrow 1$  for  $L \rightarrow 0$  and the asymptotic value (7.28) of  $\langle R \rangle$ , one readily obtains Eq. (7.31) for  $\gamma < 0$ .

In the case of amplification, the evolution equations (7.32) hold only for lengths  $L$  smaller than  $L_c \simeq l c(\gamma)/|\gamma|$ . For  $L \lesssim L_c$  stimulated emission *enhances* transmission through the waveguide. On larger length scales stimulated emission *reduces* transmission. Technically, the evolution equations (7.32) break down for  $L \rightarrow \infty$  because the integration by parts of the Fokker-Planck equation produces a non-zero boundary term if  $L > L_c$ . To

extend Eq. (7.31) to the case  $\gamma > 0$  we use the duality relation (7.7). It implies that for  $N = 1$  the distribution of the ratio  $T/R$  is an even function of  $\gamma$ . For  $\gamma > 0$  Eq. (7.31a) follows directly from the equality

$$\langle \ln T(\gamma)/R(\gamma) \rangle = \langle \ln T(-\gamma)/R(-\gamma) \rangle, \quad (7.33)$$

which holds for all  $L$ , plus Eq. (7.30), which holds for  $L \rightarrow \infty$ . The constant  $c(\gamma)$  for  $\gamma > 0$  equals  $\langle \ln R(\gamma) \rangle_\infty$  and is substituted from Eq. (7.29). The duality of  $T(\gamma)/R(\gamma)$  also implies Eq. (7.31c) for the variance, provided the covariance  $\langle \langle \ln T \ln R \rangle \rangle = \langle \ln T \ln R \rangle - \langle \ln T \rangle \langle \ln R \rangle$  remains finite as  $L \rightarrow \infty$ . We have checked this directly from the Fokker-Planck equation (7.26), and found the finite large- $L$  limit

$$\begin{aligned} \langle \langle \ln T \ln R \rangle \rangle_\infty &= -2e^{2\gamma} \text{Ei}(-2\gamma)c(\gamma) \\ &\quad - 2\gamma \int_0^\infty d\mu e^{-2\gamma\mu} \left[ \ln^2(1+\mu) - \ln^2\mu \right], \quad \gamma > 0. \end{aligned} \quad (7.34)$$

### 7.3.2 Multi-mode waveguide

We next consider a waveguide with  $N \gg 1$  modes. We compute the localization length  $\xi = -\lim_{L \rightarrow \infty} L^{-1} \langle \ln T \rangle$  in the case of absorption, and include the case of amplification invoking duality. For absorption the average reflectance  $\langle R \rangle = N^{-1} \langle \sum_k (1 + 1/\mu_k) \rangle$  remains finite as  $L \rightarrow \infty$ . The large- $L$  limit  $\langle R \rangle_\infty$  follows from the distribution (7.27), using known formulas for the eigenvalue density in the Laguerre ensemble [18]. For  $|\gamma|N^2 \gg 1$  the result is

$$\langle R \rangle_\infty = 1 + |\gamma| - \sqrt{|\gamma|(2 + |\gamma|)} + O(1/N), \quad \text{for } \gamma < 0. \quad (7.35)$$

The evolution of transmission eigenvalues is governed by the Fokker-Planck equation (7.13), with coefficients given by (7.12), (7.23), and (7.24). Each  $\mathcal{T}_n$  has its own localization length  $\xi_n = -\lim_{L \rightarrow \infty} L^{-1} \ln \mathcal{T}_n$ . We order the  $\xi_n$ 's from large to small,  $\xi_1 > \xi_2 > \dots > \xi_N$ . This implies that for  $L \rightarrow \infty$  the separation of the  $\mathcal{T}_n$ 's becomes exponentially large,  $\mathcal{T}_1 \gg \mathcal{T}_2 \gg \dots \gg \mathcal{T}_N$ . Hence we may approximate

$$\frac{\mathcal{T}_n + \mathcal{T}_m}{\mathcal{T}_n - \mathcal{T}_m} \approx \begin{cases} -1, & \text{for } n > m, \\ 1, & \text{for } n < m, \end{cases} \quad (7.36a)$$

$$\frac{\mathcal{T}_n A_{mm} + \mathcal{T}_m A_{nn}}{\mathcal{T}_n - \mathcal{T}_m} \approx \begin{cases} -A_{mm}, & \text{for } n > m, \\ A_{nn}, & \text{for } n < m. \end{cases} \quad (7.36b)$$

The Fokker-Plank equation (7.13) simplifies considerably and leads to the following equation for the largest transmission eigenvalue:

$$l \frac{\partial}{\partial L} \langle \ln \mathcal{T}_1 \rangle = \begin{cases} -1 - |\gamma| + \langle R \rangle - \frac{1}{N+1} \langle A_{11} + F_{11} \rangle, & \text{for } \beta = 1, \\ -1 - |\gamma| + \langle R \rangle - \frac{1}{N} \langle A_{11} \rangle, & \text{for } \beta = 2. \end{cases} \quad (7.37)$$

For  $|\gamma|N^2 \gg 1$  we may substitute Eq. (7.35) for  $\langle R \rangle$  and omit the terms with  $\langle A_{11} \rangle$  and  $\langle F_{11} \rangle$ . The resulting localization length is given by

$$l/\xi = \sqrt{|\gamma|(2 + |\gamma|)} + O(1/N). \quad (7.38)$$

Because of duality, Eq. (7.38) holds regardless of the sign of  $\gamma$ . It agrees with radiative transfer theory for  $\gamma < 0$ , but not for  $\gamma > 0$ . Indeed, the exponential decay of the transmitted flux in the case of amplification is an interference effect, which is not contained in the theory of radiative transfer.

Equation (7.38) is asymptotically exact for  $|\gamma| \gg 1/N^2$ . For smaller  $|\gamma|$  we cannot compute  $\xi$  rigorously because the distribution of the matrices  $\mathbf{A}$  and  $\mathbf{F}$  is not known. An interpolative formula for all  $\gamma$  can be obtained by substituting for  $\langle A_{11} \rangle$  and  $\langle F_{11} \rangle$  in Eq. (7.37) their  $L \rightarrow \infty$  limits when  $\gamma = 0$ , which are  $\langle A_{11} \rangle = \langle F_{11} \rangle = 1$ . In this way, we arrive at the localization length

$$\xi = l \left[ \frac{2}{\beta N + 2 - \beta} + \sqrt{|\gamma|(2 + |\gamma|)} \right]^{-1}, \quad (7.39)$$

which interpolates between the known [11,12,19] value for  $\xi$  for  $\gamma = 0$  and Eq. (7.38) for  $|\gamma| \gg 1/N^2$  (see Fig. 7.1).

The localization length  $\xi$  is the largest of the eigenvalue-dependent localization lengths  $\xi_n$ . What about the other  $\xi_n$ 's? For  $\gamma = 0$  it is known [12,13,19] that the inverse localization lengths are equally spaced, and satisfy the sum rule  $l \sum_n \xi_n^{-1} = N$ . We have not succeeded in deriving the spacings for  $\gamma \neq 0$ , but we have been able to derive the sum rule from the Fokker-Planck equation (by computing the  $L$ -dependence of  $\langle \sum_n \ln \mathcal{T}_n \rangle$ ). The result is exact and reads

$$l \sum_{n=1}^N \xi_n^{-1} = (1 + |\gamma|)N. \quad (7.40)$$

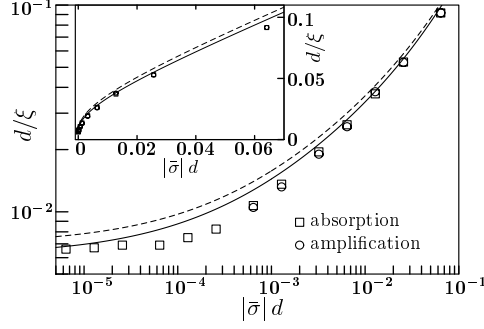


**Figure 7.1:** Localization length  $\xi = -\lim_{L \rightarrow \infty} L^{-1} \langle \ln T \rangle$  of a disordered waveguide ( $N = 10$ ) versus the modal average  $\bar{\sigma}$  of the inverse absorption or amplification length. Data points are a numerical solution of the discretized (lattice constant  $d$ ) two-dimensional Helmholtz equation for the case of absorption (squares) or amplification (circles). The curves are the analytical prediction (7.39) in the case  $\beta = 1$  (unbroken time-reversal symmetry) for  $l = 29.6d$  [solid curve, determined from Eq. (7.43)] and for  $l = 26.1d$  [dashed curve, determined from Eq. (7.44)]. The inset shows the same data on a linear, rather than logarithmic, scale.

## 7.4 Numerical results and conclusions

To test the analytical predictions on a model system, we have numerically solved a discretized version of the Helmholtz equation,

$$\left[ \nabla^2 + k^2 \varepsilon(\mathbf{r}) \right] E(\mathbf{r}) = 0, \quad (7.41)$$

on a two-dimensional square lattice (lattice constant  $d$ , length  $L$ , width  $W$ ). The real part  $\varepsilon'$  of the dielectric constant was chosen randomly from site to site with a uniform distribution between  $1 \pm \delta\varepsilon$ . The imaginary part  $\varepsilon''$  was the same at all sites. The scattering matrix was computed using the recursive Green function technique [20].

The parameter  $\bar{\sigma}$  is obtained from the analytical solution of the discretized Helmholtz equation in the absence of disorder ( $\delta\varepsilon = 0$ ). The complex longitudinal wavenumber  $k_n$  of transverse mode  $n$  then satisfies the dispersion relation

$$\cos(k_n d) + \cos(n\pi d/W) = 2 - \frac{1}{2}(kd)^2(1 + i\varepsilon''), \quad (7.42)$$

which determines  $\bar{\sigma}$  according to  $\bar{\sigma} = -2N^{-1} \text{Im} \sum_n k_n$ . Simulations with

$\varepsilon'' = 0$  were used to obtain  $l$ , either from the large- $L$  relation [12]

$$-\lim_{L \rightarrow \infty} L^{-1} \langle \ln T \rangle = [\frac{1}{2}(N+1)l]^{-1}, \quad (7.43)$$

or from the large- $N$  relation

$$\lim_{N \rightarrow \infty} \langle T \rangle = (1 + L/l)^{-1}. \quad (7.44)$$

The parameters chosen were  $W = 25d$ ,  $k = 1.22d^{-1}$ , corresponding to  $N = 10$ ,  $l = 29.6d$  from Eq. (7.43) and  $l = 26.1d$  from Eq. (7.44). The localization length was computed as a function of  $\sigma$  from the  $L$ -dependence of  $\ln T$  up to  $40l$ , averaged over 150 realizations of the disorder. Results are shown in Fig. (7.1). The localization length is the same for absorption and amplification, within the numerical accuracy. Comparison with the analytical result (7.39) for  $\beta = 1$  is plotted for the two values of the mean free path. The agreement is quite reasonable, given the approximate nature of Eq. (7.39) in the regime  $|\gamma|N^2 \simeq 1$  (corresponding to  $|\bar{\sigma}|d \simeq 10^{-4}$ ).

We can conclude that the extension of the Dorokhov-Mello-Pereyra-Kumar equation to the case of absorbing and amplifying systems leads to meaningful consequences both for single- and multi-mode waveguides. Technical difficulty of the multi-mode case is due to additional degrees of freedom contained in the matrix  $Q$ . (We have checked that a naive assumption of the uniform distribution of  $Q$  is in poor agreement with numerics.) How to overcome this difficulty is an unsolved problem.

## Bibliography

- [1] P. Erdős and R. C. Herndon, *Adv. Phys.* **31**, 65 (1982).
- [2] J. B. Pendry, *Adv. Phys.* **43**, 461 (1994).
- [3] M. E. Gertsenshtein and V. B. Vasil'ev, *Teor. Veroyatn. Primen.* **4**, 424 (1959); **5**, 3(E) (1960) [*Theor. Probab. Appl.* **4**, 3 91 (1959); **5**, 340(E) (1960)].
- [4] R. Rammal and B. Doucot, *J. Phys. (France)* **48**, 509 (1987).
- [5] V. Freilikher, M. Pustilnik, and I. Yurkevich, *Phys. Rev. Lett.* **73**, 810 (1994).
- [6] P. Pradhan and N. Kumar, *Phys. Rev. B* **50**, 9644 (1994).
- [7] A. K. Gupta and A. M. Jayannavar, *Phys. Rev. B* **52**, 4156 (1995).
- [8] Z.-Q. Zhang, *Phys. Rev. B* **52**, 7960 (1995).
- [9] V. Freilikher, M. Pustilnik, and I. Yurkevich, preprint (cond-mat/9605090).
- [10] D. J. Thouless, *Phys. Rev. Lett.* **39**, 1167 (1977).
- [11] K. B. Efetov and A. I. Larkin, *Zh. Eksp. Teor. Fiz.* **85**, 764 (1983) [*Sov. Phys. JETP* **58**, 444 (1983)].
- [12] O. N. Dorokhov, *Pisma Zh. Eksp. Teor. Fiz.* **36**, 259 (1982) [*JETP Lett.* **36**, 318 (1982)]; *Zh. Eksp. Teor. Fiz.* **85**, 1040 (1983) [*Sov. Phys. JETP* **58**, 606 (1983)].
- [13] P. A. Mello, P. Pereyra, and N. Kumar, *Ann. Phys. (N.Y.)* **181**, 290 (1988).
- [14] For a review of the theory of the DMPK equation, see C. W. J. Beenakker, *Rev. Mod. Phys.* **69**, 731 (1997).
- [15] G. L. J. A. Rikken and B. A. van Tiggelen, *Nature* **381**, 54 (1996).
- [16] N. G. van Kampen, *Stochastic Processes in Physics and Chemistry* (North-Holland, Amsterdam, 1981).
- [17] P. A. Mello and S. Tomsovic, *Phys. Rev. B* **46**, 15963 (1992).

- [18] T. Nagao and K. Slevin, *J. Math. Phys.* **34**, 2075; 2317 (1993).
- [19] A. D. Stone, P. A. Mello, K. A. Muttalib, and J.-L. Pichard, in *Mesoscopic Phenomena in Solids*, edited by B. L. Al'tshuler, P. A. Lee, and R. A. Webb (North Holland, Amsterdam, 1991).
- [20] H. U. Baranger, D. P. DiVincenzo, R. A. Jalabert, and A. D. Stone, *Phys. Rev. B* **44**, 10637 (1991).

## 8 Brightness of a phase-conjugating mirror behind a random medium

Phase conjugation is the reversal of the sign of the phase of a wave function. A phase-conjugated wave retraces the path of the original wave, thereby canceling all accumulated phase shifts. Phase conjugation was first discovered for electronic waves [1], and later for optical waves [2–4]. For electrons, phase conjugation takes place at the interface between a normal metal and a superconductor. An electron at energy  $E$  above the Fermi energy  $E_F$  is (retro-)reflected at the angle of incidence as a hole at energy  $E$  below  $E_F$ , a process known as Andreev reflection [5]. A phase-conjugating mirror for light consists of a cell containing a liquid or crystal with a large nonlinear susceptibility, pumped by two counter-propagating beams at frequency  $\omega_0$ . A wave incident at frequency  $\omega_0 + \Delta\omega$  is then retro-reflected at frequency  $\omega_0 - \Delta\omega$ , a process known as four-wave mixing [6–9].

The interplay of multiple scattering by disorder and phase conjugation has been studied extensively in the electronic case, both experimentally and theoretically. (See Ref. [10] for a review.) In the optical case the emphasis has been on weakly disordered media, which do not strongly scatter the waves [11]. Complete wave-front reconstruction is possible only if the distorted wave front remains approximately planar, since perfect time reversal upon reflection holds only in a narrow range of angles of incidence for realistic systems. (For the hypothetical case of perfect time-reversal at all angles, see Ref. [12].) McMichael, Ewbank, and Vachss [13] measured the intensity of the reconstructed wave front for a strongly inhomogeneous medium (small transmission probability  $T_0$ ), and found that it was proportional to  $T_0^2$  — in agreement with the theoretical prediction of Gu and Yeh [14]. If  $T_0 \ll 1$ , the intensity of the reconstructed wave is much smaller than the total reflected intensity. The total reflected intensity was not studied previously, perhaps because it was believed that the diffusive illumination resulting from a strongly inhomogeneous medium would render the effect of phase conjugation insignificant. In this chapter we show that a strongly disordered medium backed by a phase-conjugating mirror has unusual optical properties, different both from the weakly disordered case and from the electronic analogue.

We distinguish two regimes, depending on the relative magnitude of

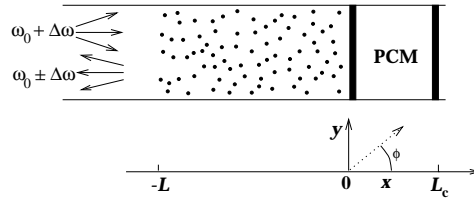


**Figure 8.1:** Schematic drawing of the disordered medium backed by a phase-conjugating mirror (PCM). Light incident at frequency  $\omega_0 + \Delta\omega$  is reflected at the two frequencies  $\omega_0 \pm \Delta\omega$ .

the frequency shift  $2\Delta\omega$  acquired at the phase-conjugating mirror and the inverse of the dwell time  $\tau_{\text{dwell}}$  of a photon in the disordered medium. (For a medium of length  $L$  and mean free path  $l$ , with light velocity  $c$ , one has  $\tau_{\text{dwell}} \simeq L^2/cl$ .) In the *coherent regime*,  $\Delta\omega \ll 1/\tau_{\text{dwell}}$ , phase conjugation leads to a constructive interference of multiply scattered light in the disordered medium. In the *incoherent regime*,  $\Delta\omega \gg 1/\tau_{\text{dwell}}$ , interference effects are insignificant. In both regimes we compute the reflectances  $R_+$  and  $R_-$ , defined as the reflected power at frequency  $\omega_0 \pm \Delta\omega$  divided by the incident power at frequency  $\omega_0 + \Delta\omega$ . A distinguishing feature of the two regimes is that (in a certain parameter range) the reflectance  $R_-$  decreases monotonically as function of  $L/l$  in the coherent regime, while in the incoherent regime it first decreases and then increases.

Our presentation is organized as follows. After having formulated the problem in section 8.1, we discuss in section 8.2 its solution using the Boltzmann equation, ignoring phase coherence. This is the theory of radiative transfer [15, 16]. A simple result is obtained if we neglect angular correlations between the scattering in the disordered medium and at the phase-conjugating mirror. We compare this approximation with an exact solution of the Boltzmann equation. In section 8.3 the phase-coherent problem is addressed, analytically using random-matrix theory, and numerically using the method of recursive Green functions. Results of this section were briefly reported in Ref. [17]. We conclude in section 8.4 with a comparison with the electronic analogue of this problem.

## 8.1 Formulation of the problem

We study the system shown in Fig. 8.1. It consists of a disordered medium (length  $L$ , mean free path  $l$ ), backed at one end by a phase-conjugating

mirror. The other end is illuminated diffusively at frequency  $\omega_+ = \omega_0 + \Delta\omega$ , where  $\omega_0$  is the pump frequency of the mirror. We are interested in the amount of light reflected at frequency  $\omega_+$  and  $\omega_- = \omega_0 - \Delta\omega$ .

To reduce the problem to the scattering of a *scalar* wave, we choose a two-dimensional geometry. The scatterers consist of dielectric rods in the  $z$ -direction, randomly placed in the  $xy$ -plane. The electric field points in the  $z$ -direction and varies in the  $xy$ -plane only. Two-dimensional scatterers are somewhat artificial, but can be realized experimentally [18]. We believe that our results apply qualitatively to a three-dimensional geometry as well, because the randomization of the polarization by the disorder renders the vector character of the light insignificant.

The  $z$ -component of the electric field at the frequencies  $\omega_+$  and  $\omega_-$  is given by

$$E_{\pm}(x, y, t) = \text{Re } \mathcal{E}_{\pm}(x, y) \exp(-i\omega_{\pm}t). \quad (8.1)$$

The phase-conjugating mirror (at  $x = 0$ ) couples the two frequencies via the wave equation [7, 8, 19, 20]

$$\begin{pmatrix} \mathcal{H}_0 & \gamma^* \\ -\gamma & -\mathcal{H}_0 \end{pmatrix} \begin{pmatrix} \mathcal{E}_+ \\ \mathcal{E}_-^* \end{pmatrix} = \frac{2\varepsilon\Delta\omega}{\omega_0} \begin{pmatrix} \mathcal{E}_+ \\ \mathcal{E}_-^* \end{pmatrix}. \quad (8.2)$$

The complex dimensionless coupling constant  $\gamma$  is zero for  $x < 0$  and for  $x > L_c$ , with  $L_c$  the length of the nonlinear medium forming the phase-conjugating mirror. For  $0 < x < L_c$  it is proportional to the electric fields  $\mathcal{E}_1, \mathcal{E}_2$  of the two pump beams and to the third-order nonlinear susceptibility  $\chi_3$ :

$$\gamma = -\frac{3}{2\varepsilon_0}\chi_3\mathcal{E}_1^*\mathcal{E}_2 \equiv \gamma_0 e^{i\psi}, \quad 0 < x < L_c. \quad (8.3)$$

The Helmholtz operator  $\mathcal{H}_0$  at frequency  $\omega_0$  is given by

$$\mathcal{H}_0 = -k_0^{-2}\nabla^2 - \varepsilon, \quad (8.4)$$

where  $\varepsilon(x, y)$  is the relative dielectric constant of the medium. We take  $\varepsilon = 1$  except in the disordered region  $-L < x < 0$ , where  $\varepsilon = 1 + \delta\varepsilon(x, y)$ . The fluctuations  $\delta\varepsilon$  lead to scattering with mean free path  $l$ . We assume  $k_0l \gg 1$ , where  $k_0 = \omega_0/c$  is the wave number of the light (velocity  $c$ ). The validity of Eq. (8.2) requires  $\Delta\omega/\omega_0 \ll 1$  and  $|\gamma| \equiv \gamma_0 \ll 1$ . The ratio of these two small parameters

$$\delta = \frac{2\Delta\omega}{\gamma_0\omega_0} \quad (8.5)$$

is a measure of the degeneracy of the incident and the reflected wave, and can be chosen freely.

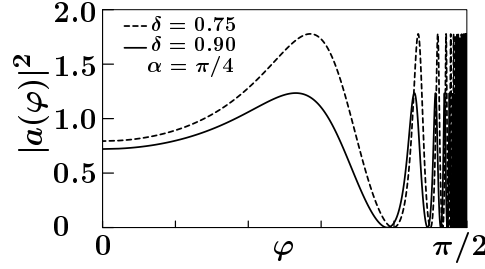


**Figure 8.2:** Reflectance of the phase-conjugating mirror as a function of the angle of incidence, computed from Eq. (8.6) for two choices of parameters.

In the absence of disorder, an incoming plane wave in the direction  $(\cos \varphi, \sin \varphi)$  is retro-reflected in the direction  $(-\cos \varphi, -\sin \varphi)$ , with a different frequency and amplitude. The scattering matrix for retro-reflection is given by [7,8,21]

$$\begin{pmatrix} \mathcal{E}_+ \\ \mathcal{E}_-^* \end{pmatrix}^{\text{out}} = \begin{pmatrix} 0 & -ia(\varphi)e^{-i\psi} \\ ia(\varphi)e^{i\psi} & 0 \end{pmatrix} \begin{pmatrix} \mathcal{E}_+ \\ \mathcal{E}_-^* \end{pmatrix}^{\text{in}}, \quad (8.6a)$$

$$a(\varphi) = [\sqrt{1 + \delta^2} \cotan(\alpha\sqrt{1 + \delta^2}/\cos \varphi) + i\delta]^{-1}, \quad (8.6b)$$

$$\alpha = \frac{1}{2}\gamma_0 k_0 L_c. \quad (8.6c)$$

In Fig. 8.2 we have plotted the reflectance  $|a|^2$  as a function of the angle of incidence  $\varphi$  for  $\alpha = \pi/4$  and two values of  $\delta = 0.75$  and  $0.9$ . The absolute value of  $a$  oscillates between 0 and  $\delta^{-1}$  as a function of the angle  $\varphi$  and the phase of  $a$  covers the range  $[-\pi, 0]$  in each oscillation. Perfect time-reversal requires  $a \approx 1$ , but this is achieved only in a limited range of angles of incidence. In particular, the  $\varphi$ -dependence of the phase of  $a$  makes it in general impossible to cancel all phase shifts. This is the crucial difference between this work and Refs. [12,22], where an angle-independent and real  $a$  was assumed.

The value  $\alpha = \pi/4$  is chosen such that  $a = 1$  for normal incidence at frequency  $\omega_0$  (i.e. for  $\varphi = 0$ ,  $\delta = 0$ ). The two values of  $\delta$  have been chosen such that the angular average of the reflectance,

$$A = \int_0^{\pi/2} d\varphi \cos \varphi |a(\varphi)|^2, \quad (8.7)$$

is  $> 1$  for  $\delta = 0.75$  and  $< 1$  for  $\delta = 0.9$ . (The  $\cos \varphi$  weight factor in Eq. (8.7) corresponds to diffusive illumination.) In most of the numerical examples throughout this chapter we will use these values of  $\alpha$  and  $\delta$ .

## 8.2 Phase-incoherent solution

### 8.2.1 Radiative transfer theory

Within the framework of radiative transfer theory [15, 16], the stationary distribution  $I(x, y, \varphi) \propto |\mathcal{E}|^2$  of the light intensity, at frequency  $\omega$  and wavevector  $(k \cos \varphi, k \sin \varphi)$ , is governed by the Boltzmann equation

$$\left( l \cos \varphi \frac{\partial}{\partial x} + l \sin \varphi \frac{\partial}{\partial y} \right) I(x, y, \varphi) = -I(x, y, \varphi) + \frac{1}{2\pi} \int_0^{2\pi} d\varphi' I(x, y, \varphi'). \quad (8.8)$$

We neglect absorption and assume isotropic scattering in the  $xy$ -plane, with mean free path  $l$ . The phase-conjugating mirror couples the intensities  $I_{\pm}$  of light at the two frequencies  $\omega_{\pm} = \omega_0 \pm \Delta\omega$ . We assume that  $l$  is independent of frequency. The symmetry of the system implies that  $I(x, y, \varphi) = I(x, |\varphi|)$ . In this section we take  $\varphi \in [0, \pi]$ . For each frequency the Boltzmann equation takes the form

$$l \cos \varphi \frac{\partial I_{\pm}(x, \varphi)}{\partial x} = \bar{I}_{\pm}(x) - I_{\pm}(x, \varphi), \quad (8.9a)$$

$$\bar{I}_{\pm}(x) = \frac{1}{\pi} \int_0^{\pi} d\varphi I_{\pm}(x, \varphi). \quad (8.9b)$$

Equation (8.9) has to be supplemented by boundary conditions at the two ends  $x = -L$  and  $x = 0$  of the disordered medium. We consider a situation that the system is illuminated at  $x = -L$  with diffusive light at frequency  $\omega_+$ , hence

$$I_+(-L, \varphi) = I_0, \quad \text{for } \cos \varphi > 0, \quad (8.10a)$$

$$I_-(-L, \varphi) = 0, \quad \text{for } \cos \varphi > 0. \quad (8.10b)$$

At  $x = 0$  the light is reflected by the phase-conjugating mirror. The intensity is multiplied by

$$|a(\varphi)|^2 = \frac{\sin^2(\alpha\sqrt{1+\delta^2}/\cos\varphi)}{\delta^2 + \cos^2(\alpha\sqrt{1+\delta^2}/\cos\varphi)}, \quad (8.11)$$

according to Eq. (8.6). The reflection is accompanied by a change in frequency  $\omega_{\pm} \rightarrow \omega_{\mp}$ , so that the boundary condition is

$$I_{\pm}(0, \varphi) = |a(\varphi)|^2 I_{\mp}(0, \pi - \varphi), \quad \text{for } \cos \varphi < 0. \quad (8.12)$$

The flux  $F_{\pm}$  associated with the intensity  $I_{\pm}$  is defined by

$$F_{\pm} = \int_0^{\pi} d\varphi \cos \varphi I_{\pm}(x, \varphi), \quad (8.13)$$

and is independent of  $x$  [ $\partial F_{\pm}/\partial x = 0$  according to Eq. (8.9)]. The reflectance  $R_-$  is defined as the ratio of the outgoing flux at frequency  $\omega_-$  and the incoming flux at frequency  $\omega_+$ ,

$$R_- = -F_-/I_0. \quad (8.14)$$

The total outgoing flux is  $(R_- + R_+)I_0$ , where

$$R_+ = 1 - F_+/I_0 \quad (8.15)$$

is the ratio of the outgoing flux and the incoming flux at the same frequency  $\omega_+$ .

### 8.2.2 Neglect of angular correlations

A simple analytical treatment is possible if the angular correlations between multiple reflections by the disorder and the phase-conjugating mirror are neglected. Here we present this simplified treatment, and in the next subsection we compare with an exact numerical solution of the Boltzmann equation.

We first consider the disordered region by itself. The plane-wave transmission probability  $|t(\varphi)|^2$  is the ratio of transmitted to incident flux when the incident light is a plane wave in the direction  $(\cos \varphi, \sin \varphi)$ . The transmission probability  $T$  for diffusive illumination is then given by

$$T = \int_0^{\pi/2} d\varphi \cos \varphi |t(\varphi)|^2, \quad (8.16)$$

such that  $T$  is the fraction of the flux incident from a diffusive source which is transmitted through the disordered region. This probability has been calculated in Ref. [23] from the Boltzmann equation (8.9). The result is

$$T = (1 + 2\eta L/\pi l)^{-1}, \quad (8.17)$$

where  $\eta$  is a numerical coefficient which depends weakly on  $L/l$ . In the ballistic limit ( $L/l \rightarrow 0$ )  $\eta$  has the value  $\pi^2/8$  and in the diffusive limit ( $L/l \rightarrow \infty$ )  $\eta$  equals 1. In this subsection (but not in the next) we take  $\eta = 1$  for all  $L/l$  for simplicity.

We use Eq. (8.17) to obtain the reflectance  $R_{\pm}$  for the case that the disordered medium is backed by a phase-conjugating mirror with reflectance

$$A = \int_0^{\pi/2} d\varphi \frac{\cos \varphi \sin^2(\alpha\sqrt{1+\delta^2}/\cos \varphi)}{\delta^2 + \cos^2(\alpha\sqrt{1+\delta^2}/\cos \varphi)}. \quad (8.18)$$

Since  $T$  and  $A$  are angular averages, we are neglecting angular correlations. The light that comes out at frequency  $\omega_-$  has been reflected an odd number of times at the mirror. The light that has been reflected once has traversed the medium twice, which leads to a contribution  $T^2A$  to  $R_-$ . Light that has been reflected three times by the mirror contributes  $T^2A^3(1-T)^2$ , since it has been reflected two times by the medium (each time with probability  $1-T$ ). Summing all contributions, one finds

$$R_- = T^2A + T^2A^3(1-T)^2 + T^2A^5(1-T)^4 + \dots = \frac{T^2A}{1 - (1-T)^2A^2}. \quad (8.19a)$$

Light that comes out at frequency  $\omega_+$  has been reflected an even number of times at the mirror. Zero reflections by the mirror contributes  $1-T$  to  $R_+$ , two reflections contributes  $T^2A^2(1-T)$ , and four reflections  $T^2A^4(1-T)^3$ . Summing the series, one finds

$$R_+ = 1 - T + \frac{T^2(1-T)A^2}{1 - (1-T)^2A^2}. \quad (8.19b)$$

The geometric series leading to Eq. (8.19) diverges if  $(1-T)A \geq 1$ . This indicates that there is only a stationary solution to the Boltzmann equation if both the gain at the mirror and the scattering in the medium are sufficiently weak. If  $A$  is increased at fixed  $\alpha = \pi/4$  by reducing  $\delta$ , the reflectances  $R_{\pm}$  diverge when  $\delta = \delta_c$ . (This divergence is preempted by depletion of the pump beams in the phase-conjugating mirror, which we do not describe.) In the approximation of this subsection,  $\delta_c$  is determined by  $(1-T)A = 1$ , or  $L/l = \frac{1}{2}\pi(A-1)^{-1}$ . In the ballistic limit,  $T = 1$  and  $A < \infty$  for any  $\delta > 0$ . In the diffusive limit,  $T = 0$  and  $A = 1$  for  $\delta = 0.78$ . Hence,  $\delta_c$  increases from 0 to 0.78 as  $L/l$  increases from 0 to  $\infty$ .

### 8.2.3 Exact solution of the Boltzmann equation

The Boltzmann equation (8.9) can be solved exactly, without neglect of angular correlations, by adapting the method of Ref. [23] to an angle-dependent boundary condition. We first rewrite Eq. (8.9) as

$$\frac{\partial}{\partial x} e^{x/l \cos \varphi} I_{\pm}(x, \varphi) = \frac{1}{l \cos \varphi} e^{x/l \cos \varphi} \bar{I}_{\pm}(x), \quad (8.20)$$

and then we integrate once over  $x$ , using the boundary conditions (8.10) and (8.12). The result is

$$I_+(x, \varphi) = \int_{-L}^x \frac{dx'}{l \cos \varphi} e^{-(x-x')/l \cos \varphi} \bar{I}_+(x') + I_0 e^{-(L+x)/l \cos \varphi}, \quad \cos \varphi > 0, \quad (8.21a)$$

$$I_+(x, \varphi) = - \int_x^0 \frac{dx'}{l \cos \varphi} e^{-(x-x')/l \cos \varphi} \bar{I}_+(x') + e^{-x/l \cos \varphi} |a(\varphi)|^2 I_-(0, \pi - \varphi), \quad \cos \varphi < 0, \quad (8.21b)$$

$$I_-(x, \varphi) = \int_{-L}^x \frac{dx'}{l \cos \varphi} e^{-(x-x')/l \cos \varphi} \bar{I}_-(x'), \quad \cos \varphi > 0, \quad (8.21c)$$

$$I_-(x, \varphi) = - \int_x^0 \frac{dx'}{l \cos \varphi} e^{-(x-x')/l \cos \varphi} \bar{I}_-(x') + e^{-x/l \cos \varphi} |a(\varphi)|^2 I_+(0, \pi - \varphi), \quad \cos \varphi < 0. \quad (8.21d)$$

Substitution of Eqs. (8.21c) and (8.21a) into, respectively, Eqs. (8.21b) and (8.21d) yields ( $\cos \varphi < 0$ )

$$I_+(x, \varphi) = \int_x^0 \frac{dx'}{l |\cos \varphi|} e^{-(x'-x)/l |\cos \varphi|} \bar{I}_+(x') + e^{x/l |\cos \varphi|} |a(\varphi)|^2 \times \int_{-L}^0 \frac{dx'}{l |\cos \varphi|} e^{x'/l |\cos \varphi|} \bar{I}_-(x'), \quad (8.22a)$$

$$I_-(x, \varphi) = \int_x^0 \frac{dx'}{l |\cos \varphi|} e^{-(x'-x)/l |\cos \varphi|} \bar{I}_-(x') + e^{x/l |\cos \varphi|} |a(\varphi)|^2 \times \left( I_0 e^{-L/l |\cos \varphi|} + \int_{-L}^0 \frac{dx'}{l |\cos \varphi|} e^{x'/l |\cos \varphi|} \bar{I}_+(x') \right) \quad (8.22b)$$

Finally, integration over  $\varphi$  leads to two coupled integral equations for the average intensities,

$$\bar{I}_+(x) = \int_{-L}^0 dx' M_1(x, x') \bar{I}_+(x') + \int_{-L}^0 dx' M_2(x, x') \bar{I}_-(x') + Q_1(x) I_0, \quad (8.23a)$$

$$\bar{I}_-(x) = \int_{-L}^0 dx' M_1(x, x') \bar{I}_-(x') + \int_{-L}^0 dx' M_2(x, x') \bar{I}_+(x') + Q_2(x) I_0. \quad (8.23b)$$

We have defined the following kernels and source terms:

$$M_1(x, x') = \frac{1}{\pi} \int_0^{\pi/2} \frac{d\varphi}{l \cos \varphi} e^{-|x-x'|/l \cos \varphi} = \frac{1}{\pi l} K_0(|x-x'|/l), \quad (8.24a)$$

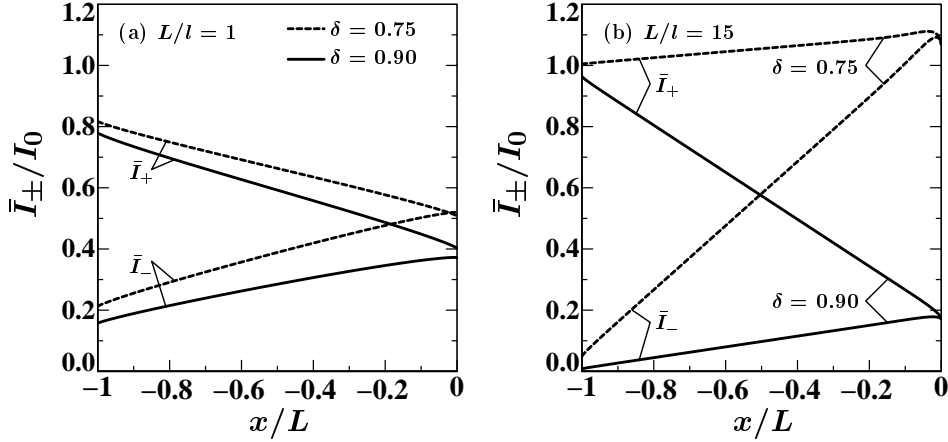


**Figure 8.3:** Intensity profiles in the disordered medium, computed from the exact numerical solution of the Boltzmann equation, for  $\alpha = \pi/4$  and two values of  $\delta$ . (a) is for a nearly ballistic system ( $L/l = 1$ ), (b) is for a diffusive system ( $L/l = 15$ ).

$$M_2(x, x') = \frac{1}{\pi} \int_0^{\pi/2} \frac{d\varphi}{l \cos \varphi} e^{(x+x')/l \cos \varphi} |a(\varphi)|^2, \quad (8.24b)$$

$$Q_1(x) = \frac{1}{\pi} \int_0^{\pi/2} d\varphi e^{-(L+x)/l \cos \varphi}, \quad (8.24c)$$

$$Q_2(x) = \frac{1}{\pi} \int_0^{\pi/2} d\varphi e^{-(L-x)/l \cos \varphi} |a(\varphi)|^2, \quad (8.24d)$$

where  $K_0$  is a Bessel function.

Equation (8.23) is the analogue for the present problem involving two coupled frequencies of the Schwarzschild-Milne equation in the theory of radiative transfer [15, 16]. We have solved it numerically by discretizing with respect to  $x$  so that the integral equation becomes a matrix equation. From the average intensities  $\bar{I}_{\pm}(x)$  one finds the intensities  $I_{\pm}(x, \varphi)$  using Eqs. (8.21) and (8.22). The reflectances  $R_{\pm}$  then follow from Eqs. (8.13)–(8.15). For numerical stability we have imposed a cut-off on the rapidly oscillating function  $a(\varphi)$  at grazing incidence, by setting  $a(\varphi) = 0$  for  $0.497\pi < \varphi < \frac{1}{2}\pi$ .

In Figs. 8.3 and 8.4 we show results for  $\bar{I}_{\pm}(x)$  and  $R_{\pm}$  for  $\alpha = \pi/4$  and  $\delta = 0.75$  and  $0.9$ . For  $\delta = 0.75$  there is an effective gain at the mirror ( $A > 1$ ), while for  $\delta = 0.9$  there is an effective loss ( $A < 1$ ). For an ordinary mirror one can show that  $\bar{I}_{\pm}(0) = \frac{1}{2}I_0$ . Instead, we find that

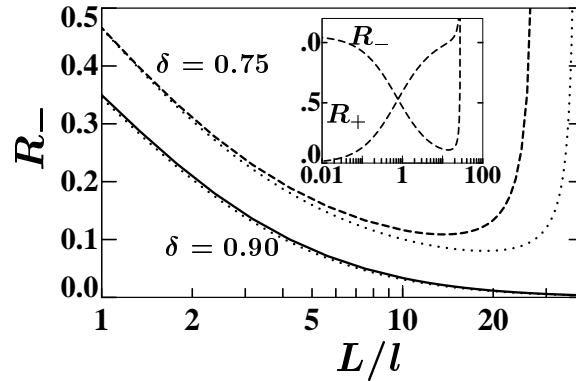


**Figure 8.4:** Reflectance  $R_-$  as a function of  $L/l$ , computed from the exact solution of the Boltzmann equation for  $\alpha = \pi/4$  and  $\delta = 0.75$  (dashed curve),  $\delta = 0.90$  (solid curve). The dotted curves are the approximate result (8.19a), in which angular correlations are neglected. The inset shows the exact reflectances  $R_{\pm}$  for  $\delta = 0.75$ , over a broader range of  $L/l$  (logarithmic scale). For  $\delta = 0.75$  the reflectances diverge at  $L/l = 28$ . No divergence occurs for  $\delta = 0.90$ .

$\bar{I}_-(0) > \bar{I}_+(0) > \frac{1}{2}I_0$  for  $\delta = 0.75$ , indicating gain, and  $\bar{I}_-(0) < \bar{I}_+(0) < \frac{1}{2}I_0$  for  $\delta = 0.9$ , indicating loss. In each case the density profiles are approximately linear in the bulk, with some bending near the boundaries at  $x = -L$  and  $x = 0$ . For  $\delta = 0.75$ , both  $R_-$  and  $R_+$  diverge when  $L/l = 28$ , while for  $\delta = 0.9$  no such divergence occurs. As discussed earlier, the divergence indicates that for  $\delta = 0.75$  and  $L/l > 28$  there is no stationary solution to the Boltzmann equation. For fixed  $L/l$  and  $\alpha$ , the divergence of  $R_{\pm}$  occurs at a critical value  $\delta_c$ , such that a stationary solution requires  $\delta > \delta_c$ . The dependence of  $\delta_c$  on  $L/l$  at fixed  $\alpha = \pi/4$  is plotted in Fig. 8.5.

In Figs. 8.4 and 8.5 we also compare the exact numerical solution of the Boltzmann equation of this subsection with the approximate analytical solution (8.19) of the preceding subsection. As one can see, the agreement with the exact results is quite good.

## 8.3 Phase-coherent solution

### 8.3.1 Scattering matrices

We now turn to a phase-coherent description of the scattering problem. To define finite-dimensional scattering matrices we embed the disordered

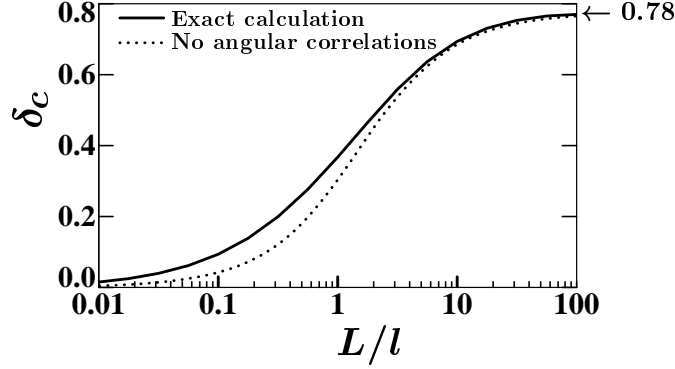


**Figure 8.5:** A stationary solution to the Boltzmann equation requires  $\delta > \delta_c$ . The solid curve is the exact result for  $\delta_c$  (at fixed  $\alpha = \pi/4$ , as a function of  $L/l$ ), the dotted curve follows from Eq. (8.19), obtained by neglecting angular correlations.

medium in a waveguide (width  $W$ ), containing  $N_{\pm} = \text{Int}(\omega_{\pm}W/c\pi) \gg 1$  propagating modes at frequency  $\omega_{\pm}$ . A basis of scattering states consists of the complex fields

$$E_{\pm,n}^{>}(x, y, t) = k_{\pm,n}^{-1/2} \sin\left(\frac{n\pi y}{W}\right) \exp(ik_{\pm,n}x - i\omega_{\pm}t), \quad (8.25a)$$

$$E_{\pm,n}^{<}(x, y, t) = k_{\pm,n}^{-1/2} \sin\left(\frac{n\pi y}{W}\right) \exp(-ik_{\pm,n}x - i\omega_{\pm}t). \quad (8.25b)$$

Here  $n = 1, 2, \dots, N_{\pm}$  is the mode index and the superscript  $>$  ( $<$ ) indicates a wave moving to the right (left), with frequency  $\omega_{\pm} = \omega_0 \pm \Delta\omega$  and wavenumber

$$k_{\pm,n} = (\omega_{\pm}^2/c^2 - n^2\pi^2/W^2)^{1/2}. \quad (8.26)$$

The normalization in Eq. (8.25) has been chosen such that each wave carries the same flux.

With respect to the basis (8.25), incoming and outgoing waves are decomposed as

$$E^{\text{in}} = \sum_{n=1}^{N_+} u_{+,n} E_{+,n}^{>} + \sum_{n=1}^{N_-} u_{-,n} E_{-,n}^{>}, \quad (8.27a)$$

$$E^{\text{out}} = \sum_{n=1}^{N_+} v_{+,n} E_{+,n}^{<} + \sum_{n=1}^{N_-} v_{-,n} E_{-,n}^{<}. \quad (8.27b)$$

The complex coefficients are combined into two vectors

$$\mathbf{u} = (u_{+,1}, u_{+,2}, \dots, u_{+,N_+}, u_{-,1}^*, u_{-,2}^*, \dots, u_{-,N_-}^*), \quad (8.28a)$$

$$\mathbf{v} = (v_{+,1}, v_{+,2}, \dots, v_{+,N_+}, v_{-,1}^*, v_{-,2}^*, \dots, v_{-,N_-}^*). \quad (8.28b)$$

The reflection matrix  $\mathbf{r}$  relates  $\mathbf{u}$  to  $\mathbf{v}$ ,

$$\mathbf{v} = \mathbf{r}\mathbf{u}, \quad \mathbf{r} = \begin{pmatrix} \mathbf{r}_{++} & \mathbf{r}_{+-} \\ \mathbf{r}_{-+} & \mathbf{r}_{--} \end{pmatrix}. \quad (8.29)$$

The dimension of  $\mathbf{r}$  is  $(N_+ + N_-) \times (N_+ + N_-)$ , the submatrices  $\mathbf{r}_{\pm,\pm}$  have dimensions  $N_{\pm} \times N_{\pm}$ . For  $\Delta\omega \ll \omega_0$  we may neglect the difference between  $N_+$  and  $N_-$  and replace both by  $N = \text{Int}(k_0W/\pi)$ .

In the absence of disorder the reflection matrix is entirely determined by the phase-conjugating mirror,

$$\mathbf{r}_{\text{PCM}} = \begin{pmatrix} 0 & -iae^{-i\psi} \\ ia e^{i\psi} & 0 \end{pmatrix}, \quad (8.30a)$$

$$a_{mn} = a(\varphi_n)\delta_{mn}, \quad \varphi_n = \arcsin(n\pi/k_0W). \quad (8.30b)$$

The elements of the  $N \times N$  diagonal matrix  $\mathbf{a}$  are obtained from Eq. (8.6) upon substitution of  $\varphi$  by  $\varphi_n$ , being the angle of incidence associated with mode  $n$ . (The difference in angle between the two frequencies  $\omega_+$  and  $\omega_-$  can be neglected if  $\Delta\omega \ll \omega_0$ .) The angular average (8.7) of the reflectance corresponds to the modal average

$$A = \frac{1}{N} \text{Tr} \mathbf{a} \mathbf{a}^\dagger. \quad (8.31)$$

In the limit  $N \rightarrow \infty$  the two averages are identical.

The disordered medium in front of the phase-conjugating mirror does not couple  $\omega_+$  and  $\omega_-$ . Its scattering properties at frequency  $\omega$  are described by two  $N \times N$  transmission matrices  $\mathbf{t}_{21}(\omega)$  and  $\mathbf{t}_{12}(\omega)$  (transmission from left to right and from right to left) plus two  $N \times N$  reflection matrices  $\mathbf{r}_{11}(\omega)$  and  $\mathbf{r}_{22}(\omega)$  (reflection from left to left and from right to right). Taken together, these four matrices constitute a  $2N \times 2N$  scattering matrix

$$\mathbf{S}_{\text{disorder}}(\omega) = \begin{pmatrix} \mathbf{r}_{11}(\omega) & \mathbf{t}_{12}(\omega) \\ \mathbf{t}_{21}(\omega) & \mathbf{r}_{22}(\omega) \end{pmatrix}, \quad (8.32)$$

which is unitary (because of flux conservation) and symmetric (because of time-reversal invariance). It is simple algebra to express the scattering

matrix  $\mathbf{r}$  of the entire system in terms of the scattering matrices  $\mathbf{r}_{\text{PCM}}$  and  $\mathbf{S}_{\text{disorder}}$  of the phase-conjugating mirror and the disordered region separately. The result is

$$\mathbf{r}_{++} = \mathbf{r}_{11}(\omega_+) + \mathbf{t}_{12}(\omega_+) \mathbf{a} \mathbf{r}_{22}^*(\omega_-) \mathbf{a} [1 - \mathbf{r}_{22}(\omega_+) \mathbf{a} \mathbf{r}_{22}^*(\omega_-) \mathbf{a}]^{-1} \mathbf{t}_{21}(\omega_+), \quad (8.33a)$$

$$\mathbf{r}_{--} = \mathbf{r}_{11}^*(\omega_-) + \mathbf{t}_{12}^*(\omega_-) \mathbf{a} \mathbf{r}_{22}(\omega_+) \mathbf{a} [1 - \mathbf{r}_{22}^*(\omega_-) \mathbf{a} \mathbf{r}_{22}(\omega_+) \mathbf{a}]^{-1} \mathbf{t}_{21}^*(\omega_-), \quad (8.33b)$$

$$\mathbf{r}_{-+} = ie^{i\psi} \mathbf{t}_{12}^*(\omega_-) \mathbf{a} [1 - \mathbf{r}_{22}(\omega_+) \mathbf{a} \mathbf{r}_{22}^*(\omega_-) \mathbf{a}]^{-1} \mathbf{t}_{21}(\omega_+), \quad (8.33c)$$

$$\mathbf{r}_{+-} = -ie^{-i\psi} \mathbf{t}_{12}(\omega_+) \mathbf{a} [1 - \mathbf{r}_{22}^*(\omega_-) \mathbf{a} \mathbf{r}_{22}(\omega_+) \mathbf{a}]^{-1} \mathbf{t}_{21}^*(\omega_-). \quad (8.33d)$$

We seek the reflectances

$$R_- = \frac{1}{N_+} \text{Tr} \mathbf{r}_{-+} \mathbf{r}_{-+}^\dagger; \quad R_+ = \frac{1}{N_+} \text{Tr} \mathbf{r}_{++} \mathbf{r}_{++}^\dagger, \quad (8.34)$$

averaged over the disorder. We will do this analytically, using random-matrix theory [24], and numerically, using the recursive Green function technique [25]. We consider two different regimes, depending on the relative magnitude of  $\Delta\omega$  and  $1/\tau_{\text{dwell}}$ , where  $\tau_{\text{dwell}} \simeq L^2/cl$  is the mean dwell time of a photon in the disordered medium. If  $\tau_{\text{dwell}}\Delta\omega \ll 1$  the difference between  $\mathbf{S}_{\text{disorder}}(\omega_+)$  and  $\mathbf{S}_{\text{disorder}}(\omega_-)$  is insignificant because the phase shifts accumulated in a time  $\tau_{\text{dwell}}$  are approximately the same for frequencies  $\omega_+$  and  $\omega_-$ . We call this the *coherent* regime. If  $\tau_{\text{dwell}}\Delta\omega \gg 1$ , on the contrary, phase shifts at  $\omega_+$  and  $\omega_-$  are essentially uncorrelated, so that  $\mathbf{S}_{\text{disorder}}(\omega_+)$  and  $\mathbf{S}_{\text{disorder}}(\omega_-)$  are independent. We call this the *incoherent* regime.

### 8.3.2 Random-matrix theory

Without loss of generality the reflection and transmission matrices of the disordered region can be decomposed as [24]

$$\begin{aligned} \mathbf{r}_{11}(\omega_\pm) &= i \mathbf{V}_\pm \sqrt{1 - \mathbf{T}_\pm} \mathbf{V}_\pm^\dagger, & \mathbf{r}_{22}(\omega_\pm) &= i \mathbf{U}_\pm \sqrt{1 - \mathbf{T}_\pm} \mathbf{U}_\pm^\dagger, \\ \mathbf{t}_{12}(\omega_\pm) &= \mathbf{V}_\pm \sqrt{\mathbf{T}_\pm} \mathbf{U}_\pm^\dagger, & \mathbf{t}_{21}(\omega_\pm) &= \mathbf{U}_\pm \sqrt{\mathbf{T}_\pm} \mathbf{V}_\pm^\dagger. \end{aligned} \quad (8.35)$$

Here  $\mathbf{U}_\pm$  and  $\mathbf{V}_\pm$  are  $N \times N$  unitary matrices (we take  $N_+ = N_- = N$  in this subsection) and  $\mathbf{T}_\pm$  is a diagonal matrix with the transmission eigenvalues  $\tau_{\pm,n} \in [0, 1]$  on the diagonal. The subscript  $\pm$  refers to the two frequencies  $\omega_+$  and  $\omega_-$ . In this so-called ‘‘polar decomposition’’ the reflectances  $R_\pm$

take the form

$$\Omega = \mathbf{U}_-^\dagger \mathbf{a} \mathbf{U}_+, \quad (8.36a)$$

$$R_- = \frac{1}{N} \text{Tr} \mathbf{T}_- \Omega \left( 1 - \sqrt{1 - \mathbf{T}_+} \Omega^\dagger \sqrt{1 - \mathbf{T}_-} \Omega \right)^{-1} \\ \cdot \mathbf{T}_+ \left( 1 - \Omega^\dagger \sqrt{1 - \mathbf{T}_-} \Omega^* \sqrt{1 - \mathbf{T}_+} \right)^{-1} \Omega^\dagger, \quad (8.36b)$$

$$R_+ = \frac{1}{N} \text{Tr}(1 - \mathbf{T}_+) \\ - \frac{1}{N} \text{Tr} \mathbf{T}_+ \sqrt{1 - \mathbf{T}_+} \left( 1 - \Omega^\dagger \sqrt{1 - \mathbf{T}_-} \Omega^* \sqrt{1 - \mathbf{T}_+} \right)^{-1} \Omega^\dagger \sqrt{1 - \mathbf{T}_-} \Omega^* \\ - \frac{1}{N} \text{Tr} \mathbf{T}_+ \sqrt{1 - \mathbf{T}_+} \Omega^\dagger \sqrt{1 - \mathbf{T}_-} \Omega \left( 1 - \sqrt{1 - \mathbf{T}_+} \Omega^\dagger \sqrt{1 - \mathbf{T}_-} \Omega \right)^{-1} \\ + \frac{1}{N} \text{Tr} \mathbf{T}_+ \Omega^\dagger \sqrt{1 - \mathbf{T}_-} \Omega \left( 1 - \sqrt{1 - \mathbf{T}_+} \Omega^\dagger \sqrt{1 - \mathbf{T}_-} \Omega \right)^{-1} \\ \cdot \mathbf{T}_+ \left( 1 - \Omega^\dagger \sqrt{1 - \mathbf{T}_-} \Omega^* \sqrt{1 - \mathbf{T}_+} \right)^{-1} \Omega^\dagger \sqrt{1 - \mathbf{T}_-} \Omega^*. \quad (8.36c)$$

To compute the averages  $\langle R_\pm \rangle$  analytically in the large- $N$  limit we make the isotropy approximation [24] that the matrices  $\mathbf{U}_\pm$  and  $\mathbf{V}_\pm$  are uniformly distributed over the unitary group  $\mathcal{U}(N)$ . This approximation corresponds to the neglect of angular correlations in the radiative-transfer theory (section 8.2.2). For  $\tau_{\text{dwell}} \Delta\omega \ll 1$  we may identify  $\mathbf{U}_+ = \mathbf{U}_-$  and  $\mathbf{V}_+ = \mathbf{V}_-$ . For  $\tau_{\text{dwell}} \Delta\omega \gg 1$  we may assume that  $\mathbf{U}_+$ ,  $\mathbf{U}_-$ ,  $\mathbf{V}_+$ , and  $\mathbf{V}_-$  are all independent. In each case the integration  $\int d\mathbf{U} f(\mathbf{U})$  over  $\mathcal{U}(N)$  with  $N \gg 1$  can be done using the large- $N$  expansion of Ref. [26]. The remaining average over  $\tau_{\pm, n}$  can be done using the known density  $\rho(\tau)$  of the transmission eigenvalues in a disordered medium [24].

The calculation is easiest in the incoherent regime ( $\tau_{\text{dwell}} \Delta\omega \gg 1$ ). The integration over  $\mathcal{U}(N)$  can be carried out using the formula [26]

$$\int d\mathbf{U} \int d\mathbf{V} \frac{1}{N} \text{Tr}(\mathbf{A}_1 \mathbf{U} \mathbf{A}_2 \mathbf{V} \mathbf{A}_3 \mathbf{U} \cdots \mathbf{A}_p) (\mathbf{B}_1 \mathbf{U} \mathbf{B}_2 \mathbf{V} \mathbf{B}_3 \mathbf{U} \cdots \mathbf{B}_q)^\dagger \\ = \delta_{pq} N^{-p} \prod_{i=1}^p \text{Tr} \mathbf{A}_i \mathbf{B}_i^\dagger + O(N^{-p-1}). \quad (8.37)$$

To apply this formula we expand the inverse matrices in Eq. (8.36) in a power series in  $\mathbf{U}_\pm$  and integrate term by term over the independent matrices  $\mathbf{U}_+$  and  $\mathbf{U}_-$ . The result is, to leading order in  $N$ ,

$$\int d\mathbf{U}_- \int d\mathbf{U}_+ R_- = \sum_{p=0}^{\infty} T_- T_+ A^{2p+1} (1 - T_-)^p (1 - T_+)^p$$

$$= \frac{T_- T_+ A}{1 - (1 - T_-)(1 - T_+)A^2}, \quad (8.38a)$$

$$\int d\mathbf{U}_- \int d\mathbf{U}_+ R_+ = 1 - T_+ + \frac{T_+^2(1 - T_-)A^2}{1 - (1 - T_-)(1 - T_+)A^2}, \quad (8.38b)$$

where we have defined the modal average

$$T_{\pm} = \frac{1}{N} \text{Tr} \mathbf{T}_{\pm} = \frac{1}{N} \sum_{n=1}^N \tau_{\pm, n}. \quad (8.39)$$

The modal average  $A$  was defined in Eq. (8.31). The quantities  $T_{\pm}$  still depend on the configuration of the scatterers, but the fluctuations around the average  $\langle T_{\pm} \rangle$  are smaller by an order  $1/N$  than the average itself. Moreover, the average  $\langle T_{\pm} \rangle$  equals the transmission probability  $T$  from radiative-transfer theory, Eq. (8.17), again up to corrections of order  $1/N$ . Replacing  $T_{\pm}$  in Eq. (8.38) by  $T$  we obtain

$$\langle R_- \rangle = \frac{T^2 A}{1 - (1 - T)^2 A^2}, \quad (8.40a)$$

$$\langle R_+ \rangle = 1 - T + \frac{T^2(1 - T)A^2}{1 - (1 - T)^2 A^2}, \quad (8.40b)$$

which is the result (8.19) of radiative transfer theory with neglect of angular correlations. The conclusion is that in the incoherent regime phase coherence has no effect on the reflectance of the system to leading order in  $N$ . In Fig. 8.6 we have plotted the analytical results from Eq. (8.40).

The situation is entirely different in the coherent regime ( $\tau_{\text{dwell}}\Delta\omega \ll 1$ ). To see the difference it is instructive to first consider the simplified model that the matrix  $a_{mn} = a_0\delta_{mn}$  is proportional to the unit matrix (a scalar). Because  $\mathbf{U}_- = \mathbf{U}_+$  for  $\tau_{\text{dwell}}\Delta\omega \ll 1$ , we then have  $\Omega_{mn} = a_0\delta_{mn}$ . There is therefore no average over  $\mathcal{U}(N)$  to perform. We only have to average over one set of transmission eigenvalues  $\tau_{+,n} = \tau_{-,n} \equiv \tau_n$ . This average amounts to the integrals

$$\langle R_- \rangle = \frac{1}{N} \int_0^1 d\tau \rho(\tau) \frac{|a_0|^2 \tau^2}{|1 - a_0^2 + a_0^2 \tau|^2}, \quad (8.41a)$$

$$\langle R_+ \rangle = 1 - \frac{1}{N} \int_0^1 d\tau \rho(\tau) \frac{\tau - |a_0|^4 \tau(1 - \tau)}{|1 - a_0^2 + a_0^2 \tau|^2}. \quad (8.41b)$$

The density  $\rho(\tau)$  for  $l \lesssim L \ll Nl$  is given by [24]

$$\rho(\tau) = \frac{N}{2(s+1)} \frac{1}{\tau\sqrt{1-\tau}} + O(s+1)^{-4}, \quad s = \frac{2L}{\pi l}. \quad (8.42)$$

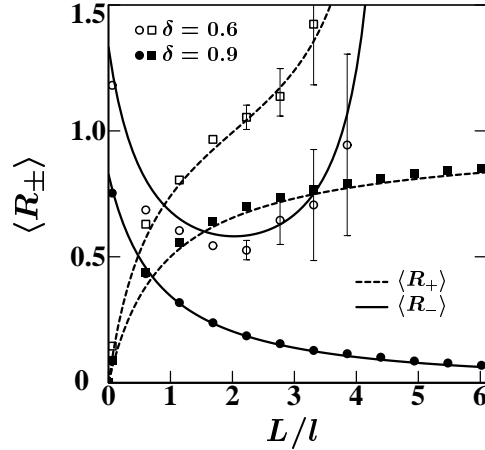


**Figure 8.6:** Average reflectances  $\langle R_{\pm} \rangle$  as a function of  $L/l$  for  $\alpha = \pi/4$  and  $\delta = 0.6, 0.9$ , in the incoherent regime. The curves are the analytical results for  $N \gg 1$ , computed from Eq. (8.19). Data points are results from numerical simulations. (Statistical error bars are shown when they are larger than the size of the marker.)

The density has a cut-off for exponentially small  $\tau$ , which is irrelevant for  $\langle R_{\pm} \rangle$  if  $a_0^2 \neq 1$ . Substitution of Eq. (8.42) into Eq. (8.41) yields the average reflectances

$$\langle R_{-} \rangle = 2T \operatorname{Re} \frac{a_0^*(a_0^2 - 1)}{a_0^2 - a_0^{*2}} \operatorname{artanh} a_0, \quad (8.43a)$$

$$\langle R_{+} \rangle = 1 - 2T \operatorname{Re} \frac{a_0^*(a_0^2 - 1)}{a_0^2 - a_0^{*2}} \operatorname{artanh} a_0^*, \quad (8.43b)$$

where  $T$  is again the transmission probability (8.17) from radiative transfer theory. Both quantities have a smooth  $L$ -dependence, with  $\langle R_{-} \rangle$  decreasing monotonically  $\propto 1/L$ . In contrast, radiative transfer theory predicts a non-monotonic  $L$ -dependence for  $A > 1$ , leading to a divergence at some  $L$ . For  $A < 1$ , radiative transfer theory predicts a quadratic decrease of  $\langle R_{-} \rangle \propto 1/L^2$ , for large  $L$ . The conclusion is that, in the coherent regime, phase coherence modifies the reflectance of the phase-conjugating mirror to leading order in  $N$ .

The result (8.43) was obtained for the simplified model of a scalar reflection matrix  $\mathbf{a}$ . The true  $\mathbf{a}$  in Eq. (8.30) is diagonal but not a scalar. This complicates the calculation because  $\Omega = \mathbf{U}_-^\dagger \mathbf{a} \mathbf{U}_+$  then needs to be averaged over  $\mathcal{U}(N)$  even though  $\mathbf{U}_- = \mathbf{U}_+$ . The calculation is outlined in

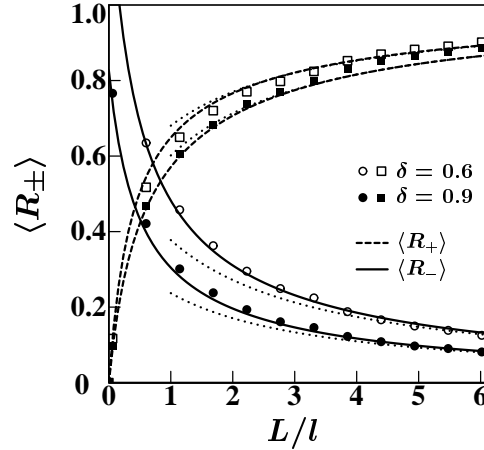


**Figure 8.7:** Average reflectances  $\langle R_{\pm} \rangle$  as a function of  $L/l$  for  $\alpha = \pi/4$  and  $\delta = 0.6, 0.9$ , in the coherent regime. The full curves are the analytical results for  $N \gg 1$ , computed from Eq. (8.76). The dotted curves are the large- $L/l$  limit given by Eqs. (8.43) and (8.45). Data points are results from numerical simulations.

appendix 8.A. The complete result is a complicated function of  $L/l$  (plotted in Fig. 8.7). For  $L/l \gg 1$  the result takes the form of Eq. (8.43), where now  $a_0$  is to be determined from the equation

$$\frac{1}{N} \text{Tr} \frac{\mathbf{a}}{1 - a_0 \mathbf{a}} = \frac{a_0}{1 - a_0^2}. \quad (8.44)$$

In the limit  $N \rightarrow \infty$  this becomes an integral equation for  $a_0$ ,

$$\int_0^{\pi/2} d\varphi \frac{\cos \varphi a(\varphi)}{1 - a_0 a(\varphi)} = \frac{a_0}{1 - a_0^2}, \quad (8.45)$$

where  $a(\varphi)$  is given by Eq. (8.6). As shown in Fig. 8.7, the large- $L$  asymptote (8.43), (8.44) is close to the complete result for  $L \gtrsim l$ . In the limit  $\delta \rightarrow 0$  the solution to Eq. (8.45) is given by  $a_0 = 1.284 - 0.0133i$ , for  $\alpha = \pi/4$ . The corresponding reflectances (for  $L \gtrsim l$ ) are  $\langle R_- \rangle = 61.1l/L$ , and  $\langle R_+ \rangle = 1 + 57.7l/L$ .

To make contact with the work on wave-front reconstruction [13, 14], we consider also the case of plane wave — rather than diffusive — illumination. A plane wave incident at frequency  $\omega_+$  in mode  $n$  is reflected into modes  $m = 1, 2, \dots, N$  at frequency  $\omega_{\pm}$  with probability  $\langle |(\mathbf{r}_{\pm+})_{mn}|^2 \rangle$ . The

calculation of this probability proceeds similarly as the calculation of  $R_-$ . (See Ref. [27] for the analogous calculation in the case of Andreev reflection.) Using Eqs. (8.33)–(8.36) we can write

$$\mathbf{r}_{-+} = ie^{i\psi} \mathbf{V}_-^* \mathbf{O} \mathbf{V}_+^T, \quad (8.46a)$$

$$\mathbf{O} = \sqrt{\mathbf{T}_-} \Omega (1 - \sqrt{1 - \mathbf{T}_+} \Omega^T \sqrt{1 - \mathbf{T}_-} \Omega)^{-1} \sqrt{\mathbf{T}_+}. \quad (8.46b)$$

For the coherent regime, we may again identify  $\mathbf{V}_+ = \mathbf{V}_- = \mathbf{V}$ . The integration over  $\mathcal{U}(N)$  can be performed using [26]

$$\int d\mathbf{V} V_{nk} V_{mj} V_{ni}^* V_{ml}^* = \frac{\delta_{ik} \delta_{jl} + \delta_{mn} \delta_{kl} \delta_{ji}}{N^2 - 1} - \frac{\delta_{kl} \delta_{ji} + \delta_{mn} \delta_{ik} \delta_{jl}}{N^3 - N}. \quad (8.47)$$

We then find

$$\int d\mathbf{V} |(\mathbf{r}_{-+})_{mn}|^2 = \frac{1 + \delta_{mn}}{N + 1} R_- + \frac{N \delta_{mn} - 1}{N^3 - N} \sum_{i \neq j} \mathbf{O}_{ii} \mathbf{O}_{jj}^*. \quad (8.48)$$

In the limit of large  $N$  we can write  $\sum_{i \neq j} \mathbf{O}_{ii} \mathbf{O}_{jj}^* = |\text{Tr } \mathbf{O}|^2$ . In the same way as before, for  $L \gg l$ , this trace can be expressed in terms of  $a_0$ , where  $a_0$  can be found from Eq. (8.30):  $N^{-1} \text{Tr } \mathbf{O} = T \text{artanh } a_0$ . The result for the averages is then

$$\langle |(\mathbf{r}_{-+})_{nn}|^2 \rangle = T^2 |\text{artanh } a_0|^2, \quad (8.49a)$$

$$\langle |(\mathbf{r}_{-+})_{mn}|^2 \rangle = N^{-1} \langle R_- \rangle, \quad m \neq n. \quad (8.49b)$$

The incident plane wave is reconstructed with an intensity  $\propto T^2$ , in agreement with Refs. [13, 14]. In the coherent regime, off-diagonal ( $m \neq n$ ) and diagonal ( $m = n$ ) reflection probabilities differ by a large factor of order  $NT$ . In fig. 8.8 we show a numerical example (to be discussed later).

In the incoherent regime, the matrices  $\mathbf{V}_+$  and  $\mathbf{V}_-$  are independent. Integration over  $\mathcal{U}(N)$  results in integrals of the form  $\int d\mathbf{V} V_{nk} V_{ni}^* = N^{-1} \delta_{ik}$ . Then the off-diagonal and diagonal reflection probabilities are both given by

$$\langle |(\mathbf{r}_{-+})_{mn}|^2 \rangle = N^{-1} \langle R_- \rangle, \quad (8.50)$$

so there is no peak in the reflected intensity at the angle of incidence. This holds for every  $N$  and  $L$ .

For both the incoherent and the coherent regime we find for the reflection without frequency shift ( $\omega_+ \rightarrow \omega_+$ ) the probability

$$\langle |(\mathbf{r}_{++})_{mn}|^2 \rangle = \frac{1 + \delta_{mn}}{1 + N} \langle R_+ \rangle. \quad (8.51)$$

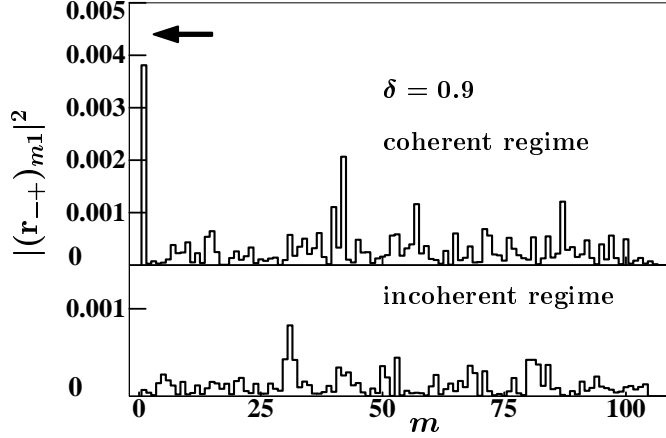


**Figure 8.8:** Histograms for the modal distribution  $|(\mathbf{r}_{-+})_{m1}|^2$  of the reflection probability with frequency shift for normal incidence. The results are for a single realization of the disorder at  $W = L = 251d$  ( $L/l = 16.2$ ),  $\alpha = \pi/4$ , and  $\delta = 0.9$ . The arrow indicates the theoretical value  $\langle |(\mathbf{r}_{-+})_{11}|^2 \rangle$  from Eq. (8.49), representing the ensemble average in the large- $N$  limit.

Here we see a much smaller backscattering peak, where the diagonal reflection probability is only twice as large as the off-diagonal reflection probability [28]. This factor is independent of the phase-conjugating mirror, and exists entirely because of time-reversal symmetry [29].

### 8.3.3 Numerical simulations

To test the analytical predictions of random-matrix theory we have carried out numerical simulations. The Helmholtz equation,

$$(-\nabla^2 - \varepsilon\omega_{\pm}^2/c^2)\mathbf{E} = 0, \quad (8.52)$$

is discretized on a square lattice (lattice constant  $d$ , length  $L$ , width  $W$ ). Disorder is introduced by letting the relative dielectric constant  $\varepsilon$  fluctuate from site to site between  $1 \pm \delta\varepsilon$ . Using the method of recursive Green functions [25] we compute the scattering matrix  $\mathbf{S}_{\text{disorder}}(\omega)$  of the disordered medium at frequencies  $\omega_+$  and  $\omega_-$ . The reflection matrix  $\mathbf{r}_{\text{PCM}}$  of the phase-conjugating mirror is calculated by discretizing Eq. (8.2). From  $\mathbf{S}_{\text{disorder}}(\omega_{\pm})$  and  $\mathbf{r}_{\text{PCM}}$  we obtain the reflection matrix  $\mathbf{r}$  of the entire system, and hence the reflectances (8.34).

We took  $W = 51d$ ,  $\delta\varepsilon = 0.5$ ,  $\alpha = \pi/4$ , and varied  $\delta$  and  $L$ . For the coherent case we took  $\omega_+ = \omega_- = 1.252c/d$ , and for the incoherent case

$\omega_+ = 1.252 c/d$ ,  $\omega_- = 1.166 c/d$ . These parameters correspond to  $N_+ = 22$ ,  $l_+ = 15.5 d$  at frequency  $\omega_+$ . The mean free path is determined using Eq. (8.17), which holds up to small corrections of order  $N^{-1}$ . In the incoherent case we have  $N_- = 20$ ,  $l_- = 20.1 d$ . This leads to  $\Delta\omega = 0.043 c/d$  and a dwell time for  $L/l \simeq 3$  of  $\tau_{\text{dwell}} \simeq L/cl \simeq 150 d/c$ . Hence we have  $\tau_{\text{dwell}}\Delta\omega \simeq 6.5$ , which should be well in the incoherent regime. For comparison with random-matrix theory, we take the large- $N$  limit and use the value  $l_+$  for  $l$ .

The numerical results are shown in Figs. 8.7 (coherent regime) and 8.6 (incoherent regime), for  $\delta = 0.6$  and  $0.9$ . As we can see, the agreement with the analytical theory is quite satisfactory. The rapid rise of  $\langle R_{\pm} \rangle$  in the incoherent regime for the smallest  $\delta$  is accompanied by large statistical fluctuations, which make an accurate comparison more difficult. Still, the striking differences between the coherent and incoherent regimes predicted by the random-matrix theory are confirmed by the simulations.

We have also studied the backscattering peak for plane-wave illumination. We considered a square sample ( $W = L = 251 d$ ) with  $\alpha = \pi/4$ ,  $\delta = 0.9$ . We calculated the reflection probabilities  $|(r_{-+})_{mm}|^2$  for normal incidence ( $n = 1$ ) in both the coherent and the incoherent regimes. The numerical results for a single realization of the disorder are shown in Fig. 8.8. The arrow denotes the analytical ensemble average (8.49) of the backscattering peak in the large- $N$  limit, which is consistent with the numerical data. Notice the absence of a backscattering peak in the incoherent regime.

## 8.4 Comparison with Andreev reflection

We have studied the reflection of light by a disordered dielectric medium in front of a phase-conjugating mirror. This problem has an electronic analogue [19, 20]. The electronic disordered system consists of a metal, in which electron or hole excitations are scattered elastically by randomly placed impurities. Retro-reflection at the phase-conjugating mirror is analogous to Andreev reflection at the interface with a superconductor. The Fermi energy  $E_F$  plays the role of the pump frequency  $\omega_0$ , while the excitation energy  $E$  corresponds to the frequency shift  $\Delta\omega$ . In spite of these similarities, the optical effects found in this study have no electronic analogue. It is instructive to see where the analogy breaks down.

To this end we compare the wave equation (8.2) with the Bogoliubov–

de Gennes equation [30]

$$\begin{pmatrix} H & \Delta \\ \Delta^* & -H \end{pmatrix} \begin{pmatrix} u \\ v \end{pmatrix} = E \begin{pmatrix} u \\ v \end{pmatrix}, \quad (8.53)$$

which determines the electron and hole wavefunctions  $u$  and  $v$ . The Hamiltonian

$$H = -\frac{\hbar^2}{2m}\nabla^2 + V - E_F \quad (8.54)$$

contains the electrostatic potential  $V(\mathbf{r})$ , which plays the role of the dielectric constant. [More precisely,  $k_0^2(\varepsilon - 1)$  corresponds to  $-(2m/\hbar^2)V$ .] The role of the nonlinear susceptibility is played here by the pair potential  $\Delta(\mathbf{r})$ , which is only nonzero in the superconductor, where it equals  $\Delta_0 e^{-i\psi}$ . Comparing Eqs. (8.53) and (8.54) for the electronic case with the optical equations (8.2) and (8.4) one notices many similarities, and some differences which amount to a redefinition of quantities. There is however one essential difference: the matrix operator in Eq. (8.53) is Hermitian, while that in Eq. (8.2) is not, because of an extra minus sign in one of the off-diagonal elements. This minus sign is the origin of the difference between Andreev reflection and optical phase conjugation.

In the optical case a disordered medium becomes transparent ( $R_- = 1$ ) [11, 12] for unit reflectance at the phase-conjugating mirror ( $a = 1$ ). This does not happen in the electronic case, where  $R_-$  is reduced by disorder even for ideal Andreev reflection. The reflection matrix of the normal-metal–superconductor (NS) interface, obtained from Eq. (8.53) for  $V \equiv 0$ ,  $E \ll \Delta_0 \ll E_F$ , is given by [1]

$$\mathbf{r}_{\text{NS}} = \begin{pmatrix} 0 & -ie^{-i\psi} \\ -ie^{i\psi} & 0 \end{pmatrix}. \quad (8.55)$$

Comparison with Eq. (8.30) for  $\mathbf{r}_{\text{PCM}}$  shows that Andreev reflection is independent of the angle of incidence; the matrix  $\mathbf{a}$  in Eq. (8.30) is replaced by the unit matrix in Eq. (8.55). This is a substantial simplification of the electronic problem, compared with the optical analogue. The matrix  $\mathbf{r}_{\text{NS}}$  is unitary, in contrast to  $\mathbf{r}_{\text{PCM}}$ , so that the appearance of gain or loss at the phase-conjugating mirror has no electronic counterpart. The reflectance  $R_- = 1 - R_+$  is a monotonically decreasing function of  $L/l$  in the electronic case [10], both in the coherent regime,

$$R_- = (2 + 4L/\pi l)^{-1}, \quad \text{if } E \ll \hbar/\tau_{\text{dwell}} \text{ and } L \gtrsim l, \quad (8.56)$$

and in the incoherent regime,

$$R_- = (1 + 4L/\pi l)^{-1}, \quad \text{if } E \gg \hbar/\tau_{\text{dwell}}. \quad (8.57)$$

The result (8.57) is what one obtains from Eq. (8.19) for the case  $A = 1$  of unit reflectance at the interface. (The transmittance  $T = (1 + 2L/\pi l)^{-1}$  of the disordered medium is the same for electrons and photons.) The result (8.56) however, is *not* what one would expect from the optical analogue. Indeed, Eq. (8.41) with  $a_0 = 1$  would give  $R_- = 1$  for all  $L$  in the case of unit reflectance at the phase-conjugating mirror. The reason that the analogy with Andreev reflection breaks down is the difference of a minus sign in the wave equations (8.2) and (8.53), which reappears in the reflection matrices (8.30) and (8.55) for phase conjugation, and ultimately in the reflectances in the coherent regime:

$$R_- = \frac{1}{N} \text{Tr} \left( \frac{\mathbf{t}\mathbf{t}^\dagger}{1 + \mathbf{r}\mathbf{r}^\dagger} \right)^2 \neq 1 \quad \text{for electrons,} \quad (8.58a)$$

$$R_- = \frac{1}{N} \text{Tr} \left( \frac{\mathbf{t}\mathbf{t}^\dagger}{1 - \mathbf{r}\mathbf{r}^\dagger} \right)^2 = 1 \quad \text{for photons if } \mathbf{a} \equiv 1. \quad (8.58b)$$

Here  $\mathbf{t}$  and  $\mathbf{r}$  are the transmission and reflection matrices of the disordered medium, which satisfy  $\mathbf{t}\mathbf{t}^\dagger + \mathbf{r}\mathbf{r}^\dagger = 1$ .

In conclusion, we have shown that the presence of a phase-conjugating mirror behind a random medium drastically changes the total reflected intensity, even when the medium is so disordered that wave-front reconstruction is ineffective. On increasing the frequency difference  $\Delta\omega$  between the incident radiation and the pump beams, a *minimum* in the disorder dependence of the reflected intensity appears. In a certain parameter range, the disordered medium reflects less radiation on reducing  $\Delta\omega$ . Experimental observation of this “darkening” would be a striking demonstration of phase-shift cancellations in a random medium.

The random-matrix approach presented here is likely to have a broad range of applicability, as in the analogous electronic problem [10,24]. One direction for future research is to include a second phase-conjugating mirror opposite system is the optical analogue of a Josephson junction [20], and it would be interesting to see how far the analogy goes.

## 8.A Calculation of reflectances in the coherent regime

In section 8.3 we computed the average reflectances  $\langle R_\pm \rangle$  for the incoherent regime. For the coherent regime we presented only a derivation for

scalar reflection matrix  $\mathbf{a}$ . This appendix contains the calculation of  $\langle R_{\pm} \rangle$  for arbitrary (diagonal) matrix  $\mathbf{a}$ . Our calculation is based on the diagrammatic method for integration over the unitary group of Refs. [31] and [26]. Integrals over the unitary group are needed for the computation of  $\langle R_{\pm} \rangle$  because of the polar decomposition (8.35) of the transmission and reflection matrices. We find it convenient to use a slightly modified version of the diagrammatic technique, in which we apply the diagrammatic rules without making explicit use of the polar decomposition. We first outline the calculation of  $\langle R_{\pm} \rangle$  in which the diagrammatic method is used for the integration of the matrices  $\mathbf{U}$  and  $\mathbf{V}$  in Eq. (8.35), and then discuss the modification of the diagrammatic method.

We start the calculation of  $\langle R_{\pm} \rangle$  with the elimination of the reflection matrix  $\mathbf{r}_{11}(\omega_0)$  and the transmission matrices  $\mathbf{t}_{12}(\omega_0)$  and  $\mathbf{t}_{21}(\omega_0)$  from the reflectances  $R_+$  and  $R_-$  [cf. Eqs. (8.33) and (8.34)], in favour of the matrix  $\mathbf{r} = \mathbf{r}_{22}(\omega_0)$ . The result is

$$\langle R_+ \rangle = \frac{1}{N} \text{Tr}[\mathbf{s}'(\mathbf{a}, \mathbf{a}) - \mathbf{s}(1, \mathbf{a}) - \mathbf{s}(\mathbf{a}, 1) + \mathbf{s}'(1, 1) + \mathbf{h}(1) + \mathbf{h}(1)^*], \quad (8.59a)$$

$$\langle R_- \rangle = \frac{1}{N} \text{Tr}\{\mathbf{s}(\mathbf{a}, \mathbf{a}) - \mathbf{s}'(1, \mathbf{a}) - \mathbf{s}'(\mathbf{a}, 1) + \mathbf{s}(1, 1) + \mathbf{a}^{-1} \mathbf{a}^{-1*} [1 - \mathbf{h}(1) - \mathbf{h}(1)^*]\}, \quad (8.59b)$$

where we defined

$$\mathbf{s}'(\mathbf{x}, \mathbf{y}) = \langle \mathbf{x}(1 - \mathbf{r}\mathbf{a}\mathbf{r}^*)^{-1} \mathbf{r}\mathbf{y}\mathbf{y}^* \mathbf{r}^* (1 - \mathbf{a}^* \mathbf{r}\mathbf{a}^* \mathbf{r}^*)^{-1} \mathbf{x}^* \rangle, \quad (8.60a)$$

$$\mathbf{s}(\mathbf{x}, \mathbf{y}) = \langle \mathbf{x}(1 - \mathbf{r}\mathbf{a}\mathbf{r}^*)^{-1} \mathbf{a}^{-1} \mathbf{y}\mathbf{y}^* \mathbf{a}^{-1*} (1 - \mathbf{a}^* \mathbf{r}\mathbf{a}^* \mathbf{r}^*)^{-1} \mathbf{x}^* \rangle, \quad (8.60b)$$

$$\mathbf{h}(\mathbf{x}) = \langle \mathbf{x}(1 - \mathbf{r}\mathbf{a}\mathbf{r}^*)^{-1} \rangle. \quad (8.60c)$$

To perform the average over  $\mathbf{r}$ , one may use the polar decomposition [cf. Eq. (8.35)]

$$\mathbf{r} = i\mathbf{U}\sqrt{1 - \mathbf{T}}\mathbf{U}^T, \quad (8.61)$$

where  $\mathbf{U}$  is a unitary matrix and  $\mathbf{T}$  is the diagonal matrix containing the  $N$  transmission eigenvalues  $\tau_j$  on the diagonal. The matrix  $\mathbf{U}$  is a member of the circular unitary ensemble (CUE), i.e. it is uniformly distributed in the unitary group. The transmission eigenvalues  $\tau_j$  have density [24]

$$\rho(\tau) = (2N/\pi) \text{Im} g(1/\tau - 1 - i0, s), \quad (8.62a)$$

$$g(\zeta, s) = \text{cotanh}[\zeta - sg(\zeta, s)], \quad s = 2L/\pi l. \quad (8.62b)$$

To integrate the matrix  $\mathbf{U}$  over the unitary group, the matrices  $\mathbf{s}$ ,  $\mathbf{s}'$ , and  $\mathbf{h}$  are first expanded as a power series in  $\mathbf{U}$ . The integration of  $\mathbf{U}$  is

then done using the general expression for the average of a polynomial function of  $\mathbf{U}$  [32],

$$\left\langle \mathbf{U}_{a_1 b_1} \cdots \mathbf{U}_{a_m b_m} \mathbf{U}_{\alpha_1 \beta_1}^* \cdots \mathbf{U}_{\alpha_n \beta_n}^* \right\rangle = \delta_{m,n} \sum_{P, P'} V_{c_1, \dots, c_k} \prod_{j=1}^n \delta_{a_j, \alpha_{P(j)}} \delta_{b_j, \beta_{P'(j)}}. \quad (8.63)$$

Here the summation is over all permutations  $P$  and  $P'$  of the numbers  $1, \dots, n$ . The numbers  $c_1, \dots, c_k$  denote the *cycle structure* of the permutation  $P^{-1}P'$ . (The permutation  $P^{-1}P'$  can be uniquely written as a product of disjoint cyclic permutations of lengths  $c_1, \dots, c_k$ , with  $n = \sum_{j=1}^k c_k$ .) To compute  $\langle R_{\pm} \rangle$  in the limit of large  $N$ , it is sufficient to know the coefficients  $V_{c_1, \dots, c_k}$  to leading order in  $N$ . These are given in Refs. [31] and [26], together with a diagrammatic method which enables one to restrict the summation over  $P$  and  $P'$  to those permutations  $P$  and  $P'$  of which the contribution to  $\langle R_{\pm} \rangle$  is of maximal order in  $N$ .

Although the computation of  $\langle R_{\pm} \rangle$  is straightforward now, the actual calculation is rather cumbersome. We find it convenient to modify the approach of Refs. [31] and [26] so that it can be applied directly to the average over the matrix  $\mathbf{r}$ , without making explicit use of the polar decomposition (8.61). This is possible because the general structure (8.63) already follows from the invariance of the distribution of  $\mathbf{U}$  under transformations

$$\mathbf{U} \rightarrow \mathbf{V} \mathbf{U} \mathbf{V}', \quad (8.64)$$

where  $\mathbf{V}$  is an arbitrary unitary matrix. The fact that  $\mathbf{U}$  itself is unitary is necessary to compute the value of the coefficients  $V_{c_1, \dots, c_k}$ , but it is not relevant for the general structure (8.63). Since the matrix  $\mathbf{r}$  is both unitary and symmetric, its distribution is invariant under transformations

$$\mathbf{r} \rightarrow \mathbf{V} \mathbf{r} \mathbf{V}^T \quad (8.65)$$

that respect the symmetry of  $\mathbf{r}$ . The same group of transformations leaves invariant the circular orthogonal ensemble (COE), consisting of uniformly distributed unitary and symmetric matrices. A diagrammatic technique for averages over the COE is presented in Ref. [26]. As before, the general structure of the average of a polynomial of a matrix from the COE is entirely determined by the invariance under the transformations (8.65), and therefore applies to the reflection matrix  $\mathbf{r}$  as well. It reads [26, 33]

$$\left\langle \mathbf{r}_{a_1 a_2} \cdots \mathbf{r}_{a_{2n-1} a_{2n}} \mathbf{r}_{\alpha_1 \alpha_2}^* \cdots \mathbf{r}_{\alpha_{2m-1} \alpha_{2m}}^* \right\rangle = \delta_{n,m} \sum_P V_{c_1, \dots, c_k} \prod_{j=1}^{2n} \delta_{a_j, \alpha_{P(j)}}, \quad (8.66)$$

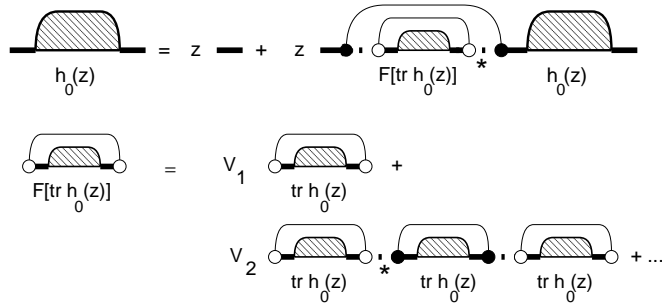


**Figure 8.9:** Diagrams for the calculation of  $h_0(z)$ .

where now the summation is over permutations  $P$  of the numbers  $1, \dots, 2n$ . We may write  $P$  as

$$P = \left( \prod_{j=1}^n \sigma_j \right) P_e P_o \left( \prod_{j=1}^n \sigma'_j \right), \quad (8.67)$$

where the permutations  $\sigma_j$  and  $\sigma'_j$  operate on the numbers  $2j-1$  and  $2j$ , and the permutation  $P_e$  ( $P_o$ ) permutes even (odd) numbers only. The numbers  $c_1, \dots, c_k$  in Eq. (8.66) are the cycle structure of the permutation  $P_e^{-1} P_o$ . The specific values of the coefficients  $V_{c_1, \dots, c_k}$  for an average of  $\mathbf{r}$  are of course different from those for the COE.

Now that we have identified the formal equivalence of an average over the (non-unitary) symmetric reflection matrix  $\mathbf{r}$  and a unitary symmetric matrix from the COE, we can directly apply the diagrammatic rules of Refs. [31] and [26] to an average over the matrix  $\mathbf{r}$ , provided we know the coefficients  $V_{c_1, \dots, c_k}$  for the ensemble of reflection matrices  $\mathbf{r}$  of a disordered waveguide. To find these coefficients, we use the fact that they factorize, to leading order in  $N$ ,

$$V_{c_1, \dots, c_k} = \prod_{j=1}^k V_{c_j}, \quad (8.68)$$

just as they do for the COE. This follows directly from the fact that, to leading order in  $N$ , the average  $\langle \prod_j \text{Tr}(\mathbf{r}\mathbf{r}^\dagger)^{c_j} \rangle$  factorizes into  $\prod_j \langle \text{Tr}(\mathbf{r}\mathbf{r}^\dagger)^{c_j} \rangle$  [34]. It remains to find the coefficients  $V_c$ . Hereto we consider the function

$$\mathbf{h}_0(z) = \left\langle \frac{z}{1 - \mathbf{r}\mathbf{r}^* z^2} \right\rangle. \quad (8.69)$$

We first compute  $\mathbf{h}_0(z)$  from the diagrammatic technique, with a priori unknown coefficients  $V_c$ . We then compare our result with a calculation of  $\text{Tr} \mathbf{h}_0(z)$  from the density of transmission eigenvalues (8.62). The relevant diagrams for the diagrammatic calculation are shown in Fig. 8.9 (for a detailed explanation of the diagrammatic notation of Fig. 8.9, we refer to Ref. [26]). The result is a self-consistency equation for  $\mathbf{h}_0(z)$  that involves the generating function  $F$  of the coefficients  $V_c$ ,

$$\mathbf{h}_0(z) = \frac{z\mathbf{1}}{1 - zF[\text{Tr} \mathbf{h}_0(z)]}, \quad (8.70)$$

$$F(x) = \sum_{j=c}^{\infty} V_c x^{2c-1}. \quad (8.71)$$

Here  $\mathbf{1}$  is the  $N \times N$  unit matrix. Direct computation of  $\text{Tr} \mathbf{h}_0(z)$  from the density  $\rho(\tau)$  of transmission eigenvalues gives

$$\text{Tr} \mathbf{h}_0(z) = \int_0^1 d\tau \frac{\rho(\tau)z}{1 - z^2(1 - \tau)}. \quad (8.72)$$

Together, Eqs. (8.68)–(8.72) determine the coefficients  $V_{c_1, \dots, c_k}$  needed for the diagrammatic evaluation of  $\langle R_{\pm} \rangle$ . In the limit of  $L \rightarrow \infty$ , the density of transmission eigenvalues tends to  $N\delta(\tau)$ . Hence  $\mathbf{h}_0(z) = z/(1 - z^2)$  and  $F(x) = (\sqrt{N^2 + 4x^2} - N)/2x$ . The corresponding coefficients  $V_c = c^{-1}N^{1-2c} \binom{2c-2}{c-1}$  are precisely those of the COE [26]. For finite  $L$ , the density  $\rho(\tau)$  is no longer a delta function, and hence the coefficients  $V_c$  deviate from those of the COE.

The fact that we can use the diagrammatic rules directly for the average over  $\mathbf{r}$  simplifies the calculation considerably. A central role in the calculation is played by the function  $\mathbf{h}(\mathbf{x})$  defined in Eq. (8.60). The diagrams for the calculation of  $\mathbf{h}(\mathbf{x})$  are similar to those of Fig. 8.9, and the result is a self-consistency equation for  $\mathbf{h}(\mathbf{x})$ ,

$$\mathbf{h}(\mathbf{x}) = \mathbf{x} (1 - \mathbf{a}F[\text{Tr} \mathbf{h}(\mathbf{a})])^{-1}. \quad (8.73)$$

Notice the formal equivalence with Eq. (8.70). The function  $F$  was defined in Eq. (8.71). Using the diagrammatic technique for the computation of  $s$  and  $s'$ , we find the linear relations

$$\mathbf{s}(\mathbf{x}, \mathbf{y}) = \mathbf{h}(\mathbf{x}) \left[ \mathbf{a}^{-1} \mathbf{y} \mathbf{y}^* \mathbf{a}^{-1*} + K \text{Tr} \mathbf{s}'(\mathbf{a}, \mathbf{y}) + L \text{Tr} \mathbf{s}(\mathbf{a}, \mathbf{y}) \right] \mathbf{h}(\mathbf{x})^*, \quad (8.74a)$$

$$\mathbf{s}'(\mathbf{x}, \mathbf{y}) = \mathbf{h}(\mathbf{x}) \left[ K \text{Tr} \mathbf{s}(\mathbf{a}, \mathbf{y}) + L \text{Tr} \mathbf{s}'(\mathbf{a}, \mathbf{y}) \right] \mathbf{h}(\mathbf{x})^*, \quad (8.74b)$$

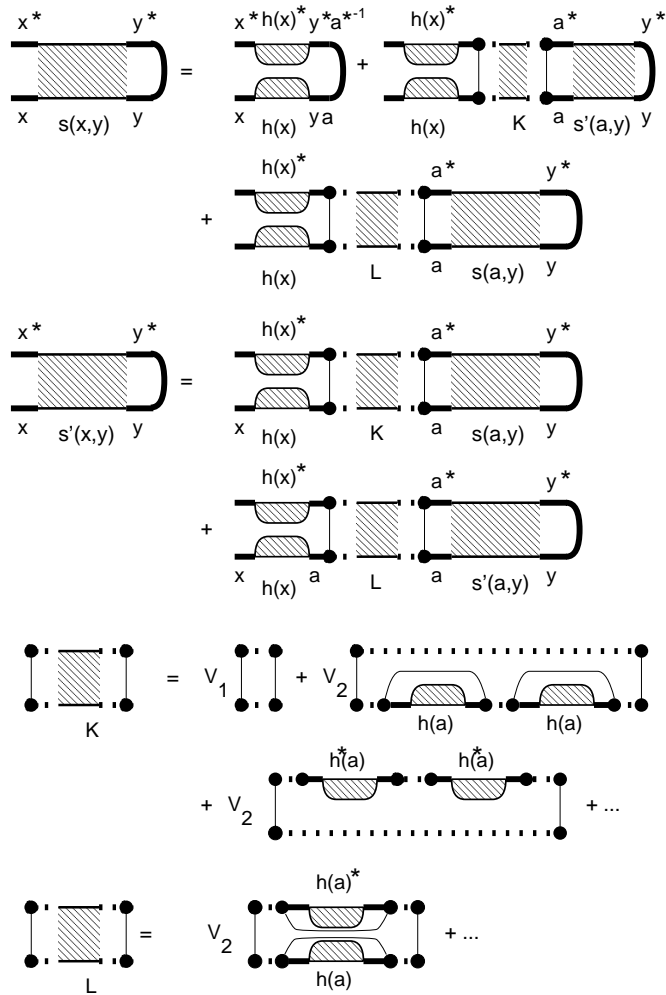


Figure 8.10: Diagrams for the calculation of  $s(x, y)$  and  $s'(x, y)$ .

where we have defined

$$h = \text{Tr } \mathbf{h}(\mathbf{a}), \quad (8.75a)$$

$$K = \sum_{i,j=1}^{\infty} V_{i+j-1} h^{2i-2} (h^*)^{2j-2} = \frac{hF(h) - h^*F(h)^*}{h^2 - h^{*2}}, \quad (8.75b)$$

$$L = \sum_{i,j=1}^{\infty} V_{i+j} h^{2i-1} (h^*)^{2j-1} = \frac{h^*F(h) - hF(h)^*}{h^2 - h^{*2}}. \quad (8.75c)$$

We have shown the relevant diagrams leading to Eqs. (8.74) and (8.75) in Fig. 8.10. They are similar to those of Ref. [31], where the case of a chaotic cavity was considered, instead of a disordered waveguide. Together, Eqs. (8.73)–(8.75) form a closed set of equations, from which  $\mathbf{h}(\mathbf{x})$  and subsequently  $\mathbf{s}(\mathbf{x}, \mathbf{y})$  and  $\mathbf{s}'(\mathbf{x}, \mathbf{y})$  can be calculated. The average reflectances  $\langle R_{\pm} \rangle$  are obtained upon substitution of  $\mathbf{s}(\mathbf{x}, \mathbf{y})$ ,  $\mathbf{s}'(\mathbf{x}, \mathbf{y})$ , and  $\mathbf{h}(\mathbf{x})$  into Eq. (8.59). The final result is expressed as a function of  $h = \text{Tr } \mathbf{h}(\mathbf{a})$ ,

$$N\langle R_{+} \rangle = \frac{(I^2 + J^2)K - 2J(1 - IL)}{(1 - IL)^2 - (KI)^2} + 2 \text{Re Tr}[1 - \mathbf{a}F(h)]^{-1}, \quad (8.76a)$$

$$N\langle R_{-} \rangle = \frac{(I + LJ^2)(1 - IL) + KIJ(KI - 2)}{(1 - IL)^2 - (KI)^2} + J|F(h)|^2, \quad (8.76b)$$

where we defined

$$I = \text{Tr } \mathbf{a}[1 - \mathbf{a}F(h)]^{-1}[1 - \mathbf{a}^*F(h)^*]^{-1}\mathbf{a}^*, \quad (8.77a)$$

$$J = \text{Tr}[1 - \mathbf{a}F(h)]^{-1}[1 - \mathbf{a}^*F(h)^*]^{-1}. \quad (8.77b)$$

These expressions simplify in the large- $L/l$  limit, when  $\rho(\tau)$  takes the form (8.42). Substitution in Eq. (8.72) gives

$$\text{Tr } \mathbf{h}_0(z) = \frac{Nz}{1 - z^2} \left( 1 - \frac{z \text{artanh } z}{1 + s} \right) + O(1 + s)^2, \quad s = 2L/\pi l. \quad (8.78)$$

and hence allows us to find  $F(z)$  from Eq. (8.70). Expanding the expressions (8.76) for  $\langle R_{\pm} \rangle$  and the self-consistency equation (8.73) to lowest order in  $(1 + s)^{-1}$  we find the results (8.43) and (8.44), with the effective reflectance  $a_0 = z$ .

## Bibliography

- [1] A. F. Andreev, Zh. Eksp. Teor. Fiz. **46**, 1823 (1964); **49**, 655 (1965) [Sov. Phys. JETP **19**, 1228 (1964); **22**, 455 (1966)].
- [2] J. P. Woerdman, Opt. Comm. **2**, 212 (1970).
- [3] B. I. Stepanov, E. V. Ivakin, and A. S. Rubanov, Dokl. Akad. Nauk USSR **196**, 567 (1971) [Sov. Phys. Dokl. **16**, 46 (1971)].
- [4] B. Ya. Zel'dovich, V. I. Popovichev, V. V. Ragul'skii, and F. S. Faizullof, ZhETF Pis. Red. **15**, 160 (1972) [JETP Lett. **15**, 109 (1972)].
- [5] A. A. Abrikosov, *Fundamentals of the Theory of Metals* (North-Holland, Amsterdam, 1988).
- [6] R. W. Hellwarth, J. Opt. Soc. Am. **67**, 1 (1977).
- [7] A. Yariv and D. M. Pepper, Opt. Lett. **1**, 16 (1977).
- [8] R. A. Fisher, editor, *Optical Phase Conjugation* (Academic, New York, 1983).
- [9] B. Ya. Zel'dovich, N. F. Pilipetskiĭ, and V. V. Shkunov, *Principles of Phase Conjugation* (Springer, Berlin, 1985).
- [10] C. W. J. Beenakker, in: *Mesoscopic Quantum Physics*, edited by E. Akkermans, G. Montambaux, J.-L. Pichard, and J. Zinn-Justin (North-Holland, Amsterdam, 1995).
- [11] Yu. N. Barabanenkov, Yu. A. Kravtsov, V. D. Ozrin, and A. I. Saichev, in: *Progress in Optics XXIX*, edited by E. Wolf (North-Holland, Amsterdam, 1991).
- [12] R. Mittra and T. M. Habashy, J. Opt. Soc. Am. A **1**, 1103 (1984).
- [13] I. McMichael, M. D. Ewbank, and F. Vachss, Opt. Comm. **119**, 13 (1995).
- [14] C. Gu and P. Yeh, Opt. Comm. **107**, 353 (1994).
- [15] S. Chandrasekhar, *Radiative Transfer* (Dover, New York, 1960).
- [16] A. Ishimaru, *Wave Propagation and Scattering in Random Media* (Academic, New York, 1978).

- [17] J. C. J. Paasschens, P. W. Brouwer, and C. W. J. Beenakker, *Europhys. Lett.* **38**, 651 (1997).
- [18] I. Freund, M. Rosenbluh, R. Berkovits, and M. Kaveh, *Phys. Rev. Lett.* **61**, 1214 (1988); M. I. Mishchenko, J. M. Dlugach, and E. G. Yanovitskij, *J. Quant. Spectrosc. Radiat. Transfer* **47**, 401 (1992).
- [19] D. Lenstra, in: *Huygens Principle 1690–1990; Theory and Applications*, edited by H. Blok, H. A. Ferweda, and H. K. Kuiken (North-Holland, Amsterdam 1990).
- [20] H. van Houten and C. W. J. Beenakker, *Physica B* **175**, 187 (1991).
- [21] H. F. Arnoldus and T. F. George, *J. Mod. Opt.* **36**, 31 (1989).
- [22] A. T. Friberg and E. P. Rantala, *Opt. Comm.* **54**, 236 (1985).
- [23] M. J. M. de Jong, *Phys. Rev. B* **49**, 7778 (1994).
- [24] Two reviews of the random-matrix theory of phase-coherent scattering are: A. D. Stone, P. A. Mello, K. A. Muttalib, and J.-L. Pichard, in: *Mesoscopic Phenomena in Solids*, edited by B. L. Altshuler, P. A. Lee, and R. A. Webb (North-Holland, Amsterdam, 1991); C. W. J. Beenakker, *Rev. Mod. Phys.* **69**, 731 (1997).
- [25] H. U. Baranger, D. P. DiVincenzo, R. A. Jalabert, and A. D. Stone, *Phys. Rev. B* **44**, 10637 (1991).
- [26] P. W. Brouwer and C. W. J. Beenakker, *J. Math. Phys.* **37**, 4904 (1996).
- [27] C. W. J. Beenakker, J. A. Melsen, and P. W. Brouwer, *Phys. Rev. B* **51**, 13882 (1995).
- [28] P. A. Mello, E. Akkermans, and B. Shapiro, *Phys. Rev. Lett.* **61**, 459 (1988).
- [29] G. Bergmann, *Phys. Rep.* **107**, 1 (1984).
- [30] P. G. de Gennes, *Superconductivity of Metals and Alloys* (Benjamin, New York, 1966).
- [31] N. Argaman and A. Zee, *Phys. Rev. B* **54**, 7406 (1996).
- [32] S. Samuel, *J. Math. Phys.* **21**, 2695 (1980).
- [33] P. A. Mello and T. H. Seligman, *Nucl. Phys. A* **344**, 489 (1980).
- [34] P. A. Mello and A. D. Stone, *Phys. Rev. B* **44**, 3559 (1991).

# Samenvatting

## Over de transmissie van licht door wanordelijke media

Een wanordelijk medium in de optica is een systeem waar de brekingsindex varieert als functie van de positie en wel op een wanordelijke manier. Als er nu licht door dit medium beweegt, dan wordt het verstrooid door die brekingsindexverschillen. In dit proefschrift beschrijven we de transmissie van licht door zulke systemen.

Een volledige oplossing van het probleem volgt uit de Maxwellvergelijkingen voor het elektromagnetische veld, met een plaatsafhankelijke brekingsindex. In veel gevallen echter is zo'n volledige beschrijving niet zinvol maar onnodig gecompliceerd. Dit geldt met name voor wanordelijke media, waar veelvuldige verstrooiing vraagt om een statistische theorie. Wij zijn niet in staat om gedetailleerde analytische beschrijvingen te geven van individuele systemen. Wel kunnen we een statistische beschrijving geven van een ensemble van wanordelijke systemen, die microscopisch verschillend zijn, maar macroscopisch gelijkwaardig.

De verschillende theoretische beschrijvingen die wij gebruiken hebben een verschillend niveau van details die meegenomen worden. In alle gevallen zullen we de polarisatie van het licht verwaarlozen. Voor systemen waar interferentie verwaarloosd mag worden, gebruiken we een kinetische theorie, de "stralingstransporttheorie", oorspronkelijk ontwikkeld voor toepassing op de voortplanting van licht door het heelal. Deze theorie bevat slechts de energie van het elektromagnetische veld en niet de fase. Indien de wanorde groot genoeg is, volstaan we met de diffusiebenadering, waarin slechts de totale energiestroom wordt meegenomen en niet die van individuele lichtstralen.

In sommige gevallen zijn interferentie-effecten van essentieel belang en kan de fase van het elektromagnetische veld dus niet verwaarloosd worden. We maken dan gebruik van een verstrooiingstheorie, die de relaties tussen in- en uitgaande velden beschrijft door een matrix, de "verstrooiingsmatrix". Om deze matrix voor een gegeven systeem te vinden zouden we de Maxwellvergelijkingen moeten oplossen. Dit kan nume-

riek, door de ruimte te discretiseren op een rooster. Analytisch kunnen we dit probleem omzeilen door gebruik te maken van bepaalde statistische eigenschappen van grote matrices met toevallig gekozen elementen. Deze theoretische aanpak heet "toevalsmatrixtheorie" en is oorspronkelijk ontwikkeld voor toepassing op verstrooiingsexperimenten in de kernfysica.

In de hoofdstukken 2 en 3 vergelijken we de diffusiebenadering met de stralingstransporttheorie. Als eerste beschouwen we de transmissie door een wanordelijke laag, waarbij er een brekingsindexverschil is met de omgeving. Voor dikke lagen is bekend dat de diffusiebenadering uitstekend is. Door nu een exacte berekening te geven van hetzelfde systeem in de stralingstransporttheorie kunnen we nagaan onder welke omstandigheden de diffusiebenadering bruikbaar is. Het blijkt dat zelfs voor lagen die slechts enkele vrije weglengtes dik zijn, dit nog best aardig gaat.

In hoofdstuk 3 beschouwen we een oneindig uitgestrekt wanordelijk medium, waarin op een zeker moment een korte lichtpuls wordt gegenereerd. We bestuderen de intensiteit als functie van tijd en plaats in het medium. De diffusiebenadering veronderstelt dat licht alle snelheden kan hebben. Licht heeft echter een constante en eindige snelheid en dus geeft de diffusiebenadering met name voor kleine tijden een onjuist resultaat. Wij hebben een exacte oplossing gevonden voor dit probleem met behulp van de stralingstransporttheorie, waar de constante lichtsnelheid wel wordt meegenomen. Een nieuw resultaat is dat de ballistische piek, bestaande uit het onverstrooide licht, een staart heeft die een gevolg is van licht dat slechts eenmaal en in de voorwaartse richting is verstrooid.

In hoofdstuk 4 wordt gekeken naar medische toepassingen, de oorspronkelijke motivatie voor dit onderzoeksproject. Gebruik makend van de diffusiebenadering hebben we de invloed van inhomogeniteiten in een wanordelijk medium op de transmissie bestudeerd. (De toepassing betreft de detectie met licht van een tumor in een borst, hetgeen veiliger is dan detectie met Röntgenstraling.) Eerst geven we een algemene beschrijving die het ons mogelijk maakt verschillende soorten objecten te karakteriseren. Daarna bekijken we wat de invloed is van de randen van het medium op de gevoeligheid voor objecten, en vergelijken we met experimenten aan modelsystemen.

In de hoofdstukken 5, 6 en 7 bestuderen we een systeem dat niet alleen wanorde bevat, maar ook de mogelijkheid heeft tot het versterken van licht door gestimuleerde emissie, zoals in een laser. Zo'n systeem wordt wel een wanordelijke laser genoemd. Interferentie is essentieel en we gebruiken dus de verstrooiingstheorie, die we uitbreiden om ook ge-

stimuleerde emissie te bevatten. Voor de reflectiviteit van zo'n systeem hebben we het verschijnsel van "superreflectie" gevonden, waarbij het gereflecteerde vermogen niet recht evenredig is met het beschenen oppervlak, maar juist met het kwadraat daarvan. We hebben ook de transmissie onderzocht. Wanorde zorgt voor exponentiële afname van de transmissie voor grote lengtes, hetgeen "localisatie" wordt genoemd. Absorptie versterkt deze exponentiële afval. Het ligt voor de hand te veronderstellen dat versterkende systemen precies het tegenovergestelde zouden doen, namelijk het verzwakken van de exponentiële afval. Hoewel dit voor korte systemen inderdaad zo is, hebben wij verrassenderwijs gevonden dat voor lange systemen versterking in dezelfde mate de localisatie vergroot als absorptie. Dit volgt uit een dualiteitsrelatie tussen verstrooiingsmatrices met absorptie en met versterking.

In het laatste hoofdstuk bestuderen we het optische analogon van het elektronische systeem bestaande uit een metaal in contact met een supergeleider. Het systeem dat we beschouwen is een wanordelijke laag waarachter zich een fase-conjugerende spiegel bevindt. Het effect van fase-conjugatie op een invallende golf lijkt op het omkeren van de tijd, zoals een elektron aan een supergeleider gereflecteerd wordt als gat (= "tijdsomgekeerd elektron"). Dit kan gebruikt worden voor golffront-reconstructie, als de wanorde niet te groot is. Wij hebben het geval van grote wanorde onderzocht, zowel met de stralingstransporttheorie als met de verstrooiingstheorie.



## List of Publications

- *Probability of reflection by a random laser*, C. W. J. Beenakker, J. C. J. Paasschens, and P. W. Brouwer, *Physical Review Letters* **76**, 1368–1371 (1996) [chapter 5].
- *Localization of light: Dual symmetry between absorption and amplification*, J. C. J. Paasschens, T. Sh. Misirpashaev, and C. W. J. Beenakker, *Physical Review B* **54**, 11887–11890 (1996) [chapter 6].
- *Localization in a disordered multi-mode waveguide with absorption or amplification*, T. Sh. Misirpashaev, J. C. J. Paasschens, and C. W. J. Beenakker, *Physica A* **236**, 189–201 (1997) [chapter 7].
- *Solution of the time-dependent Boltzmann equation*, J. C. J. Paasschens, *Physical Review E* **56**, 1135–1141 (1997) [chapter 3].
- *Brightness of a phase-conjugating mirror behind a random medium*, J. C. J. Paasschens, P. W. Brouwer, and C. W. J. Beenakker, *Europhysics Letters* **38**, 651–656 (1997).
- *Reflection of light from a disordered medium backed by a phase-conjugating mirror*, J. C. J. Paasschens, M. J. M. de Jong, P. W. Brouwer, and C. W. J. Beenakker, *Physical Review A* (November 1997) [chapter 8].
- *Tomographic image reconstruction from optical projections in light-diffusing media*, S. B. Colak, D. G. Papaioannou, G. W. 't Hooft, M. B. van der Mark, H. Schomberg, J. C. J. Paasschens, J. B. M. Melissen, and N. A. A. J. van Asten, *Applied Optics* **36**, 180–213 (1997).
- *Influence of boundaries on the imaging of objects in turbid media*, J. C. J. Paasschens and G. W. 't Hooft, submitted to *Journal of the Optical Society of America A* [chapter 4].
- *Comment on "Direction of optical energy flow in a transverse magnetic field"*, G. W. 't Hooft, G. Nienhuis, and J. C. J. Paasschens, submitted to *Physical Review Letters*.



## Curriculum Vitæ

Ik ben op 14 maart 1970 in Valkenswaard geboren. Mijn middelbare schooltijd heb ik doorgebracht op het Pius X-college te Bladel, waar ik vanaf 1982 voorbereidend wetenschappelijk onderwijs heb genoten, afgesloten door het eindexamen in 1988. Twee jaar daarvoor nam ik deel aan de Nederlandse Wiskunde Olympiade, evenals het jaar daarop. In 1988 heb ik deelgenomen aan de Nederlandse Natuurkunde Olympiade en vervolgens aan de Internationale Natuurkunde- en aan de Internationale Wiskunde Olympiade. Beide keren won ik een bronzen medaille.

In hetzelfde jaar ben ik begonnen aan mijn studie natuurkunde aan de Katholieke Universiteit Nijmegen, en in 1989 haalde ik daar mijn propædeuse. Tijdens mijn studie heb ik 8 semesters lang werkcolleges gegeven voor verscheidene vakken. Ik ben twee jaar student-vertegenwoordiger geweest in de disciplineraad van natuurkunde. Verder heb ik twee jaar bestuurswerk verricht bij de studievereniging "Marie Curie", waar ik me heb bezig gehouden met het organiseren van studiereizen, naar onder andere Engeland en Rusland. Mijn afstudeerwerk over de elektronische eigenschappen van één-dimensionale quasi-kristallen heb ik verricht in de vakgroep theoretische vaste-stoffysica onder begeleiding van prof. dr. T. Janssen.

In februari 1994 ben ik begonnen met mijn promotie onder leiding van prof. dr. C. W. J. Beenakker van de Rijksuniversiteit te Leiden, als Onderzoeker in Opleiding bij de Nederlandse organisatie voor Wetenschappelijk Onderzoek. Dit heeft, met financiële steun van Philips N.V., in zijn geheel plaats gevonden op het Philips Natuurkundig Laboratorium te Eindhoven, eerst in groep van dr. H. van Houten en later in de groep van dr. ir. E. J. van Loenen. De belangrijkste resultaten van het onderzoek zijn in dit proefschrift opgenomen. Een deel van de resultaten heb ik gepresenteerd op nationale en internationale symposia.

# STELLINGEN

behorende bij het proefschrift

## **On the Transmission of Light through Random Media**

van Jeroen Paasschens

1. De door Rikken en Van Tiggelen gevonden polarizatie-afhankelijkheid van de energiestroom in een niet-absorberend medium met een magneetveld-afhankelijke diëlektrische constante verdwijnt als de golfvector loodrecht op het magneetveld staat.

*G. L. J. A. Rikken en B. A. van Tiggelen,  
Physical Review Letters 78, 847 (1997).*

2. De voorwaarde van Loss, Schoeller en Goldbart voor adiabaticiteit van de elektronspin in een roterend magneetveld is te zwak.

*D. Loss, H. Schoeller en P. M. Goldbart,  
Physical Review B 48, 15218 (1993).*

3. De door Schep en Bauer berekende dichtheid van transmissie-eigenwaarden van een wanordelijk grensvlak volgt uit de toevalsmatrixtheorie voor een reflectiematrix die niet veel van de eenheidsmatrix afwijkt.

*K. M. Schep en G. E. W. Bauer,  
Physical Review Letters 78, 3015 (1997).*

4. De door Neijzen *et al.* gemeten lineaire dikte-afhankelijkheid van het contrast van een vloeibaar kristal in een polymeermatrix wordt beschreven door de formule

$$\text{contrast} = (1 + n_{\text{matrix}})^4 \frac{1 - g}{8\theta_0^2} (d/l_{\text{scat}} - 2).$$

*J. H. M. Neijzen, H. M. J. Boots, F. A. M. A. Paulissen,  
M. B. van der Mark en H. J. Cornelissen,  
Liquid Crystals 22, 255 (1997).*

5. De veronderstelling van Movaghar, Ries en Grünewald, dat er in hun model voor de dynamica van excitaties in wanordelijke organische halfgeleiders geen correlatie bestaat tussen de sprongkans en eerder bezochte posities, is onjuist.

*B. Movaghar, B. Ries en M. Grünewald  
Physical Review B 34, 5574 (1986).*

6. Kolossale magnetoweerstand is een kritiek verschijnsel.
7. De gangbare absorptiecorrectie van de diffusieconstante heeft geen theoretische rechtvaardiging.
8. De theoretische beschrijving van de relatie tussen Poyntingvector en groepsnelheid in systemen die zowel absorberend als anisotroop zijn, behoeft een niet-triviale uitbreiding van de afzonderlijke gevallen.
9. Er bestaan superposities van twee vlakke elektromagnetische golven in vacuüm waarbij de elektrische en magnetische componenten op elk punt evenwijdig zijn.
10. De stelling van Butler *et al.*, dat onze wereld beschreven wordt door de Lorentzmetriek  $g = \text{diag}(1, -1, -1, -1)$  en niet door de anti-Lorentzmetriek  $g = \text{diag}(-1, 1, 1, 1)$ , is niet falsifieerbaar.

*P. H. Butler, J. G. Williamson, P. F. Renaud en  
M. B. van der Mark.*

11. Zonder fotografen was het fenomeen Diana er nu niet geweest.

Eindhoven, 16 oktober 1997.